PHYSIOLOGICALLY-BASED PHARMACOKINETIC MODELING APPROACH FOR DRUG DISPOSITION IN HUMAN AND PREGNANT RAT

by

TING LI

(Under the Direction of Catherine A. White)

ABSTRACT

Physiologically-based pharmacokinetic (PBPK) modeling is a useful approach to investigate the absorption, distribution, metabolism and elimination (ADME) of a compound in animals as well as humans. In this dissertation, a PBPK model was constructed to describe dose and time dependent pharmacokinetics of dichloroacetic acid (DCA) in humans. DCA is used clinically to treat metabolic acidosis and is also a potential carcinogenic contaminate in drinking water. DCA inactivates its own metabolic enzyme, glutathione transferase zeta (GSTzeta) which leads to an increased half-life after repeated dosing. GSTzeta is also a major enzyme in tyrosine catabolism and deficiency in this metabolic pathway resulting in the accumulation of intermediate metabolites is proposed as the mechanism behind DCA carcinogenicity. Therefore, quantitative evaluation of DCA pharmacokinetics and compromised GSTzeta activity following repeated dosing is critical in understanding the pharmacological and toxicological effects arising from human exposure.

Nucleoside reverse transcriptase inhibitors (NRTIs) are the primary antiretroviral drugs used in highly active antiretroviral therapy (HAART), which is successful in reducing mother-to-child transmission (MTCT) of HIV. However, limited *in vivo* pharmacokinetic data are available

for NRTI disposition in pregnant women as well as their fetuses. PBPK models are advantageous in that assessment of special physiological situations, such as pregnancy and the compounds pharmacokinetics behavior, in animal, tissues that otherwise can never been assessed in human, such as placenta and fetus. The first PBPK models describing perinatal exposure to NRTIs and the potential drug-drug interactions are reported in this dissertation. Based on the model simulations, NRTIs cross placenta through active transport, not only passive diffusion. Consequently, when co-administered, NRTI clearance from maternal tissues may be altered. Drug-drug interactions on transplacental transfer suggest a complex mechanism including up-regulated/down-regulated transport, which may be the result of multiple NRTIs transporters located on both the maternal and fetal side of the placenta. Because of the similarity between human and rat placenta, including similar transporter compositions, the interactions identified in present study may have clinical significance and thus, require careful monitoring during administration to pregnant women to protect against mother-to-child transmission (MTCT) of HIV.

INDEX WORDS: physiologically-based pharmacokinetic model, dichloroacetic acid, nucleoside reverse transcriptase inhibitors, pregnancy, drug-drug interaction, suicide inhibition

PHYSIOLOGICALLY-BASED PHARMACOKINETIC MODELING APPROACH FOR DRUG DISPOSITION IN HUMAN AND PREGNANT RAT

by

TING LI

B.S., Huazhong Agricultural University, China, 2002

A Dissertation Submitted to the Graduate Faculty of The University of Georgia in Partial Fulfillment of the Requirements for the Degree

DOCTOR OF PHILOSOPHY

ATHENS, GEORGIA

2007

PHYSIOLOGICALLY-BASED PHARMACOKINETIC MODELING APPROACH FOR DRUG DISPOSITION IN HUMAN AND PREGNANT RAT

by

TING LI

Major Professor:	Catherine A. White
Committee:	Robert D. Arnold Brian S. Cummings Jeffrey W. Fisher Arthur Grider Ethan Will Taylor

Electronic Version Approved:

Maureen Grasso
Dean of the Graduate School
The University of Georgia
August 2007

ACKNOWLEDGEMENTS

First of all, I would like to thank my family whose love and support through the years have provided me with the strength to be successful in all my endeavors. Being an independent and intelligent human being, like one of you, has been my motivation in life. I would like to give very special thanks to my husband, Dr. Jerry Campbell. Marrying you was the luckiest thing that has happened to me. I would like to thank my major advisor, Dr. Catherine A. White for providing me the opportunity to advance as a scientist. I would like to thank Dr. Ethan Will Taylor whom I believe is one of the most talented and generous people in the world. I would also like to thank Dr. Jeffrey W. Fisher whose guidance has been invaluable. I would like to thank Dr. Brian S. Cummings who sets a high academic standard for my work and for always having the time to assist me; Dr. Robert D. Arnold for all your knowledge, advice and encouragement; and Dr. Arthur Grider for your unfailing optimism that was always there when I needed it. Finally, I would also like to thank all of my friends whose friendship is the most cherished thing I have gained in my life.

TABLE OF CONTENTS

Page

LIST OF TABLES

Page

LIST OF FIGURES

Page

CHAPTER 1

INTRODUCTION

A specialized class of pharmacokinetic models, physiological-based pharmacokinetic (PBPK) models, is a set of interconnected compartments that incoporate the physiology and anatomy of the animals along with the biochemistry of the chemical of interest in the description. PBPK models provide a quantitative tool allowing for dose-to-dose, route-to-route and species-to-species extrapolations. PBPK models are useful in the investigation of the absorption, distribution, metabolism and elimination (ADME) of compounds in different tissues. This dissertation describes the development of PBPK models for dichloroacetic acid (DCA) in human and nucleoside reverse transcriptase inhibitors (NRTIs) in pregnant rats as well as the pharmacokinetic interactions of NRTIs following combination therapies.

In Chapter 2, studeis addressing critical issues in PBPK model development and application are reviewed. Special topics related to the present study, such as the mathematical description of enzyme suicide inhibition, PBPK models developed for pregnancy and perinatal exposure of xenobiotics and drug-drug interactions are discussed. In Chapter 3, a PBPK model created to describe the plasma pharmacokinetics of DCA in human is discussed. The model was used to estimate the loss in metabolic capacity of glutathione transferase zeta (GSTzeta) along with its impact on the DCA eliminaiton. Human equivalent doses are calculated with the model based on the 10% increased risk of liver tumor in mice. In Chapter 4, models for perinatal exposure of NRTIs (abacavir (ABC), lamivudine (3TC), zalcitabine (ddC) and zidovudine (AZT)) in rat are described. The mechanism of transplacental transfer of these nucleoside anlog

drugs was investigated with several alternative model structures. In Chapter 5, PBPK models for the individual NRTIs are combined to describe the co-administration of two NRTIs (AZT-3TC and AZT-ABC) to investigate the altered pharmacokinetic by incorporating drug-drug interactions on the maternal clearance and transplacental transfers. Chapter 6 summarizes the major discoveries gleaned from the three PBPK modeling projects. In Appendix A, a study investigating the biological function of pro-fs, a peptide encoded by HIV, and its *in vitro* interactions with host proteins were reported. This study suggested that pro-fs can stimulate gene expression through a NF-κB mediated pathway and may play a significant role in auto-regulation of virus gene expression. Appendix B documents the Advanced Continuous Simulation Language (ACSL) code for all PBPK models reported in Chapters 3 through 5.

CHAPTER 2

LITERATURE REVIEW

Physiologically-Based Pharmacokinetic (PBPK) Models and Their Applications

Physiologically-based pharmacokinetics modeling is a dynamic tool useful for the prediction of experimental kinetic data (i.e., the uptake, distribution and elimination of a chemical) including the mechanisms underlying these pharmacokinetic processes. The major distinctive feature of a PBPK model compared to an empirical model is the incorporation of physiological processes, such as tissue volumes and blood flows, as is shown in the example model structure (Fig. 2.1). The structure of an empirical model is determined by the 'best fit' to the experimental data. For example, in the 2-compartment empirical model, the disposition of a drug in the body is described by oral or IV administration into the central compartment (blood and other rapidly distributed tissues, such as liver and kidney) and distribution to the peripheral compartment (slowly distributed tissues, such as muscle and fat). The loss of drug from the body is described as elimination from the central compartment (Fig. 2.1a). Empirical models are data driven and do not require additional information related to the modeled compound, such as partition coefficients, and provide good fits to the experimental data along with estimations of PK parameters such as volume of distribution and clearance. Due to these attributes, empirical models are used extensively by the pharmaceutical industry. On the other hand, PBPK model structures are predetermined by the anatomical and physiological structures of the organism studied, encompassing body tissues, fluids, organs and/or systems (Fig. 2.1b) (Nestorov, 2003). PBPK models are not only derived to capture the kinetic data, but also to answer important

questions related to factors and/or mechanisms that are influencing the pharmacokinetic behavior.

With "physiological reality" as a base, PBPK models may provide more accurate characterization of xenobiotic PK behavior in each of the tissues across various exposure scenarios and can also be extrapolated across species. Therefore, PBPK models have been well implemented in toxicological studies and risk assessments where tissue dosemetrics of chemicals and metabolites are assessed in target tissues of animals first and then extrapolated to humans (Andersen *et al.*, 1987; Clewell *et al.*, 2005; U.S.EPA, 2006a).

PBPK models are also particularly advantagous for drug development and research (Nestorov, 2003). For example, PBPK model have been used to predict the *in vivo* volume of distributions based on the chemical properties of several drug and tissue compositions prior to *in vivo* studies and the early stages of drug development to facilitate *in vitro* to *in vivo* extrapolation and candidate selection (Poulin and Theil, 2002). A mechanism-based PBPK model successfully described multiple non-linear factors, such as saturable tissue distribution and hepatic clearances, for cyclosporine (an immunosuppresive agent) dispostion. The model further demonstrated that the observed apparent linear pharmacokinetics of cyclosporine over a wide dose range resulted from a counterbalance of these saturable factors (Tanaka *et al.*, 1999). Another PBPK model was constructed to characterize the pharmacokinetics of capecitabine and its three serial metabolites in humans. Capecitabine, a pro-drug of 5-fluorouracil (5-FU), is used in tumor chemotherapy. Because capecitabine undergoes extensive metabolism in multiple tissues, its pharmacokinetic and pharmacodynamic activity was poorly predicted with empirical PK models (Blesch *et al.*, 2003). Physiological alterations that occur with medications can also be incorporated into PBPK models. For example, a PBPK model was employed to describe dose-dependent dynamic

changes in blood flow to target tissues caused by inaperisone, a muscle relaxant. (Nagata *et al.*, 1990).

PBPK Model Development

Tissue Compartments

Though a PBPK model is designed to simulate the "real body," determining which tissues to be included as compartments is based primarily on the intended use of the model. Tissue compartments generally included are a) essential elimination organs, such as liver and kidney; b) important depots, such as adipose for lipophilic drugs (Fiserovabergerova, 1992); c) plasma/blood compartment for compounds with significant binding to plasma protein or accumulation in red blood cells (Tanaka *et al.*, 1999); d) tissues related to specific exposure routes, such as lung for inhalation exposure and skin for dermal exposure (Sarangapani *et al.*, 2002b; Reddy *et al.*, 2005); e) target tissues, such as brain for CNS drugs (Blakey *et al.*, 1997). At the same time, model development should follow the principle of parsimony in order to avoid unnecessary over-parameterization.

Model Equations

PBPK models are a set of interconnected compartments (i.e., continuous stirred tank reactors). The set of differential equations for a model are derived as mass balance across various compartments integrated over time**.** The amount of chemical within a given compartment at any point time is equal to the amount of compound distributed to the compartment from arterial supply minus the amount leaving the tissue in the venous return (Fig. 2.2). Two commonly used descriptions for the uptake of a compound into a compartment are flow-limited and diffusion-limited (Nestorov, 2003). In a flow-limited model, the rate of transport of the drug into the tissue is limited by blood flow to that particular tissue as the uptake of drug by the tissue

is assumed to be very rapid (Fig. 2.2a). In a diffusion-limited model, the rate of uptake from the tissue blood into the tissue rather than amount arriving from the blood flow limits the uptake of the drug into the tissue compartment (Fig. 2.2b). The permeability-area cross product (PA_T) for the tissue determines the rate at which the drug can enter the tissue compartment. Tissues subdivided into compartments representing capillary bed, interstitial fluid and intracellular space, have been developed to describe more complicated tissue distributions (Kawai *et al.*, 1998; Brightman *et al.*, 2006). In the elimination organs (*i.e.*, liver and kidney), except the amount of drug getting into the tissue through arterial blood flow and leaving the tissue through venous blood flow, the mass balance includes the amount of drug eliminated through either metabolism or urinary excretion. The renal excretion of many chemicals from the kidney compartment was described as a first-order elimination. However more 'realistic' kidney models have been developed to include glomerular filtration, tubular secretion and saturable re-absorption when the simple first-order model failed to predict the urinary data or when the chemical disposition in the kidney is a tissue of primary interest (Corley *et al.*, 2005; Brightman *et al.*, 2006). Metabolic elimination is generally described as a Michaelis-Menten process (*i.e.*, with a maximum metabolic activity V_{max} and affinity constant K_m) to capture the non-linear elimination pharmacokinetics. Meanwhile, more complicated mathematical descriptions were incorporated into the PBPK mdoel to account for the alteration of V_{max} and apparent K_m over time due to enzyme induction/inhibition and competitive inhibition. (Andersen *et al.*, 1997; Sarangapani *et al.*, 2002a; Campbell and Fisher, 2007).

Model Parameterization

There are two types of parameters employed in a PBPK model: physiological parameters, and chemical-specific parameters such as partition coefficient and biochemical parameters.

Physiological parameters such as blood flow and tissue volumes are well documented for most laboratory animals and humans (Brown *et al.*, 1997). In PBPK models, physiological parameters are scaled to body weight or surface area providing the foundation for inter-species extrapolation. That is, PBPK models, through incorporation of species specific physiological parameters, allow for cross-species extrapolation where limited data are available.

Partition coefficients (PCs) in biological tissues include the chemical solubility within a tissue and the macromolecular binding within the tissue. PCs can be measured *in vitro* by vial-equilibriation method (*i.e.*, volatile) (Gargas *et al.*, 1989), centrifugal ultrafiltration method (*i.e.*, nonvolatile) (Jepson *et al.*, 1994) or estimated *in vivo* by calculating steady state ratio of tissue to blood concentrations (Kang *et al.*, 1997; U.S. EPA, 2006a). When experimental values are not available, algorithms have been derived to predict tissue:blood PCs (Poulin and Krishnan, 1995; El-Masri and Portier, 1998). This method is very useful at the earlier drug development stage when the *in vivo* experiments have not been conducted. Biochemical parameters, such as metabolic rate constants, can be measured by several methods (Knaak *et al.*, 1995). *In vitro* measurements are accomplished using microsomal protein, hepatocyte cellular cultures, or liver slice and then extrapolated to *in vivo* based on protein content (U.S. EPA, 2006b). When the *in vivo* measurements of parent chemicals and metabolite products in tissue and blood are available, the metabolic parameters may be estimated by PBPK model (Clewell *et al.*, 2000; Fisher, 2000).

Two prediction based methods have been employed to estimate chemical-specific parameters for PBPK models including visual and statistical fitting of the kinetic data. Visual fitting is an iterative process where parameters are estimated by trial and error until the model predictions reasonably fits to the data (usually within 2-factors of the experimental data) and no further adjustments are required. Statistical estimation methodologies, such as maximum

likelihood methods, are generally incorporated into the simulation software (i.e., acslXtreme, Aegis Technologies Group, Inc., Huntsville, AL). Using standard statistical optimization methods can increase the accuracy of the estimation and remove operator bias from the parameter estimation process.

PBPK Modeling of Dicloroacetic Acid (DCA) in Humans

Pharmacology and Toxicology of DCA

DCA is used clinically to treat metabolic disorders such as lactic acidosis and diabetes mellitus due to its ability to reduce circulating glucose, lactate and pyruvate. DCA stimulates the activity of pyruvate dehydrogenase by inhibiting the pyruvate dehydrogenase kinase. Thus, it decreases lactate production by shifting the metabolism of pyruvate from glycolysis towards oxidation in the mitochondria (Stacpoole, 1989). DCA was recently proposed as an anti-cancer treatment (Bonnet *et al.*, 2007) after DCA was found to stimulate apoptosis in cancer cell lines and shrink the human tumors implanted in rats. Adverse effects following years of DCA treatment include mild liver dysfunction, transient central neuropathy, peripheral neuropathy and hypocalcemia (Stacpoole *et al.*, 1998b; U.S.EPA., 2003; Mori *et al.*, 2004). DCA is also an environmental contaminant produced primarily when water is disinfected with chlorine. The reported median concentration of DCA in surface water system is 15 μg/L with maximum concentration of 74 μg/L (Boorman *et al.*, 1999). No cancer incidence has yet to be reported in humans, however the carcinogenicity of DCA in rodents has been proved (U.S. EPA., 2003).

DCA is eliminated by hepatic metabolism with less than 1% excreted in the urine (Stacpoole *et al.*, 1998a). The metabolism of DCA involves oxidative dechlorination to form glyoxylate, which is oxidized further to oxalate and then to carbon dioxide (Tong *et al.*, 1998b; EPA, 2001). Glutathione transferase zeta (GSTzeta) is the only enzyme identified in the

biotransformation of DCA (Tong *et al.*, 1998a; Lim *et al.*, 2004). DCA inhibits its own metabolism through inactivation of GSTzeta by covalent modification of the enzyme (Anderson *et al.*, 2002). In a 5-repeated dosing study (i.e., 50mg/kg IV infusion) at 2-hour intervals, the half-life of DCA after the fifth dose increased 6-fold compared to the half-life after the first dose (6 hour *vs.* 1 hour) (Curry *et al.*, 1991). The half-life of DCA changes following a second DCA administration indicated that it took more than 4 weeks before the half-life returned to the initial value after the first 50mg/kg administration (Curry *et al.*, 1991). Four functional allelic variants of GSTZ 1-1 (GSTZ 1a-1a GSTZ 1d-1d) have been identified in humans. These allelic variants have different metabolic capacities and inhibition characteristics for DCA in *in vitro* studies (Blackburn *et al.*, 2000; Tzeng *et al.*, 2000). GSTzeta (GSTZ1-1) is also known as maleylacetoacetate isomerase (MAAI), an essential enzyme in the phenylalanine/tyrosine catabolism pathway.

Disruption of tyrosine catabolism by competitive inhibition has been proposed as a mechanism of DCA induced toxicity (Ammini *et al.*, 2003; Lantum *et al.*, 2003). The metabolite product of DCA, glyoxylate, which reacts with amino acids and other cellular macromolecules, may also play a role in DCA toxicity (Anderson *et al.*, 2004).

Rodent PBPK Models for DCA

DCA PBPK models for rodents were first published nearly 10 years ago. The first rodent models were developed to track DCA as a metabolite of trichloroethylene (Abbas and Fisher, 1997; Greenberg *et al.*, 1999; Clewell *et al.*, 2000). Barton *et al.* (1999) published a mouse PBPK model for DCA to better understand the hepatic dosimetry of DCA and its carcinogenicity. The latest DCA PBPK model for rodents developed by Keys *et al.* is the first model to incorporate suicide inhibition of GSTzeta by DCA (Keys *et al.*, 2004). In order to

describe the lack of accumulation of DCA in the body after repeated administration, a first-order non-inhibitable pathway was proposed, although this non-GSTzeta mediated pathway has not been proven experimentally. The model then was used to estimate the impact of reduced hepatic metabolism (through suicide inhibition of GSTzeta) on the plasma kinetics of DCA after multiple administrations in mouse and rat.

Modeling Decreased Enzyme Capacity Caused by Suicide Inhibition

When enzyme-mediated biotransformation is the major elimination pathway of a chemical, the change in enzyme activity (the amount of activity enzyme available) over time leads to dose and time dependent alterations in pharmacokinetics. Suicide inhibition is a special circumstance in that enzyme is irreversibly inhibited during this catalysis process. Lilly *et al.*(1998) derived equations to account for different mechanisms of action describing the loss of trans-1,2-dichloroethylene (*t*DCE) metabolizing capacity over time (Lilly *et al.*, 1998) (Table 2.1). The possible mechanisms resulting in suicide inhibition that were reported include: 1) reactive metabolite reacts with enzyme-substance complex; 2) reactive metabolite reacts with total enzyme present; 3) reactive metabolite reacts with free enzyme; 4) bound intermediate inactivates enzyme in a first-order process; and 5) free parent drug (*i.e.*, trichloroethylene) or metabolite formed in a first-order process reacts with bound enzyme. Previous PBPK models describing suicide inhibition have focused on mechanism 1, where Fisher *et al.* (2004) described the inhibition of cytochrome P450 system (CYP 2E1) by carbon tetrachloride, and mechanism 4, where Keys *et al.* (2004) described DCA-mediated inhibition of GSTzeta.

In addition to the chemical-induced reduction of enzyme activity, *in vivo*, the natural recovery of an enzyme (V_{resyn}) is described as:

$$\frac{dV_{resyn}}{dt} = k_s - k_{\deg} \times V_{mt} \qquad (2.1)$$

where k_s is the zero-order synthesis rate constant, k_{deg} is first-order degradation rate constant and V_{mt} is the enzyme activity. In the absence of drug, enzyme synthesis and degradation maintain an equilibrium in which $k_s = k_{deg} \times V_{m(0)}$. $V_{m(0)}$ is initial value of V_{mt} (Anderson *et al.*, 1999). The apparent rate of change for enzyme activity is the sum of $\frac{dV_{resyn}}{dt}$ and $\frac{dV_{mt}}{dt}$.

Interindividual Variability in Human PBPK model

Compared to inbred laboratory animals, humans present significant interindividual variability in chemical disposition. This interindividual variability can be the result of environmental and genetic factors (Clewell and Andersen, 1996). Human PBPK models describe individual kinetic data using subject-specific physiological parameters such as body weight, body fat, blood flow and some other physiological parameters determined by the subject's gender and age (Fisher *et al.*, 1998; Clewell *et al.*, 2004; Bjorkman, 2005). Parameters for key pharmacological processes such as metabolic enzyme activity, urinary excretion activity can be estimated for each subject as well (Nihlen and Johanson, 1999; Sweeney *et al.*, 2004; Merrill *et al.*, 2005). Genetic polymorphisms in metabolic enzymes are a major contributor to interindividual variability in xenobiotic elimination (Haber *et al.*, 2002). PBPK models, in combination with Monte Carlo analysis can be used to incorporate information on polymorphisms, have been developed to analyze the kinetic variability of warfarin and parathion (Gentry *et al.*, 2002b). All the critical issues in application of PBPK model to quantify the impact of interindividual differences as well as human age in xenobiotic dispostion and susceptibity to toxicity were reviewed in a recently report published by U.S. EPA (U.S. EPA, 2006b).

PBPK Modeling of Nucleoside Reverse Transcriptase Inhibitors (NRTIs) in Pregnant Rats

Pharmacology and Toxicology of NRTIs in Pregnancy

Zidovudine (AZT) is the first approved antiretroviral agents used in pregnant women. AZT belongs to the largest class of antiretroviral drugs - nucleoside reverse transcriptase inhibitors (NRTIs). Other NRTIs include: abacavir (ABC), didanosine (ddI), emtricitabine (FTC), lamivudine (3TC), stavudine (d4T), zalcitabine (ddC). NRTIs are pro-drugs as the active forms are the triphosphate anabolites (NRTI-TPs) that are formed intracellularly. The activated NRTI competes with natural deoxynucleotides for incorporation into the viral DNA and inhibiting the viral reverse transcriptase. Unlike the natural deoxynucleotide substrates, NRTIs lack a 3'-hydroxyl group on the deoxyribose moiety. As a result, incorporation of an NRTI blocks the incorporation of the next incoming deoxynucleotide as there is no 5'-3' phosphodiester bond can be formed to extend the DNA chain terminating synthesis of the viral DNA (Peter and Gambertoglio, 1998). Intracellular concentrations of NRTI-TPs are very low, and the anti-HIV activity is dependent upon the concentration ratio of NRTI-TPs and the endogenous nucleotides (Stein and Moore, 2001). Quantitatively, the intracellular metabolism is such a minor pathway that accounts for less then 1% of total dose of AZT is phosphorylated inracellularly (Veal and Back, 1995). The half-life of NRTI-TPs exceeds that of the parent drug in plasma, allowing for once or twice daily dosing of the pro-drug (Sharma *et al.*, 2004). No clinically significant alterations in the pharmacokinetics of NRTIs following oral administration have been identified in pregnant woman compared with non-pregnant adults, consequently no dose adjustments are required during in pregnant women (P.H.G.W.G., 2006). All NRTIs have been shown to cross human placenta (Capparelli *et al.*, 2005). NRTIs-TPs, the active form, have been measured in fetal plasma after maternal administration, thus providing a sound pharmacological basis to

protect the fetus from HIV transmission (Williams *et al.*, 2003). The chief pharmacokinetic information for NRTIs during pregnancy is summarized in Table 2.2 (Sharma *et al.*, 2004; Capparelli *et al.*, 2005; Pacifici, 2005).

Due to rapid development of drug resistance to NRTIs, combination antiretroviral therapies, usually consisting of two NRTIs and a protease inhibitor (PI), are the recommended treatment for HIV-1-infected adults who are not pregnant (CDC, 2006). In pregnant women, combination therapies have been shown to successfully reduce the risk of mother-to-child transmission to less than 2% (Mandelbrot *et al.*, 2001; Cooper *et al.*, 2002). The potential drug-drug interactions among these antiretroviral agents not only affect treatment efficiency, but also the toxicity to mother and fetus. Unfortunately, little information is available on the drug-drug interactions in pregnant women or the neonate. *In vivo* study conducted in the pregnant pigtailed macaque showed that AZT did not affect transplacental transfer or systemic clearance of ddC, ddI and d4T (Pereira *et al.*, 1995; Odinecs *et al.*, 1996; Tuntland *et al.*, 1996). No maternal pharmacokinetic interactions were identified in pregnant women treated with AZT/3TC (Moodley *et al.*, 1998). However, co-administration of AZT/3TC and AZT/ABC and AZT/acyclovir (ACV) in pregnant rats showed substantial drug-drug interactions in both maternal and fetal drug disposition (Brown *et al.*, 2003; Lewis, 2006). The failure of identifying ineractions in human might be partly due to large inter-individual differences. The drug-drug interactions among antiviral agents in non-pregnant adults have been reviewed by Barry *et al.* (1999) and the potential interactions between NRTIs are summarized in Table 2.3.

The adverse effects of NRTIs are related to defective mitochondrial DNA replication secondary to the NRTI-induced inhibition of the mitochondrial DNA polymerase gamma (Kakuda, 2000). Long-term treatment with NRTIs gives rise to toxicity in a broad spectrum of

tissues, including hematologic disorders, myopathy, cardiotoxic effects, peripheral neuropathies, and hepatotoxic effects (Squires, 2001). Mitochondrial dysfunction related toxicities have been observed in pregnant and their new born babies (Blanche *et al.*, 2006; Venhoff and Walker, 2006). For example, pregnant women receiving NRTI treatment showed a significant decrease in mtDNA copies per cell in placenta and cord blood (Shiramizu *et al.*, 2003). Asymptomatic hyperlactatemia and severe neurological symptoms caused by persistent mitochondrial dysfunction were identified in children after *in utero* exposure to either AZT/3TC or AZT alone (Blanche *et al.*, 1999; Benhammou *et al.*, 2007). The potency of NRTIs-induced mitochondrial compromise in infant monkeys after *in utero* exposure was reported as: d4T/3TC > AZT/ddI > AZT/3TC > 3TC (Divi *et al.*, 2007). ddT and d4T co-administration is not recommended due to an increased risk of fetal lactic acidosis. Carcinogenicity of NRTIs has only been shown after long term high dose exposure (~ 2 to 3 orders of magnitude higher than therapeutic doses) (Briggs, 2005).

Placental Transporters for NRTIs

The placental transfer of NRTIs directly affects fetal exposure to the drug and also affects the efficacy of treatment and toxicity in the fetus. ddI, d4T, AZT, 3TC, ddC and ABC were shown to cross the placenta by passive diffusion using placenta perfusion and *in vivo* animal models (Capparelli *et al.*, 2005).However, the estimated AZT placental clearance from the fetus to the mother was found to be larger than in the opposite direction in pregnant baboons (Garland *et al.*, 1998). Substantial alterations in placental transfer and fetal exposure of NRTIs have been shown in pregnant rats (Brown *et al.*, 2003; Lewis, 2006). If passive diffusion is the only mechanism in placental transfer of NRTIs, the placental transfer rate should be equal in both the fetal and maternal directions for single NRTI and no alterations should be observed when two

NRTIs are administered together. Meanwhile, multiple NRTI transporters have been identified in rat and human placenta (Ganapathy *et al.*, 2000; Leazer and Klaassen, 2003; Unadkat *et al.*, 2004). NRTI transporters include nucleoside transporters (ENTs and CNTs), organic anion transporters (OAT), organic cation transporters (OCTs), multidrug resistance proteins (MRPs), and breast cancer resistance proteins (BCRPs) (Table 2.4). These transporters are located on the apical and basal side of placenta and can either transport the substance along or against the concentration gradient. Therefore, based on the *in vitro* transporter study and *in vivo* kinetic information, transporter-mediated transfer of NRTIs across the placenta can not be excluded.

PBPK Models for Perinatal Pharmacokinetics

PBPK models have been developed to study maternal and embryonic/fetal disposition of drugs such as methadone (Gabrielsson *et al.*, 1985), morphine (Gabrielsson and Paalzow, 1983) and vitamin A acid (Clewell *et al.*, 1997) and other chemicals such as trichloroethylene and perchlorate (Fisher *et al.*, 1989; Clewell *et al.*, 2003). Changes in body weight, tissue volumes and blood flows are well documented for both maternal and fetal tissues during pregnancy (Oflaherty *et al.*, 1992; Gentry *et al.*, 2002a). Several alternative structures have been described previously for PBPK pregnancy models and are shown in Fig. 2.4. Passive diffusion has been the primary description for placental transfer of chemicals (Gabrielsson and Paalzow, 1983). Terry *et al.* (1995) devised several model structures based on theoretical mechanisms for the perinatal transfer of methoxyacetic acid (2-MAA). PH- trapping of ionized 2-MAA assumed distribution of the weak acid to the tissue compartments was solely dependent upon the pH gradient. For a weak acid like 2-MAA, at physiology pH (7.4), the majority of the drug is ionized, while only un-ionized free drug can cross the tissue membrane. One drawback of pH trapping model is the tissue pH was estimated by fitting the model to the observed kinetic data of the interested

chemical. The active transport model structure assumed the distribution clearance between the placental and fetal compartment differed between influx and efflux. The active transport model structure provided the best fit to the experimental data, even though the mechanism of transport remains unknown. The reversible binding model structure was based on the assumption that 2-MAA significantly binds to macromolecules within tissue compartments, and only free drug is avialabe to transfer between compartments.

PBPK Models for Drug-Drug Interactions

Several approaches have been used to describe drug-drug interactions in PBPK models. Kang (1997) included altered partitioning to account for increased exposure of ddI in pancreas and muscle when pentamidine was co-administered. Alteration in the metabolism of one drug can result from co-administration of other drugs metabolized by the same enzyme. For example, PBPK models were developed to describe the competitive inhibition of CYP3A4-mediated metabolism of co-administered PIs, simvastatin and itraconazole (Ishigam *et al.*, 2001; Shibata *et al.*, 2002). Drug-drug interactions with transporters are often described as competitive, uncompetitive or noncompetitive inhibition in empirical models (Bhattacharya and Boje, 2006). However, there are few PBPK models published investigating interactions of transporters. A PBPK model was developed for the P-glycoprotein knockout mouse (mdr 1a -/-) to simulate digoxin pharmacokinetics similar to the inhibition of P-glycoprotein.

References

Abbas, R., and Fisher, J. W. (1997). A physiologically based pharmacokinetic model for trichloroethylene and its metabolites, chloral hydrate, trichloroacetate, dichloroacetate, trichloroethanol, and trichloroethanol glucuronide in B6C3F1 mice. *Toxicology and Applied Pharmacology* **147**, 15-30.

Ammini, C. V., Fernandez-Canon, J., Shroads, A. L., Cornett, R., Cheung, J., James, M. O., Henderson, G. N., Grompe, M., and Stacpoole, P. W. (2003). Pharmacologic or genetic ablation of maleylacetoacetate isomerase increases levels of toxic tyrosine catabolites in rodents. *Biochemical Pharmacology* **66**, 2029-2038.

Andersen, M. E., Birnbaum, L. S., Barton, H. A., and Eklund, C. R. (1997). Regional hepatic CYP1A1 and CYP1A2 induction with 2,3,7,8-tetrachlorodibenzo-p-dioxin evaluated with a multicompartment geometric model of hepatic zonation. *Toxicology and Applied Pharmacology* **144**, 145-155.

Andersen, M. E., Clewell, H. J., Gargas, M. L., Smith, F. A., and Reitz, R. H. (1987). Physiologically based pharmacokinetics and the risk assessment process for methylene-chloride. *Toxicology and Applied Pharmacology* **87**, 185-205.

Andersen, M. E., Sarangapani, R., Reitz, R. H., Gallavan, R. H., Dobrev, I. D., and Plotzke, K. P. (2001). Physiological modeling reveals novel pharmacokinetic behavior for inhaled octamethylcyclotetrasiloxane in rats. *Toxicological Sciences* **60**, 214-231.

Anderson, W. B., Board, P. G., and Anders, M. W. (2004). Glutathione transferase zeta-catalyzed bioactivation of dichloroacetic acid: Reaction of glyoxylate with amino acid nucleophiles. *Chemical Research in Toxicology* **17**, 650-662.

Anderson, W. B., Liebler, D. C., Board, P. G., and Anders, M. W. (2002). Mass spectral characterization of dichloroacetic acid-modified human glutathione transferase zeta. *Chemical Research in Toxicology* **15**, 1387-1397.

Benhammou, V., Tardieu, M., Warszawski, J., Rustin, P., and Blanche, S. (2007). Clinical mitochondrial dysfunction in uninfected children born to HIV-infected mothers following

perinatal exposure to nucleoside analogues. *Environmental and Molecular Mutagenesis* **48**, 173-178.

Bhattacharya, I., and Boje, K. M. K. (2006). Potential gamma-hydroxybutyric acid (GHB) drug interactions through blood-brain barrier transport inhibition: A pharmacokinetic simulation-based evaluation. *Journal of Pharmacokinetics and Pharmacodynamics* **33**, 657-681.

Bjorkman, S. (2005). Prediction of drug disposition in infants and children by means of physiologically based pharmacokinetic (PBPK) modelling: theophylline and midazolam as model drugs. *British Journal of Clinical Pharmacology* **59**, 691-704.

Blackburn, A. C., Tzeng, H. F., Anders, M. W., and Board, P. G. (2000). Discovery of a functional polymorphism in human glutathione transferase zeta by expressed sequence tag database analysis. *Pharmacogenetics* **10**, 49-57.

Blakey, G. E., Nestorov, I. A., Arundel, P. A., Aarons, L. J., and Rowland, M. (1997). Quantitative structure-pharmacokinetics relationships: I. Development of a whole-body physiologically based model to characterize changes in pharmacokinetics across a homologous series of barbiturates in the rat. *Journal of Pharmacokinetics and Biopharmaceutics* **25**, 277-312.

Blanche, S., Tardieu, M., Benhammou, V., Warszawski, J., and Rustin, P. (2006). Mitochondrial dysfunction following perinatal exposure to nucleoside analogues. *Aids* **20**, 1685-1690.

Blanche, S., Tardieu, M., Rustin, P., Slama, A., Barret, B., Firtion, G., Ciraru-Vigneron, N., Lacroix, C., Rouzioux, C., Mandelbrot, L., Desguerre, I., Rotig, A., Mayaux, M. J., and Delfraissy, J. F. (1999). Persistent mitochondrial dysfunction and perinatal exposure to antiretroviral nucleoside analogues. *Lancet* **354**, 1084-1089.

Blesch, K. S., Gieschke, R., Tsukamoto, Y., Reigner, B. G., Burger, H. U., and Steimer, J. L. (2003). Clinical pharmacokinetic/pharmacodynamic and physiologically based pharmacokinetic modeling in new drug development: The capecitabine experience. *Investigational New Drugs* **21**, 195-223.

Bonnet, S., Archer, S. L., Allalunis-Turner, J., Haromy, A., Beaulieu, C., Thompson, R., Lee, C. T., Lopaschuk, G. D., Puttagunta, L., Bonnet, S., Harry, G., Hashimoto, K., Porter, C. J., Andrade, M. A., Thebaud, B., and Michelakis, E. D. (2007). A mitochondria-K+ channel axis is suppressed in cancer and its normalization promotes apoptosis and inhibits cancer growth. *Cancer Cell* **11**, 37-51.

Boorman, G. A., Dellarco, V., Dunnick, J. K., Chapin, R. E., Hunter, S., Hauchman, F., Gardner, H., Cox, M., and Sills, R. C. (1999). Drinking water disinfection byproducts: Review and approach to toxicity evaluation. *Environmental Health Perspectives* **107**, 207-217.

Briggs, G. G. (2005). *Drugs In Pregnancy And Lactation*. Lippincott Williams & Wilkins.

Brightman, F. A., Leahy, D. E., Searle, G. E., and Thomas, S. (2006). Application of a generic physiologically based pharmacokinetic model to the estimation of xenobiotic levels in rat plasma. *Drug Metabolism and Disposition* **34**, 84-93.

Brown, S. D., Bartlett, M. G., and White, C. A. (2003). Pharmacokinetics of intravenous acyclovir, zidovudine, and acyclovir-zidovudine in pregnant rats. *Antimicrobial Agents and Chemotherapy* **47**, 991-996.

Campbell, J. L., and Fisher, J. W. (2007). A PBPK Modeling assessment of the competitive metabolic interactions of JP-8 vapor with two constituents, m-xylene and ethylbenzene. *Inhalation Toxicology* **19**, 265-273.

Capparelli, E., Rakhmanina, N., and Mirochnickc, M. (2005). Pharmacotherapy of perinatal HIV. *Seminars in Fetal & Neonatal Medicine* **10**, 161-175.

CDC (2006). Guidlines for the Use of Antiretroviral Agents in HIV-1-Infected Adults and Adolescents. the DHHS Panel on Antiretroviral Guidelines for Adults and Adolescents - A Working Group of the Office of AIDS Research Advisory Concil.

Clewell, H. J. (1993). Coupling of computer modeling with invitro methodologies to reduce animal usage in toxicity testing. *Toxicology Letters* **68**, 101-117.

Clewell, H. J., and Andersen, M. E. (1996). Use of physiologically based pharmacokinetic modeling to investigate individual versus population risk. *Toxicology* **111**, 315-329.

Clewell, H. J., Andersen, M. E., Wills, R. J., and Latriano, L. (1997). A physiologically based pharmacokinetic model for retinoic acid and its metabolites. *Journal of the American Academy of Dermatology* **36**, S77-S85.

Clewell, H. J., Gentry, P. R., Covington, T. R., and Gearhart, J. M. (2000). Development of a physiologically based pharmacokinetic model of trichloroethylene and its metabolites for use in risk assessment. *Environmental Health Perspectives* **108**, 283-305.

Clewell, H. J., Gentry, P. R., Covington, T. R., Sarangapani, R., and Teeguarden, J. G. (2004). Evaluation of the potential impact of age- and gender-specific pharmacokinetic differences on tissue dosimetry. *Toxicological Sciences* **79**, 381-393.

Clewell, H. J., Gentry, P. R., Kester, J. E., and Andersen, M. E. (2005). Evaluation of physiologically based pharmacokinetic models in risk assessment: An example with perchloroethylene. *Critical Reviews in Toxicology* **35**, 413-433.

Clewell, R. A., Merrill, E. A., Yu, K. O., Mahle, D. A., Sterner, T. R., Mattie, D. R., Robinson, P. J., Fishert, J. W., and Gearhart, J. M. (2003). Predicting fetal perchlorate dose and

inhibition of iodide kinetics during gestation: A physiologically-based pharmacokinetic analysis of perchlorate and iodide kinetics in the rat. *Toxicological Sciences* **73**, 235-255.

Cooper, E. R., Charurat, M., Mofenson, L., Hanson, I. C., Pitt, J., Diaz, C., Hayani, K., Handelsman, E., Smeriglio, V., Hoff, R., and Blattner, W. (2002). Combination antiretroviral strategies for the treatment of pregnant HIV-1-infected women and prevention of perinatal HIV-1 transmission. *Journal of Acquired Immune Deficiency Syndromes* **29**, 484-494.

Corley, R. A., Bartels, M. J., Carney, E. W., Weitz, K. K., Soelberg, J. J., Gies, R. A., and Thrall, K. D. (2005). Development of a physiologically based pharmacokinetic model for ethylene glycol and its metabolite, glycolic acid, in rats and humans. *Toxicological Sciences* **85**, 476-490.

Covington, T. R., Gentry, P. R., Van Landingham, C. B., Andersen, M. E., Kester, J. E., and Clewell, H. J. (2007). The use of Markov chain Monte Carlo uncertainty analysis to support a Public Health Goal for perchloroethylene. *Regulatory Toxicology and Pharmacology* **47**, 1-18.

Curry, S. H., Lorenz, A., Chu, P. I., Limacher, M., and Stacpoole, P. W. (1991). Disposition and Pharmacodynamics of Dichloroacetate (Dca) and Oxalate Following Oral Dca Doses. *Biopharmaceutics & Drug Disposition* **12**, 375-390.

Divi, R. L., Leonard, S. L., Kuo, M. M., Nagashima, K., Thamire, C., St Claire, M. C., Wade, N. A., Walker, V. E., and Poirier, M. C. (2007). Transplacentally exposed human and monkey newborn infants show similar evidence of nucleoside reverse transcriptase inhibitor-induced mitochondrial toxicity. *Environmental and Molecular Mutagenesis* **48**, 201-209.

El-Masri, H. A., and Portier, C. J. (1998). Physiologically based pharmacokinetics model of primidone and its metabolites phenobarbital and phenylethylmalonamide in humans, rats, and mice. *Drug Metabolism and Disposition* **26**, 585-594.

Fiserovabergerova, V. (1992). Inhalation anesthesia using physiologically based pharmacokinetic models. *Drug Metabolism Reviews* **24**, 531-557.

Fisher, J. W., Whittaker, T. A., Taylor, D. H., Clewell, H. J., and Andersen, M. E. (1989). Physiologically based pharmacokinetic modeling of the pregnant rat - a multiroute exposure model for trichloroethylene and its metabolite, trichloroacetic-acid. *Toxicology and Applied Pharmacology* **99**, 395-414.

Fisher, J. W. (2000). Physiologically based pharmacokinetic models for trichloroethylene and its oxidative metabolites. *Environmental Health Perspectives* **108**, 265-273.

Fisher, J., Lumpkin, M., Boyd, J., Mahle, D., Bruckner, J., and El-Masri, H. A. (2004). PBPK modeling of the metabolic interactions of carbon tetrachloride and tetrachloroethylene in B6C3F1 mice. *Environmental Toxicology and Pharmacology* **16**, 93-105.

Fisher, J. W., Mahle, D. A., and Abbas, R. (1998). A Human Physiological Based Pharmacokinetic Model for trichloroethylene and Its Matabolites, Trichloroacetic Acid and Free Trichloroethanol. *Toxicology and Applied Pharmacology* **152**, 339-359.

Gabrielsson, J. L., Johansson, P., Bondesson, U., and Paalzow, L. K. (1985). Analysis of methadone disposition in the pregnant rat by means of a physiological flow model. *Journal of Pharmacokinetics and Biopharmaceutics* **13**, 355-372.

Gabrielsson, J. L., and Paalzow, L. K. (1983). A physiological pharmacokinetic model for morphine disposition in the pregnant rat. *Journal of Pharmacokinetics and Biopharmaceutics* **11**, 147-163.

Ganapathy, V., Prasad, P. D., Ganapathy, M. E., and Leibach, F. H. (2000). Placental transporters relevant to drug distribution across the maternal-fetal interface. *Journal of Pharmacology and Experimental Therapeutics* **294**, 413-420.

Gargas, M. L., Burgess, R. J., Voisard, D. E., Cason, G. H., and Andersen, M. E. (1989). Partition-coefficients of low-molecular-weight volatile chemicals in various liquids and tissues. *Toxicology and Applied Pharmacology* **98**, 87-99.

Garland, M., Szeto, H. H., Daniel, S. S., Tropper, P. J., Myers, M. M., and Stark, R. I. (1998). Placental transfer and fetal metabolism of zidovudine in the baboon. *Pediatric Research* **44**, 47-53.

Gentry, P. R., Covington, T. R., Andersen, M. E., and Clewell, H. J. (2002a). Application of a physiologically based pharmacokinetic model for isopropanol in the derivation of a reference dose and reference concentration. *Regulatory Toxicology and Pharmacology* **36**, 51-68.

Gentry, P. R., Hack, C. E., Haber, L., Maier, A., and Clewell, H. J. (2002b). An approach for the quantitative consideration of genetic polymorphism data in chemical risk assessment: Examples with warfarin and parathion. *Toxicological Sciences* **70**, 120-139.

Greenberg, M. S., Burton, G. A., and Fisher, J. W. (1999). Physiologically based pharmacokinetic modeling of inhaled trichloroethylene and its oxidative metabolites in B6C3F(1) mice. *Toxicology and Applied Pharmacology* **154**, 264-278.

Haber, L. T., Maier, A., Gentry, P. R., Clewell, H. J., and Dourson, M. L. (2002). Genetic Polymorphisms in assessing interindividual variability in delivered dose. *Regulatory Toxicology and Pharmacology* **35**, 177-197.

Hack, C. E. (2006). Bayesian analysis of physiologically based toxicokinetic and toxicodynamic models. *Toxicology* **221**, 241-248.

Hong, M., Schlichter, L., and Bendayan, R. (2001). A novel zidovudine uptake system in microglia. *Journal of Pharmacology and Experimental Therapeutics* **296**, 141-149.

Ishigam, M., Uchiyama, M., Kondo, T., Iwabuchi, H., Inoue, S., Takasaki, W., Ikeda, T., Komai, T., Ito, K., and Sugiyama, Y. (2001). Inhibition of in vitro metabolism of simvastatin by itraconazole in humans and prediction of in vivo drug-drug interactions. *Pharmaceutical Research* **18**, 622-631.

Jepson, G. W., Hoover, D. K., Black, R. K., McCafferty, J. D., Mahle, D. A., and Gearhart, J. M. (1994). A partition-coefficient determination method for nonvolatile chemicals in biological tissues. *Fundamental and Applied Toxicology* **22**, 519-524.

Jia, M. H., Coats, B., Chadha, M., Frentzen, B., Perez-Rodriguez, J., Chadik, P. A., Yost, R. A., Henderson, G. N., and Stacpoole, P. W. (2006). Human kinetics of orally and intravenously administered low-dose 1,2-C-13-dichloro acetate. *Journal of Clinical Pharmacology* **46**, 1449-1459.

Kang, H. J. K., Wientjes, M. G., and Au, J. L. S. (1997). Physiologically based pharmacokinetic models of 2',3'-dideoxyinosine. *Pharmaceutical Research* **14**, 337-344.

Kawai, R., Mathew, D., Tanaka, C., and Rowland, M. (1998). Physiologically based pharmacokinetics of Cyclosporine A: Extension to tissue distribution kinetics in rats and scale-up to human. *Journal of Pharmacology and Experimental Therapeutics* **287**, 457-468.

Keys, D. A., Schultz, I. R., Mahle, D. A., and Fisher, J. W. (2004). A quantitative description of suicide inhibition of dichloroacetic acid in rats and mice. *Toxicological Sciences* **82**, 381-393.

Keys, D. A., Wallace, D. G., Kepler, T. B., and Conolly, R. B. (2000). Quantitative evaluation of alternative mechanisms of blood disposition of di(n-butyl) phthalate and mono(n-butyl) phthalate in rats. *Toxicological Sciences* **53**, 173-184.

Knaak, J. B., Albayati, M. A., and Raabe, O. G. (1995). Development of partition-coefficients, v-max and k-m values, and allometric relationships. *Toxicology Letters* **79**, 87-98.

Kong, W., Engel, K., and Wang, J. (2004). Mammalian nucleoside transporters. *Current Drug Metabolism* **5**, 63-84.

Lantum, H. B. M., Cornejo, J., Pierce, R. H., and Anders, M. W. (2003). Perturbation of maleylacetoacetic acid metabolism in rats with dichloroacetic acid-induced glutathione transferase zeta deficiency. *Toxicological Sciences* **74**, 192-202.

Leazer, T. M., and Klaassen, C. D. (2003). The presence of xenobiotic transporters in rat placenta. *Drug Metabolism and Disposition* **31**, 153-167.

Leung, S., and Bendayan, R. (2001). Uptake properties of lamivudine (3TC) by a continuous renal epithelial cell line. *Canadian Journal of Physiology and Pharmacology* **79**, 59-66.

Lewis, S. R. (2006). Maternal and fetal disposition of antiviral agents in the pregnent rats. In *College of Pharamcy*. University of Georgia, Athens.

Lilly, P. D., Thornton-Manning, J. R., Gargas, M. L., Clewell, H. J., and Andersen, M. E. (1998). Kinetic characterization of CYP2E1 inhibition in vivo and in vitro by the chloroethylenes. *Archives of Toxicology* **72**, 609-621.

Lim, C. E. L., Matthaei, K. I., Blackburn, A. C., Davis, R. P., Dahlstrom, J. E., Koina, M. E., Anders, M. W., and Board, P. G. (2004). Mice deficient in glutathione transferase zeta/maleylacetoacetate isomerase exhibit a range of pathological changes and elevated expression of Alpha, Mu, and Pi class glutathione transferases. *American Journal of Pathology* **165**, 679-693.

Mandelbrot, L., Landreau-Mascaro, A., Rekacewicz, C., Berrebi, A., Benifla, J. L., Burgard, M., Lachassine, E., Barret, B., Chaix, M. L., Bongain, A., Ciraru-Vigneron, N., Crenn-Hebert, C., Delfraissy, J. F., Rouzioux, C., Mayaux, M. J., and Blanche, S. (2001). Lamivudine-zidovudine combination for prevention of maternal-infant transmission of HIV-1. *Jama-Journal of the American Medical Association* **285**, 2083-2093.

Merrill, E. A., Clewell, R. A., Robinson, P. J., Jarabek, A. M., Gearhart, J. M., Sterner, T. R., and Fisher, J. W. (2005). PBPK model for radioactive iodide and perchlorate kinetics and perchlorate-induced inhibition of iodide uptake in humans. *Toxicological Sciences* **83**, 25-43.

Moodley, J., Moodley, D., Pillay, K., Coovadia, H., Saba, J., van Leeuwen, R., Goodwin, C., Harrigan, P. R., Moore, K. H. P., Stone, C., Plumb, R., and Johnson, M. A. (1998). Pharmacokinetics and antiretroviral activity of lamivudine alone or when coadministered with zidovudine in human immunodeficiency virus type 1-infected pregnant women and their offspring. *Journal of Infectious Diseases* **178**, 1327-1333.

Mori, M., Yamagata, T., Goto, T., Saito, S., and Momoi, M. Y. (2004). Dichloroacetate treatment for mitochondrial cytopathy: long-term effects in MELAS. *Brain & Development* **26**, 453-458.

Morita, N., Kusuhara, H., Sekine, T., Endou, H., and Sugiyama, Y. (2001). Functional characterization of rat organic anion transporter 2 in LLC-PK1 cells. *Journal of Pharmacology and Experimental Therapeutics* **298**, 1179-1184.

Nagata, O., Murata, M., Kato, H., Terasaki, T., Sato, H., and Tsuji, A. (1990). Physiological pharmacokinetics of a new muscle-relaxant, inaperisone, combined with its pharmacological effect on blood-flow rate. *Drug Metabolism and Disposition* **18**, 902-910.

Nestorov, I. (2001). Modelling and simulation of variability and uncertainty in toxicokinetics and pharmacokinetics. *Toxicology Letters* **120**, 411-420.

Nestorov, I. (2003). Whole body pharmacokinetic models. *Clinical Pharmacokinetics* **42**, 883-908.

Nihlen, A., and Johanson, G. (1999). Physiologically based toxicokinetic modeling of inhaled ethyl tertiary-butyl ether in humans. *Toxicological Sciences* **51**, 184-194.

Odinecs, A., Nosbisch, C., and Unadkat, J. D. (1996). Zidovudine does not affect transplacental transfer or systemic clearance of stavudine (2',3'-didehydro-3'-deoxythymidine) in the pigtailed macaque (Macaca nemestrina). *Antimicrobial Agents and Chemotherapy* **40**, 1569-1571.

Oflaherty, E. J., Scott, W., Schreiner, C., and Beliles, R. P. (1992). A physiologically based kinetic-model of rat and mouse gestation - disposition of a weak acid. *Toxicology and Applied Pharmacology* **112**, 245-256.

Pastor-Anglada, M., Cano-Soldado, P., Molina-Arcas, M., Lostao, M. P., Larrayoz, I., Martinez-Picado, J., and Casado, E. J. (2005). Cell entry and export of nucleoside analogues. *Virus Research* **107**, 151-164.

Pereira, C. M., Nosbisch, C., Baughman, W. L., and Unadkat, J. D. (1995). Effect of Zidovudine on Transplacental Pharmacokinetics of Ddi in the Pigtailed Macaque (Macaca-Nemestrina). *Antimicrobial Agents and Chemotherapy* **39**, 343-345.

Perinatal HIV Guidlines Working Group (P. H. G. W.). (2006). Public Health Service Task Force Recommendations for Use of Antiretroviral Drugs in Pregnant HIV-1-Infected Womean for Maternal Health and Interventions to Reduce Perinatal HIV-1 Transmission in the United States. In *AIDSinfo*.

Peter, K., and Gambertoglio, J. G. (1998). Intracellular phosphorylation of zidovudine (ZDV) and other nucleoside reverse transcriptase inhibitors (RTI) used for Human Immunodeficiency Virus (HIV) infection. *Pharmaceutical Research* **15**, 819-825.

Poulin, P., and Krishnan, K. (1995). An Algorithm for Predicting Tissue-Blood Partition-Coefficients of Organic-Chemicals from N-Octanol-Water Partition-Coefficient Data. *Journal of Toxicology and Environmental Health* **46**, 117-129.

Poulin, P., and Theil, F. P. (2002). Prediction of pharmacokinetics prior to in vivo studies. 1. Mechanism-based prediction of volume of distribution. *Journal of Pharmaceutical Sciences* **91**, 129-156.

Reddy, M. B., Yang, R. S. H., Clewell, H. J., and Andersen, M. E. (2005). Dermal Exposure Models. In *Physiologically Based Pharmacokinetic Modeling*.

Reid, G., Wielinga, P., Zelcer, N., De Haas, M., Van Deemter, L., Wijnholds, J., Balzarini, J., and Borst, P. (2003). Characterization of the transport of nucleoside analog drugs by the human multidrug resistance proteins MRP4 and MRP5. *Molecular Pharmacology* **63**, 1094-1103.

Sarangapani, R., Teeguarden, J., Plotzke, K. P., McKim, J. M., and Andersen, M. E. (2002a). Dose-response modeling of cytochrome P450 induction in rats by octamethylcyclotetrasiloxane. *Toxicological Sciences* **67**, 159-172.

Sarangapani, R., Teeguarden, J. G., Cruzan, G., Clewell, H. J., and Andersen, M. E. (2002b). Physiologically based pharmacokinetic modeling of styrene and styrene oxide respiratory-tract dosimetry in rodents and humans. *Inhalation Toxicology* **14**, 789-834.

Schuetz, J. D., Connelly, M. C., Sun, D. X., Paibir, S. G., Flynn, P. M., Srinivas, R. V., Kumar, A., and Fridland, A. (1999). MRP4: A previously unidentified factor in resistance to nucleoside-based antiviral drugs. *Nature Medicine* **5**, 1048-1051.

Sharma, P. L., Nurpeisov, V., Hernandez-Santiago, B., Beltran, T., and Schinazi, R. F. (2004). Nucleoside inhibitors of human immunodeficiency virus type 1 reverse transcriptase. *Current Topics in Medicinal Chemistry* **4**, 895-919.

Shibata, N., Gao, W., Okamoto, H., Kishida, T., Iwasaki, K., Yoshikawa, Y., and Takada, K. (2002). Drug interactions between HIV protease inhibitors based on physiologically-based pharmacokinetic model. *Journal of Pharmaceutical Sciences* **91**, 680-689.

Shiramizu, B., Shikuma, K. M., Kamemoto, L., Gerschenson, M., Erdem, G., Pinti, M., Cossarizza, T., and Shikuma, C. (2003). Placenta and cord blood mitochondrial DNA toxicity in HIV-infected women receiving nucleoside reverse transcriptase inhibitors during pregnancy. *Jaids-Journal of Acquired Immune Deficiency Syndromes* **32**, 370-374.

Squires, K. E. (2001). An introduction to nucleoside and nucleotide analogues. *Antiviral Therapy* **6**, 1-14.

Stacpoole, P. W. (1989). The Pharmacology of Dichloroacetate. *Metabolism-Clinical and Experimental* **38**, 1124-1144.

Stacpoole, P. W., Henderson, G. N., Yan, Z. M., Cornett, R., and James, M. O. (1998a). Pharmacokinetics, metabolism, and toxicology of dichloroacetate. *Drug Metabolism Reviews* **30**, 499-539.

Stacpoole, P. W., Henderson, G. N., Yan, Z. M., and James, M. O. (1998b). Clinical pharmacology and toxicology of dichloroacetate. *Environmental Health Perspectives* **106**, 989-994.

Stein, D. S., and Moore, K. H. P. (2001). Phosphorylation of nucleoside analog antiretrovirals: A review for clinicians. *Pharmacotherapy* **21**, 11-34.

Sweeney, L. M., Kirman, C. R., Morgott, D. A., and Gargas, M. L. (2004). Estimation of interindividual variation in oxidative metabolism of dichloromethane in human volunteers. *Toxicology Letters* **154**, 201-216.

Takeda, M., Khamdang, S., Narikawa, S., Kimura, H., Kobayashi, Y., Yamamoto, T., Cha, S. H., Sekine, T., and Endou, H. (2002). Human organic anion transporters and human organic cation transporters mediate renal antiviral transport. *Journal of Pharmacology and Experimental Therapeutics* **300**, 918-924.

Takubo, T., Kato, T., Kinami, J., Hanada, K., and Ogata, H. (2002). Uptake of lamivudine by rat renal brush border membrane vesicles. *Journal of Pharmacy and Pharmacology* **54**, 111-117.

Tanaka, C., Kawai, R., and Rowland, M. (1999). Physiologically based pharmacokinetics of cyclosporine A: Reevaluation of dose-nonlinear kinetics in rats. *Journal of Pharmacokinetics and Biopharmaceutics* **27**, 597-623.

Tong, Z., Board, P. G., and Anders, M. W. (1998a). Glutathione transferase zeta-catalyzed biotransformation of dichloroacetic acid and other alpha-haloacids. *Chemical Research in Toxicology* **11**, 1332-1338.

Tong, Z., Board, P. G., and Anders, M. W. (1998b). Glutathione transferase Zeta catalyses the oxygenation of the carcinogen dichloroacetic acid to glyoxylic acid. *Biochemical Journal* **331**, 371-374.

Tuntland, T., Nosbisch, C., Baughman, W. L., Massarella, J., and Unadkat, J. D. (1996). Mechanism and rate of placental transfer of zalcitabine (2',3'-dideoxycytidine) in Macaca nemestrina. *American Journal of Obstetrics and Gynecology* **174**, 856-863.

Tzeng, H. F., Blackburn, A. C., Board, P. G., and Anders, M. W. (2000). Polymorphism- and species-dependent inactivation of glutathione transferase zeta by dichloroacetate. *Chemical Research in Toxicology* **13**, 231-236.

Unadkat, J. D., Dahlin, A., and Vijay, S. (2004). Placental drug transporters. *Current Drug Metabolism* **5**, 125-131.

U. S. EPA (2001). Stage 2 Occurrence Assessment for Disfectants and Disinfection Byproducts (*D/DBPs*). *Washington, DC, US Enviromental Protection Agency.*

U. S. EPA (2003). Toxicological Review of Dichloroacetic Acid. *U.S. Envirometnal Protection Agency, Washington, DC*.

U. S. EPA (2006a). Approaches for the Application of Physiologically Based Pharmacokinetic (PBPK) Models and Supporting Data in Risk Assessment. *U.S. Envirometnal Protection Agency, Washington, DC*.

U.S.EPA (2006b). Use of Physiologically Based Pharmacokientic Modles to Quantify the Impact of Human Age and Interinvididual Differences in Pgysiology and Biochemistry Pertinent to Risk-Final Report. *U.S. Envirometnal Protection Agen, Washington, DC*.

Veal, G. J., and Back, D. J. (1995). Metabolism of zidovudine. *General Pharmacology* **26**, 1469-1475.

Venhoff, N., and Walker, U. A. (2006). Mitochondrial disease in the offspring as a result of antiretroviral therapy. *Expert Opinion on Drug Safety* **5**, 373-381.

Wada, S., Tsuda, M., Sekine, T., Cha, S. H., Kimura, M., Kanai, Y., and Endou, H. (2000). Rat multispecific organic anion transporter 1 (rOAT1) transports zidovudine, acyclovir, and other antiviral nucleoside analogs. *Journal of Pharmacology and Experimental Therapeutics* **294**, 844-849.

Wang, J., and Giacomini, K. M. (1997). Molecular determinants of substrate selectivity in Na+-dependent nucleoside transporters. *Journal of Biological Chemistry* **272**, 28845-28848.

Wang, X., Nitanda, T., Shi, M. Y., Okamoto, M., Furukawa, T., Sugimoto, Y., Akiyama, S., and Baba, M. (2004). Induction of cellular resistance to nucleoside reverse transcriptase inhibitors by the wild-type breast cancer resistance protein. *Biochemical Pharmacology* **68**, 1363-1370.

Weiss, J., Theile, D., Ketabi-Kiyanvash, N., Lindenmaier, H., and Haefeli, W. E. (2007). Inhibition of MRP1/ABCC1, MRP2/ABCC2, and MRP3/ABCC3 by nucleoside, nucleotide, and non-nucleoside reverse transcriptase inhibitors. *Drug Metabolism and Disposition* **35**, 340-344.

Williams, L. D., Von Tungeln, L. S., Beland, F. A., and Doerge, D. R. (2003). Liquid chromatographic-mass spectrometric determination of the metabolism and disposition of

the anti-retroviral nucleoside analogs zidovudine and lamivudine in C57BL/6N and B6C3F1 mice. *Journal of Chromatography B-Analytical Technologies in the Biomedical and Life Sciences* **798**, 55-62.

Table 2.1 Mathematical descriptions of possible mechanisms of suicide inhibition (Lilly *et al.*, 1998).

Mechanism 1: Reactive metabolite reacts with enzyme-substance complex $\frac{dV_{mt}}{dt} = -k_d \times (\frac{V_{mt} \times Cl}{K_m + Cl}) \times (\frac{V_{mt} \times Cl}{K_m + Cl})$
Mechanism 2: Reactive metabolite reacts with total enzyme present, reactive metabolite reacts with free enzyme $\frac{dV_{mt}}{dt} = -k_d \times (\frac{V_{mt} \times Cl}{K_m + Cl}) \times V_{mt}$
Mechanism 3: Reactive metabolite reacts with free enzyme $\frac{dV_{mt}}{dt} = -k_d \times (\frac{V_{mt} \times Cl}{K_m + Cl}) \times (\frac{V_{mt} \times K_m}{K_m + Cl})$
Mechanism 4: Bound intermediate inactivates enzyme in a first-order process $\frac{dV_{mt}}{dt} = -k' \times (\frac{V_{mt} \times Cl}{K_m + Cl})$
Mechanism 5: Free parent drug (i.e., trichloroethylene) or metabolite form in a first-order process reacts with bound enzyme $\frac{dV_{mt}}{dt} = -k' \times (\frac{V_{mt} \times Cl}{K_m + Cl})^{n1} \times (TCE)^{n2}$

K_m: M-M affinity constant (mg/l); V_{mt}: maximum rate of inhibitable metabolism (mg/h); k_d: inhibition constant (mg^{-1}); k': first-order constant (h^{-1}); Cl: the free concentration of the chemical in liver (mg/l).

Table 2.2 Pharmacokinetics of NRTIs in pregnant patints (Sharma *et al.*, 2004; Capparelli *et al.*, 2005; Pacifici, 2005).

Drug	Dose regimen (mg/day)	V_{ss} (L/kg)	Half-life pro-drug (intracellular) (h)	Elimination	System Clearances (L/h-kg)	Alteration in pregnancy	Cord/blood ratio	US FDA pregnancy category*
AZT	200	1.6	1.1(3-4)	Hepatic metabolism	1.0 -2.6	no	1.2	C
3TC	300	1.3	6 (15)	Urine excretion	0.27-0.39	no	~1	C
ABC	600	0.86	1.3 (>12)	Hepatic metabolism	0.56-1.04	no	0.83	B
ddC†	0.75 every 8 hrs	0.5	2 (10)	80% Urinary excretion	0.14-0.30	N/A	N/A	C
ddI	400	1.5	1.5 (12)	Metabolism	0.69-0.88	Oral: No IV: clearance↑ 30%	0.38	B
d4T	80	0.7	1 (3.5)	40% urinary excretion; 60% metabolism	0.40-0.50	no	1.3	C
FTC†	200	1.4	10 (39)	86% Urinary excretion	0.7	N/A	N/A	B

* The US FDA categories are: A- adequate and well-controlled studies have failed to demonstrate a risk to the fetus in the first trimester of pregnancy (and there is no evidence of risk in later trimesters); B- Animal reproduction studies have failed to demonstrate a risk to the fetus and there are no adequate and well-controlled studies in pregnant women OR Animal studies which have shown an adverse effect, but adequate and well-controlled studies in pregnant women have failed to demonstrate a risk to the fetus in any trimester; C- Animal reproduction studies have shown an adverse effect on the fetus and there are no adequate and well-controlled studies in humans, but potential benefits may warrant use of the drug in pregnant women despite potential risks; D- There is positive evidence of human fetal risk based on adverse reaction data from investigational or marketing experience or studies in humans, but potential benefits may warrant use of the drug in pregnant women despite potential risks; X- Studies in animals or humans have demonstrated fetal abnormalities and/or there is positive evidence of human fetal risk based on adverse reaction data from investigational or marketing experience, and the risks involved in use of the drug in pregnant women clearly outweigh potential benefits. † No clinical data in pregnant women.

Table 2.3 Drug-drug interactions of NRTIs in non-pregnant women*.

NRTIs	ABC	ddI	FTC	3TC	d4T	AZT
ABC		N/A	N/A	No significant interaction, while High rate of virological failure and emergence of resistance reported	N/A	No interaction
ddI			N/A	Renal elimination interaction unlikely. High rate of virological failure and of emergence of resistance	No significant PK interaction observed; Due to toxicity, Coadministration not recommended	No interaction
FTC				Potential competition for metabolism with other cytidine analogues. Coadministration not recommended	No interaction	No interaction
3TC					No interaction	No interaction
d4T						Coadministration not recommended due to competition for metabolism with other thymidine analogues
ddC	N/A	N/A	Potential competition for metabolism with other cytidine analogues. Coadministration not recommended	Coadministration not recommended due to competition for metabolism with other cytidine analogues	No interaction	No PK significant interaction observed. Do not co-administer due to modest antiviral effect

* Based on the information from http://www.hiv-druginteractions.org/.

Table 2.4 Experimentally proved NRTI transporters (Ganapathy *et al.*, 2000; Leazer and Klaassen, 2003; Unadkat *et al.*, 2004).

Transporters	Nucleoside Analogs K_m (μM)	Natural substrates	Physiological Function in	Placental Localization	References
ENT1	AZT inhibited ENT1-mediated nucleoside transport but not a substrate of ENT1 itself. ddC	purine and pyrimidine	Equilibrative transporter mediate facilitated diffusion	Apical	(Kong *et al.*, 2004) (Pastor-Anglada *et al.*, 2005)
ENT2	AZT ddC >7500 ddI 3000	purine, pyrimidine and nucleobases	Equilibrative transporter mediate facilitated diffusion	Unknown	(Kong *et al.*, 2004)
CNT1	AZT 550 ddC 500 3TC poor inhibitor	pyrimidine and adenosine	Na+-dependent concentrative transporter	Unknown	(Kong *et al.*, 2004)
CNT2	ddI	Purine and uridine	Na+-dependent concentrative transporter		(Wang and Giacomini, 1997)
CNT3	AZT ddC ddI	purine and pyrimidine	Na+-dependent concentrative transporter	Basolateral	(Kong *et al.*, 2004)
OAT1	AZT 45.9 (h) 68 (r) 3TC ddC ddI d4T	organic anions, weak acid	Na+-independent facilitative transporter organic anions	Basolateral	(Wada *et al.*, 2000) (Takeda *et al.*, 2002)
OAT2	AZT 26.8 (h) 26 (r) ddC 3080 (r)	organic anions, weak acid	Na+-independent facilitative transporter of organic anions	Basolateral	(Takeda *et al.*, 2002) (Morita *et al.*, 2001)
OAT3	AZT 145.1	organic anions, weak acid	Na+-independent facilitative transporter of organic anions	Basolateral	(Takeda *et al.*, 2002)

Table 2.4 –continued. Experimentally proved NRTI transporters (Ganapathy *et al.*, 2000; Leazer and Klaassen, 2003; Unadkat *et al.*, 2004).

Transporters	Nucleoside Analogs K_m (μM)	Natural substrates	Physiological Function in	Placental Localization	References
OCT1	AZT	organic cations, weak bases also non-charged compounds and some anions	Facilitative transporter of cationic substrates	Apical	(Pastor-Anglada *et al.*, 2005)
OCT3	AZT	organic cations, weak bases	Facilitative transporter of cationic substrates	Basolateral	(Pastor-Anglada *et al.*, 2005)
BCRP	AZT 3TC ddC ddI d4T	broad range of cytotoxics and xenobiotics	ATP-dependent efflux transporter	Apical	(Wang *et al.*, 2004)
MRP1	ABC 3TC FTC	broad range of substrates	ATP-dependent efflux transporter	Apical or Basolateral	(Weiss *et al.*, 2007)
MRP2	ABC 3TC FTC	broad range of substrates	ATP-dependent efflux transporter	Apical or Basolateral	(Weiss *et al.*, 2007)
MRP3	ABC 3TC FTC	broad range of substrates	ATP-dependent efflux transporter	Apical or Basolateral	(Weiss *et al.*, 2007)
MPR4	AZT 3TC ABC	broad range of substrates	ATP-dependent efflux transporter	Apical or Basolateral	(Reid *et al.*, 2003)
MPR5	ABC	broad range of substrates	ATP-dependent efflux transporter	Apical or Basolateral	(Reid *et al.*, 2003)
Unidentified organic cation transporter	3TC 2280 AZT ddC	antiviral nucleosides	pH-sensitive uptake	Rat renal brush border membrane vesicles (BBMV)	(Takubo *et al.*, 2002)
	AZT 1024	unknown	pH-sensitive uptake	Rat microglia cell (MLS-9)	(Hong *et al.*, 2001)
	3TC 1200	unknown	pH-sensitive uptake	Renal epithelial cell line	(Leung and Bendayan, 2001)

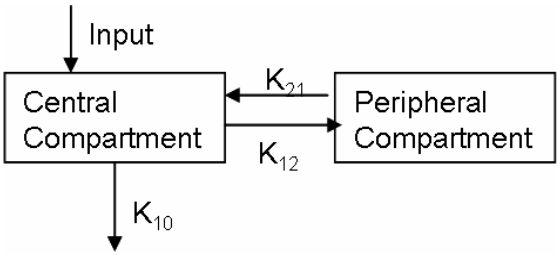

a.

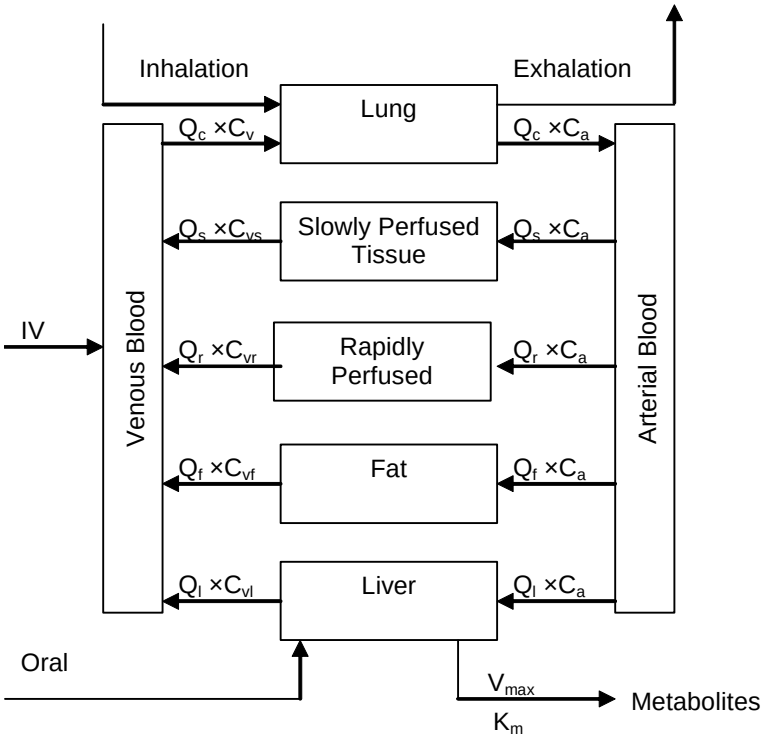

b.

Figure 2.1 Examples of model structures. (a) 2-compartment empirical model; (b) PBPK model. K_{10} is the system elimination rate constant from the central compartment. K_{12} and K_{21} are microconstants that describe the drug distribution rate between central compartment and the peripheral compartment. Q_i: the blood flow to the tissue, i = each tissue compartment. C_{vi}: the drug concentration in venous blood out of each tissue. C_a: drug concentration in the arterial blood. V_{max}: the maximum metabolic capability of an enzyme; K_m: the affinity constant of a chemical to the enzyme. V_{max} and K_m together represent the biotransformation of a chemical in the liver.

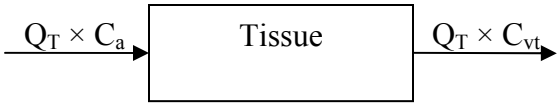

$$V_T \frac{dC_T}{dt} = Q_T \times (C_a - \frac{C_T}{P_T}) \qquad \text{a.}$$

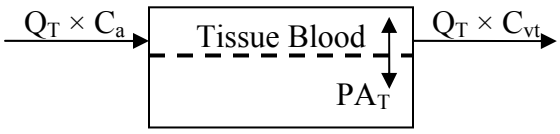

$$V_{T,E} \frac{dC_{T,E}}{dt} = Q_T \times (C_a - C_{T,E}) + PA_T \times (\frac{C_{T,I}}{P_T} - C_{T,E})$$

$$V_{T,I} \frac{dC_{T,I}}{dt} = PA_T \times (C_{T,E} - \frac{C_{T,I}}{P_T}) \qquad \text{b.}$$

Figure 2.2 Scheme and equations for tissue distribution. (a) Flow-limited tissue. V_T; tissue volume, C_T: drug concentration in the flow-limited tissue, Q_T: blood flow to the tissue, C_a: drug concentration in the arterial blood, P_T: tissue: plasma partition coefficient. (b) Diffusion-limited tissue. $V_{T,E}$; extracellular (blood) portion of tissue, $V_{T,I}$; intracellular portion of tissue, $C_{T,E}$: drug concentration in tissue blood, $C_{T,I}$: drug concentration in the tissue, PA_T: permeability-area cross product.

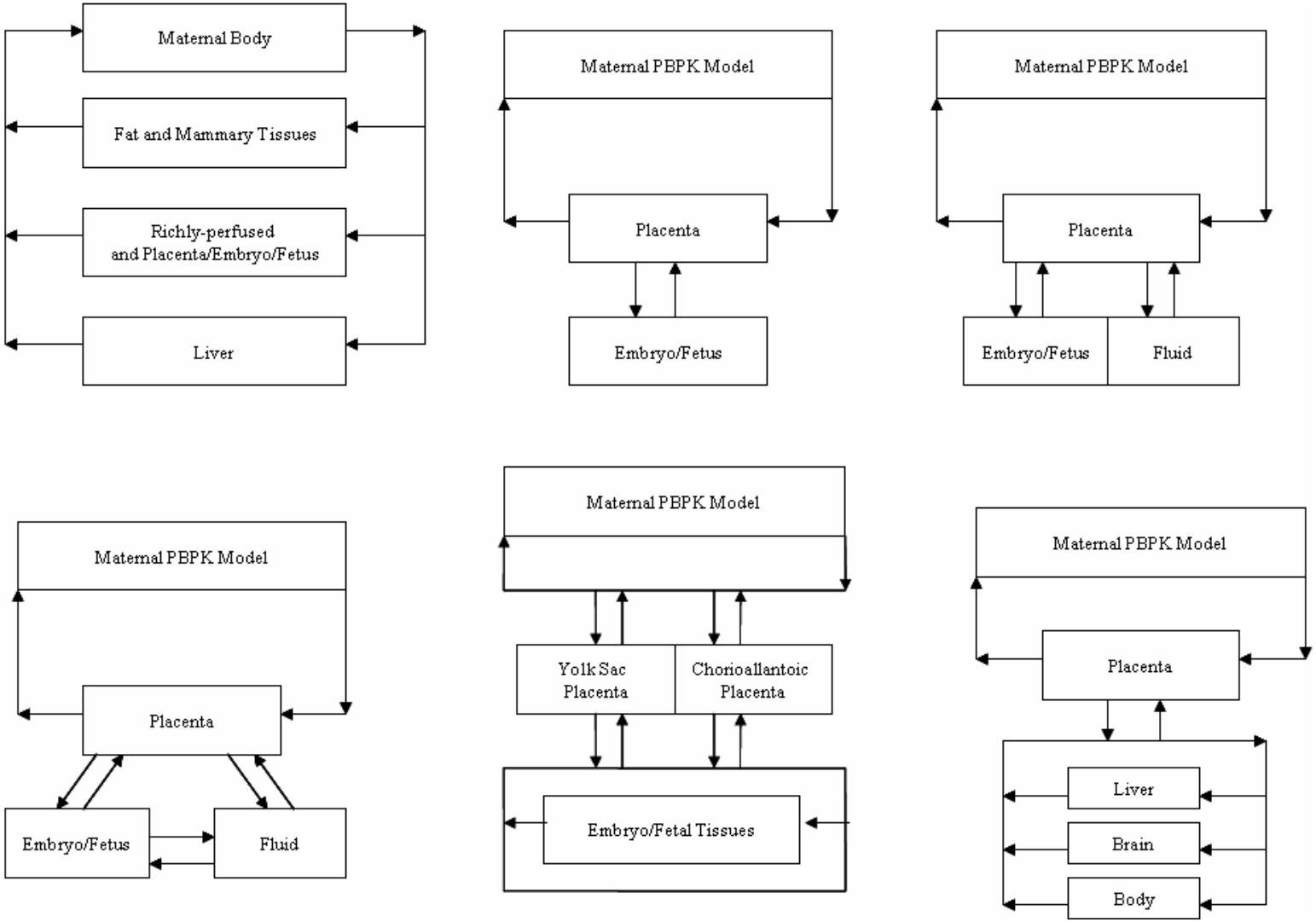

Figure 2.3 Six major model structures for pregnancy. Addapted from Fig. 3 of Corley *et al.*, 2003.

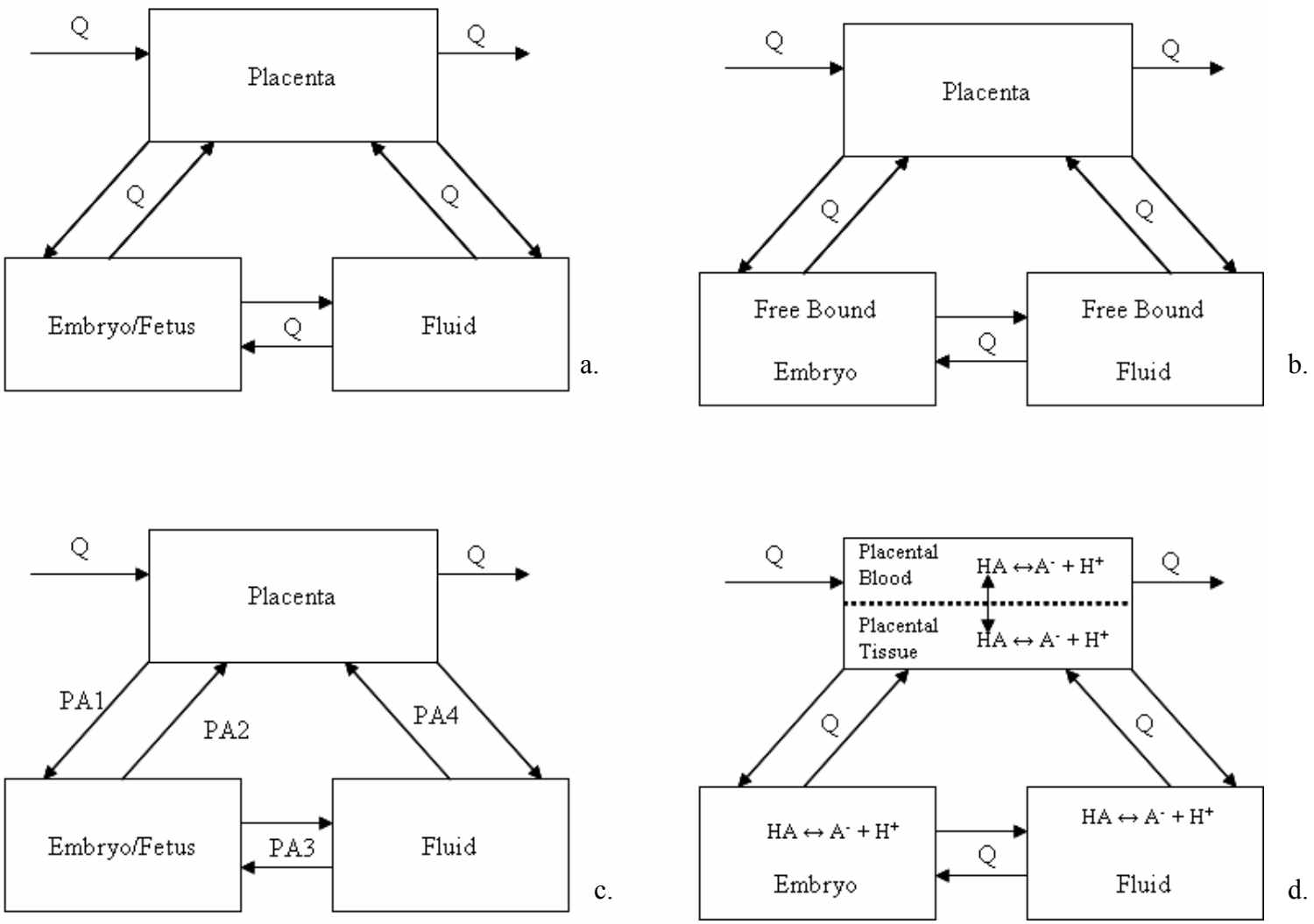

Figure 2.4 PBPK model structures for 4 potential perinatal transfer mechanism. (a) Flow-limited; (b) Reversible binding; (c) Active-transport; d)pH-trapping. Q: blood flow to the placenta. PA: permeability-area cross product. Addapted from Fig. 2 of Terry *et al.* 1999.

CHAPTER 3

QUANTITATIVE EVALUATION OF DICHOLOROACETIC ACID KINETICS IN HUMAN – A PHYSIOLOGICALLY-BASED PHARMACOKINETIC MODELING INVESTIGATION

Ting Li, Irv Schultz, Deborah Keys, Jerry Campbell, and Jeff Fisher. Submitted to *Toxicology*, 07/05/2007

Abstract

Dichloroacetic acid is a common disinfection byproduct in surface waters and is a probable minor metabolite of trichloroethylene. DCA liver carcinogenicity has been demonstrated in rodents but epidemiological evidence in humans is not available. High doses of DCA (~50mg/kg) are used clinically to treat metabolic acidosis. Biotransformation of DCA by glutathione transferase zeta (GSTzeta) in the liver is the major elimination pathway in humans. GSTzeta is also inactivated by DCA, leading to slower systemic clearance and nonlinear pharmacokinetics after multiple doses. A physiologically-based pharmacokinetic (PBPK) model was developed to quantitatively describe DCA biotransformation and kinetics in humans administered DCA by intravenous infusion and oral ingestion. GSTzeta metabolism was described using a Michaelis-Menten equation coupled with rate constants to account for normal GSTzeta synthesis, degradation and irreversible covalent binding and inhibition by the glutathione-bound-DCA intermediate. With some departures between observation and model prediction, the human DCA PBPK model adequately predicted the DCA plasma kinetics over a 20,000 fold range in administered doses. Apparent inhibition of GSTzeta mediated metabolism of DCA was minimal for low doses of DCA (μg/kg/day), but was significant for therapeutic doses of DCA. Serum protein binding of DCA was an important factor influencing the kinetics of low doses of DCA (μg/kg/day). GSTzeta polymorphisms may help explain inter-individual variability in DCA plasma kinetics and warrant future research. In conclusion, using the human DCA PBPK model to predict a human equivalent dose for the dosimetric, area under the curve (AUC) for total DCA in plasma and the point of departure liver cancer in mice (2.1 mg/kg/day), a 10% increase in incidence of liver cancer is equated to ingestion of 700 μg DCA per L of water assuming 2 L consumed per day.

Introduction

Dichloroacetic acid (DCA) is an environmental contaminant produced primarily by disinfection of water with chlorine. The reported median concentration of DCA in surface water systems is 15 μg/L with a maximum concentration of 74 μg/L (Boorman *et al.*, 1999) and the concentration as high as 133 μg/L may also occur (Uden and Miller, 1983). DCA is classified as a possible human carcinogen based on sufficient evidence of carcinogenicity in rats and mice (DeAngelo *et al.*, 1999; U.S.EPA, 2003).

Clinically, DCA has been used to treat metabolic disorders such as lactic acidosis and diabetes mellitus due to its ability to reduce circulating glucose, lactate and pyruvate. Pharmacological doses of DCA range from 10 to 50 mg/kg/day. Adverse effects from therapeutic use included mild liver dysfunction, transient central neuropathy, peripheral neuropathy and hypocalcemia The clinical effects are generally reversible after withdrawal of treatments (Stacpoole *et al.*, 1998b; U.S.EPA, 2003; Mori *et al.*, 2004).

DCA is absorbed readily by the gastrointestinal tract and only 1% of the total dose is excreted in urine after a single administration of 50 mg/kg in humans. The plasma half-life of DCA in healthy humans is approximately 1 hour and increases somewhat with repeated dosing (Curry *et al.*, 1991; Stacpoole *et al.*, 1998a). The metabolism of DCA involves oxidative dechlorination to form glyoxylate, which is further oxidized to oxalate, carbon dioxide or incorporated into amino acids nucleophiles and other cellular molecules (Tong *et al.*, 1998b; U.S.EPA, 2003; Anderson *et al.*, 2004). GSTzeta is the only enzyme identified in the biotransformation of DCA (Tong *et al.*, 1998a; Ammini *et al.*, 2003; Lim *et al.*, 2004). DCA has been shown to inhibit GSTzeta, through covalent modification of the enzyme, in both *in vivo* animal studies and *in vitro* studies (Anderson *et al*., 1999; Anderson *et al.*, 2002; Schultz *et al.*,

2002). GSTzeta (GSTZ1-1), also known as maleylacetoacetate isomerase (MAAI), is an essential enzyme in phenylalanine/tyrosine catabolism pathway. Disruption of tyrosine catabolism by competitive inhibition was proposed as a possible mechanism for DCA toxicity (Cornett *et al.*, 1999; Schultz *et al.*, 2002; Ammini *et al.*, 2003; Lantum *et al.*, 2003). Four functional allelic variants of GSTZ 1-1 (GSTZ 1a-1a GSTZ 1d-1d) have been identified in humans. These GSTZ allelic variants have different metabolic capacities and inhibition characteristics towards DCA *in vitro* (Tzeng *et al.*, 2000; Blackburn *et al.*, 2001).

The first rodent physiologically based pharmacokinetic (PBPK) models for DCA were created to track trace amounts of DCA, presumably formed as a metabolite of trichloroethylene (Abbas and Fisher, 1997; Greenberg *et al.*, 1999; Clewell *et al.*, 2000). In addition, Barton et al. (1999) created a mouse DCA PBPK model to understand the relationship between hepatic cancer incidence and DCA hepatic dosimetry for orally ingested DCA. The inhibitory effect of DCA on its own metabolism was not accounted for in PBPK models until Keys *et al.* (2004) developed rodent DCA PBPK models. The rodent PBPK models of Keys *et al.* (2004) were used to evaluate the impact of reduced hepatic metabolism (by suicide inhibition of GSTzeta) on DCA blood time course kinetics. In the present paper we report on the development of a human PBPK model for DCA formulated to account for reduced hepatic metabolism of DCA *via* suicide inhibition of the GSTzeta enzyme. The development of a human PBPK model for DCA was possible, in part, because several pharmacokinetic studies of administered DCA have been reported (Lukas *et al.*, 1980; Wells *et al.*, 1980; Chu, 1987; Curry *et al.*, 1991; Fox *et al.*, 1996; Shangraw and Fisher, 1999; Jia *et al.*, 2006; Schultz and Shangraw, 2006).

Materials and methods

DCA Human Kinetic Studies Used for PBPK Modeling

Therapeutic DCA Dosing Studies. Curry et al. (1991) intravenously infused 4 male (average weight = 77 kg) and 4 female (average weight = 54 kg) healthy subjects over a 30 min period with 50 mg/kg DCA. Blood samples were collected at 0.125 h intervals for the first h post dosing, at 0.25 h intervals for the 2nd h, at 0.5 h intervals for the 3rd to 6th h post dosing and then at 1 h intervals till the 12th h post dosing. These particular kinetic studies and other kinetic studies are reported in a dissertation by Chu (1987). Chu (1987) collected urine from each of these 8 subjects at various intervals up to 12 h post dosing and calculated the cumulative amount of DCA excreted and urinary clearance. In other studies Chu (1987) reported DCA serum kinetics after a single oral dose of 50 mg/kg DCA given to 4 male subjects administered in gelatin capsules. The blood sampling schedule was similar to the intravenous experiments. Chu (1987) also administered 5 repeated 30 min iv doses of DCA two hours apart to adult volunteers. Four males and one female received 25 mg/kg of DCA and one male and three females received repeated doses of 50 mg/kg of DCA. Blood samples were collected at 30 min intervals for the first 8.5-9 h after the first infusion and subsequently every 3-4 h for a 24 h period.

Three published kinetic studies with therapeutic doses of DCA were used to test the ability of the model to predict plasma kinetics. Lukas et al. (1980) intravenously administered either 10 or 20 mg/kg of DCA in saline to two adult subjects over a 20 min period. Blood samples were drawn every hour for the first 4 hours, then every two hours for the next 8 hours. Shangraw and Fisher (1996) treated cirrhosis patients with 30 min iv infusions of 35 mg/kg DCA. Five healthy men and one healthy woman were included in the control group. In these individuals blood samples were withdrawn at 0, 0.25, 0.5, 1, 2, 4, 6, 10, 14, 20, and 24 h post

dosing. In a somewhat complicated dosing schedule, Fox et al. (1996a) administered two 30 min intravenous infusions of DCA 8 hours apart to 9 subjects in each dose group. Doses were (first + second infusions): 30+15, 60+30 or 100+50 mg/kg. Blood samples were collected at several predetermined times over a 14 hour period.

Sub-therapeutic DCA Dosing Studies. Schultz and Shangraw (2006) administered an oral dose of 2 mg/kg of $^{12}C_1$-DCA in 0.5 L of water followed 5 min later by an iv dose of 0.3 mg/kg $^{13}C_1$-DCA to 16 healthy subjects. Blood samples were collected at 5 min intervals for the first 0.5 h, then 10 min intervals for remainder of the first hour, followed by collections at 1.25, 1.50 and 2.0 hour post dosing. These subjects were then kept on a daily oral bolus dose of 0.02 mg/kg of $^{12}C_1$-DCA for 14 days to mimic drinking water contaminated with DCA. At the end of the last day of treatment (day 15), the subjects were again given an oral bolus dose 2 mg/kg of $^{12}C_1$-DCA followed by an iv dose of 0.3 mg/kg $^{13}C_1$-DCA.

Jia et al. (2006) administered 2.5 μg/kg 1,2-^{13}C-DCA daily to twenty healthy adult volunteers (8 male and 12 female) either by oral or intravenous administration. In one study, fifteen of these volunteers (6 male and 9 female) received orally administered 1,2-^{13}C-DCA in 200 mL distilled water after an overnight fast for either 5 or 15 consecutive days. Blood was sampled on days 1, 5 and 15 to determine 1,2-^{13}C-DCA plasma kinetics. In another study 16 volunteers (7 male and 9 female) received iv administered 1,2-^{13}C-DCA for up to 5 days. Intravenous 1,2-^{13}C-DCA (2.5 μg/kg) was infused at a constant rate in saline over 10 minutes into a forearm vein after an overnight fast. Blood was sampled on days 1 and 5 to determine 1,2-^{13}C-DCA plasma kinetics. On each blood sampling Day, 2 mL of venous whole blood was withdrawn at 10 minutes before administration of 1,2-^{13}C-DCA, and then 0, 5, 10, 20, 30 minutes, and 1, 2, 3, 4, 6, 8, 12 and 24 hours after administration of 1,2-^{13}C-DCA. Urine was

also collected at 12 and 24 hours during each kinetic study. Selected volunteers participated in both the oral and iv dosing study. These 11 volunteers (5 male and 6 female) had a lapse in treatment of at least 30 days between two routes of exposures.

Human PBPK Model for DCA

All model code was written in ACSL (acslXtreme V 2.0.1.2, Aegis Technologies Group Inc., Huntsville, AL). The model compartments include plasma, liver, kidney, slowly perfused, and rapidly perfused tissues (Fig. 3.1). Blood flows to these compartments were described using venous equilibration equations. Intravenous dosing was described as an infusion rate directly into the mixed venous blood supply. A two compartment modeling approach (Abbas and Fisher, 1997) was used to describe oral ingestion of DCA. The hepatic metabolism of DCA by GSTzeta was described with a Michaelis-Menten equation modified to account for suicide inhibition (Lilly *et al.*, 1998). Minor elimination of DCA through the urine was described using a first-order rate constant. Two PBPK models for DCA with identical structure and model parameter values were used to describe the competitive metabolism of two isotopes of DCA after co-administration (Schultz and Shangraw, 2006). Competitive inhibition of metabolism for chemical mixtures has been successfully incorporated into PBPK models for chemicals that are metabolized by the same enzymes (Campbell and Fisher, 2007). Suicide inhibition of GSTzeta was also retained in both models where co-administration of DCA isotopes was simulated.

The metabolism of DCA under co-exposure conditions is presented in Equations 3.1 and 3.2. The amount of each isotope (^{12}C DCA in this example) that is metabolized with respect to time (dAm/dt, mg/h) in the liver is given by:

$$RAM^{12} = \frac{dA_m^{12}}{dt} = \frac{V_{\max} \times Cv_l^{12}}{K_m \times (1 + Cv_l^{13} / K_m) + Cv_l^{12}} \qquad (3.1)$$

Assuming both isotopes have the same affinity to GST-zeta, the K_m values for each isotope are the same, thus Equation (3.1) for ^{12}C DCA can be rearranged as:

$$RAM^{12} = \frac{V_{\max} \times Cv_l^{12}}{K_m + Cv_l^{13} + Cv_l^{12}} \tag{3.2}$$

Similarly, the rate of metabolism of ^{13}C DCA is described as:

$$RAM^{13} = \frac{dA_m^{13}}{dt} = \frac{V_{\max} \times Cv_l^{13}}{K_m + Cv_l^{12} + Cv_l^{13}} \tag{3.3}$$

where the Michaelis-Menten equation represents metabolic conversion by the GSTzeta enzyme; K_m is the Michaelis-Menten affinity constant (mg/L), V_{max} (mg/h) is the current metabolic capacity (inhibitable), Cv_l^{12} and Cv_l^{13} are the ^{12}C-DCA, and ^{13}C-DCA concentrations in the venous blood leaving the liver, respectively.

The proposed mechanism of DCA-mediated inactivation of GSTzeta involves the covalent binding of the glutathione-bound-DCA intermediate metabolic product with a nucleophilic site on GSTzeta. This covalent modification results in dose-dependent inactivation of GSTzeta (Anderson *et al.*, 2002). In the present human model, the inactivation reaction rate was described mathematically as a second order process (bimolecular rate constant, k_d, mg^{-1}) which is dependent upon the intermediate reactive metabolic product(s) and free GSTzeta concentrations in the liver (Lilly *et al*., 1998). The rate of change in the initial value of maximal velocity of metabolism (V_{max0}) with respect to time (dV_{max}/dt, mg/h^2) equals

$$\frac{dV_{\max}}{dt} = -k_d \times \left(\frac{V_{\max} \times Cv_l}{K_m + Cv_l}\right) \times \left(\frac{V_{\max} \times K_m}{K_m + Cv_l}\right) + [k_s - k_{de} \times V_{\max}] \tag{3.4}$$

The resynthesis (k_s, mg/h^2) and the natural degradation (k_{de}, 1/hr) of GSTzeta (Equation (3.4)) was described in a similar fashion to the Keys *et al.* (2004) PBPK model for rodents. Integration

of Equation (4) provided the value of V_{max} as a function of inhibition of GSTzeta using starting maximal velocity in the absence of DCA (V_{max0}).

$$V_{\max} = \int_0^t \frac{dV_{\max}}{dt} + V_{\max 0} \tag{3.5}$$

To maintain equilibrium of enzyme at steady state, $k_s = k_{de} \cdot V_{max0}$. The percentage of reduction of the GSTzeta metabolic capacity (PV_{max}) was calculated as:

$$PV_{\max} = \frac{V_{\max(t)}}{V_{\max 0}} \times 100\% \tag{3.6}$$

where $V_{max(t)}$ is the maximum metabolism rate at time t.

This PBPK model accounts for low capacity, high affinity binding of DCA to plasma proteins. DCA has been shown to be bound weakly to rat serum protein (e.g., 10%, Schultz *et al.*, 1999). Chu (1987) reported that 23% of DCA is bound in human plasma. To describe the rate of binding of DCA to plasma proteins in this paper, the methods of Clewell et al. (2003) were used, where the binding (association) of DCA to plasma proteins was described as Michaelis-Menten kinetics and the rate of dissociation (unbinding) was assumed to be a first-order process (Clewell et al., 2003).

Physiological parameters used in the human model are summarized in Table 3.1. Average body weight for each pharmacokinetic study was used when reported. Gender differences in DCA kinetics were evaluated in selected studies. No appreciable gender differences were observed. In the Shultz and Shangraw (2006) study, individual subject DCA kinetic data was reported. In this case, physiological model parameters were developed for males and females (Table 3.1) and also by lumping sexes through averaging body weight, and blood flows to the liver and kidney, which are slightly different between the sexes.

Calibration of Human PBPK Model for DCA

DCA is highly hydrophilic with an octanol/water partition coefficient ($logP_{o/w}$) of 0.92. Chemical-specific parameters for DCA are listed in Table 3.2. DCA tissue/blood partition coefficient (PC) values determined for mice (Abbas and Fisher, 1997) were used for humans, except where noted. A small urinary clearance constant (Cl_{rc}, l/h/kg) value was calculated by allometrically scaling the clearance rates reported in Curry *et al.* (1991). Cl_{rc} was fixed prior to further model parameterization. The following sequence was used to estimate metabolic parameters describing suicide inhibition of DCA metabolism. The value of the Michaelis Menten affinity constant (K_m) was set to 6 mg/L, which was measured using human liver cytosol (Tong *et al*. 1998a). The initial value of the inhibition rate constant (k_d) was set to 0.001 mg^{-1}. The degradation rate (k_{de}) was initially set to the value used for rodents (0.00875 h^{-1}; Keys *et al.*, 2004). It was necessary to lower the slowly perfused (PS) partition coefficient value obtained in mice (0.37, Abbas and Fisher, 1997) to 0.11 to improve the agreement between observation and model prediction following 0.3 mg/kg ^{13}C-DCA IV bolus on day 0 (Schultz and Shangraw, 2006). The initial estimate for the maximal rate of DCA metabolism (V_{maxc0}) was then obtained by visual inspection using the same data set of Schultz and Shangraw (2006). This low dose of DCA was considered to have a minimal effect on GSTzeta activity. The metabolic inhibition constant, k_d, was then fit to the high dose DCA plasma concentration-time course data following 5-repeated infusion of 50 mg/kg and 25 mg/kg DCA at 2 h interval in the study of Chu (1987) by the maximum likelihood method with all other parameters fixed. After this, the value of V_{maxc0} was again visually adjusted, this time, to fit the concentration-time course data following 50 mg/kg single iv infusion (Curry *et al.*, 1991).

Diminished systemic clearance of DCA after multiple or single high doses of DCA indicated that all individuals (n =12) needed more than 4 weeks to recover (Chu, 1987; Curry *et al.*, 1991), suggesting a very slow recovery for GSTzeta activity. The GSTzeta resynthesis rate, k_{de}, was set to a value that would provide a recovery rate for GSTzeta enzymatic activity equal to 8 weeks after a single 50 mg/kg dose of DCA (2 out of 4 subjects recovered by 8 weeks). The values of the oral absorption rate constants following drinking water administration were estimated by fitting the ^{12}C-DCA concentration time course data after 2 mg/kg ^{12}C-DCA oral ingestion in 500 ml of drinking water reported in the study of Schultz and Shangraw (2006). K_{a1} was set to 0.01 h^{-1} and the values of K_{a2}, K_{a3} were estimated visually. To describe low capacity binding of DCA to plasma proteins, the parameters for protein binding (B_{MAX}, $K_{mb,}$ and K_{unb}) were estimated visually by fitting the kinetic data after iv and oral administration of 2.5 μg/kg 1,2-^{13}C-DCA in days 1, 5 and 15 (Jia *et al.*, 2006). Plasma protein binding was important for describing the plasma kinetics of DCA after administration of 2.5 μg/kg of DCA.

Individual metabolic capacities were estimated for the 16 subjects reported in Schultz and Shangraw (2006) to assess the inter-individual variation as inferred by differences in clearance kinetics of DCA across the study participants. Gender specific values of physiological parameters were used (Table 3.1), but not considered essential because gender appears to have little influence on DCA kinetics (Stacpoole *et al.*, 1998a; Schultz and Shangraw, 2006). V_{maxc0}, k_d and the oral absorption parameters (K_{a2} and K_{a3}) for each subject were estimated by maximum likelihood methods. Firstly, the initial estimations of V_{maxc0}, k_d, K_{a2} and K_{a3} were fit simultaneously to the individual ^{12}C-DCA and ^{13}C-DCA concentration-time course data of each subject. Secondly, K_{a2} and K_{a3} were fixed to the initial estimated values and V_{maxc0} and k_d were re-optimized by fitting ^{12}C-DCA and ^{13}C-DCA concentration-time course data. Finally, K_{a2} and

K_{a3} were re-optimized by fitting to ^{12}C-DCA concentration-time course data with all other parameters fixed.

Sensitivity Analysis of Parameters.

A sensitivity analysis using the wizard provided in acslXtreme was carried out using area AUC for DCA in plasma. Briefly, the equation used to calculate the sensitivity coefficient for each parameter is:

$$\text{Sensitivity Coefficient} = \frac{(A-B)/B}{(C-D)/D} \tag{3.7}$$

where A is the DCA plasma AUC predicted with a 1% increased parameter value, B is the DCA plasma AUC predicted at the starting parameter value, C is the parameter value after a 1% increase, and D is the original parameter value. Parameters with large absolute value of coefficients indicate the parameter has an important effect on the model. A positive value indicates that the output and the corresponding model parameter are positively related and a negative value indicates they are inversely related. The calculation was performed using the forward difference algorithm with delta equals to 0.01 and normalized to both response variables and parameters.

Cancer Risk Estimates.

The theoretical cancer risk for ingestion of DCA was calculated using a previously reported mouse PBPK model for DCA (Keys *et al.*, 2004) and the current human PBPK model for DCA. A point of departure (POD) for a 10% increase in cancer risk for DCA is reported to be 2.1 mg/kg/day (estimated as 95% lower confidence limit of benchmark dose) (U.S.EPA., 2003) for liver carcinomas in B6C3F$_1$ mice exposed to DCA in drinking water (DeAngelo *et al.*, 1999). The previously published DCA model for mouse (Keys *et al.*, 2004) was used to estimate the daily plasma AUC (day·mg/L) and the average daily amount of DCA metabolized per kg of

liver ($A_{ml,}$ mg/kg) at steady state following 2.1 mg/kg/day DCA exposure in drinking water. Assuming a 70-kg human ingests 1 L each 12 hours, the present human model was used to estimate the human equivalent doses (HEDs) which correspond to the mouse daily plasma AUC and A_{ml} when administered 2.1 mg/kg/day of DCA in drinking water.

Results

The range of administered intravenous and oral ingestion doses of DCA described with this PBPK model was a remarkable 20,000 fold (2.5 μg/kg to 50 mg/kg) with studies conducted at several laboratories. Also noteworthy, one set of model parameter values (Tables 3.1 and 3.2) was used in the PBPK model to describe the entire DCA data set with the exception of individual subject optimized kinetic data reported by Schultz and Shangraw (2006). Perhaps the most challenging pharmacokinetic data to describe with the present PBPK model were the high dose DCA studies conducted in the laboratory of Chu (1987). The model over-predicted systemic clearance of DCA over a 6 hour period in 4 male and 4 female subjects (Fig. 3.2) after a single iv infusion of 50 mg/kg (reported by Curry *et al.*, 1991) and modestly under-predicted following 5-repeated administrations of DCA (50 and 25 mg/kg) at 2 hour intervals over a 10 hour period (Fig. 3.3). The cumulative urinary excretion of DCA was somewhat variable (Fig. 3.4) in these subjects accounting for less than 1% of the administrated dose. The PBPK model predicted and observed cumulative amount of DCA excreted in urine was in good agreement, but slightly under predicted the mean cumulative amount of urine observed in these subjects (Fig. 3.4).

In other high dose studies (Lukas *et al.*, 1980), with two individuals each intravenously administered 10 or 20 mg/kg, good agreement was obtained between model predictions and observations (Fig. 3.5). In another group of six individuals administered 35 mg/kg of DCA (Shangraw and Fisher, 1999), the systemic clearance of DCA was slightly over- predicted (Fig.

3.5). In the final high dose simulation study (Fig. 3.6) in which groups of individuals were intravenously administer a second dose of DCA 8 hours after the first dose (Fox *et al.*, 1996a), favorable agreement was obtained between model prediction and observation.

Two independent clinical studies were used for low dose DCA simulation studies. In the Schultz and Shangraw (2006) study, individuals were initially dosed orally with 2 mg/kg of ^{12}C-DCA followed within minutes by an intravenous dose of 0.3 mg/kg of ^{13}C-DCA and after 14 days of daily treatment with a low dose (0.02 mg/kg) of ^{12}C-DCA, this oral/iv dosing schedule was repeated and serial blood samples were collected. Figure 3.7a depicts the entire prediction of both oral and iv dosing of men at the beginning and end of the study as well as the daily low dose treatment. In panels' b and c of Fig. 3.7, model predicted and observed plasma concentrations are shown for a two hour period after oral and then iv administration of the two isotopes of DCA at the beginning and end of the treatment period. Generally speaking, good agreement was observed between computer predicted DCA concentrations and measured values. The model predicted clearance of iv administered DCA in men was somewhat slower than observed for both days. Similar trends between model prediction and observation were found for women (Fig. 3.8). When individual DCA clearance kinetics was evaluated by adjusting the values for metabolism (V_{maxc0}, k_d) and oral absorption (K_{a2}, K_{a3}) (Table 3.3), the fitted values for V_{maxc0} had the largest range of estimated values (36.7 to 280 mg/h/kg$^{0.75}$), while values for k_d ranged from zero (no metabolic inhibition) to 0.016 mg^{-1}. The individual values of K_{a2}, K_{a3} are relatively similar and the average values are about 8.0 h^{-1}. The simultaneously optimized values for V_{maxc0}, k_d, K_{a2} and K_{a3} were very close to the final values obtained after the re-optimization was conducted separately for the metabolic parameters (V_{maxc0}, k_d) and the oral absorption parameters (K_{a2} and K_{a3}). This was expected because the metabolic parameters influence the

AUC of both ^{12}C-DCA and ^{13}C-DCA while the oral uptake parameters only influence the shape of ^{12}C-DCA concentration-time profiles (i.e., peak concentration (C_{max}) and time to reach the peak concentration, T_{max}).

In the Jia *et al.* (2006) clinical study, individuals were administered a very low dose of 2.5 μg/kg/day for 5 days by iv infusion or per orally for 15 days. Blood was collected on specified days following treatment for analysis of DCA concentration. These low dose kinetic data demonstrated the requirement for serum protein binding of DCA (Fig. 3.9a). The DCA plasma kinetic behavior could not be described (Fig. 3.9b) without assuming serum protein binding. In the other higher dose DCA studies, the influence of this low capacity, high affinity serum protein binding on DCA kinetics was not readily apparent. The binding of DCA to these unspecified plasma proteins were assumed to be reversible. When 2.5 μg/kg/day of DCA was administered orally, peak plasma DCA concentrations were moderately under-predicted on days 1, 5 and 15 of treatment (Fig. 3.10).

Sensitivity assay

Since the sensitivity analysis is both dose and time dependent, this analysis was applied using dosimetrics that reflect integrated measures over time, such as AUC (Table 3.4). Normalized sensitivity coefficients with absolute values that were determined to be most sensitive (>0.5) are in bold. Cardiac output and blood flow to the liver were found to be sensitive for low intravenous doses of DCA (0.3 mg/kg and 2.5 μg/kg), while the metabolic parameters (V_{maxc0}, K_m and k_d) were the most sensitive parameters at therapeutic doses. The protein binding parameters (B_{max} and K_{unb}) were sensitive model parameters only for the lowest DCA dose of 2.5 μg/kg/day.

HED for cancer risk estimate

Under steady state conditions, the estimated daily plasma AUC in mice treated with 2.1 mg/kg/day of DCA in drinking water was 0.05 mg/L/day and the average daily amount of DCA metabolized per kg of liver (A_{ml}) was 38.5 mg/kg liver. In the present human model, oral administration of 0.02 mg/kg/day resulted in a plasma AUC equal to 0.05 mg/L/day, while oral administration of 1.0 mg/kg/day results in an A_{ml} equal to 38.5 mg/kg/day.

Discussion

In the present study PBPK modeling was used to quantitatively describe intravenous and oral intake of DCA in humans. The range of administered doses of DCA reported in the pharmacokinetic literature was exceptionally wide (μg to mg per kg) and included both single and repetative dose administration. Collectively, these published clinical pharmacokinetic studies provided an excellent data base for the development of a human PBPK model fpr DCA, especially when coupled with information derived from published PBPK models of DCA in laboratory animals. The historical focus of research on DCA metabolism has been on how DCA is metabolized and how DCA inhibits its own metabolism. Our present human model for DCA suggests that at low doses, such as those encountered in the environment (μg/L in drinking water), inhibition of its metabolism is a minor contributor to the pharmacokinetic behavior of DCA, but serum protein binding probably plays an important role. For higher doses of DCA, such as therapeutic doses, inhibition of its own metabolism can be substantial; resulting in slowed clearance of DCA from the body while metabolic recovery from the insult also appears to be very slow.

Varying degrees of success were obtained in describing these diverse and sometimes highly variable kinetic data sets for DCA with the present human PBPK model. The model

parameters were constrained to single values to represent the mean kinetic behavior for groups of individuals. When inter-individual variability was evaluated for metabolism and oral uptake of DCA, a wide range of metabolic capacity values were obtained (Table 3.3). The variability in kinetic data across the clinical studies and even between individuals may reflect polymorphisms in GSTzeta, the primary hepatic enzyme responsible for metabolism of DCA and well as other possible factors.

In the present simulations, the breakdown of DCA was assumed to occur only by hepatic GSTzeta and depending on dose; its metabolism was partially inhibited by covalent binding of a reactive intermediate metabolite. This process was described as a second order process which depends on the concentration of reactive intermediate available to bind to GSTzeta and availability of GSTzeta in the liver (Equation 3.4). Experimental evidence has demonstrated the dose dependent inactivation of GSTzeta by DCA (Tzeng *et al.*, 2000) and the subsequent degradation of the GSTzeta protein (Anderson *et al.*, 1999). With the current formulation of the human PBPK model for DCA, repeated intravenous administration of the lowest reported clinical dose of DCA (2.5 μg/kg/day) would result in less than 1% reduction in GSTzeta activity under steady state conditions. With combined doses of 2 mg/kg oral and 0.3 mg/kg iv (Schultz and Shangraw, 2006), the model predicted decrease in metabolic capacity was nearly 13 % which persisted until the second dose 15 days later due to the slow recovery of GSTzeta as well as 0.02 mg/kg DCA administered daily in drinking water between the two challenges. If a person was administered 50 by mg/kg/day iv infusion until steady state was reached, only about 13 % of the initial metabolic capacity is predicted to remain.

The PBPK model predicted human equivalent dose (using the dosimetric AUC for DCA in plasma) for oral administration of 2.1 mg/kg/day in mice was 0.02 mg/kg/day of DCA in

humans. Theoretically this exposure corresponds to a 10% increase in incidence in liver cancer based on 2 year rodent bioassay data (DeAngelo *et al.*, 1999). If a 70 kg person ingested two liter of water each day, this would be equivalent to ingestion of 700 μg DCA per L of water. The current maximum contaminant level (MCL) is 60 μg/L for five haloacetic acids including DCA (U.S. EPA, 2002).

In conclusion, the present DCA PBPK model in humans is able to quantitatively describe the DCA kinetics across different populations and diverse exposure scenarios. Model simulations suggest that environmental exposure of DCA in drinking water (~ 0.5 μg/kg/day) is expected to have very limited effects on GSTzeta activity. Future studies such as genotyping of individual subjects will allow determination of the effect GSTZ polymorphism has on *in vivo* DCA pharmacokinetics.

Acknowledgments

This research was funded in part by Department of Energy Cooperative Agreement #DE-FC09-02CH11109 and a graduate assistantship from the Department of Pharmaceutical and Biomedical Sciences at the University of Georgia.

References

Abbas, R., and Fisher, J. W. (1997). A physiologically based pharmacokinetic model for trichloroethylene and its metabolites, chloral hydrate, trichloroacetate, dichloroacetate, trichloroethanol, and trichloroethanol glucuronide in B6C3F1 mice. *Toxicology and Applied Pharmacology* **147**, 15-30.

Ammini, C. V., Fernandez-Canon, J., Shroads, A. L., Cornett, R., Cheung, J., James, M. O., Henderson, G. N., Grompe, M., and Stacpoole, P. W. (2003). Pharmacologic or genetic

ablation of maleylacetoacetate isomerase increases levels of toxic tyrosine catabolites in rodents. *Biochemical Pharmacology* **66**, 2029-2038.

Anderson, W. B., Board, P. G., and Anders, M. W. (2004). Glutathione transferase zeta-catalyzed bioactivation of dichloroacetic acid: Reaction of glyoxylate with amino acid nucleophiles. *Chemical Research in Toxicology* **17**, 650-662.

Anderson, W. B., Board, P. G., Gargano, B., and Anders, M. W. (1999). Inactivation of glutathione transferase zeta by dichloroacetic acid and other fluorine-lacking alpha-haloalkanoic acids. *Chemical Research in Toxicology* **12**, 1144-1149.

Barshop, B. A., Naviaux, R. K., McGowan, K. A., Levine, F., Nyhan, W. L., Loupis-Geller, A., and Haas, R. H. (2004). Chronic treatment of mitochondrial disease patients with dichloroacetate. *Molecular Genetics and Metabolism* **83**, 138-149.

Barton, H. A., Bull, R., Schultz, I., and Andersen, M. E. (1999). Dichloroacetate (DCA) dosimetry: interpreting DCA-induced liver cancer dose response and the potential for DCA to contribute to trichloroethylene-induced liver cancer. *Toxicology Letters* **106**, 9-21.

Blackburn, A. C., Coggan, M., Tzeng, H. F., Lantum, H., Polekhina, G., Parker, M. W., Anders, M. W., and Board, P. G. (2001). GSTZ1d: a new allele of glutathione transferase zeta and maleylacetoacetate isomerase. *Pharmacogenetics* **11**, 671-678.

Blackburn, A. C., Tzeng, H. F., Anders, M. W., and Board, P. G. (2000). Discovery of a functional polymorphism in human glutathione transferase zeta by expressed sequence tag database analysis. *Pharmacogenetics* **10**, 49-57.

Boorman, G. A., Dellarco, V., Dunnick, J. K., Chapin, R. E., Hunter, S., Hauchman, F., Gardner, H., Cox, M., and Sills, R. C. (1999). Drinking water disinfection byproducts: Review and approach to toxicity evaluation. *Environmental Health Perspectives* **107**, 207-217.

Brown, R. P., Delp, M. D., Lindstedt, S. L., Rhomberg, L. R., and Beliles, R. P. (1997). Physiological parameter values for physiologically based pharmacokinetic models. *Toxicology and Industrial Health* **13**, 407-484.

Campbell, J. L., and Fisher, J. W. (2007). A PBPK Modeling assessment of the competitive metabolic interactions of JP-8 vapor with two constituents, m-xylene and ethylbenzene. *Inhalation Toxicology* **19**, 265-273.

Chu, P. I. (1987). Pharmacokinetics of sodium dichloroacetics. Ph. D. Dissertation. *College of Pharmacy*. University of Florida, Gainesville.

Clewell, H. J., Gentry, P. R., Covington, T. R., and Gearhart, J. M. (2000). Development of a physiologically based pharmacokinetic model of trichloroethylene and its metabolites for use in risk assessment. *Environmental Health Perspectives* **108**, 283-305.

Clewell, R. A., Merrill, E. A., Yi, K. Y., Mahle, D. A., Sterner, T. R., Fisher, J. W., and Gearhart, J. M. (2003). Predicting neonatal perchlorate dose and inhibition of iodide uptake in the rat during lactation using physiologically-based pharmacokinetic modeling. *Toxicological Sciences* **74**, 416-436.

Cornett, R., James, M. O., Henderson, G. N., Cheung, J., Shroads, A. L., and Stacpoole, P. W. (1999). Inhibition of glutathione S-transferase zeta and tyrosine metabolism by dichloroacetate: A potential unifying mechanism for its altered biotransformation and toxicity. *Biochemical and Biophysical Research Communications* **262**, 752-756.

Curry, S. H., Chu, P. I., Baumgartner, T. G., and Stacpoole, P. W. (1985). Plasma-Concentrations and Metabolic Effects of Intravenous-Sodium Dichloroacetate. *Clinical Pharmacology & Therapeutics* **37**, 89-93.

Curry, S. H., Lorenz, A., Chu, P. I., Limacher, M., and Stacpoole, P. W. (1991). Disposition and Pharmacodynamics of Dichloroacetate (Dca) and Oxalate Following Oral Dca Doses. *Biopharmaceutics & Drug Disposition* **12**, 375-390.

Fisher, J. W., Mahle, D. A., and Abbas, R. (1998). A Human Physiological Based Pharmacokinetic Model for trichloroethylene and Its Matabolites, Trichloroacetic Acid and Free Trichloroethanol. *Toxicology and Applied Pharmacology* **152**, 339-359.

Fox, A. W., Sullivan, B. W., Buffini, J. D., Neichin, M. L., Nicora, R., Hoehler, F. K., Orourke, R., and Stoltz, R. R. (1996). Reduction of serum lactate by sodium dichloroacetate, and human pharmacokinetic-pharmacodynamic relationships. *Journal of Pharmacology and Experimental Therapeutics* **279**, 686-693.

Gonzalez-Leon, A., Merdink, J. L., Bull, R. J., and Schultz, I. R. (1999). Effect of pre-treatment with dichloroacetic or trichloroacetic acid in drinking water on the pharmacokinetics of a subsequent challenge dose in B6C3F1 mice. *Chemico-Biological Interactions* **123**, 239-253.

Gonzalez-Leon, A., Schultz, I. R., Xu, G. H., and Bull, R. J. (1998). Pharmacokinetics and metabolism of dichloroacetate in the F344 rat after prior administration in drinking water (vol 146, pg 189, 1997). *Toxicology and Applied Pharmacology* **148**, 194-194.

Gonzalez-Leon, A., Schultz, I. R., Xu, G. H., and Bull, R. J. (1997). Pharmacokinetics and metabolism of dichloroacetate in the F344 rat after prior administration in drinking water. *Toxicology and Applied Pharmacology* **146**, 189-195.

Greenberg, M. S., Burton, G. A., and Fisher, J. W. (1999). Physiologically based pharmacokinetic modeling of inhaled trichloroethylene and its oxidative metabolites in B6C3F(1) mice. *Toxicology and Applied Pharmacology* **154**, 264-278.

Guo, X., Dixit, V., Liu, H. P., Shroads, A. L., Henderson, G. N., James, M. O., and Stacpoole, P. W. (2006). Inhibition and recovery of rat hepatic glutathione S-transferase zeta and alteration of tyrosine metabolism following dichloroacetate exposure and withdrawal. *Drug Metabolism and Disposition* **34**, 36-42.

Haber, L. T., Maier, A., Gentry, P. R., Clewell, H. J., and Dourson, M. L. (2002). Genetic Polymorphisms in Assessing Interindividual Variability in Delivered Dose. *Regulatory Toxicology and Pharmacology* **35**, 177-197.

James, M. O., Cornett, R., Yan, Z., Henderson, G. N., and Stacpoole, P. W. (1997). Glutathione-dependent conversion to glyoxylate, a major pathway of dichloroacetate biotransformation in hepatic cytosol from humans and rats, is reduced in dichloroacetate-treated rats. *Drug Metabolism and Disposition* **25**, 1223-1227.

Jia, M. H., Coats, B., Chadha, M., Frentzen, B., Perez-Rodriguez, J., Chadik, P. A., Yost, R. A., Henderson, G. N., and Stacpoole, P. W. (2006). Human kinetics of orally and intravenously administered low-dose 1,2-C-13-dichloro acetate. *Journal of Clinical Pharmacology* **46**, 1449-1459.

Keys, D. A., Schultz, I. R., Mahle, D. A., and Fisher, J. W. (2004). A quantitative description of suicide inhibition of dichloroacetic acid in rats and mice. *Toxicological Sciences* **82**, 381-393.

Lantum, H. B. M., Cornejo, J., Pierce, R. H., and Anders, M. W. (2003). Perturbation of maleylacetoacetic acid metabolism in rats with dichloroacetic acid-induced glutathione transferase zeta deficiency. *Toxicological Sciences* **74**, 192-202.

Larson, J. L., and Bull, R. J. (1992). Metabolism and Lipoperoxidative Activity of Trichloroacetate and Dichloroacetate in Rats and Mice. *Toxicology and Applied Pharmacology* **115**, 268-277.

Lilly, P. D., Thornton-Manning, J. R., Gargas, M. L., Clewell, H. J., and Andersen, M. E. (1998). Kinetic characterization of CYP2E1 inhibition in vivo and in vitro by the chloroethylenes. *Archives of Toxicology* **72**, 609-621.

Lim, C. E. L., Matthaei, K. I., Blackburn, A. C., Davis, R. P., Dahlstrom, J. E., Koina, M. E., Anders, M. W., and Board, P. G. (2004). Mice deficient in glutathione transferase zeta/maleylacetoacetate isomerase exhibit a range of pathological changes and elevated expression of Alpha, Mu, and Pi class glutathione transferases. *American Journal of Pathology* **165**, 679-693.

Lukas, G., Vyas, K. H., Brindle, S. D., Lesher, A. R., and Wagner, W. E. (1980). Biological Disposition of Sodium Dichloroacetate in Animals and Humans after Intravenous Administration. *Journal of Pharmaceutical Sciences* **69**, 419-421.

Lumpkin, M. H., Bruckner, J. V., Campbell, J. L., Dallas, C. E., White, C. A., and Fisher, J. W. (2003). Plasma binding of trichloroacetic acid in mice, rats, and humans under cancer bioassay and environmental exposure conditions. *Drug Metabolism and Disposition* **31**, 1203-1207.

Merrill, E. A., Clewell, R. A., Robinson, P. J., Jarabek, A. M., Gearhart, J. M., Sterner, T. R., and Fisher, J. W. (2005). PBPK model for radioactive iodide and perchlorate kinetics and

perchlorate-induced inhibition of iodide uptake in humans. *Toxicological Sciences* **83**, 25-43.

Mori, M., Yamagata, T., Goto, T., Saito, S., and Momoi, M. Y. (2004). Dichloroacetate treatment for mitochondrial cytopathy: long-term effects in MELAS. *Brain & Development* **26**, 453-458.

Schultz, I. R., Merdink, J. L., Gonzalez-Leon, A., and Bull, R. J. (1999). Comparative toxicokinetics of chlorinated and brominated haloacetates in F344 rats. *Toxicology and Applied Pharmacology* **158**, 103-114.

Schultz, I. R., Merdink, J. L., Gonzalez-Leon, A., and Bull, R. J. (2002). Dichloroacetate toxicokinetics and disruption of tyrosine catabolism in B6C3F1 mice: dose-response relationships and age as a modifying factor. *Toxicology* **173**, 229-247.

Schultz, I. R., and Shangraw, R. E. (2006). Effect of Short-Term Drinking Water Exposure to Dichloroacetate on its Pharmacokinetics and Oral Bioavailability in Human Volunteers: A Stable Isotope Study. *Toxicology Sciences*.

Shangraw, R. E., and Fisher, D. M. (1999). Pharmacokinetics and pharmacodynamics of dichloroacetate in patients with cirrhosis. *Clinical Pharmacology & Therapeutics* **66**, 380-390.

Stacpoole, P. W., Henderson, G. N., Yan, Z. M., Cornett, R., and James, M. O. (1998a). Pharmacokinetics, metabolism, and toxicology of dichloroacetate. *Drug Metabolism Reviews* **30**, 499-539.

Stacpoole, P. W., Henderson, G. N., Yan, Z. M., and James, M. O. (1998b). Clinical pharmacology and toxicology of dichloroacetate. *Environmental Health Perspectives* **106**, 989-994.

Tong, Z., Board, P. G., and Anders, M. W. (1998a). Glutathione transferase zeta-catalyzed biotransformation of dichloroacetic acid and other alpha-haloacids. *Chemical Research in Toxicology* **11**, 1332-1338.

Tong, Z., Board, P. G., and Anders, M. W. (1998b). Glutathione transferase Zeta catalyses the oxygenation of the carcinogen dichloroacetic acid to glyoxylic acid. *Biochemical Journal* **331**, 371-374.

Tzeng, H. F., Blackburn, A. C., Board, P. G., and Anders, M. W. (2000). Polymorphism- and species-dependent inactivation of glutathione transferase zeta by dichloroacetate. *Chemical Research in Toxicology* **13**, 231-236.

Uden, P. C., and Miller, J. W. (1983). Chlorinate Acids and Chloral in Drinking-Water. *Journal American Water Works Association* **75**, 524-527.

U.S.EPA (2002). National Primary Drinking Water Regulations. *Fed Registr* Sec.141.64, 430

U.S.EPA (2003). Toxicological Review of Dichloroacetic Acid. *U.S. Envirometnal Protection Agency, Washington, DC*.

Wells, P. G., Moore, G. W., Rabin, D., Wilkinson, G. R., Oates, J. A., and Stacpoole, P. W. (1980). Metabolic Effects and Pharmacokinetics of Intravenously Administered Dichloroacetate in Humans. *Diabetologia* **19**, 109-113.

Williams, P. J., Lane, J. R., Turkel, C. C., Capparelli, E. V., Dziewanowska, Z., and Fox, A. W. (2001). Dichloroacetate: Population pharmacokinetics with a pharmacodynamic sequential link model. *Journal of Clinical Pharmacology* **41**, 259-267.

Yan Z, H. G., James MO, Stacpoole PW. (1997). Determination of dichloroacetate and its metabolites in human plasma by gas chromatography-mass spectrometry. *J Chromatogr B Biomed Sci Appl.* **703**, 75-84.

Table 3.1. Physiological model parameter values used in human PBPK model for DCA.

Parameters	Symbol	Human	Source
Bodyweight(kg)	BW	~70.0	Subject -specific when provided
Cardiac output (l/h/kg$^{3/4}$)	QCC	16.5 15.87 ♂ 17.73 ♀	Gender-specific when provided. (Brown *et al.*, 1997; Fisher *et al.*, 1998)
Blood flows (% of cardiac output)			
Liver	QLC	26.5 25.0 ♂ 27.0 ♀	Gender-specific when provided. (Brown *et al.*, 1997; Fisher *et al.*, 1998)
Kidney	QKC	17.5 19.0 ♂ 17.0 ♀	Gender-specific when provided. (Brown *et al.*, 1997; Fisher *et al.*, 1998)
Rapidly perfused	QRC	32.0	(Brown *et al.*, 1997; Fisher *et al.*, 1998)
Slowly perfused	QSC	24.0	(Brown *et al.*, 1997; Fisher *et al.*, 1998)
Tissue Volumes (% of body weight)			
Plasma	VPLAC	4.4	(Merrill *et al.*, 2005)
Liver	VLC	2.6	(Brown *et al*., 1997)
Kidney	VKC	0.44	(Brown *et al*., 1997)
Rapidly perfused	VRC	9.86	(Brown *et al*., 1997)
Slowly perfused	VSC	74.7	(Brown *et al*., 1997)

Table 3.2. Chemical specific parameter values for human PBPK model for DCA.

Parameters	Symbol	Value	Source
Partition coefficient			
Liver:Blood	PL	1.08	Abbas and Fisher, 1997
Kidney:Blood	PK	0.74	Abbas and Fisher, 1997
Rapidly perfused:Blood	PR	1.08	Abbas and Fisher, 1997
Slowly perfused:Blood	PS	0.11	Abbas and Fisher, 1997*
Metabolic and clearance parameters			
Maximal rate of GSTzeta velocity ($mg/h/kg^{0.75}$)	V_{maxc0}	50	Estimated
Michaelic-Menten affinity constant (mg/l)	K_m	6.0	Tong *et al.*, 1998a
Inhibition constant (mg^{-1})	k_d	0.004	Estimated
Degradation rate constant (h^{-1})	k_{de}	0.004	Estimated
Urinary excretion (l/h-kg)	Cl_{rc}	0.7×10^{-3}	Curry *et al.*, 1991
Oral absorption parameters following drinking water injection			
Transfer rate from the 1st GI compartment to the liver (h^{-1})	K_{a1}	0.01	Estimated
Transfer rate from the 1st to the 2nd GI compartment (h^{-1})	K_{a2}	7.0	Estimated
Transfer rate from the 2nd GI compartment to the liver (h^{-1})	K_{a3}	7.0	Estimated
Plasma protein binding parameters			
Maximum capacity (mg)	B_{max}	0.06	Estimated
Affinity constant (mg/l)	K_{mb}	0.001	Estimated
Dissociation constant (h^{-1})	K_{unb}	0.16	Estimated

* Abbas and Fisher (1997) value of 0.37 reduced to 0.11 for humans.

Table 3.3. Optimized parameter values for metabolic constants (V_{maxc0} and k_d) and oral uptake constants (K_{a2} and K_{a3}) using individual DCA plasma pharmacokinetic data from Shultz and Shangraw (2006).

Subject	Gender	Weight (kg)	V_{maxc0} ($mg/h/kg^{0.75}$)	k_d (mg^{-1})	K_{a2} (h^{-1})	K_{a3} (h^{-1})
1	M	90	113.2	0.001	5.1	5.1
2	F	66	71.1	0.0	5.3	5.3
3	F	74.5	118.8	0.011	9.3	9.1
5	M	66.6	113.2	0.002	5.6	2.9
6	F	78.3	252.2	0.016	6.9	6.9
7	M	64.2	89.3	0.0	4.6	4.0
8	F	59	61.4	0.005	7.9	7.9
9	M	79	97.9	0.005	9.0	9.0
10	F	45	225.8	0.011	7.7	12.5
11	F	69.5	36.7	0.006	9.5	9.5
12	M	78.6	280.0	0.010	8.8	8.9
13	M	73.5	58.4	0.0	11.8	12.0
15	F	67.4	60.0	0.006	17.7	5.7
16	M	55.9	83.1	0.0	8.0	8.1
17	F	67.8	51.1	0.0	7.7	13.3
18	M	73.2	45.8	0.0	8.9	8.9
Mean		69.3	109.9	0.005	8.4	8.1
SD		10.6	75.7	0.005	3.1	3.0

Table 3.4. Normalized sensitivity coefficients of selected parameters in the PBPK model for DCA, based on model predictions of DCA plasma AUC in various exposure scenarios.

Model Parameters	Normalized sensitivity coefficients					
	50mg/kg iv (single) $AUC_{0\rightarrow24h}$	**50mg/kg iv (2 h interval) $AUC_{0\rightarrow24h}$**	**0.3mg/kg iv (day 0) $AUC_{0\rightarrow24h}$**	**2mg/kg oral (day 0) $AUC_{0\rightarrow24h}$**	**2.5 µg/kg/day iv $AUC_{0\rightarrow120h}$**	**2.5 µg/kg/day oral $AUC_{0\rightarrow360h}$**
QCC	-0.05	-0.02	**-0.54**	-0.02	**-0.64**	-0.15
QLC	-0.09	-0.03	**-0.50**	_	**-0.57**	-0.12
V_{maxc0}	**-0.88**	**-0.53**	**-0.50**	**-1.05**	-0.33	**-0.72**
K_m	0.47	0.41	0.43	**0.92**	0.33	**0.72**
k_d	**0.76**	0.22	0.21	0.42	_	_
k_{de}	_	_	_	_	_	_
K_{a2}	_	_	_	0.04	_	-0.09
K_{a3}	_	_	_	0.03	_	-0.08
B_{max}	_	_	0.14	0.06	**0.96**	**1.01**
K_{mb}	_	_	_	_	-0.07	-0.08
K_{unb}	_	_	-0.10	-0.05	**-0.81**	**-0.90**

Note. The coefficients less that 0.01 are not reported.

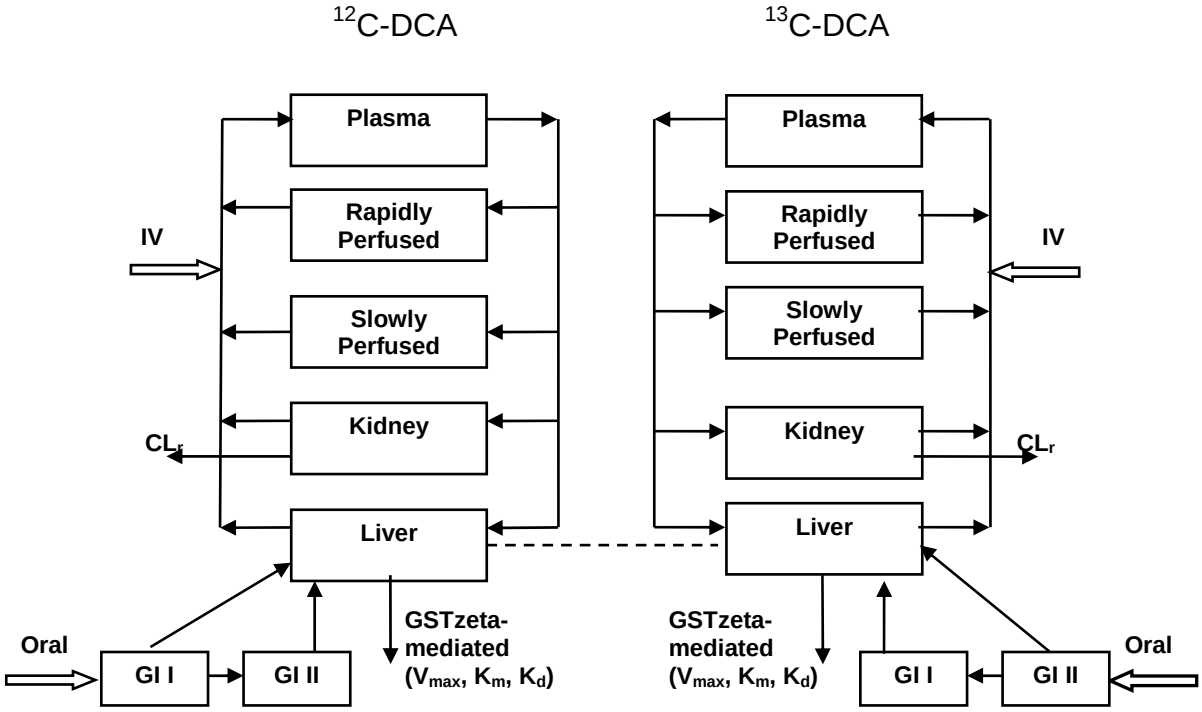

Figure 3.1 Schematic of DCA PBPK model of human. Each isotope was described separately to simulate the data of Schultz and Shangraw (2006). Metabolic Interaction was added to the liver compartment to maintain the separate description of the isotopes.

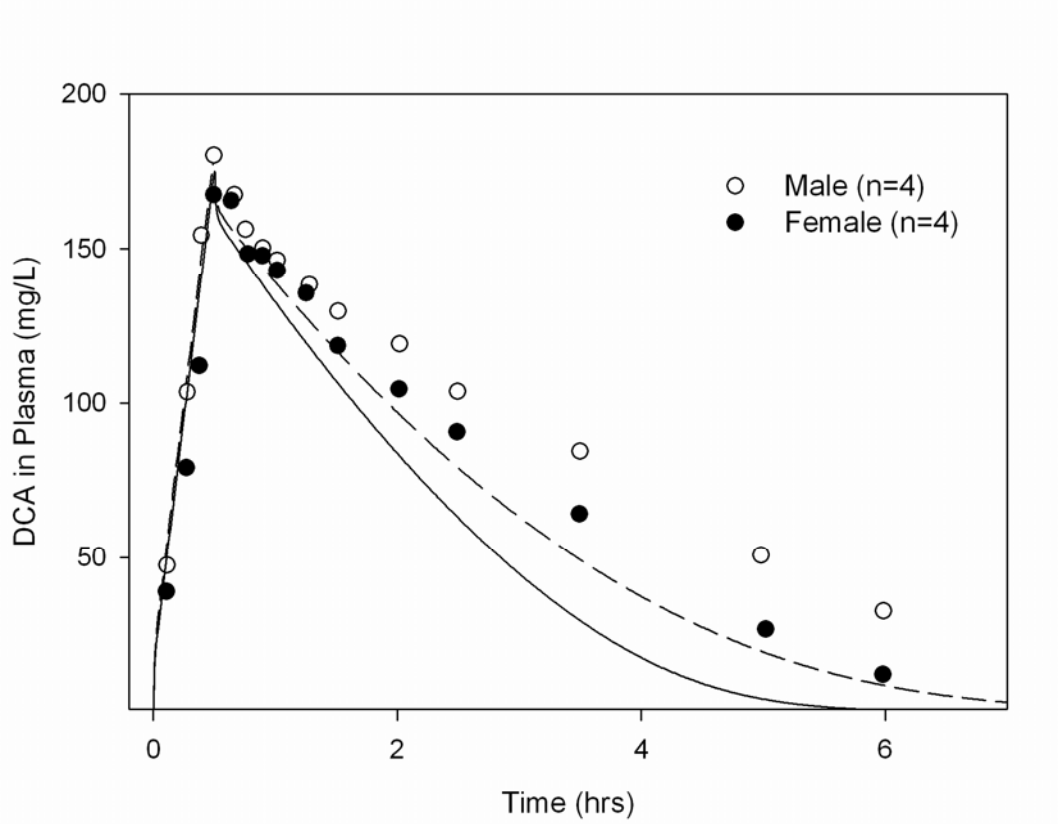

Figure 3.2 Model predicted (—) *vs.* observed mean DCA plasma concentrations for four female (●) and model predicted (----) *vs.* observed mean DCA plasma concentrations for four male (○) subjects following a 0.5 h intravenous infusion of 50 mg/kg DCA. The measured values were originally reported by Chu (1987).

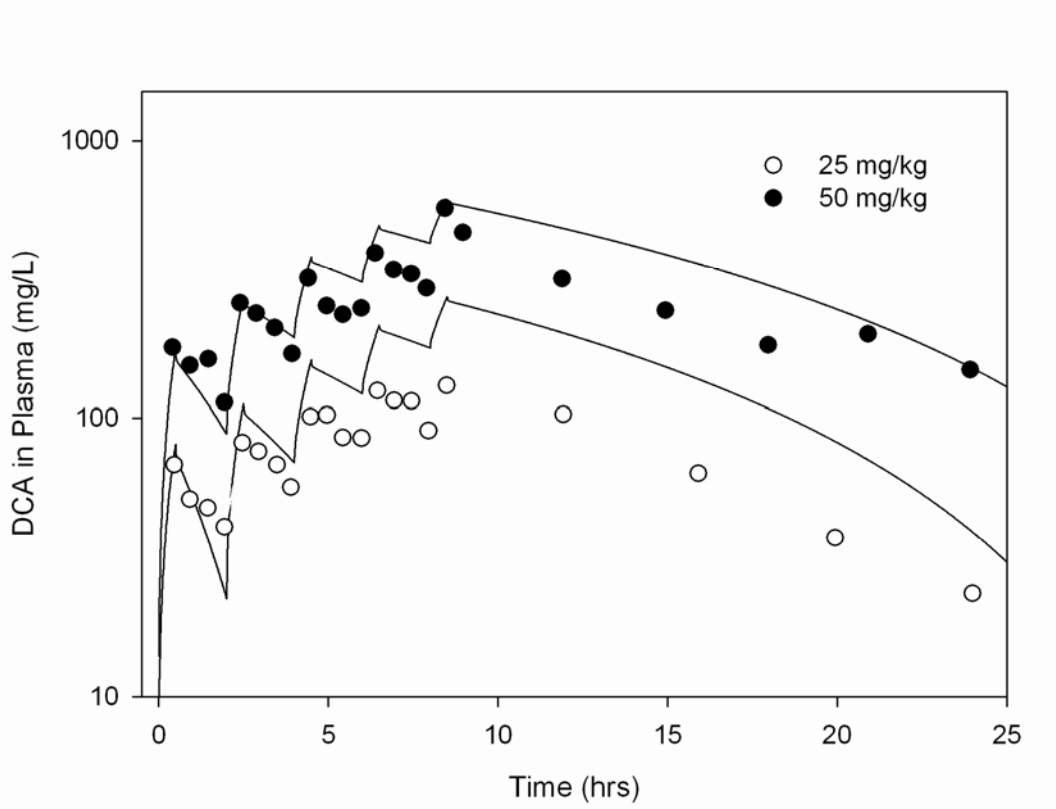

Figure 3.3 Model predicted and observed mean DCA plasma concentrations following 5-repeated 0.5 h intravenous infusions at 2 h intervals. The concentration-time course data for two doses are presented: 25 mg/kg (○, n=5) and 50 mg/kg (●, n=4). The measured data was originally reported by Chu (1987).

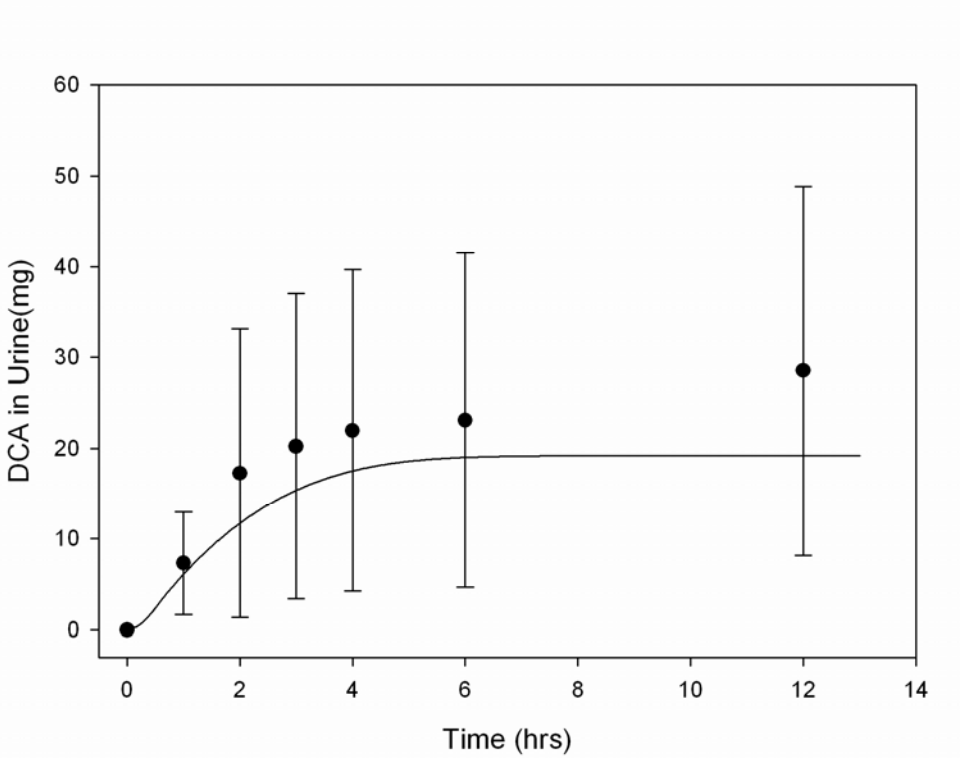

Figure 3.4 Model prediction (—) of cumulative amount of DCA excretion in the urine vs. average of 8 subjects after a single 50mg/kg iv administration (● ± S.D.). Measured data originally reported by Chu (1987).

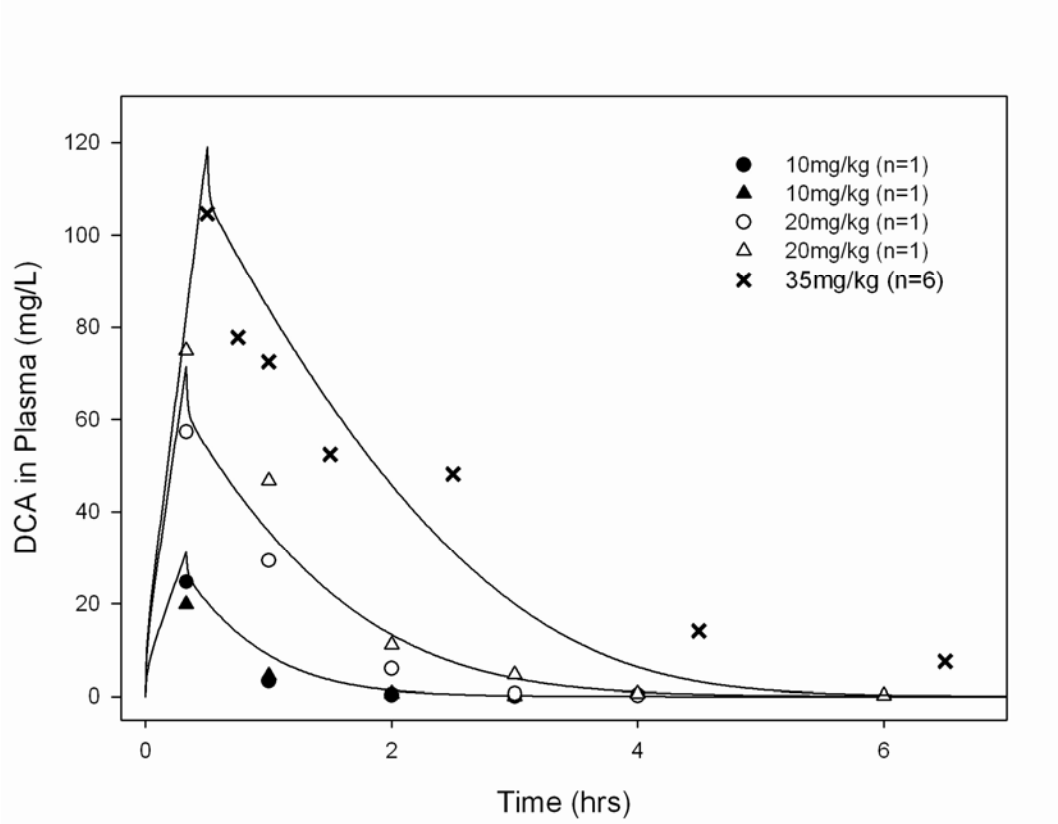

Figure 3.5 Model predicted (—) and observed DCA plasma concentrations of 2 subjects following 10 mg/kg (●,▲), 2 subjects following 20 mg/kg (○, Δ) intravenous infusions (20 min) of DCA (originally reported by Lukas *et al.* 1980) and the mean plasma concentrations (**x**, n=6) following 0.5 h intravenous infusion of 35 mg/kg DCA reported by Shangraw and Fisher (1996).

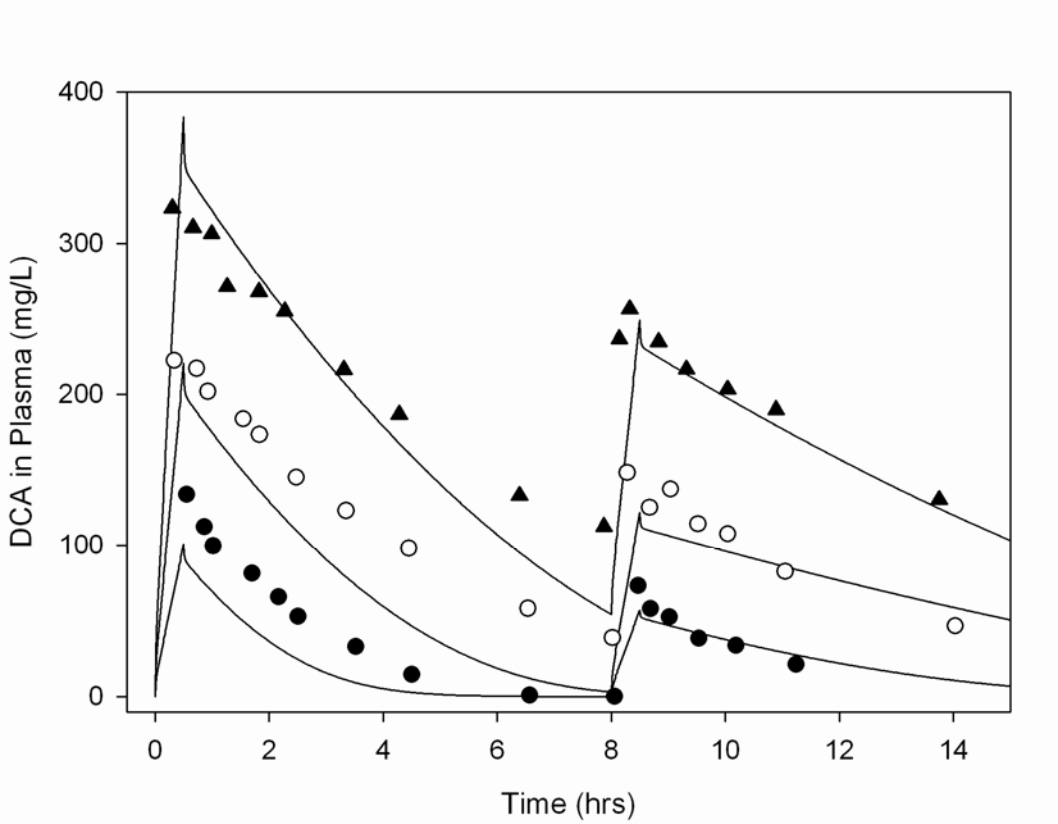

Figure 3.6 Model predicted (—) and observed mean DCA plasma concentrations after two 0.5 h intravenous infusions of DCA at 0 and 8 h. The administered doses of DCA were 30 + 15 mg/kg (●, n=9), 60 +30 mg/kg (○, n=9) and 100 +50 mg/kg (▲, n=9). Experimental data was originally reported by Fox *et al.* (1996).

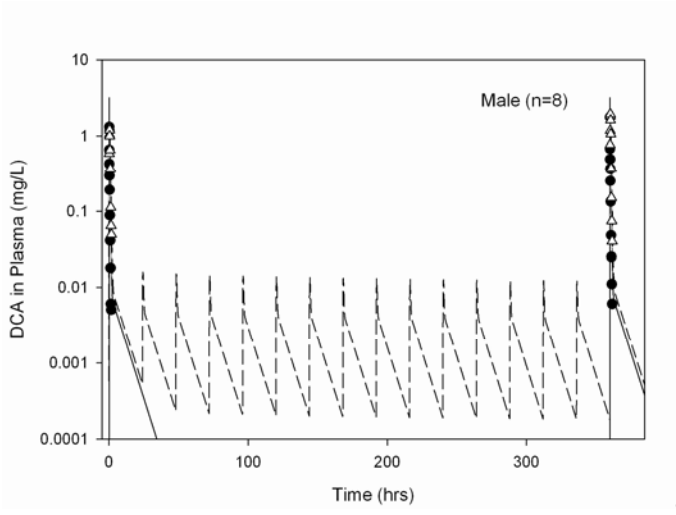

a.

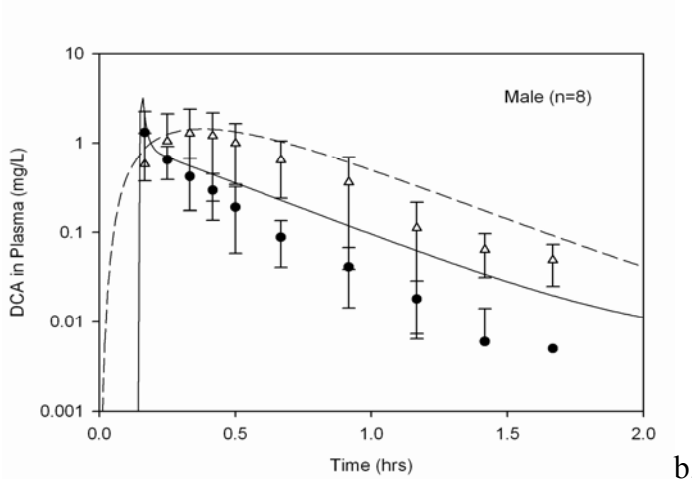

b.

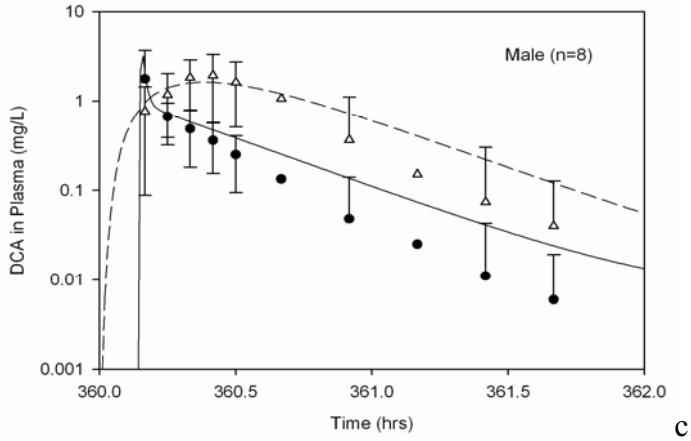

c.

Figure 3.7 Model predictions of ^{12}C-DCA (----) and ^{13}C-DCA (—) vs. observed ^{12}C-DCA plasma concentration (Δ ± SD) and ^{13}C-DCA plasma concentration (● ± SD) in males; (a) the period of study (15 days); (b) the initial 2 h following the first 2mg/kg oral and 0.3mg/kg iv administration on day 0, and (c) the initial 2 h following the second 2mg/kg oral and 0.3mg/kg iv administration on day 15. Data from Schultz and Shangraw (2006).

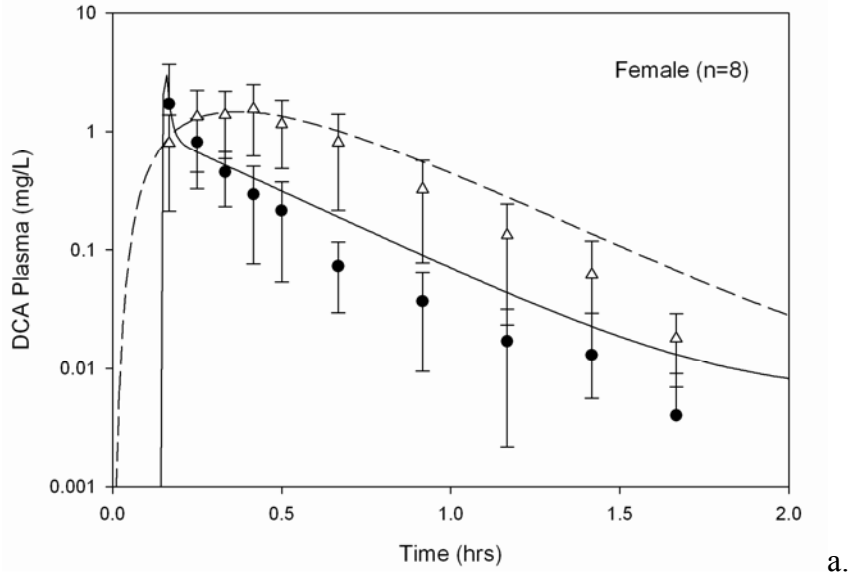

a.

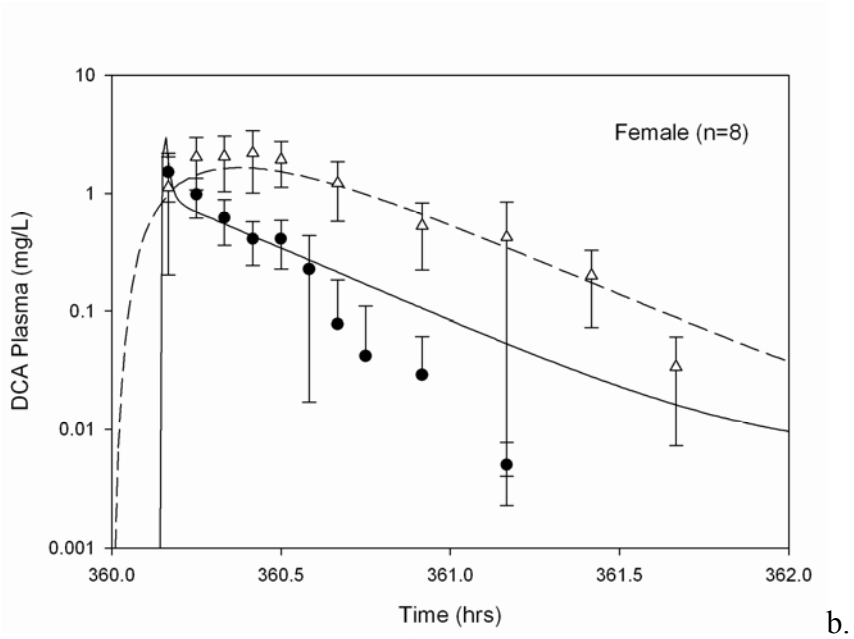

b.

Figure 3.8 Model predictions of ^{12}C-DCA (----) and ^{13}C-DCA (—) vs. observed ^{12}C-DCA plasma concentration (Δ ± SD) and ^{13}C-DCA plasma concentration (● ± SD) in females; (a) the initial 2 h following the first 2mg/kg oral and 0.3mg/kg iv administration on day 0, and (b) the initial 2 h following the second 2mg/kg oral and 0.3mg/kg iv administration on day 15. Data from Schultz and Shangraw (2006).

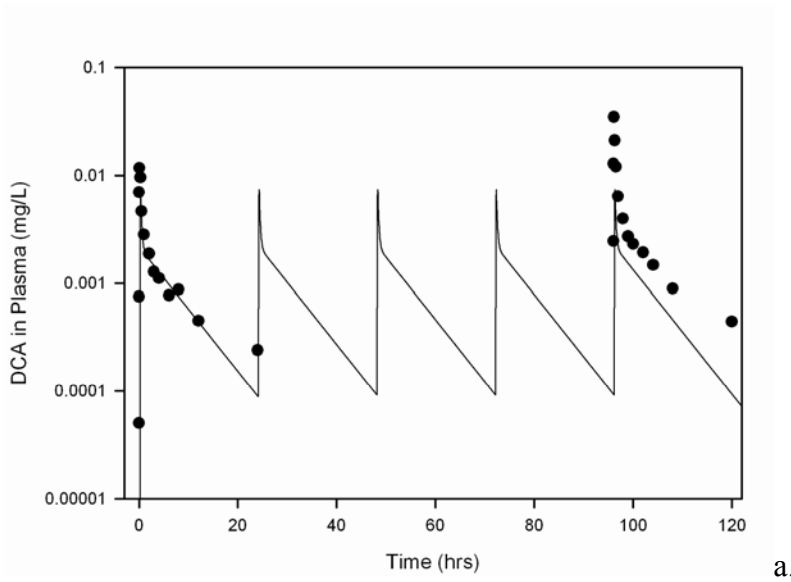

a.

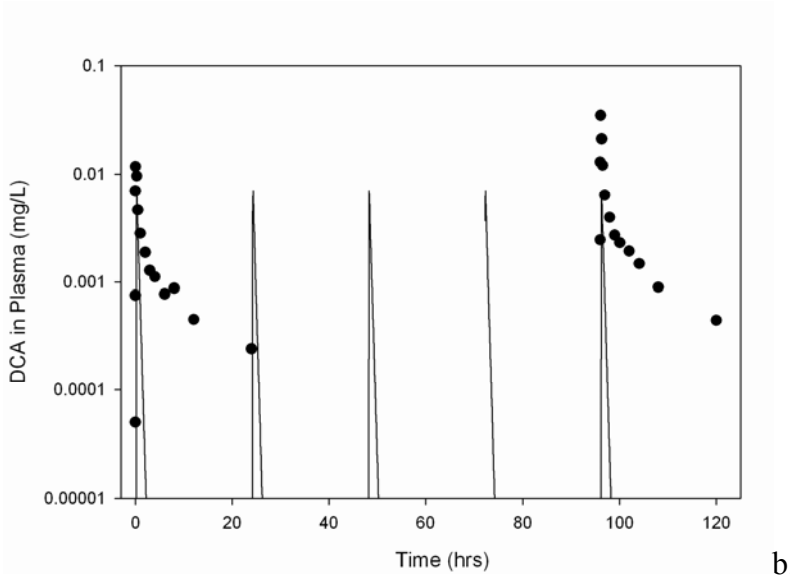

b.

Figure 3.9 Model predicted (—) and observed ^{13}C-DCA (●) concentrations following a 10 min intravenous infusion of 2.5 μg/kg/day for 5 days. Inset (a) shows the final model with the added low capacity plasma protein binding and inset (b) shows the initial model without binding. The measured data originally reported by Jia *et al.*(2006).

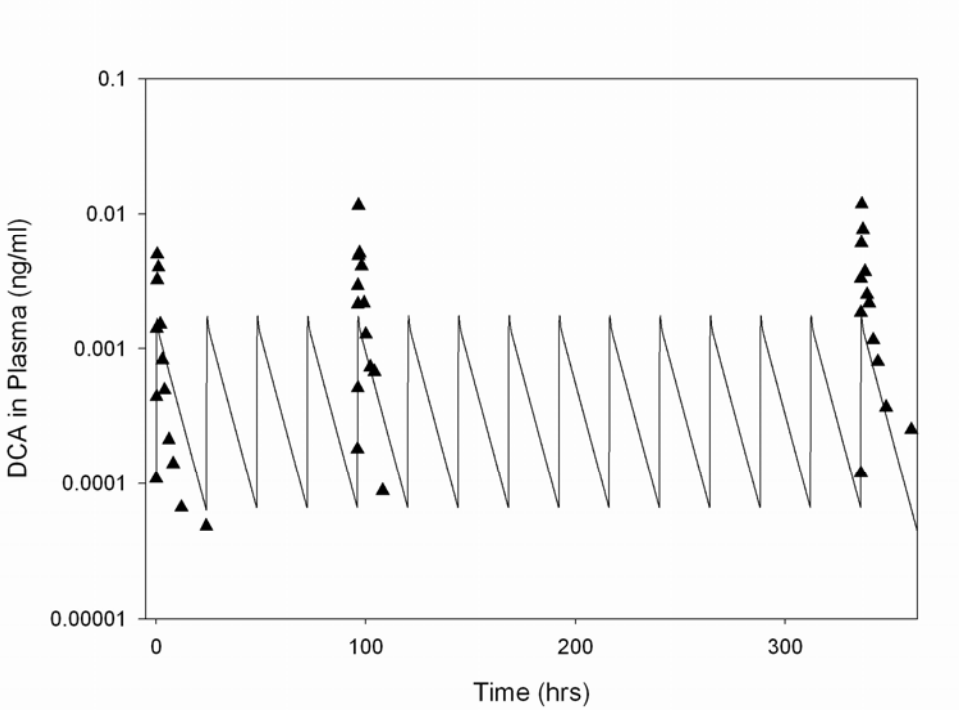

Figure 3.10. Model predicted (—) and observed ^{13}C-DCA concentration (▲) following water ingestion of 2.5 μg/kg/day DCA in 200 mL of water for 15 days. Data originally reported by Jia *et al.* (2006).

CHAPTER 4

QUANTITATIVE DESCRIPTION OF MATERNAL-FETAL TRANSPORT OF NUCLEOSIDE REVERSE TRANSCRIPTASE INHIBITORS IN PREGNANT RATS: A PHYSIOLOGICALLY-BASED PHARMACOIKNETIC MODELING STUDY

Ting Li, S.R. Lewis, and C.A.White. To be submitted to *Journal of Pharmaceutical Sciences*.

Abstract

Zalcitabine (ddC), lamivudine (3TC), zidovudine (AZT) and abacavir (ABC) are nucleoside analogue reverse transcriptase inhibitors (NRTIs) that are used alone or in highly active antiretroviral therapy (HAART) to treat human immunodeficiency virus-infection in pregnant women. However, the in vivo information about the placental transport and fetal disposition of these drugs is limited. A physiologically based pharmacokinetic (PBPK) model was developed to describe the disposition of NRTIs in pregnant rats. The model was composed of seven compartments: plasma, liver, kidney, rest of the body, placenta, fetuses and amniotic fluid. The kinetics of each drug was described by a set of mass balance differential equations for each tissue compartments. Model parameters were obtained either from the literature or optimized to the experimental data. Three hypotheses of placental transfer of NRTIs were tested using different model structures: flow-limited, simple-diffusion limited and active-transport. The active transport model provided the best fit to all the experimental data. Thus, our model suggests active transport may be an important mechanism of NRTIs fetal disposition in pregnant rats.

Introduction

Zalcitabine (ddC), Lamivudine (3TC), zidovudine (AZT) and abacavir (ABC) are nucleosides analogs belonging to the largest class of antiretroviral drugs called nucleoside reverse transcriptase inhibitors (NRTIs) (Table 4.1). NRTIs are pro-drugs and the active forms are the triphosphate anabolite formed intracellularly, which compete with natural deoxynucleotides for incorporation into the viral DNA and inhibit viral reverse transcriptase. NRTIs are used widely in HIV-infected pregnant women to prevent mother-to-child HIV transmission (MTCT) as well as primary therapy of maternal HIV infection. For example, a three-part regimen of AZT reduces the risk of MTCT by 70% (P.H.G.W.G., 2006). Doses of 3TC, AZT and ABC administered during pregnancy are equal to those prescribed for non-pregnant adults (Capparelli *et al.*, 2005). Currently, there have been no published clinical studies of ddC in pregnant women. When administered near term, the concentration ratios of 3TC, AZT and ABC in the mother plasma, cord blood are approximately 1 (Mirochnick and Capparelli, 2004). ddC, 3TC, AZT and ABC have been shown to cross the placenta in human placenta perfusion studies and *in vivo* animal models (Capparelli *et al.*, 2005; Pacifici, 2005). Nucleoside analogue drugs are known to induce mitochondrial dysfunction related toxicity in HIV infected patients. Very limited data exist regarding the safety of NRTIs in pregnancy. No carcinogenicity and teratogenicity has been observed for all the NRTIs in mice or rats at therapeutic doses, though ddC and ABC have shown teratogenic effects and developmental toxicities in rats at high doses (Briggs, 2005).

The placental transfer of NRTIs directly affects fetal exposure to the drug and also affects the efficacy of treatment and toxicity in the fetus. The placental transport rate of a compound correlates to its chemical properties. Drugs with low molecular weight (<500 Da), low

ionization, low protein binding and high lipid solubility pass the placenta through simple diffusion (Polin *et al.*, 2004). Diffusion of these substances is governed by Fick's law. With highly lipid soluble molecules, placental uptake becomes rate-limited by blood flow to the placenta. On the other hand, polar, hydrophilic molecules pass through the membrane slowly, hence their transfer across the placenta will be membrane-permeation limited (Unadkat *et al.*, 2004). In addition, transporters in the placental tissue may play a crucial role in the transfer of chemicals through facilitative diffusion and efflux transport. Several transporters have been identified in both human and rat placentas that take nucleoside analogues as substrates (Ganapathy *et al.*, 2000; Leazer and Klaassen, 2003; Unadkat *et al.*, 2004). Transporters may not only affect the maternal-fetal transfer of single drug but also lead to drug-drug interaction in combination therapies.

Clinical studies and e*x vivo* human placental infusion experiments suggest NRTIs pass the placenta by simple diffusion (Mirochnick and Capparelli, 2004). However, due to the ethical and technical difficulties, the available *in vivo* pharmacokinetic data are limited to the drug concentrations in the maternal plasma, newborn plasma, cord blood and amniotic fluid during labor. Under these non-steady state conditions, the maternal and fetal blood drug concentrations are consistently changing in a non-parallel fashion and normally no kinetic data are available for the placenta. Rats have been used successfully used as animal models to study drug dispositions in during pregnancy because rat placenta is similar to that of humans (*i.e.*, hemodynamic and hemochorial) (Boike *et al.*, 1989; Brown *et al.*, 2002; Clark *et al.*, 2006). Recent studies in pregnant rats using mono- and dual-therapy (3TC/AZT or ABC/AZT) suggest complex mechanisms and drug-drug interactions related to the placental transport of NRTIs (Lewis, 2006).

Physiologically-based pharmacokinetic (PBPK) models are an effective tool to study the disposition of drugs during pregnancy because the model structures are based, to a large extent, on physiological and biomedical reality. PBPK models of pregnancy employ developmental equations to describe the physiological changes of both the mother and the embryo/fetuses (O'Flaherty *et al.*,1992; Gentry *et al.*, 2002). Several general pregnancy formats along with five hypothetical model structures have been developed to investigate the mechanisms of the placental transport of chemicals (Terry *et al.*, 1995; Welsch *et al.*, 1995; Corley *et al.*, 2003). The objective of this research was to develop a PBPK model to investigate the mechanisms of trnasplacnetal transfer of NRTIs (ddC, ABC, 3TC and AZT) and quantitatively describe their fetal exposures in pregnant rats.

Materials and methods

Experimental data. The kinetic data used in developing the PBPK model were reported in a previous study (Lewis, 2006). Briefly, pregnant Sprague-Dawley rats with an average weight of 328 ± 20 g were dosed *via* intravenous bolus on day 19 of gestation. Four dosing groups were used in the study: (i) ddC monotherapy (25mg/kg) (n=6); (ii) 3TC monotherapy (25 mg/kg) (n = 6); (iii) AZT monotherapy (25 mg;/kg) (n = 6); and (iv) ABC monotherapy (25mg/kg) (n=6). Blood samples of 150 to 250 µl were collected at 5, 15, 30, 45, 60, 90, 120, 180, 240, 300, 360 min after dosing. Fetuses were harvested at 5, 15, 30, 45, 60, 90, 120, 180, 240, 300, 360 min. Placental and fetal tissues were homogenized in two volumes of deionized water (wt/vol). Amniotic fluid samples were withdrawn from the fetal sacs with an 18-gauge needle prior to harvesting the fetus. All samples were stored at –20 °C until analysis. ddC, 3TC, AZT and ABC concentrations in mother plasma, placenta, fetus and amniotic fluid were determined by HPLC or

LC-MS (Lewis, 2006). The measured concentration-time course data in different tissues following each NRTI therapy are shown in Fig. 4.1.

Physiological parameters. Physiological parameters used in the PBPK model are summarized in Table 4.2. All tissue volumes and blood flows were scaled to body weight. Volumes of the placenta, fetuses and amniotic fluid were measured by Lewis (2006). The maternal blood flow to each conceptus through yolk sac and chorioallantoic placenta on gestation day 19 was calculated using the equation of O'Flaherty *et al.* (1992) and multiplied by a factor of 10 (as an average number of fetuses per dam). The equation used to calculate the placenta blood flow to each fetus was:

$$Q_{pla} = 2.2/24 \times \exp(-0.23 \times (GD - 10)) + 0.1207 \times (GD - 12)^{4.36} \qquad (4.1)$$

where Q_{pla} is the blood flow to the placenta, GD is the gestation days. The blood volume for placenta is expressed as a fraction of the tissues total volume and was taken from literature (Emond *et al.*, 2004)

Partition coefficients. The octanol:buffer partition coefficient (LogP) for ddC, 3TC, AZT and ABC are -1.3, -0.97, 0.01 and 1.2, respectively (Strazielle and Ghersi-Egea, 2005). Liver:blood, kidney:blood and muscle:blood partition coefficients for each drug was estimated from $K_{o/w}$ by the algorithm of Poulin and Krishnan (1995). Because placneta is richly perfused with blood flow, the partition coefficients for placenta:blood was set to the same value as liver:blood (Gargas *et al.*, 2000; Clewell *et al.*, 2003). The partition coefficient for fetus:blood was set to the same as muscle:blood partition coefficient (Gabrielsson *et al.*, 1984; Fisher *et al.*, 1989). The partition coefficients for body:blood along with the permeability-surface area products (PS_b) were estimated by fitting the maternal plasma kinetic data (Table 4.3).

Model development for pregnant rat. The model consists of seven compartments (plasma, liver, kidney, rest of the body, placenta, fetuses and amniotic fluid (Fig. 4.2a). The distribution into the liver and kidney were blood-flow limited and the distribution of each drug into 'rest of the body' was described as diffusion limited (i.e., the body was divided into extracellular and intracellular compartments). The primary elimination routes of ddC, 3TC and AZT in rats are urinary excretion and were described as first-order eliminations (CL_r) from the kidney. However, ABC in rats is eliminated by metabolism in the liver (Kumar et al., 1999) so the elimination of ABC from the dam was described as first-order clearance (CL_h) from the liver compartment. Because the experimental data were available for the homogenized fetuses, the fetuses were treated as a single compartment. Exchange of the drug between fetuses and amniotic fluid was described by bidirectional clearance. The drug transfer from the fetuses to the amniotic fluid (CL_{faf}) was assumed to be fetal urinary excretion and the drug transfer from the amniotic fluid to the fetuses (CL_{aff}) was assumed to due to the re-uptake (swallowing and diffusion) of the drug from the amniotic fluid by the fetuses. Physiologically speaking, exchange of the drug between amniotic fluid and placental compartments was minor compared to the circulation between amniotic fluid and fetuses (Brace, 2004). In order to keep the model simple, placental-amniotic fluid drug transfer was was not included in present model. Three model structures were developed to describe the placental transport of NRTIs: flow-limited, simple-diffusion and active-transport models.

Flow-limited model (FLM). In the FLM, the distribution of the drug into the placenta is assumed instantaneous and the rate of transport of drug into the placenta is limited by blood flow to the placenta on day 19 of gestation (Fig. 4.2a). The drug was transferred to the fetuses through

the maternal blood flow to the fetuses. The rates of change of drugs in the placental, fetal and amniotic fluid compartments are given by:

$$Vpla\frac{dCv_{pla}}{dt} = Q_{pla} \times (Ca - Cv_{pla}) + Q_{con} \times C_{fet} / P_{fet} - Q_{con} \times Cv_{pla} \quad (4.2)$$

$$Vfet\frac{dC_{fet}}{dt} = Q_{con} \times (Cv_{pla} - C_{fet} / P_{fet}) - CL_{faf} \times C_{fet} / P_{fet} + CL_{aff} \times C_{af} \quad (4.3)$$

$$Vaf\frac{dC_{af}}{dt} = CL_{faf} \times C_{fet} / P_{fet} - CL_{aff} \times C_{af} \quad (4.4)$$

where V_{pla}, V_{fet} , and V_{af} are the volume of placental, fetal and amniotic fluid compartments, respectively. Cv_{pla}, C_{fet} are the drug concentration in placental venous blood and in the fetuses, respectively. Q_{con} is the blood flow to the conceptus, P_{fet} is the fetus:blood partition coefficient and P_{pla} is the placenta:blood partition coefficients. CL_{faf} and CL_{aff} are the bidirectional clearance from fetuses to amniotic fluid.

Simple diffusion model (SDM). In the SDM, the placental compartment was described as diffusion-limited and the tissue was divided into extracellular and intracellular compartments. The transfer of the drug to the placental tissue was controlled by passive diffusion from the extracellular compartment (tissue blood) to the intracellular compartment (tissue cellular matrices). The transport of the drug from the placenta to the fetus was also described with passive diffusion (Fig. 4.2b). The rate of change of each drug in the placenta was given by:

$$Vpla_{extra}\frac{dCv_{pla}}{dt} = Q_{pla} \times (Ca - Cv_{pla}) + PA_{pla} \times (C_{plat} / P_{pla} - Cv_{pla}) \quad (4.5)$$

$$Vpla_{\text{int}ra}\frac{dC_{plat}}{dt} = PA_{pla} \times (Cv_{pla} - C_{plat}) + PA_{pf} \times (C_{fet} / P_{fet} - C_{plat} / P_{pla}) \quad (4.6)$$

where $Vpla_{extra}$ and $Vpla_{intra}$ are the placental blood volume, the placenta tissue volume. PA_{pla} and PA_{pf} are the permeation coefficient-surface area-cross products (l/h); Ct_{pla} is the drug concentration in intracellular portion of placenta.

The rate of change of drugs in the fetuses is given by:

$$Vfet\frac{dC_{fet}}{dt} = PA_{pf} \times (C_{plat} / P_{pla} - C_{fet} / P_{fet}) - CL_{faf} \times C_{fet} / P_{fet} + CL_{aff} \times C_{af} \quad (4.7)$$

Active-transport model (ATM). In the prior classical PK analysis (Lewis, 2006), the estimated clearance from the placental to maternal compartment was twice as large as the clearance from the maternal to the placental compartment for both 3TC and AZT. This observation suggested that passive diffusion may not be the only mechanism involved in the placental transfer of NRTIs. In the ATM structure, the drug transfer rates from the maternal blood to the placenta and from placenta to the maternal blood were allowed to differ from each other (Fig. 4.2c). The equations used to describe the rates of change of each drug in the placenta were:

$$Vpla_{exra}\frac{dCv_{pla}}{dt} = Q_{pla} \times (Ca - Cv_{pla}) - CL_{mp} \times Cv_{pla} + CL_{pm} \times C_{plat} / P_{pla} \quad (4.8)$$

$$Vpla_{intra}\frac{dC_{plat}}{dt} = CL_{mp} \times Cv_{pla} - CL_{pm} \times C_{plat} / P_{pla} + CL_{fp} \times C_{fet} / P_{fet} - CL_{pf} \times C_{plat} / P_{pla} \quad (4.9)$$

where Cl_{mp} is the distribution clearance from maternal blood portion to the intracellular portion of the placenta; CL_{pm} is the distribution clearance from intracellular portion to the maternal blood portion the placenta, Cl_{pf} is the distribution clearance from placenta to the fetuses and CL_{fp} is the distribution clearance from fetuses to the placenta.

Parameter estimation. All simulations were performed in acslXtreme (V 2.0.1.2, Aegis Technologies Group Inc., Huntsville, AL). The maximum likelihood method implemented in the optimization function was used to estimate adjustable parameters. The Nelder-Mead algorithm

was used and error model was allowed to vary to find the best fit. In all three model descriptions, the partition coefficient for rest of the body:blood (PB), the permeability-surface area products (PS_B) and the maternal clearance (CL_{renal} for ddC, 3TC and AZT; CL_{int} for ABC) were estimated simultaneously by fitting the concentration-time course data in the maternal plasma. CL_{faf} and CL_{aff} in FLM, PA_{pla}, PA_{pf}, CL_{faf} and CL_{aff} in SDM, CL_{mp}, CL_{pm}, CL_{pf}, CL_{fp}, CL_{faf} and CL_{aff} in ATM were then estimated simultaneously for each model by fitting the concentration-time course data in all the tissues.

Statistical analysis. The optimal value of the log-likelihood (LLF) of each model was reported by the software. The acceptability of the models was compared using Akaike Information Criterion (AIC). The test statistic was calculated as:

$$AIC = -2 \times LLF_i + 2P \tag{4.10}$$

where LLF_i is the optimal value of the log-likelihood of the ith model and P is the number of adjustable parameters for the particular model. The model with the smallest AIC the model is superior. The AIC of each model was calculated for each drug therapy and then added together to derive a grand total AIC for all the experimental data.

Results

Predictions of disposition of ddC. The FLM, SDM and ATM model structures provided good fits to the ddC concentration in the maternal plasma and amniotic fluid (Fig. 4.3 a-c). As shown in Fig. 4.3a, the FLM under-predicted ddC concentration in the placenta compartment and over predicted the ddC concentration in the fetuses within the first 2 hours post-administration while adequately describing the later time points. The SDM improved the model fit to the fetal ddC concentration in the early time points compared with FLM but over-predicted the fetal concentration over the whole 6 hours (Fig. 4.3b). The ATM model fit the ddC concentration in

all the tissues adequately (Fig. 4.3c). Estimated CL_{mp} and CL_{pm}, CL_{pf} and CL_{fp}, CL_{faf} and CL_{aff} for ddC (along with 3TC, AZT and ABC) by ATM are listed in Table 4.4.

Predictions of disposition of 3TC. The FLM fit the 3TC concentration in the maternal plasma and amniotic fluid well but over-predicted the concentration in both placenta and fetuses (Fig. 4.4a). The SDM improved the predication as compared to the FLM (Fig. 4.4b). However, the model over-predicted the concentration in the placental and fetal compartments. Fig. 4.4c demonstrates that the ATM successfully described the observed 3TC concentrations in all the compartments.

Predictions of disposition of AZT. The FLM over-predicted the AZT concentration in the placental and fetal compartments immediately after the administration, but provided reasonable fits to the drug disposition in the maternal plasma and amniotic fluid (Fig. 4.5a). The SDM over-predicted AZT concentration in the placenta and fetuses (Fig. 4.5b). The ATM described adequately the observed concentrations of AZT in all the tissues (Fig. 4.5c).

Predictions of disposition of ABC. FLM over predicted the observed ABC concentration in the placental and fetal compartment within 1 hour post-administration though the clearance of ABC was described adequately (Fig. 4.6a). The SDM failed to simulate the clearance of ABC in the placental and fetal compartments (Fig. 4.6b). Fig. 4.6c demonstrates that ATM was able to describe the disposition of ABC in all the tissues.

Model discrimination. The AIC values of FLM, SDM and ATM are listed in Table 4.5 The active-transport model had the smallest individual and grand total AIC, thus the ATM provided the best description for NTRI disposition in pregnant rats.

Discussion

Different PBPK model structures were developed in multiple studies to investigate the mechanism of chemical disposition in the body (Collins *et al.*, 1999; Keys *et al.*, 1999; Keys *et al.*, 2000). Terry et al. (1995) developed 5 model structures to study the disposition of 2-Methoxyacetic acid in the pregnant mouse (Terry *et al.*, 1995). In present study, the active transport model structure adequately captured the observed disposition data of four NTRIs in pregnant rats on GD 19. The flow-limited placental transport model predicted the higher peak concentration in the placental and fetal compartment almost immediately after the administration (Fig. 4.3a, 4.4a, 4.5a and 4.6a). The passive diffusion placental transport model predicted that the drug reach the equilibrium at a higher concentration than the experimental data in the placental and fetal compartment (Fig. 4.3b, 4.4b, 4.5b and 4.6b). The ATM, when compared with FLM and SDM, provided the best fit as determined by visual inspection and smallest AIC (Table 4.5).

Though ddC and 3TC are both structurally related to cytidine, they exhibit quite different PK behavior. During the 6 hours post-administration, in the maternal plasma, ddC had the second lowest concentrations (ABC had the lowest concentrations) while 3TC had the second highest drug concentrations. However, in the placenta, ddC had higher drug concentrations than 3TC, AZT and ABC. The PK behavior of ddC and 3TC were similar in the fetal and amniotic fluid compartments with relative slower uptake at the beginning compared to AZT and ABC (Fig. 4.1). The placental concentration of ddC exceeded the maternal plasma concentration 1 hour post-administration, while the placental concentration of 3TC was lower than the maternal plasma concentration till 6 hour post-administration (Fig. 4.3c and Fig. 4.4c). Accordingly, the distribution clearances of ddC between maternal-blood and the placenta are equal and the clearance from fetuses to the placenta is 2.6-fold larger than the opposite direction. For 3TC,

there is a consistent trend to pump the drug out of the fetuses back to the maternal blood (CL_{pm} ≈1.8 CL_{mp} and CL_{fp} ≈ 2.2 CL_{pf}). Both AZT and ABC have larger distribution of placenta to maternal blood than the opposite direction (CL_{pm} ≈ 2 CL_{mp} for AZT and CL_{pm} ≈ 1.6 CL_{mp} for ABC). Their distribution clearances between placenta and the fetuses are equal in both direction (CL_{pf} ≈ CL_{fp} = 0.17 l/h for AZT and CL_{pf} ≈ CL_{fp}= 0. 2 l/h for ABC) (Table 4.4 and Fig. 4.7). Specially, the placental-fetal clearance of ABC reaches the maternal blood flow to the conceptus, which is consistent with its larger lipophilicity. The drug with larger lipophilicity (LogP) has larger CL_{mp}, CL_{pm}, CL_{pf} and CL_{fp}, which suggested that passive diffusion and active-transporter work together to control NRTIs pass placenta (Fig. 4.7).

One possible mechanism for the asymmetrical maternal-placental-fetal transfer is transporter-mediated active transport. Studies have shown that NRTIs are substrates for multiple transporters that are known to be expressed in placenta. For example, AZT, 3TC and ddC are substrates for OAT_1 and BCRP (Wada *et al.*, 2000; Wang *et al.*, 2004). Both OAT_1 and BCPR were found in the placenta (Leazer and Klaassen, 2003; Syme *et al.*, 2004). Unfortunately, there is no direct information about transporter-mediated placental transfer of NRTIs thus far. AZT metabolism in human placenta has been demonstrated, but the metabolism of NRTIs in placenta is believed to be minor and will not alter distribution of the drugs (Collier *et al.*, 2003; Syme *et al.*, 2004). In most in vivo pregnancy pharmacokinetic studies, the drug concentration-time profile in the placenta is not available. Therapeutic and toxicological effects of a drug may be exerted directly on the fetus but also may occur indirectly by altering placental function. In present study, the disposition of drugs in the placenta was studied. This information is of critical importance because the placenta is the last barrier before the virus reaches the fetus during

pregnancy. The toxicity of NRTIs in placenta has been demonstrated (Collier *et al.*, 2003; Shiramizu *et al.*, 2003).

NRTIs accumulated in the amniotic fluid in the pregnant rats, which was also observed in clinical human studies (Chappuy *et al.*, 2004). In present model, the accumulation of drug is adequately predicted by transfer clearance between fetuses and amniotic fluid compartment. The transfer clearance between fetuses and amniotic fluid are very similar in both directions for ddC, 3TC and AZT. ABC has the largest transfer clearances between fetuses and amniotic fluid and the transfer clearance from the fetuses to the amniotic fluid is almost 1.8 times of the clearance from the amniotic to the fetuses (Table 4.4). This model estimation is consistent with faster uptake of ABC in the amniotic fluid compared to other NRTIs in present study (Fig. 4.1d).

Species differences in NRTI elimination exists. AZT is metabolized extensively in humans while most AZT is excreted unchanged in the urine of rats. Though 50% of ABC constantly binds to the plasma protein in humans, none of the NRTIs included in present study showed significant plasma protein binding in rats. All the estimated permeability-surface area cross products in the body compartment (PS_b) are smaller than the blood-flow to the body compartment (3.9 L/h) (Table 4.4), which justifies the diffusion-limited distribution of NRTIs in the rest of the body.

In summary, a PBPK model for NTRIs in pregnant rat was developed. The active-transport model predicted the disposition of NRTIs. Thus, active transport, not only simple diffusion, may be an important mechanism allowing transport of NRTIs across the placenta in rats. Furhter studies, such as multiple administrations at different doses may helpul to show the non-linear activity of the placental transfer of NRTIs due to saturation of the transporters.

References

Boike, G. M., Deppe, G., Young, J. D., Gove, N. L., Bottoms, S. F., Malone, J. M., Malviya, V. K., and Sokol, R. J. (1989). Chemotherapy in a Pregnant Rat Model .1. Mitomycin-C - Pregnancy-Specific Kinetics and Placental-Transfer. *Gynecologic Oncology* **34**, 187-190.

Briggs, G. G. (2005). *Drugs In Pregnancy And Lactation*. Lippincott Williams & Wilkins.

Brown, S. D., White, C. A., Chu, C. K., and Bartlett, M. G. (2002). Determination of acyclovir in maternal plasma, amniotic fluid, fetal and placental tissues by high-performance liquid chromatography. *Journal of Chromatography B-Analytical Technologies in the Biomedical and Life Sciences* **772**, 327-334.

Capparelli, E., Rakhmanina, N., and Mirochnickc, M. (2005). Pharmacotherapy of perinatal HIV. *Seminars in Fetal & Neonatal Medicine* **10**, 161-175.

Chappuy, H., Treluyer, J. M., Jullien, V., Dimet, J., Rey, E., Fouche, M., Firtion, G., Pons, G., and Mandelbrot, L. (2004). Maternal-fetal transfer and amniotic fluid accumulation of nucleoside analogue reverse transcriptase inhibitors in human immunodeficiency virus-infected pregnant women. *Antimicrobial Agents and Chemotherapy* **48**, 4332-4336.

Clark, T. N., White, C. A., and Bartlett, M. G. (2006). Determination of didanosine in maternal plasma, amniotic fluid, fetal and placental tissues by high-performance liquid chromatography-tandem mass spectrometry. *Biomedical Chromatography* **20**, 605-611.

Collier, A. C., Helliwell, R. J. A., Keelan, J. A., Paxton, J. W., Mitchell, M. D., and Tingle, M. D. (2003). 3'-Azido-3'-deoxythymidine (AZT) induces apoptosis and alters metabolic enzyme activity in human placenta. *Toxicology and Applied Pharmacology* **192**, 164-173.

Collins, A. S., Sumner, S. C. J., Borghoff, S. J., and Medinsky, M. A. (1999). A physiological model for tert-amyl methyl ether and tert-amyl alcohol: Hypothesis testing of model structures. *Toxicological Sciences* **49**, 15-28.

Corley, R. A., Mast, T. J., Carney, E. W., Rogers, J. M., and Daston, G. P. (2003). Evaluation of physiologically based models of pregnancy and lactation for their application in children's health risk assessments. *Critical Reviews in Toxicology* **33**, 137-211.

Emond, C., Birnbaum, L. S., and DeVito, M. J. (2004). Physiologically based pharmacokinetic model for developmental exposures to TCDD in the rat. *Toxicological Sciences* **80**, 115-133.

Fisher, J. W., Whittaker, T. A., Taylor, D. H., Clewell, H. J., and Andersen, M. E. (1989). Physiologically based pharmacokinetic modeling of the pregnant rat - a multiroute exposure model for trichloroethylene and its metabolite, trichloroacetic-acid. *Toxicology and Applied Pharmacology* **99**, 395-414.

Gabrielsson, J. L., Paalzow, L. K., and Nordstrom, L. (1984). A physiologically based pharmacokinetic model for theophylline disposition in the pregnant and nonpregnant rat. *Journal of Pharmacokinetics and Biopharmaceutics* **12**, 149-165.

Ganapathy, V., Prasad, P. D., Ganapathy, M. E., and Leibach, F. H. (2000). Placental transporters relevant to drug distribution across the maternal-fetal interface. *Journal of Pharmacology and Experimental Therapeutics* **294**, 413-420.

Gargas, M. L., Tyler, T. R., Sweeney, L. M., Corley, R. A., Weitz, K. K., Mast, T. J., Paustenbach, D. J., and Hays, S. M. (2000). A toxicokinetic study of inhaled ethylene glycol monomethyl ether (2-ME) and validation of a physiologically based

pharmacokinetic model for the pregnant rat and human. *Toxicology and Applied Pharmacology* **165**, 53-62.

Gentry, P. R., Covington, T. R., Andersen, M. E., and Clewell, H. J. (2002). Application of a physiologically based pharmacokinetic model for isopropanol in the derivation of a reference dose and reference concentration. *Regulatory Toxicology and Pharmacology* **36**, 51-68.

Keys, D. A., Wallace, D. G., Kepler, T. B., and Conolly, R. B. (1999). Quantitative evaluation of alternative mechanisms of blood and testes disposition of di(2-ethylhexyl) phthalate and mono(2-ethylhexyl) phthalate in rats. *Toxicological Sciences* **49**, 172-185.

Keys, D. A., Wallace, D. G., Kepler, T. B., and Conolly, R. B. (2000). Quantitative evaluation of alternative mechanisms of blood disposition of di(n-butyl) phthalate and mono(n-butyl) phthalate in rats. *Toxicological Sciences* **53**, 173-184.

Kong, W., Engel, K., and Wang, J. (2004). Mammalian nucleoside transporters. *Current Drug Metabolism* **5**, 63-84.

Leazer, T. M., and Klaassen, C. D. (2003). The presence of xenobiotic transporters in rat placenta. *Drug Metabolism and Disposition* **31**, 153-167.

Lewis, S. R. (2006). Maternal and fetal disposition of antiviral agents in the pregnent rats. In *College of Pharamcy*. University of Georgia, Athens.

Mirochnick, M., and Capparelli, E. (2004). Pharmacokinetics of antiretrovirals in pregnant women. *Clinical Pharmacokinetics* **43**, 1071-1087.

Pacifici, G. M. (2005). Transfer of antivirals across the human placenta. *Early Human Development* **81**, 647-654.

Pastor-Anglada, M., Cano-Soldado, P., Molina-Arcas, M., Lostao, M. P., Larrayoz, I., Martinez-Picado, J., and Casado, E. J. (2005). Cell entry and export of nucleoside analogues. *Virus Research* **107**, 151-164.

Perinatal HIV Guidlines Working Group (P.H.G.W.G.) (2006). Public Health Service Task Force Recommendations for Use of Antiretroviral Drugs in Pregnant HIV-1-Infected Women for Maternal Health and Interventions to Reduce Perinatal HIV-1 Transmission in the United States. *AIDSinfo*.

Polin, R. A., Fox, W. W., and Abman, S. H. (2004). *Fetal and Neonatal Physiology*. Elsevier.

Reid, G., Wielinga, P., Zelcer, N., De Haas, M., Van Deemter, L., Wijnholds, J., Balzarini, J., and Borst, P. (2003). Characterization of the transport of nucleoside analog drugs by the human multidrug resistance proteins MRP4 and MRP5. *Molecular Pharmacology* **63**, 1094-1103.

Shiramizu, B., Shikuma, K. M., Kamemoto, L., Gerschenson, M., Erdem, G., Pinti, M., Cossarizza, T., and Shikuma, C. (2003). Placenta and cord blood mitochondrial DNA toxicity in HIV-infected women receiving nucleoside reverse transcriptase inhibitors during pregnancy. *Jaids-Journal of Acquired Immune Deficiency Syndromes* **32**, 370-374.

Strazielle, N., and Ghersi-Egea, J. F. (2005). Factors affecting delivery of antiviral drugs to the brain. *Reviews in Medical Virology* **15**, 105-133.

Syme, M. R., Paxton, J. W., and Keelan, J. A. (2004). Drug transfer and metabolism by the human placenta. *Clinical Pharmacokinetics* **43**, 487-514.

Takeda, M., Khamdang, S., Narikawa, S., Kimura, H., Kobayashi, Y., Yamamoto, T., Cha, S. H., Sekine, T., and Endou, H. (2002). Human organic anion transporters and human organic

cation transporters mediate renal antiviral transport. *Journal of Pharmacology and Experimental Therapeutics* **300**, 918-924.

Terry, K. K., Elswick, B. A., Welsch, F., and Conolly, R. B. (1995). Development of a Physiologically-Based Pharmacokinetic Model Describing 2-Methoxyacetic Acid Disposition in the Pregnant Mouse. *Toxicology and Applied Pharmacology* **132**, 103-114.

Unadkat, J. D., Dahlin, A., and Vijay, S. (2004). Placental drug transporters. *Current Drug Metabolism* **5**, 125-131.

Wada, S., Tsuda, M., Sekine, T., Cha, S. H., Kimura, M., Kanai, Y., and Endou, H. (2000). Rat multispecific organic anion transporter 1 (rOAT1) transports zidovudine, acyclovir, and other antiviral nucleoside analogs. *Journal of Pharmacology and Experimental Therapeutics* **294**, 844-849.

Wang, X., Nitanda, T., Shi, M. Y., Okamoto, M., Furukawa, T., Sugimoto, Y., Akiyama, S., and Baba, M. (2004). Induction of cellular resistance to nucleoside reverse transcriptase inhibitors by the wild-type breast cancer resistance protein. *Biochemical Pharmacology* **68**, 1363-1370.

Weiss, J., Theile, D., Ketabi-Kiyanvash, N., Lindenmaier, H., and Haefeli, W. E. (2007). Inhibition of MRP1/ABCC1, MRP2/ABCC2, and MRP3/ABCC3 by nucleoside, nucleotide, and non-nucleoside reverse transcriptase inhibitors. *Drug Metabolism and Disposition* **35**, 340-344.

Welsch, F., Blumenthal, G. M., and Conolly, R. B. (1995). Physiologically based pharmacokinetic models applicable to organogenesis: Extrapolation between species and potential use in prenatal toxicity risk assessments. *Toxicology Letters* **82-3**, 539-547.

Table 4.1 Chemical structures and octanol/buffer partition coefficients of NRTIs

NRTIs	ddC	3TC	AZT	ABC
Structures	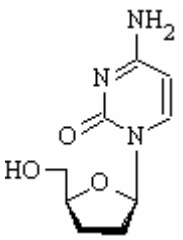	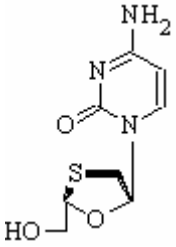	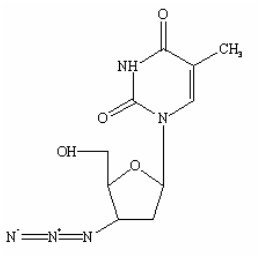	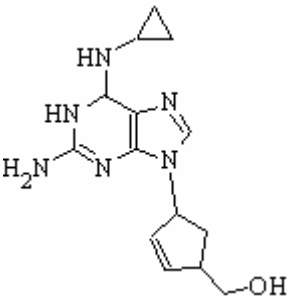
Natural nucleoside	cytidine	cytidine	Thymidine	guanosine
Molecular weight	211.2	229.3	267.2	286.3
LogP	-1.1	-0.97	0.1	0.82
pK_a	weak base 4.4	weak base 4.3	weak acid 9.7	weak base 5.1
Example Transporters	ENT1,2[1] CNT3[1] OAT1,2[2]	OAT1[2] MRP4[3]	ENT2[1] CNT1, 3[1] OAT1,2,3,4[2] OCT1,3[4] MRP4[3]	MRP1,4,5[5]

[1]Reported by Kong *et al.*, 2004.
[2]Reported by Takeda *et al.*, 2002.
[3]Reported by Reid *et al.*, 2003.
[4]Reported by Pastro-Anglada *et al.*, 2005.
[5]Reported by Weiss *et al.*, 2007.

Table 4.2 Physiological Parameters for pregnant rats on gestation day 19.

Physiological Parameters	Values	Source
Body weight of non-pregnant rat BW (kg)	0.3	Lewis (2006)
Cardiac output QCC (l/h/kg)	14.0	Clewell *et al.* (2003)
Blood Flow		
Body QB (%QC)	68.0	Brown *et al.* (1997)
Kidney QKc (%QC)	14.0	Brown *et al.* (1997)
Liver QLc (%QC)	18.0	Brown *et al.* (1997)
Placenta QPL (l/h)	0.32	O'Flaherty *et al.* (1992)
Conceptus QCON (l/h)	0.20	O'Flaherty *et al.* (1992)
Tissue Volume		
Extracellular body VB_E (%BW)	30	Collins *et al.* (1999)
Intracellular body VB_I (%BW)	56	Collins *et al.* (1999)
Kidney VKc (%BW)	1.7	Brown et al. (1997)
Liver VLc (%BW)	3.4	Brown et al. (1997)
Plasma Vblc (%BW)	4.0	Brown et al. (1997)
Placenta Vpla (kg)	0.0045	Lewis (2006)
Fetuses Vfet (kg)	0.025	Lewis (2006)
Amniotic Fluid Vaf (kg)	0.0032	Lewis (2006)
Compartment blood volume (% of tissue volume)		
Placenta	50	Emond *et al.* (2004)

Table 4.3 Tissue: blood partition coefficients of NRTIs.

Partition coefficients	NRTIs			
	ddC	**3TC**	**AZT**	**ABC**
Body: blood[a] (PB)	2.25	1.28	0.93	2.30
Kidney : blood (PK)	0.94	0.94	0.96	1.32
Liver : blood (PL)	0.87	0.87	0.89	1.28
Placenta : blood[b] (PPL)	0.87	0.87	0.89	1.28
Fetuses : blood[c] (PE)	0.90	0.91	0.92	1.13

[a] Estimated by fitting the maternal plasma kinetic data.
[b] Set to be the same as PL.
[c] Set to be the partition coefficients of muscle:blood.

Table 4.4 Active transport model specific parameters.

Parameter	Symbols	NRTI therapy			
		ddC	**3TC**	**AZT**	**ABC**
Transfer from maternal blood to placenta (l/h)	CL_{mp}	0.010	0.007	0.030	0.058
Transfer from placenta to maternal blood (l/h)	CL_{pm}	0.008	0.013	0.061	0.095
Transfer from placenta to fetus (l/h)	CL_{pf}	0.008	0.020	0.163	0.20
Transfer from fetus to placenta (l/h)	CL_{fp}	0.026	0.042	0.180	0.20
Transfer from fetus to amniotic fluid (l/h)	CL_{faf}	0.002	0.002	0.002	0.012
Transfer from amniotic fluid to fetus (l/h)	CL_{aff}	0.003	0.001	0.002	0.006
Permeability-surface area products (l/h)	PS_b	0.32	0.31	0.32	0.69
Maternal clearance (l/h/kg)	CL_r or CL_h	1.30	0.79	0.65	2.76

Table 4.5 Akaike Information Criterion (AIC) values of the different model structures

	Flow limited Model	Simple Diffusionn Model	Active Transport Model
Number of adjustable parameters	5	7	9
ddC	107.0	91.4	53.7
3TC	138.6	95.6	25.5
AZT	129.2	130.5	97.3
ABC	137.8	128.6	91.5
Grand Total	512.7	446.1	268.1

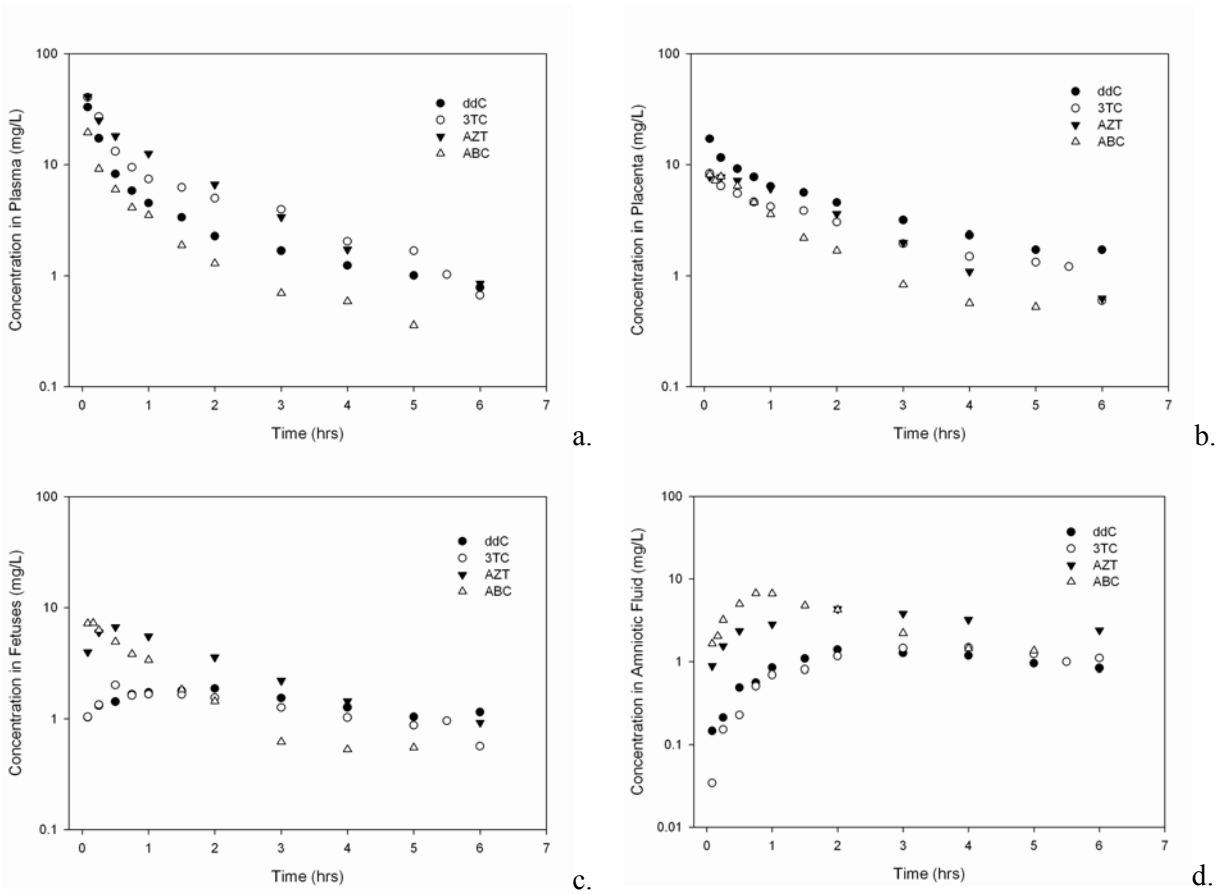

Figure 4.1 Measured ddC (●), 3TC (○), AZT (▼) and ABC (Δ) concentrations in pregnant rat at gestation day 19 (n = 6 for each drug). (a) NRTI concentrations in maternal plasma. (b) NRTI concentrations in placenta. (c) NRTI concentrations in fetuses. (d). NRTI concentrations in amniotic fluid.

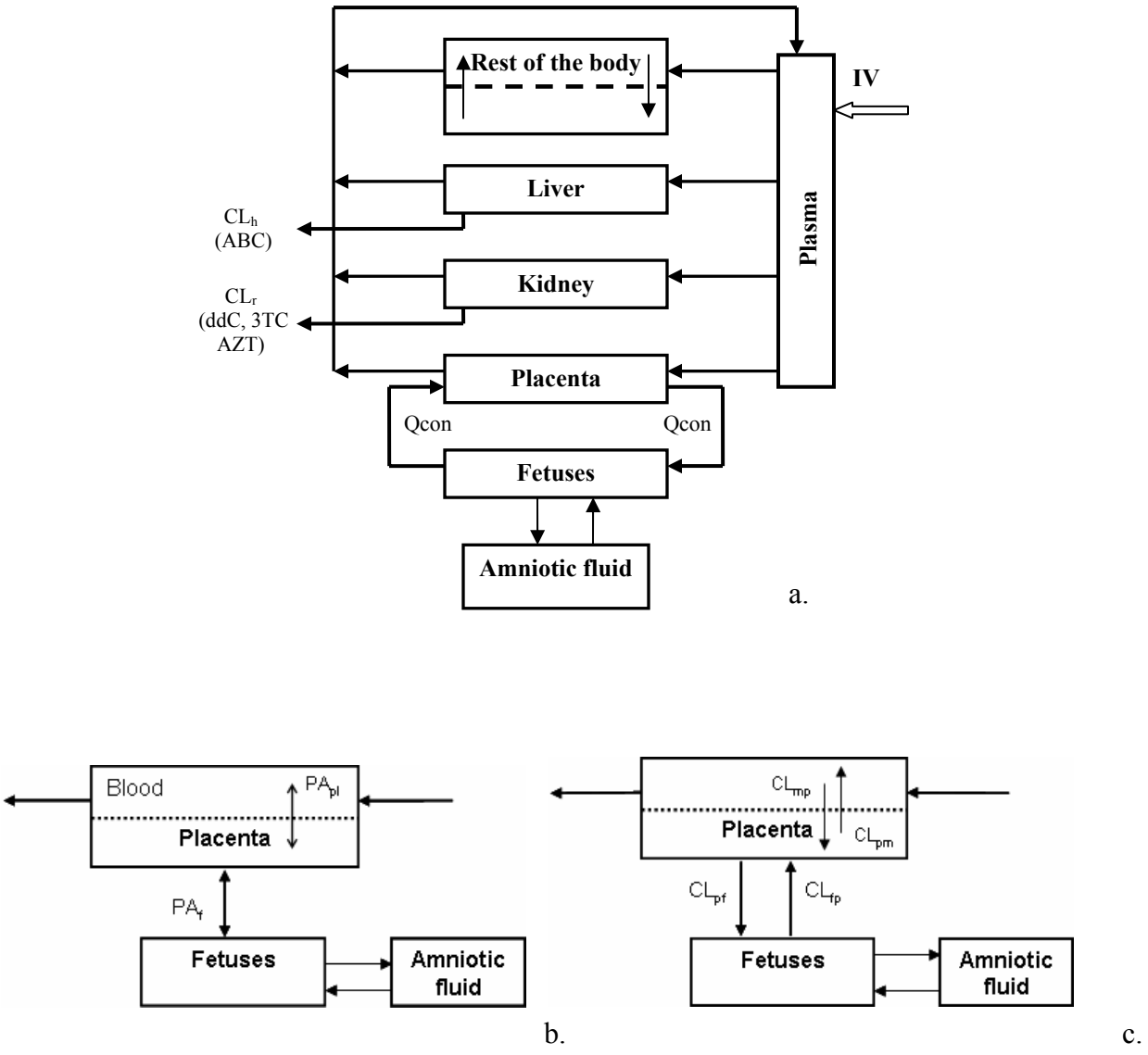

Figure 4.2 PBPK model structures. (a) flow-limited model structure of placenta compartment, (b) diffusion-limited model structure of placenta compartment, (c) active –transport model structure of placental and fetal compartments.

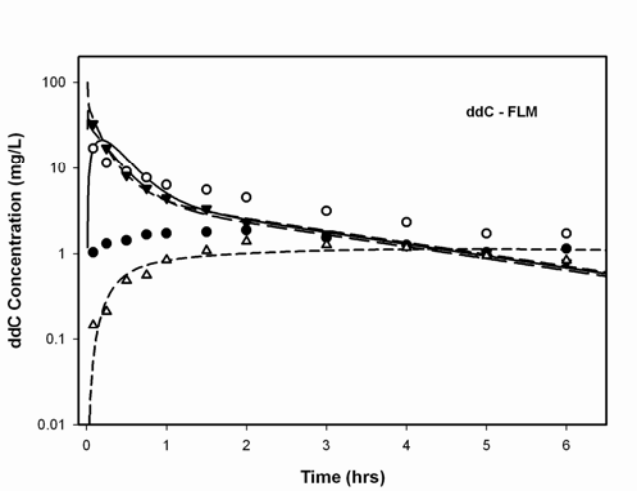

a.

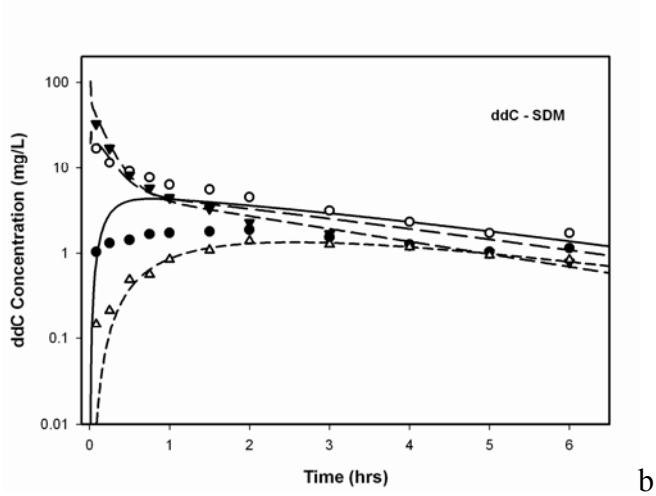

b.

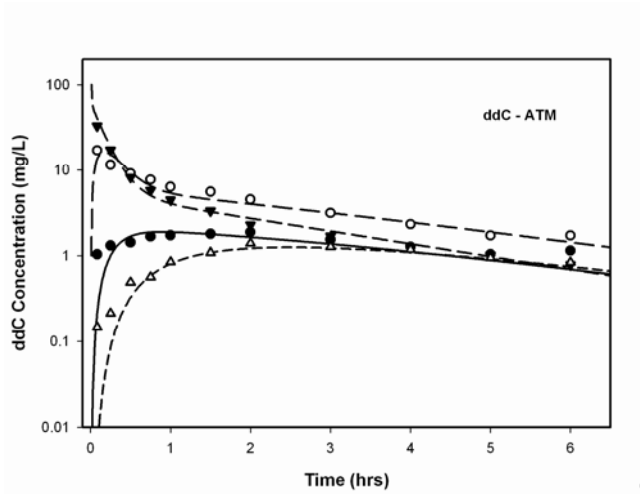

c.

Figure 4.3 Model predictions and observed ddC concentrations in maternal plasma (▼), placenta (○), fetuses (●) and amniotic fluid (Δ) following 25 mg/kg iv bolus in pregnant rats at gestation day 19. (a) FLM, (b) SDM, (c) ATM.

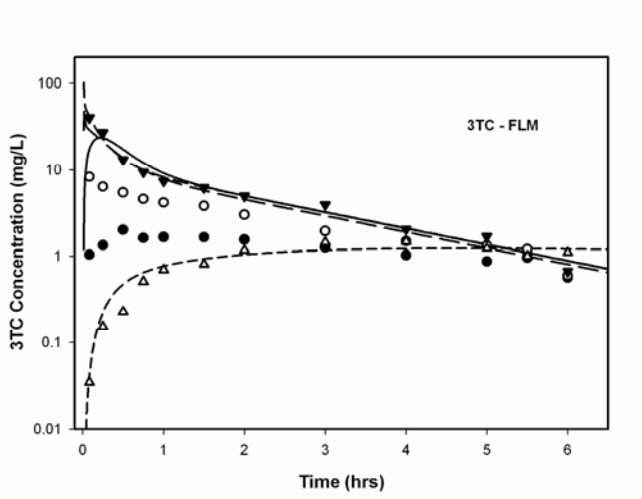

a.

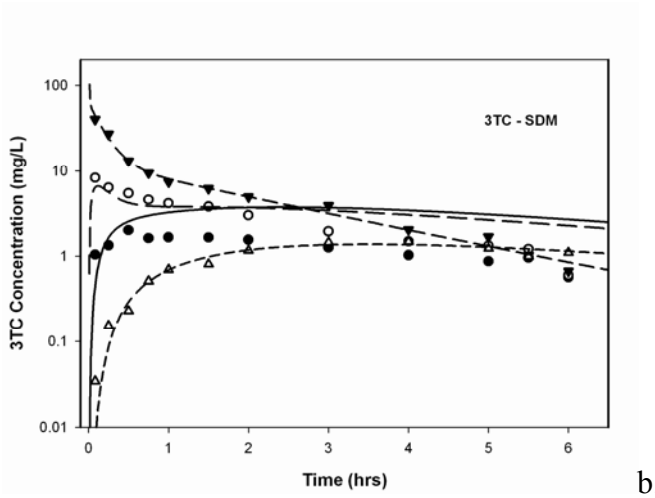

b.

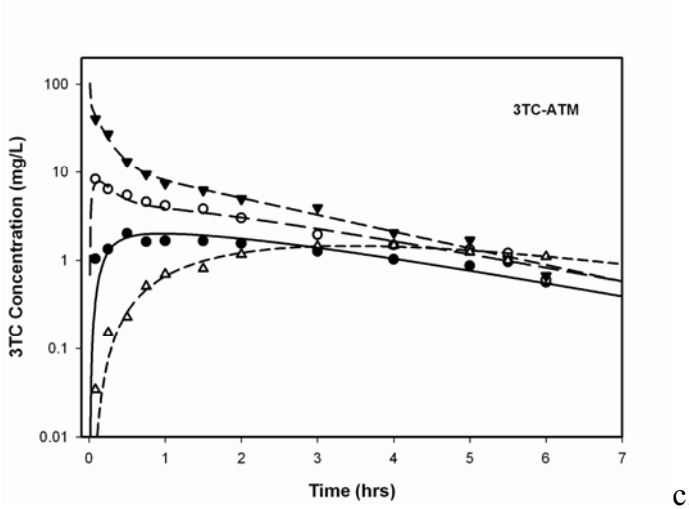

c.

Figure 4.4 Model predictions and observed 3TC concentrations in maternal plasma (▼), placenta (○), fetuses (●) and amniotic fluid (Δ) following 25 mg/kg iv bolus in pregnant rats at gestation day 19. (a) FLM, (b) SDM, (c) ATM.

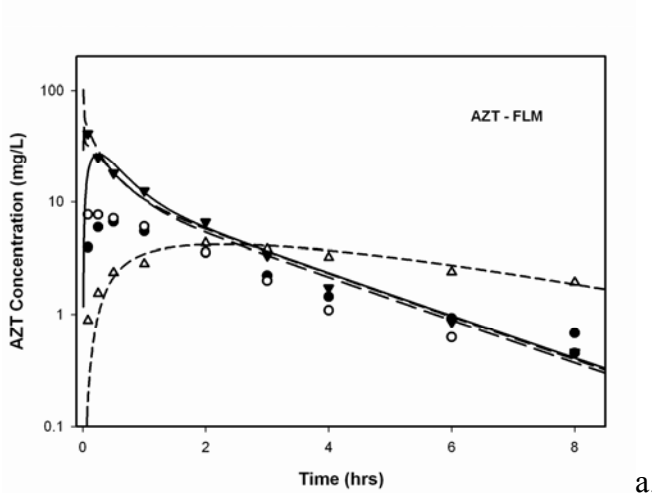

a.

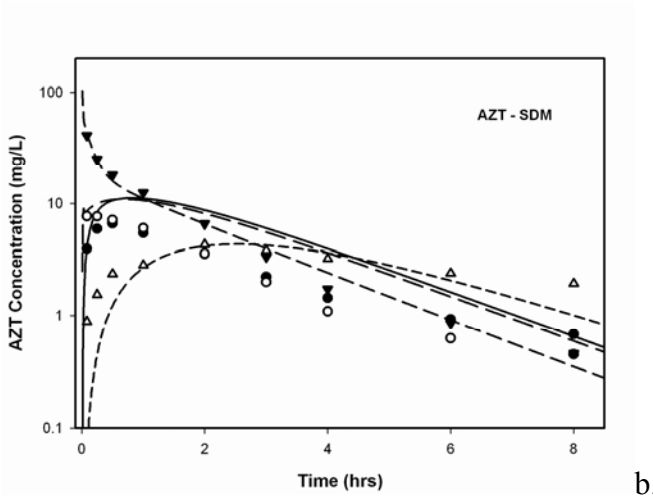

b.

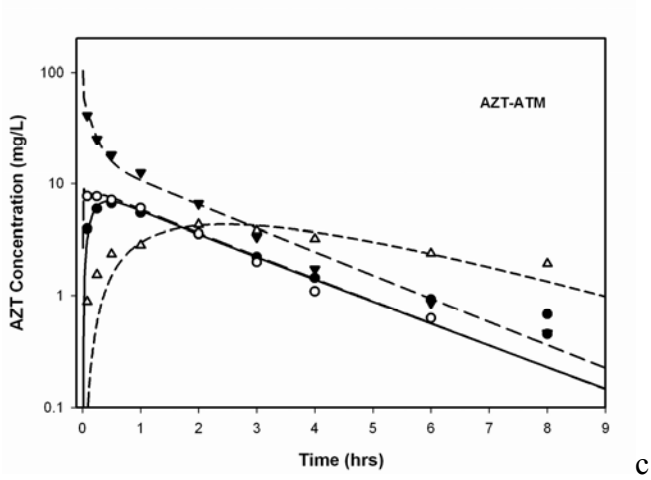

c.

Figure 4.5 Model predictions and observed AZT concentrations in maternal plasma (▼), placenta (○), fetuses (●) and amniotic fluid (Δ) following 25 mg/kg iv bolus in pregnant rats at gestation day 19. (a) FLM, (b) SDM, (c) ATM.

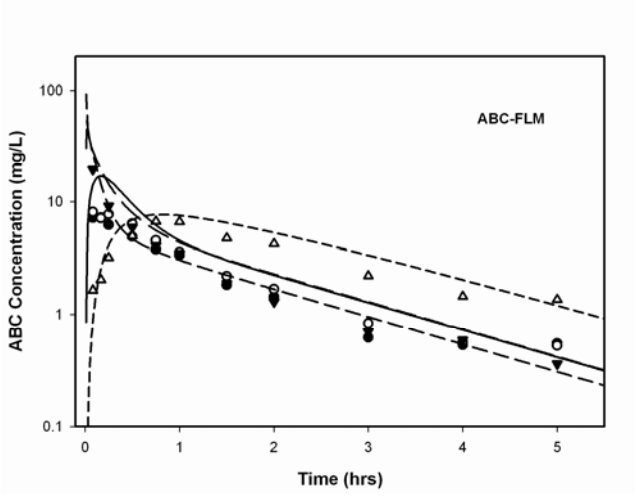

a.

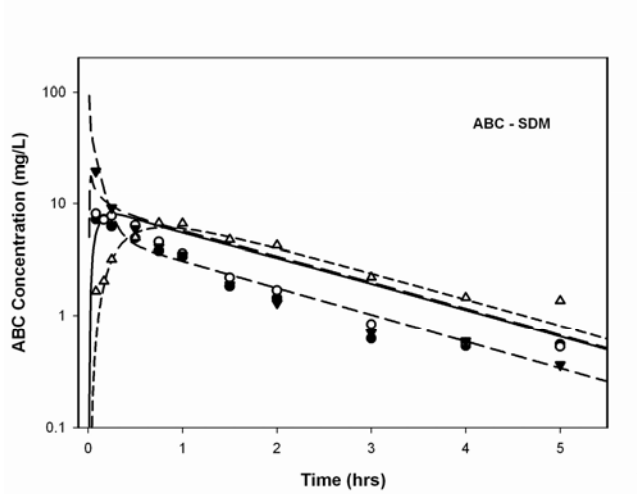

b.

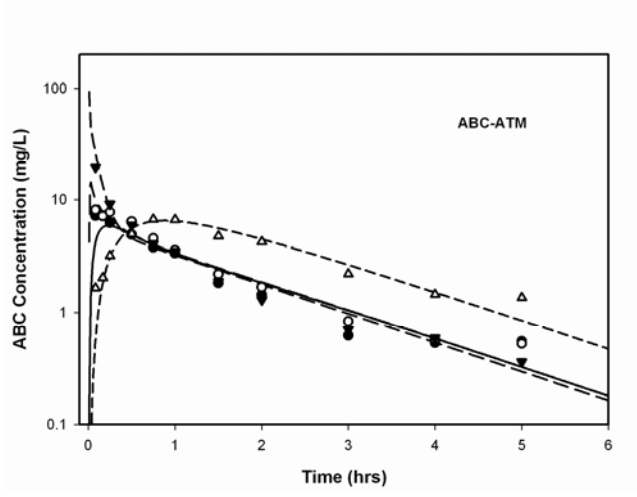

c.

Figure 4.6 Model predictions and observed ABC concentrations in maternal plasma (▼), placenta (○), fetuses (●) and amniotic fluid (Δ) following 25 mg/kg iv bolus in pregnant rats at gestation day 19. (a) FLM, (b) SDM, (c) ATM.

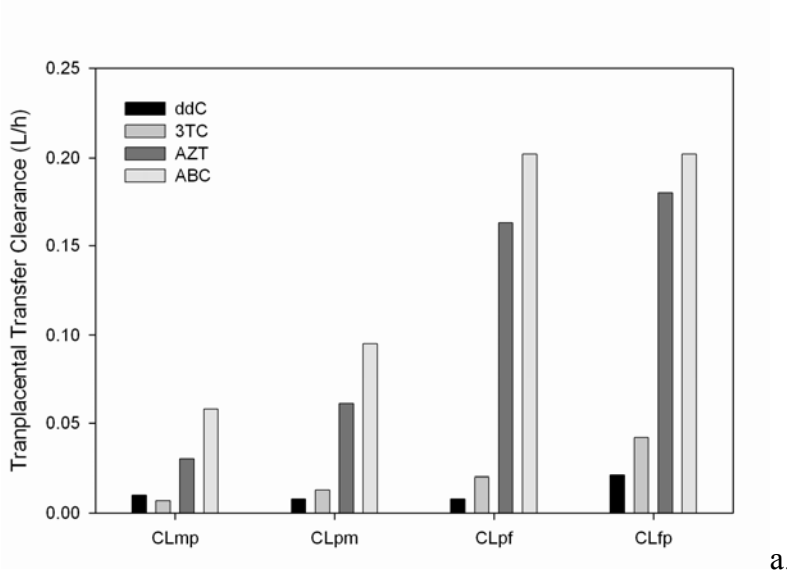

a.

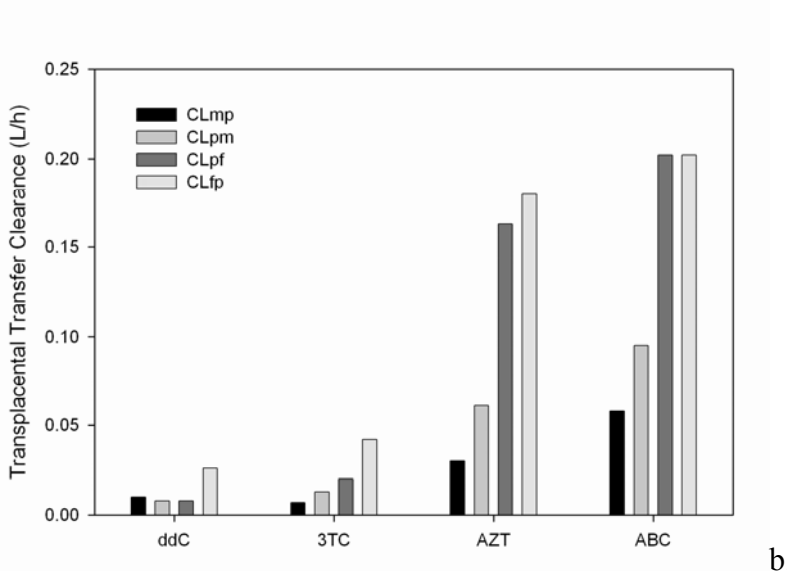

b.

Figure 4.7 Histogram of the transplacental transfer clearances (CL_{mp}, CL_{pm}, CL_{pf} and CL_{fp}) for ddC, 3TC, AZT and ABC. The transplacental transfer clearances were estimated by active-transport (ATM) model fitting to the observed NRTI concentration-time course data in the placenta and fetuses in pregnant rats at gestation day 19.

CHAPTER 5

INVESTIGATION OF THE DRUG-DRUG INTERACTIONS FOR NUCLEOSIDE REVERSE TRANSCRIPTASE INHIBITORS IN PREGNANT RATS- A PHYSIOLOGICALLY-BASED PHARMACOKINETIC MODLEING APPROACH

Ting Li, S.R.Lewis, and C.A.White. To be submistted to *Journal of Pharmacokinetics and Biopharmaceutics.*

Abstract

Nucleoside reverse transcriptase inhibitors (NRTIs) are a class of drugs used in highly antiretroviral therapy (HARRT) for the treatment of HIV-infection. HAART has been successful in reducing mother-to-child transmission (MTCT) to less then 2%. However, the *in vivo* pharmacokinetic mode of action for placental transport and fetal disposition of NRTIs has been limited and inconclusive. In the present study, a physiologically-based pharmacokinetic (PBPK) model was constructed to explore the pharmacokinetics of NRTIs and potential drug-drug interactions in pregnant rats receiving combination-therapies. Active-transport PBPK models for two NRTIs were run simultaneously to mimic the co-administration of lamivudine-zidovudine (3TC-AZT) and abacavir–zidovudine (ABC-AZT). The effect of one NRTI on the other (the change in the maternal clearances and transplacental distribution clearances) was presumed to be linearly related to the drug's concentration by first-order interaction constants (Kint's). The model predicted substantial drug-drug interactions in both maternal and fetal dispositions for these combination therapies. Alterations of maternal pharmacokinetics were not able to explain all pharmacokinetic changes in placental, fetal and amniotic fluid compartments which support the theory that the NRTIs interact at the placenta, altering transplacental distribution as well as fetal exposure after combination therapy. These interactions are most likely mediated through multiple transporters located in kidney, liver and placenta. The drug-drug interactions identified in pregnant rats may be clinically relevant to humans impacting the NRTIs treatment efficacy and safety in pregnant women and their newborns.

Introduction

Most children living with HIV acquire the infection through mother-to-child transmission (MTCT), which can occur during pregnancy, labor and delivery, or breastfeeding. Without treatment, approximately 15-30% of babies born to HIV positive women will become infected with HIV during pregnancy and delivery (WHO, 2006). Though the mechanism of virus transmission from mother to fetus during pregnancy is not fully understood, anti-retroviral drugs originally used in non-pregnant adults have proved successful in reducing MTCT of HIV (P.H.G.W.G., 2006). Zidovudine (AZT), a nucleoside reverse transcriptase inhibitor (NRTI), the first FDA approved drug to treat HIV-infection during pregnancy, reduces MTCT by nearly 70% (CDC, 2006). Other drugs in this class include: abacavir (ABC), didanosine (ddI), emtricitabine (FTC), lamivudine (3TC), stavudine (d4T) and zalcitabine (ddC). The risk of MTCT is further reduced, to less than 2%, when the pregnant women are treated with combination therapies (P.H.G.W.G., 2006). Highly active antiretroviral therapy (HARRT), the standard treatment for HIV-infection, typically consists of two NRTIs and a protease inhibitor (PI) (CDC, 2006). Because AZT has the most extensive safety information available regarding use during pregnancy, it is the primary drug prescribed to HIV-infected pregnant women (Briggs, 2005). Potential interactions between AZT and other antiretroviral agents may alter drug disposition, treatment efficiency and drug safety. However, little pharmacokinetic information is available for the combination therapy in pregnant women and their neonates.

In many international guidelines, AZT-3TC is the recommended dual NRTIs for combination therapy during pregnancy (CDC, 2006). AZT, 3TC and ABC are co-formulated as Trizivir® (150 mg 3TC, 300 mg AZT and 300 mg ABC) and oral administered twice a day (GlaxoSmithKline, 2006). No significant alterations in pharmacokinetics have been identified

among AZT, 3TC and ABC when either two or three of these drugs were dosed together in non-pregnant patients (Wang *et al.*, 1999; McDowell *et al.*, 2000; Ibbotson and Perry, 2003; GlaxoSmithKline, 2006). In a clinical study with 10 pregnant women, no significant interactions were identified for AZT and 3TC on maternal pharmacokinetics (Moodley *et al.*, 1998). There is no current information available for ABC and AZT combination therapy in pregnancy.

Adverse effects have been associated with NRTIs treatments including hyperlactataemia and lactic acidosis, neuropathy, pancreatitis and lipoatrophy (Nolan and Mallal, 2004). The adverse effects are, at least in part, related to defective mitochondrial DNA replication caused by NRTIs (Cote *et al.*, 2002). Serious and sometimes fatal hypersensitivity reactions have been associated with ABC (CDC, 2006). It is not clear whether the combination therapy is associated with adverse pregnancy outcomes such as premature delivery (P.H.G.W.G., 2006). Mitochondrial dysfunction has been identified in infants with *in utero* or neonatal exposure to either AZT-3TC or AZT alone (Blanche *et al.*, 1999; Benhammou *et al.*, 2007). Other serious adverse events seen in children after perinatal exposure to AZT-3TC were neutropenia and anemia (Mandelbrot *et al.*, 2001). Developmental toxicity and carcinogenicity after perinatal exposure to single NRTI at therapeutic doses was not observed in animal studies (Briggs, 2005).

Perfusion experiments with human placenta suggest NRTIs cross the placenta by passive diffusion (Pacifici, 2005). The observation of comparable concentrations in maternal and cord blood supports passive diffusion as the mechanism behind NRTIs transplacental transfer (Capparelli *et al.*, 2005). However, competitive interactions for the same transporters among AZT, 3TC and ABC have been shown *in vitro* (Kong *et al.*, 2004). Many of these transporters are also expressed on rat and human placenta (Ganapathy *et al.*, 2000; Leazer and Klaassen, 2003; Unadkat *et al.*, 2004). Recently, co-administration of AZT-3TC, AZT-ABC and AZT-

acyclovir (ACV) in pregnant rats showed substantial drug-drug interactions for both maternal and fetal pharmacokinetics (Brown *et al.*, 2003; Lewis, 2006).

As a part of the ongoing pharmacokinetic investigations of antiretroviral drugs in pregnancy, the interactions of AZT-3TC and AZT-ABC on the maternal clearance and placental transfer are characterized by a PBPK modeling approach in the present study. PBPK models have been created to describe the perinatal exposure of chemicals (Corley *et al.*, 2003; Reddy *et al.*, 2005). Based on previously developed PBPK model for single NRTIs, PBPK models were developed to investigate changes in pharmacokinetics of each NRTI following two combination therapies (AZT-3TC and AZT-ABC).

Materials and methods

Experimental Data. The kinetic data used in developing the NRTI PBPK model were reported in previous study (Lewis, 2006). Briefly, pregnant Sprague-Dawley rats (n= 19) with an average weight of 328 ± 20 g were dosed by intravenous bolus on day 19 of gestation. Five dosing groups were used in the study: (i) 3TC monotherapy (25 mg/kg) (n = 6), (ii) AZT monotherapy (25 mg/kg) (n = 6), (iii) ABC monotherapy (25 mg/kg) (n = 7), (iv) 3TC-AZT combination therapy (25 mg/kg each) (n = 7) and (v) ABC-AZT combination therapy (25 mg/kg each) (n = 6). Blood samples of 150 to 250 µl were collected at 5, 15, 30, 45, 60, 90, 120, 180, 240, 300, 360 min after dosing. Fetuses, amniotic fluid and placenta were harvested at 5, 15, 30, 45, 60, 90, 120, 180, 240, 300, and 360 min. Placental and fetal tissues were homogenized in two volumes of deionized water (wt/vol). Amniotic fluid samples were pulled from the fetal sacs with an 18-gauge needle and deposited into microfuge tubes. All samples were stored at –20 °C until analysis. 3TC and AZT concentrations in mother plasma, placenta, fetus and amniotic fluid were determined by an HPLC or LC-MS method developed previously (Lewis, 2006).

Fixed parameters. Physiological parameters used in the NRTI PBPK model are summarized in Table 5.1. All tissue volumes and blood flows were scaled to body weight. Volumes of the placenta, fetuses and amniotic fluid were measured by Lewis (2006). The maternal blood flow to each conceptus through yolk sac and chorioallantoic placenta on gestation day 19 was calculated using the equation of O'Flaherty *et al.* (1992) and multiplied by a factor of 10 (as an average number of fetuses per dam). The placental blood volume was expressed as a fraction of the tissues total volume and was taken from literature (Emond *et al.*, 2004). The tissue: blood partition coefficients in active transport model for each drug were directly used in present model (Table 5.2).

Altered pharmacokinetics in combination therapy. To gain insight into what pharmacokinetic affects result from the co-administration of NRTIs, the independent active transport model for one NRTI was fit to the kinetic data of each NRTI from the combination therapy. The PBPK model structure was adapted from the active-transport model (ATM) for NRTIs developed previously for mono-therapy data (Chapter 4). The model structure consists of seven compartments plasma, liver, kidney, rest of the body, placenta, fetuses and amniotic fluid. The distribution of NRTIs into the liver and kidney were blood-flow limited and the distribution into 'rest of the body' was described as diffusion limited. Urinary excretion is the primary elimination pathway for 3TC and AZT, while hepatic metabolism is the major elimination pathway for ABC. The maternal system clearance (CL_{rc} for 3TC and AZT, CL_{hc} for ABC) and the distribution clearances between maternal-blood and placenta (CL_{mp} and CL_{pm}), between placenta and fetuses (CL_{pf} and CL_{fp}) and between fetuses and amniotic fluid (CL_{faf} and CL_{aff}) were optimized by fitting to the concentration-time course data of each drug in following combination therapy. The estimated parameter values for the combination-therapy were

compared to the correspondent estimated parameter values for the mono-therapy by two-sample T-test.

Modeling drug-drug interactions. To mimic the co-administration and interaction of two drugs dosed simultaneously, each drug in the combination-therapy was described separately by a PBPK model and run simultaneously. The potential interactions of the drugs were assumed to occur in the maternal elimination tissues (i.e., kidney and liver) and placenta, fetus and amniotic fluid (Fig. 5.1). The effect of one NRTI on another (i.e., the change in the maternal clearances and transplacental distribution clearances) was presumed to be linearly related to the drug's concentration by first-order interaction constants (Kint's). Obtaining a positive value of Kint suggests a stimulation effect and a negative value of Kint suggests an inhibition effect. If the value of Kint is not significantly different from 0, then it suggests there is no interaction on the corresponding process. The interaction for the maternal elimination tissues (i.e., kidney and liver) and placenta, fetus and amniotic fluid were described similarly. For example, the altered maternal-blood to placenta transfer clearance of AZT following combination therapy with 3TC was described as:

$$RCLmp_{AZT} = \frac{dCLmp_{AZT}^{+3TC}}{dt} = K\,\mathrm{int}_{mp}^{3TC:AZT} \times Cplacb_{3TC}^{+AZT} \tag{5.1}$$

$$CLmp_{AZT}^{+3TC} = CLmp_{AZT}^{0} + \int_0^t RCLmp_{AZT} \tag{5.2}$$

where $RCLmp_{AZT}$ is rate of change of maternal-blood to placenta transfer clearance of AZT, $CLmp_{AZT}^{+3TC}$ is the maternal-blood to placenta transfer clearance of AZT when 3TC was administered together, $K\,\mathrm{int}^{3TC:AZT}$ is the interaction constant (i.e., the effect of 3TC on maternal-blood to placenta transfer of AZT), $Cplacb_{3TC}^{+AZT}$ is the 3TC concentration in the placental blood,

and $CLmp^{0}_{AZT}$ is the AZT maternal-blood to placenta transfer clearance estimated for the mono-therapy data.

First, the Kint's for drug-drug interactions in the maternal clearances were fit to maternal plasma concentration time course data. The Kint's for transplacental clearances of NRTIs were then estimated by fitting the observed kinetic data of the two drugs in placental and fetal compartments at the same time. In order to reduce parameter redundancy, the backward model selection methods were applied to identify the most important interactions and the unnecessary interactions (Kint's) were then removed from the model. Briefly, the selection process was started using the full model, which contains a total of 8 possible interaction constants: 3TC effects on AZT distribution clearance from maternal-blood to placenta($K\,\mathrm{int}^{3TC:AZT}_{mp}$), from placenta to maternal-blood($K\,\mathrm{int}^{3TC:AZT}_{pm}$), from placenta to fetuses($K\,\mathrm{int}^{3TC:AZT}_{pf}$), from fetuses to placenta($K\,\mathrm{int}^{3TC:AZT}_{fp}$) and AZT effects on 3TC (accordinly, $K\,\mathrm{int}^{AZT:3TC}_{mp}$, $K\,\mathrm{int}^{AZT:3TC}_{pm}$, $K\,\mathrm{int}^{AZT:3TC}_{pf}$, $K\,\mathrm{int}^{AZT:3TC}_{pf}$) for 3TC-AZT concentration-time profile in placenta and fetuses; similarly, $K\,\mathrm{int}^{ABC:AZT}_{mp}$, $K\,\mathrm{int}^{ABC:AZT}_{pm}$, $K\,\mathrm{int}^{ABC:AZT}_{pf}$, $K\,\mathrm{int}^{ABC:AZT}_{fp}$ and $K\,\mathrm{int}^{AZT:ABC}_{mp}$, $K\,\mathrm{int}^{AZT:ABC}_{pm}$, $K\,\mathrm{int}^{AZT:ABC}_{pf}$, $K\,\mathrm{int}^{AZT:ABC}_{fp}$ for ABC-AZT concentration-time profile in placenta and fetuses. All Kint's were temporarily set to their initial estimations from the mono-therapy model and then optimized by fitting to the observed data from the combination-therapy. Following this, the least significant Kint's (the optimized Kint with the smallest absolute values and large S.E.) were set to zero, as long as it did not significantly sacrifice the feasibility of the model predictions. This process was continued by successively re-fitting the PBPK model using reduced number of Kint's until all remaining interaction constants are statistically significant (95% CIs for all the remaining estimated Kint's do not contain 0). For the alteration of the distribution clearance of AZT from

maternal-blood to placenta in the combination-therapy, the initial estimation for the $K\,\mathrm{int}_{mp}^{3TC:AZT}$ ($^{0}K\,\mathrm{int}_{mp}^{3TC:AZT}$) was calculated as:

$$^{0}K\,\mathrm{int}_{mp}^{3TC:AZT} = \frac{CLmp_{AZT}^{+3TC} - CLmp_{AZT}^{0}}{Cplacb_{3TC}^{+AZT}} \tag{5.3}$$

where $CLmp_{AZT}^{+3TC}$ was the optimized value for the combination-therapy from the independent PBPK models for each drug in the combination-therapy without taking into account the effect of the other drug described in the previous section. Finally, with all other parameters fixed, the Kint's for the fetal-amniotic fluid transfer were estimated simultaneously by fitting the concentration time profiles of two co-administered drugs in the amniotic fluid.

All predictions were performed in acslXtreme (V 2.0.1.2, Aegis Technologies Group Inc., Huntsville, AL). The maximum likelihood method implemented in the optimization function was used to estimate the adjustable parameters. The Nelder-Mead algorithm was used. The relative error model was used for maternal plasma, placental and fetal concentrations and constant error model was used for drug concentrations in amniotic fluid. Finally, model fits to the observed data were inspected visually to ensure reasonable estimations of parameters were obtained.

Statistical analysis. The ability of the reduced model (with less than 8 Kint's for the transplacnetal interactions) to fit the experimental data was compared directly to the full model (with all 8 possible Kint's for the transplacnetal interactions), using log-likelihood ratio (LLR) test, because the reduced models are essentially nested models of the full model. The test statistic, L, was calculated as:

$$L = 2 \times (LLF_{full} - LLF_{reduced}) \tag{5.4}$$

where LLF_{full} and $LLF_{redcued}$ are the optimal values of the log-likelihood (LLF) of the full and reduced models generated by acslXtreme, respectively. The degree of freedom for each test was the number of removed parameters in each reduced model compared to the full model. The test statistic L was compared to the critical value of the χ^2 statistic with $\alpha = 0.05$ as the level of significance. At the same time, the Akaike Information Criterion (AIC) value of each model was calculated as:

$$AIC = -2 \times LLF_i + 2P \qquad (5.5)$$

where LLF_i is the optimal value of the log-likelihood of the ith model and P is the number of adjustable parameters for the particular model (i.e., 8 for the full model). The model with the smallest AIC is considered to be superior.

Results

Alterations of PK parameters in combination-therapy. The independent PBPK model was used to estimate PK parameters of each drug in the combination therapy of 3TC-AZT and ABC-AZT. The maternal system clearance (CL_{rc} for 3TC and AZT, CL_{hc} for ABC) and the distribution clearances between maternal-blood and placenta (CL_{mp} and CL_{pm}), between placenta and fetuses (CL_{pf} and CL_{fp}) and between fetuses and amniotic fluid (CL_{faf} and CL_{aff}) were fit to the kinetic data of each drug. As expected, the independent models fit the observed kinetic data following combination therapy well (Fig. 5.2 and 5.3). The estimated parameter values and their standard error (S.E.) were shown in Table 5.3. Based on a T-test ($\alpha = 0.05$), the maternal system clearances of AZT were increased significantly in the combination with 3TC. The transfer clearances (CL_{pm}) of 3TC and AZT from maternal-blood to placenta were decreased significantly compared to the values estimated for their mono-therapy data. No significant alterations were identified for the distribution clearances between placental and fetal

compartment and between fetal and amniotic fluid compartment. When ABC and AZT were coadministered, maternal system clearance of ABC was decreased significantly while maternal clearance of AZT was increased significantly. The distribution clearance of ABC from placenta tissue back to maternal-blood (CL_{pm}) was increased by 80%, though due to the large S.E., this increase was not statistically significant. There were no changes in the distribution clearances between placental and fetal compartment. The distributions between fetal and amniotic fluid compartment were decreased significantly by AZT. The distribution clearances of AZT between maternal-blood and placental compartment were increased in both directions, though again due to a relatively large S.E., these differences were not significant statistically. The distributions of AZT between fetal and amniotic fluid compartments followed an increased trend. Noteworthy, the S.E.'s are only an approximation and not accurate in non-linear regression. The T-tests constructed here and the test results are not used as a restricted statistical standard.

3TC pharmacokinetics affected by AZT. The estimated Kint's for NRTI interactions following combination therapy are shown in Table 5.4. Co-administration model predictions and observed kinetic data for 3TC-AZT combination therapy and mono-therapy (3TC or AZT) are presented in Fig. 5.4 and Fig. 5.5. Based on the model simulations, AZT did not affect the maternal clearance of 3TC and the estimated $K\,\mathrm{int}_{mcl}^{AZT:3TC}$ is not significantly different from 0 (Fig. 5.4a). However, AZT increased significantly 3TC concentration in the placental and fetal tissues (Fig. 5.4b and 5.4c). The interaction model predicted adequately the higher 3TC concentrations in the placenta for the first few time points after dosing that resulted from the increased uptake of 3TC into the placenta ($K\,\mathrm{int}_{mp}^{AZT:3TC} = +\,0.3$) and the higher 3TC concentrations in the placenta over the later time points, which resulted from the slowed efflux of 3TC from placenta to maternal blood ($K\,\mathrm{int}_{pm}^{AZT:3TC} = -\,0.3$). The interaction constants ($K\,\mathrm{int}_{mp}^{AZT:3TC}$

and $K\,\mathrm{int}_{pm}^{AZT:3TC}$) for maternal blood and placental tissue were able to predict the alterations in 3TC concentrations in both placental and fetal compartments, consequently the co-administration model predicted no impact of AZT on the 3TC placental distribution clearances on the fetal side (i.e., $K\,\mathrm{int}_{pf}^{AZT:3TC}$ and $K\,\mathrm{int}_{fp}^{AZT:3TC}$ are not different from 0). The increased 3TC concentrations in both placental and fetal compartments did not result in higher accumulation of 3TC in amniotic fluid (Fig. 5.4d). Accordingly, the estimated interaction constant ($K\,\mathrm{int}_{aff}^{AZT:3TC}$) for the 3TC transfer clearance from the amniotic fluid to the fetal compartment was + 0.25, while the interaction constant ($K\,\mathrm{int}_{faf}^{AZT:3TC}$) for transfer clearance from fetal to amniotic fluid was not different from 0. The increased amniotic fluid-fetal transfer clearance prevented increased accumulation of 3TC in amniotic fluid.

AZT pharmacokinetics affected by 3TC. Maternal clearance of AZT was increased after combination therapy with 3TC as can be seen with the estimated $K\,\mathrm{int}_{mcl}^{3TC:AZT}$ value of + 8.2 (Fig. 5. 5a). The AZT concentrations, after co-administration with 3TC, in the placental and fetal compartment showed a decreasing trend compared to the AZT mono-therapy (Fig. 5.5b and 5.5c). The co-administration model predicted decreased distribution clearances between maternal blood and placental compartments with negative Kint values ($K\,\mathrm{int}_{mp}^{AZT:3TC}$ and $K\,\mathrm{int}_{pm}^{AZT:3TC}$, Table 5.4). The distribution clearances between fetal and amniotic fluid compartment are not dissimilar with the mono-therapy (Fig. 5.5d).

ABC pharmacokinetics affected by AZT. The co-administration model predictions and observed data for ABC-AZT combination therapy (ABC or AZT) are presented in Fig. 5.6 and 5.7. When dosed in combination with AZT, the maternal elimination of ABC was significantly inhibited. Accordingly, the estimated $K\,\mathrm{int}_{mcl}^{AZT:ABC}$ was -577.8 (Table 5.4). Without a lower

boundary for maternal clearance of ABC, the large negative interaction constant reduced the maternal clearance to 0 immediately after dosing. In order to fit the observed clearance, albeit slight, in the later time points, a minimum residual clearance was estimated at the same time as the interaction constants. The estimated minimum maternal clearance of ABC was 0.2 l/h/kg (Fig. 5.6a). The co-administration model predicted the positive effects of AZT on the ABC distribution clearances from placenta to maternal blood ($K\,\mathrm{int}_{pm}^{AZT:ABC}$, Table 5.3). The model was also successful in predicting the ABC concentration time course for both placental and fetal tissues (Fig. 5.6b and 5.6c). The distribution of ABC into amniotic fluid increased more slowly and reached a higher plateau as compared to the mono-therapy observations (Fig. 5.6d). Accordingly, the interaction model predicted that AZT inhibited ABC transfer from fetal to amniotic fluid resulting in a large negative interaction constant ($Kint_{faf}$ = -30.3). The amniotic fluid-fetal distribution clearance was also decreased by AZT though the effect was much smaller compared to the effects on fetal-amniotic fluid direction ($Kint_{aff}$ = -3.0). Residual distribution clearances were required to predict the plateau ABC concentrations after 2 hours post dosing. The residual distribution clearances, estimated simultaneously with $Kint_{faf}$ and $Kint_{aff}$, were 3.6 ml/h in both directions between fetal and amniotic fluid compartments.

AZT pharmacokinetics affected by ABC. The maternal clearance of AZT was increased by ABC ($Kint_{mcl}$ = + 2.5) (Fig. 5.7a). Higher peak concentrations of AZT in the placental and fetal compartment were seen immediately after the administration compared to the mono-therapy data (Fig. 5.7b and 5.7c). Accordingly, the interaction model predicted that ABC had positive effects on the transplacental distribution clearances of AZT (Table 5.4). The estimated positive interactions constants ($Kint_{faf}$ =0.4 and $Kint_{aff}$ = 0.3) for the AZT transfer clearances between fetal and amniotic fluid compartments described the higher peak concentration of AZT at early

time points while a more rapid clearance was seen in the later time points for the amniotic fluid (Fig. 5.7d).

Alteration in maternal clearances and transplacental distribution clearances estimated by independent models and co-administration drug-drug interaction models were in good agreement (Table 5.3 and 5.4). Increased/decreased parameter values estimated by the independent model are consistent with positive/negative Kint values in the co-administration drug-drug interaction model. Calculated LLR test support the conclusion that the interaction constants (Kint's) in Table 5.4 are the most important parameters necessary for the describing the alteration in transplacental exposure. As presented in Table 5.5, the final models (Model 3) for 3TC-AZT combination therapy and ABC-AZT combination therapy were able to provide similar predictions on par with the full model based on the calculated LLR test, but with less parameters.

Discussion

PBPK models were developed to describe the concentration-time profiles of NRTIs in pregnant rats following 3TC-AZT and ABC-AZT combination therapy. The pharmacokinetic alterations in maternal clearances and transplacental distribution of one NRTI compared to the mono-therapy were mathematically described as a first order process related to the concentration of another co-administered NRTI. The models were able to predict the observed kinetic data in present study quite well (Fig. 5.4-5.7).

The pharmacokinetic models suggest alterations of NRTIs following the combination therapy in multiple tissues. Maternal clearance of AZT was increased in the presence of both 3TC and ABC. In view of the fact that urinary excretion is the primary elimination pathway of AZT and multiple transporters (i.e., organic anion and organic cation transporters) have been shown to mediate renal transport of NRTIs (Takeda *et al.*, 2002), the increased clearance may be

due to up-regulation of transporter-mediated urinary excretion or inhibition of the re-absorption (Chatton *et al.*, 1990). Though the same transporters are also involved in 3TC urinary excretion (Wada *et al.*, 2000), the maternal clearance of 3TC was not affected by the co-administration of 25mg/kg AZT.

This study first time identified significantly decreased maternal clearance of ABC when dosed with AZT. The primary routes of elimination of ABC in humans are *via* metabolism by alcohol dehydrogenase (to form the 5'-carboxylic acid, 30% of total oral dose) and glucuronyl transferase (to form the 5'-glucuronide, 36% of total oral dose). Only 1.2% unchanged ABC was recovered in the urine (GlaxoSmithKline, 2002). The primary elimination routes for AZT in humans are metabolism by glucuronyl transferase (to 5'-glucuronyl AZT) and CYP450/P450-reductase (to form 3'-amino-3'-deoxythymidine). 14% AZT is excreted in urine unchanged (Veal and Back, 1995). Though ABC and AZT have common metabolic pathways via glucuronyl transferase, no clinically relevant drug-drug interactions were identified from the combination therapy (GlaxoSmithKline, 2002), which may be explained the low therapeutic doses (~ 4 mg/kg for both drugs). The interaction between AZT and ABC identified in present study are not likely the result of simple competitive inhibition of the biotransformation. First of all, in the rat, 80% of AZT was excreted in urine unchanged. The rat glucuronyl transferase (as compared to the human enzyme) has a much lower affinity and lower catalytic efficiency (5-6-fold lower) toward AZT which leads to the negligible glucuronidation of the drug (Cretton *et al.*, 1990; Mays *et al.*, 1991; Collins, 2001). Though there is no information in terms of species differences for metabolism of ABC, the fact that AZT is a poor substrate for glucuronidation would lead one to conclude that AZT would not be able to inhibit the system clearance of ABC so dramatically even when the maternal plasma concentration ratio of ABC/AZT was about 10 at

5 hours post dosing (Fig. 5.6a and 5.7a). Secondly, simple competitive inhibition would lead to lower rate of elimination for both ABC and AZT, while the elimination of AZT was increased in the presence ABC. Therefore, it is more likely that AZT would reduce the metabolism of ABC by inhibiting the uptake or stimulate the efflux of ABC in the liver. Multiple transporters carrying NRTIs have been found in liver. For example, OAT2 and OCT1 function for hepatic uptake, while MRP1 and MRP3 move substrates from liver to blood (Faber *et al.*, 2003). This transporter-mediated interaction theory of AZT and ABC is further supported by the slower accumulation of ABC in amniotic fluid following combination therapy. The model simulated a 2-fold higher peak concentration at around 1 hour post-administration, if the distribution transfer rates of ABC between the fetus and amniotic fluid were not affected by AZT ($Kint_{faf} = Kint_{aff} = 0$) because of the increase in fetal concentration.

Based on the model predictions, alterations of maternal pharmacokinetics were not able to explain all the changes in placental, fetal and amniotic fluid compartments which support the theory that the NRTIs affect each other's transplacental transfer and fetal exposure. Both LLR and AIC statistics (Table 5.5) show that the goodness of fit of the models, when assuming no interactions on transplacental transfer, was significantly worse than the final interaction models. Both 3TC and AZT are pyrimidine analogs. Without affecting the maternal clearance of 3TC, AZT increased 3TC accumulation in placental and fetal compartment by increase the distribution clearances from maternal blood to placental compartment and decrease the efflux rate from placenta back to maternal blood. 3TC reduced the fetal exposure to AZT by reducing the distribution clearances from maternal blood to the placenta and increasing the efflux transfer rate from fetuses to placenta. When the alteration in maternal PK was filtered, AZT increased the efflux transfer of ABC (a purine analog) from placenta back to the maternal blood and decreased

the transfer between fetuses and amniotic fluid. ABC up-regulate the transplacental distribution rate of AZT in both directions, which led to greater and earlier peak concentrations in both placental and fetal compartments. The most likely mechanisms behind the observed complex interactions are that NRTIs interfering with each other though multiple influx/efflux transporters located on both maternal and fetal side of the placenta. Moreover, because most of these transporters can function in either direction under appropriate driving force, the direction of transport is determined by the magnitude of the ionic gradient driving forces and the substrate concentration gradients (Ganapathy *et al.*, 2000). However, based on the information used in developing the models presented here, it is not possible to determine which transporters and specific mechanisms are responsible for these complex interactions.

Many of the NRTIs transporters are pH-dependent and fetal plasma is slightly less basic (pH = 7.3) compared to maternal plasma and it is not clear if this slight local pH gradient would affect the transporter's activity. As nearly all of the 3TC, AZT and ABC are unionized at pH =7.4, it is unlikely that the local pH is altered following combination therapy, thus the amount of unionized drug available for transport would be the same. With the exception of the hypothesized transporter-mediate interactions, the alteration of free drug concentrations due to the changes in protein binding could affect the drug transplacental distributions. However, 3TC, AZT and ABC are not significantly bound to plasma protein in rats, so this mechanism is not believed to play an important role. Another possibility is that NRTIs alter the intracellular metabolism of each other and result in decreased/increased accumulation of the pro-drug. However, this proposed interactions should be minor considering that the only very small amount of NRTI is phosphorylated intracellularly (e.g., less than 1% of the total dose for AZT) (Veal and Back, 1995). Meanwhile, different enzymes mediate the phosphorylation of AZT, 3TC

and ABC, therefore cross-talk in these pathways would not be expected. Interestingly, Kewn *et al.* (1997) found that high doses of AZT could inhibit 3TC phospharlation in peripheral blood mononuclear cells (PBMC) and monocytic cell lines (U937). These researchers concluded that this is effect was due to toxicity or an effect on endogenous dCTP pools and not direct inhibition of the kinase enzyme (Kewn *et al.*, 1997).

NRTIs can alter the accumulation and catabolism of themselves and other NRTIs through regulating transporter activities. Jorajuria *et al* (2004) found long term exposure (14 days) to AZT increases the expression of multidrug transporters (MRPs) on human monocyte-derived macrophages (MDMs) and lymphocytes (Jorojuria *et al.*, 2004). Prolonged 3TC exposure (4 months) up-regulated ATP-cassette C11 (ABCC1) in a human T lymphoblastoid cell line and decreased the intracellular accumulation of 3TC (Turriziani *et al.*, 2002). Chronic treatment of a human T-lymphoblastoid cell line with a combination of AZT, 3TC and ABC induced expression multidrug resistance protein 4 (MRP4) leading to 3TC resistance. Meanwhile the acitivity of thymidine kinase (TK) was reduced, which led to AZT resistance (Turriziani *et al.*, 2006). Purcet *et al.* (2006) proved that the uptake of AZT in to peripheral blood mononuclear cells is inhibited by itself and up-regulated by phytohaemagglutinin (PHA, an OAT inhibitor) and higher temperature and concluded that AZT uptake into T-cells is associated with a mediated and regulated transport mechanism not only passive diffusion (Purcet *et al.*, 2006).

In this first generation PBPK model, the impact of one drug upon another was modeled to be proportional to the drug concentrations in related compartments. By using the first order interaction constants, the co-administration models were able to predict the observed kinetic data and also be robust enough to show maternal clearance and transplacental transport stimulation/inhibition. More experimental data, such as repeated dosing at different dose are

necessary for refinement of the mathematical descriptions of the NRTIs interactions. Since multiple transporters in different tissues such as kidney, liver and both maternal and fetal sides of the placenta, might play important roles in the interactions seen in this work, more information on the specific transporters is required to fully describe the interaction mechanism. Co-administration NRTIs with known cellular transporter inhibitors and even transporter gene knock-out animals will help identify the critical transporters and their functions on maternal clearance and tranplacental distribution of NRTIs (Aiba *et al.*, 1995; Gibbs *et al.*, 2003).

References

Aiba, T., Sakurai, Y., Tsukada, S., and Koizumi, T. (1995). Effects of probenecid and cimetidine on the renal excretion of 3'-azido-3'-deoxythymidine in rats. *Journal of Pharmacology and Experimental Therapeutics* **272**, 94-99.

Benhammou, V., Tardieu, M., Warszawski, J., Rustin, P., and Blanche, S. (2007). Clinical mitochondrial dysfunction in uninfected children born to HIV-infected mothers following perinatal exposure to nucleoside analogues. *Environmental and Molecular Mutagenesis* **48**, 173-178.

Blanche, S., Tardieu, M., Rustin, P., Slama, A., Barret, B., Firtion, G., Ciraru-Vigneron, N., Lacroix, C., Rouzioux, C., Mandelbrot, L., Desguerre, I., Rotig, A., Mayaux, M. J., and Delfraissy, J. F. (1999). Persistent mitochondrial dysfunction and perinatal exposure to antiretroviral nucleoside analogues. *Lancet* **354**, 1084-1089.

Brace, R. A. (2004). Amniotic fluid dynamics. In *Maternal-Fetal Medicine: Principles and Practice*, pp. 50. Elsevier Inc.

Briggs, G. G. (2005). *Drugs In Pregnancy And Lactation*. Lippincott Williams & Wilkins.

Brown, S. D., Bartlett, M. G., and White, C. A. (2003). Pharmacokinetics of intravenous acyclovir, zidovudine, and acyclovir-zidovudine in pregnant rats. *Antimicrobial Agents and Chemotherapy* **47**, 991-996.

Capparelli, E., Rakhmanina, N., and Mirochnickc, M. (2005). Pharmacotherapy of perinatal HIV. *Seminars in Fetal & Neonatal Medicine* **10**, 161-175.

CDC (2006). Guidlines for the Use of Antiretroviral Agents in HIV-1-Infected Adults and Adolescents. the DHHS Panel on Antiretroviral Guidelines for Adults and Adolescents - A Working Group of the Office of AIDS Research Advisory Concil.

Chatton, J. Y., Odone, M., Besseghir, K., and Rochramel, F. (1990). Renal secretion of 3'-azido-3'-deoxythymidine by the rat. *Journal of Pharmacology and Experimental Therapeutics* **255**, 140-145.

Collins, J. M. (2001). Inter-species differences in drug properties. *Chemico-Biological Interactions* **134**, 237-242.

Corley, R. A., Mast, T. J., Carney, E. W., Rogers, J. M., and Daston, G. P. (2003). Evaluation of physiologically based models of pregnancy and lactation for their application in children's health risk assessments. *Critical Reviews in Toxicology* **33**, 137-211.

Cote, H. C. F., Brumme, Z. L., Craib, K. J. P., Alexander, C. S., Wynhoven, B., Ting, L. L., Wong, H., Harris, M., Harrigan, P. R., O'Shaughnessy, M. V., and Montaner, J. S. G. (2002). Changes in mitochondrial DNA as a marker of nucleoside toxicity in HIV-infected patients. *New England Journal of Medicine* **346**, 811-820.

Cretton, E. M., Waterhous, D. V., Bevan, R., and Sommadossi, J. P. (1990). Glucuronidation of 3'-azido-3'-deoxythymidine by rat and human liver-microsomes. *Drug Metabolism and Disposition* **18**, 369-372.

Faber, K. N., Muller, M., and Jansen, P. L. M. (2003). Drug transport proteins in the liver. *Advanced Drug Delivery Reviews* **55**, 107-124.

Ganapathy, V., Prasad, P. D., Ganapathy, M. E., and Leibach, F. H. (2000). Placental transporters relevant to drug distribution across the maternal-fetal interface. *Journal of Pharmacology and Experimental Therapeutics* **294**, 413-420.

Gibbs, J. E., Rashid, T., and Thomas, S. A. (2003). Effect of transport inhibitors and additional anti-HIV drugs on the movement of lamivudine (3TC) across the guinea pig brain barriers. *Journal of Pharmacology and Experimental Therapeutics* **306**, 1035-1041.

GlaxoSmithKline (2002). ZIAGEN prescribing information, Research Triangle Park, NC.

GlaxoSmithKline (2006). Trizivir® Medication Guide. Research Triangle Park, NC.

Ibbotson, T., and Perry, C. M. (2003). Lamivuldine/zidovuldine/abacavir - Triple combination tablet. *Drugs* **63**, 1089-1098.

Jorojuria, S., Dereuddre-Bosquet, N., Becher, F., Martin, S., Porcheray, F., Garrigues, A., Mabondzo, A., Benech, H., Grassi, J., Orlowski, S., Dormont, D., and Clayette, P. (2004). ATP binding cassette multidrug transporters limit the anti-HIV activity of zidovudine and indinavir in infected human macrophages. *Antiviral Therapy* **9**, 519-528.

Kewn, S., Veal, G. J., Hoggard, P. G., Barry, M. G., and Back, D. J. (1997). Lamivudine (3TC) phosphorylation and drug interactions in vitro. *Biochemical Pharmacology* **54**, 589-595.

Kong, W., Engel, K., and Wang, J. (2004). Mammalian nucleoside transporters. *Current Drug Metabolism* **5**, 63-84.

Leazer, T. M., and Klaassen, C. D. (2003). The presence of xenobiotic transporters in rat placenta. *Drug Metabolism and Disposition* **31**, 153-167.

Lewis, S. R. (2006). Maternal and fetal disposition of antiviral agents in the pregnent rats. In *College of Pharamcy*. University of Georgia, Athens.

Mandelbrot, L., Landreau-Mascaro, A., Rekacewicz, C., Berrebi, A., Benifla, J. L., Burgard, M., Lachassine, E., Barret, B., Chaix, M. L., Bongain, A., Ciraru-Vigneron, N., Crenn-Hebert, C., Delfraissy, J. F., Rouzioux, C., Mayaux, M. J., and Blanche, S. (2001). Lamivudine-zidovudine combination for prevention of maternal-infant transmission of HIV-1. *Jama-Journal of the American Medical Association* **285**, 2083-2093.

Mays, D. C., Dixon, K. F., Balboa, A., Pawluk, L. J., Bauer, M. R., Nawoot, S., and Gerber, N. (1991). A nonprimate animal-model applicable to zidovudine pharmacokinetics in humans - inhibition of glucuronidation and renal excretion of zidovudine by probenecid in rats. *Journal of Pharmacology and Experimental Therapeutics* **259**, 1261-1270.

McDowell, J. A., Lou, Y., Symonds, W. S., and Stein, D. S. (2000). Multiple-dose pharmacokinetics and pharmacodynamics of abacavir alone and in combination with zidovudine in human immunodeficiency virus-infected adults. *Antimicrobial Agents and Chemotherapy* **44**, 2061-2067.

Moodley, J., Moodley, D., Pillay, K., Coovadia, H., Saba, J., van Leeuwen, R., Goodwin, C., Harrigan, P. R., Moore, K. H. P., Stone, C., Plumb, R., and Johnson, M. A. (1998). Pharmacokinetics and antiretroviral activity of lamivudine alone or when coadministered with zidovudine in human immunodeficiency virus type 1-infected pregnant women and their offspring. *Journal of Infectious Diseases* **178**, 1327-1333.

Nolan, D., and Mallal, S. (2004). Complications associated with NRTI therapy: update on clinical features, and possible pathogenic mechanisms. *Antiviral Therapy* **9**, 849-863.

Pacifici, G. M. (2005). Transfer of antivirals across the human placenta. *Early Human Development* **81**, 647-654.

Perinatal HIV Guidlines Working Group(P.H.G.W.G.) (2006). Public Health Service Task Force Recommendations for Use of Antiretroviral Drugs in Pregnant HIV-1-Infected Womean for Maternal Health and Interventions to Reduce Perinatal HIV-1 Transmission in the United States.

Purcet, S., Minuesa, G., Molina-Arcas, M., Erkizia, I., Casado, F. J., Clotet, B., Martinez-Picado, J., and Pastor-Anglada, M. (2006). 3 '-Azido-2 ',3 '-dideoxythymidine (zidovudine) uptake mechanisms in T lymphocytes. *Antiviral Therapy* **11**, 803-811.

Reddy, M. B., Yang, R. S. H., Clewell, H., and Andersen, M. E. (2005). Drugs. In *Physiologically Based Pharmacokinetic Modeling*. John Wiley & Sons, Inc.

Takeda, M., Khamdang, S., Narikawa, S., Kimura, H., Kobayashi, Y., Yamamoto, T., Cha, S. H., Sekine, T., and Endou, H. (2002). Human organic anion transporters and human organic cation transporters mediate renal antiviral transport. *Journal of Pharmacology and Experimental Therapeutics* **300**, 918-924.

Turriziani, O., Pagnotti, P., Pierangeli, A., Focher, F., Baranello, C., Bellomi, F., Falasca, F., Morgan, J., Schuetz, J. D., and Antonelli, G. (2006). The effects of prolonged treatment with zidovudine, lamivudine, and abacavir on a T-lymphoblastoid cell line. *Aids Research and Human Retroviruses* **22**, 960-967.

Turriziani, O., Schuetz, J. D., Focher, F., Scagnolari, C., Sampath, J., Adachi, M., Bambacioni, F., Riva, E., and Antonelli, G. (2002). Impaired 2 ',3 '-dideoxy-3 '-thiacytidine accumulation in T-lymphoblastoid cells as a mechanism of acquired resistance

independent of multidrug resistant protein 4 with a possible role for ATP-binding cassette C11. *Biochemical Journal* **368**, 325-332.

Unadkat, J. D., Dahlin, A., and Vijay, S. (2004). Placental drug transporters. *Current Drug Metabolism* **5**, 125-131.

Veal, G. J., and Back, D. J. (1995). Metabolism of zidovudine. *General Pharmacology* **26**, 1469-1475.

Wada, S., Tsuda, M., Sekine, T., Cha, S. H., Kimura, M., Kanai, Y., and Endou, H. (2000). Rat multispecific organic anion transporter 1 (rOAT1) transports zidovudine, acyclovir, and other antiviral nucleoside analogs. *Journal of Pharmacology and Experimental Therapeutics* **294**, 844-849.

Wang, L. H., Chittick, G. E., and McDowell, J. A. (1999). Single-dose pharmacokinetics and safety of abacavir (1592U89), zidovudine, and lamivudine administered alone and in combination in adults with human immunodeficiency virus infection. *Antimicrobial Agents and Chemotherapy* **43**, 1708-1715.

WHO (2006). Antiretroviral drugs for treating pregnant women and preventing HIV infection in infants: towards universal access.

Appendix

Below are the equations used to describe interactions in the PBPK model following 3TC-AZT and ABC-AZT combination therapy. Drug A and drug B represent the two drugs in two combination therapies. When one drug is considered as drug A, the other drug is considered as drug B. For interactions in the maternal elimination tissues, 3TC and AZT interactions were assumed in maternal kidney and interactions between ABC and AZT were assumed in the maternal liver.

Maternal clearance (CLm)

$$RCLm_A = \frac{dCLm_A^{+B}}{dt} = K\,\mathrm{int}_m^{B:A} \times \frac{Ci_B^{+A}}{PCi_B}$$

$$CLm_A^{+B} = CLm_A^0 + \int_0^t RCLm_A$$

$RCLm_A$ is the rate of change of the maternal clearance, CLm_A^{+B} is the maternal clearance of drug A in the presence of B, $K\,\mathrm{int}_m^{B:A}$ is the first order interaction constant describing the effect of drug B to A on maternal clearance, Ci_B^{+A} is the drug B concentration in elimination tissue (kidney or liver), PCi_B is the drug B tissue: blood partition coefficient, CLm_A^0 is the maternal clearance of A when dosed alone.

Transfer clearance from placenta blood to placenta tissue (CLmp)

$$RCLmp_A = \frac{dCLmp_A^{+B}}{dt} = K\,\mathrm{int}_{mp}^{B:A} \times Cplacb_B^{+A}$$

$$CLmp_A^{+B} = CLmp_A^0 + \int_0^t RCLmp_A$$

$RCLmp_A$ is the rate of change of transfer clearance of drug A from placental blood to placental tissue in presence of drug B, $CLmp_A^{+B}$: transfer clearances of drug A from placental blood to placental tissue, $K\,\mathrm{int}_{mp}^{B:A}$ is the 1st order interaction constant describing the effect of drug B on drug A placental blood to tissue transfer clearance, $Cplacb_B^{+A}$ is the drug B concentration in the placental blood in presence of drug A, $CLmp_A^0$ is the transfer clearance of drug A from placental blood to placental tissue of drug A was dosed alone.

Transfer clearance from placental tissue to placental blood (CLpm)

$$RCLpm_A = \frac{dCLpm_A^{+B}}{dt} = K\,\mathrm{int}_{pm}^{B:A} \times \frac{Cplac_B^{+A}}{PCpl_B}$$

$$CLpm_A^{+B} = CLpm_A^0 + \int_0^t RCLpm_A$$

$RCLpm_A$ is the rate of change of transfer clearance of drug A from placental tissue to placental blood in presence of drug B, $CLpm_A^{+B}$ is the transfer clearance of drug A from placental tissue to placenta blood in presence of drug B, $K\,\mathrm{int}_{pm}^{B:A}$ is the 1st order interaction constant describing the effect of drug B on drug A transfer clearance from placental tissue to placental blood, $Cplac_B^{+A}$ is the drug B concentration in placental tissue in presence of drug A, $PCpl_B$ is the placenta: blood partition coefficient of drug B, $CLpm_A^0$ is the transfer clearance of drug A from placental tissue to placental blood when dosed alone.

Transfer clearance from placental tissue to fetuses (CLpf)

$$RCLpf_A = \frac{dCLpf_A^{+B}}{dt} = K\,\mathrm{int}_{pf}^{B:A} \times \frac{Cplac_B^{+A}}{PCpl_B}$$

$$CLpf_A^{+B} = CLpf_A^0 + \int_0^t RCLpf_A$$

$RCLpf_A$ is the rate of change of transfer clearance of drug A from placental tissue to fetuses in presence of drug B, $CLpf_A^{+B}$ is the transfer clearance of drug A from placental tissue to fetuses in presence of drug B, $K\,\mathrm{int}_{pf}^{B:A}$ is the 1st order interaction constant describing the effect of drug B on A transfer clearance from placental tissue to fetuses, $Cplac_B^{+A}$ is drug B concentration in placental tissue in presence of drug A, $PCpl_B$ is the placenta:blood partition coefficient of drug B, $CLpf_A^0$ is the transfer clearance of drug A from placental tissue to fetuses when dosed alone.

Transfer clearance from fetuses to placental tissue (CLfp)

$$RCLfp_A = \frac{dCLfp_A^{+B}}{dt} = K\,\mathrm{int}_{fp}^{B:A} \times \frac{Cf_B^{+A}}{PCf_B}$$

$$CLfp_A^{+B} = CLfp_A^0 + \int_0^t RCLfp_A$$

$RCLfp_A$ is the rate of change of the transfer clearance of drug A from fetuses to placenta, $CLfp_A^{+B}$ is the transfer clearance of drug A from fetuses to placenta in presence of drug B, $K\,\mathrm{int}_{fp}^{B:A}$ is the 1st order interaction constant describing the effect of drug B to A on transfer clearance from fetuses to placenta, Cf_B^{+A} is the drug B concentration in fetuses in presence of drug A, PCf_B is the fetus:blood partition coefficient for drug B, $CLfp_A^0$ is the transfer clearance of drug A from fetuses to placental tissue when dosed alone.

Transfer clearance from fetuses to amniotic fluid (CLfaf)

$$RCLfaf_A = \frac{dCLfaf_A^{+B}}{dt} = K\,\mathrm{int}_{faf}^{B:A} \times \frac{Cf_B^{+A}}{PCf_B}$$

$$CLfaf_A^{+B} = CLfaf_A^0 + \int_0^t RCLfaf_A$$

$RCLfaf_A$ is the rate of change of transfer clearance of drug A from fetuses to amniotic fluid in presence of drug B, $CLfaf_A^{+B}$ is the transfer clearance of drug A from fetuses to amniotic fluid, $K\,\mathrm{int}_{faf}^{B:A}$ is the 1st order interaction constant describing the effect of drug B on A transfer clearance from fetuses to amniotic fluid, Cf_B^{+A} is the fetal concentration of drug B in the presence of drug A, PCf_B is the fetus:blood partition coefficient for drug B, $CLfaf_A^0$ is the transfer clearance of drug A from fetuses to amniotic fluid when dosed alone.

Transfer clearance from amniotic fluid to fetuses (CLfaf)

$$RCLaff_A = \frac{dCLaff_A^{+B}}{dt} = K\,\mathrm{int}_{aff}^{B:A} \times Caf_B^{+A}$$

$$CLaff_A^{+B} = CLaff_A^0 + \int_0^t RCLaff_A$$

$RCLaff_A$ is the rate of change of transfer clearance of drug A from amniotic fluid to fetuses, $CLaff_A^{+B}$ is the transfer clearance of drug A from amniotic fluid to fetuses, $K\,\mathrm{int}_{aff}^{B:A}$ is the 1st order interaction constant describing the effect of drug B on drug A transfer clearance from amniotic fluid to fetuses, Caf_B^{+A} is the drug B concentration in amniotic fluid in the presence

of drug A, $CLaff_A^0$ is the transfer clearance of drug A from amniotic fluid to fetuses when dosed alone.

Table 5.1 Physiological Parameters for pregnant rats on genstation day 19.

Physiological Parameters	Values	Source
Body weight of non-pregnant rat BW (kg)	0.3	Lewis (2006)
Cardiac output QCC (l/h/kg$^{0.75}$)	14.0	Brown *et al.* (2003)
Blood Flow		
Body QB (%QC)	68.0	Brown *et al.* (1997)
Kidney QKc (%QC)	14.0	Brown *et al.* (1997)
Liver QLc (%QC)	18.0	Brown *et al.* (1997)
Placenta QPL (l/h)	0.315	O'Flaherty *et al.* (1992)
Conceptus QCON (l/h)	0.202	O'Flaherty *et al.* (1992)
Tissue Volume		
Extracellular body VB_E (%BW)	30	Collins *et al.* (1999)
Intracellular body VB_I (%BW)	56	Collins *et al.* (1999)
Kidney VKc (%BW)	1.7	Brown et al. (1997)
Liver VLc (%BW)	3.4	Brown et al. (1997)
Plasma Vblc (%BW)	4	Brown et al. (1997)
Placenta VPL (kg)	0.0045	Lewis (2006)
Fetuses (kg)	0.025	Lewis (2006)
Amniotic Fluid VAF (kg)	0.0032	Lewis (2006)
Compartment blood volume (% of tissue volume)		
Placenta	50	Emond *et al.* (2004)

Table 5.2 Tissue-to-blood partition coefficients of NRTIs.

Partition coefficients	NRTIs		
	3TC	ABC	AZT
Body: blood (PCb)	1.28	2.30	0.93
Kidney : blood (PCk)	0.94	1.29	0.97
Liver : blood (PCl)	0.87	1.25	0.89
Placenta : blood (PCpl)	0.87	1.25	0.89
Fetuses : blood (PCf)	0.91	1.11	0.92
Permeability-surface area products PS_b (l/h)	0.31	0.69	0.32

Table 5.3 Estimated parameters (S.E.) for each NRTI in active-transport models.

Parameter	Symbols	NRTI Therapy						
		3TC	**AZT**	**ABC**	**3TC (+AZT)**	**AZT (+3TC)**	**ABC (+AZT)**	**AZT (+ABC)**
Transfer from maternal blood to placenta (ml/h)	CLmp	6.8 (0.5)	29.7 (1.4)	58.0 (14.4)	8.0 (0.7)	18.7 (5.8)	76.3 (31.0)	83.2* (27.2)
Transfer from placenta to maternal blood (ml/h)	CLpm	12.2 (1.1)	61.2 (3.8)	95.4 (23.5)	5.2* (0.6)	31.9* (9.8)	167.2 (70.5)	150.5 (58.6)
Transfer from placenta to fetus (ml/h)	CLpf	19.3 (3.6)	163.3 (13.0)	200.0 (68.5)	19.6 (4.0)	164.2 (71.5)	200.9 (57.7)	202.0 (121.8)
Transfer from fetus to placenta (ml/h)	CLfp	42.2 (9.1)	179.9 (15.4)	202.0 (68.4)	41.0 (9.9)	202.0 (98.3)	202.0 (65.7)	202.0 (136.0)
Transfer from fetus to amniotic fluid (ml/h)	CLfaf	1.5 (0.1)	1.8 (0.3)	11.9 (2.1)	1.2 (0.4)	2.7 (0.8)	2.1* (0.3)	3.6 (1.1)
Transfer from amniotic fluid to fetus (ml/h)	CLaff	1.4 (0.2)	1.3 (0.3)	6.4 (1.1)	2.8 (1.0)	2.5 (0.8)	2.0* (0.4)	2.6 (0.9)
Maternal clearance (l/h-kg)	CLr or CLh	0.79 (0.03)	0.65 (0.04)	2.76 (0.3)	0.76 (0.01)	1.0* (0.09)	0.2* (0.04)	0.87* (0.09)

***** T-test P-value < 0.05. Estimated parameter values in the mono-therapy *vs.* estimated parameter values in the combination therapy.

Table 5.4 Interaction constants for combination therapy in co-administration models (estimated values (S.E.))

Interaction Constants	Combination Therapy			
	AZT (+3TC)	3TC (+AZT)	AZT (+ABC)	ABC (+AZT)
$Kint_{mcl}$ for maternal clearance	+ 8.2 (1.2)	–	+ 2.5 (0.9)	-577.8 (1281.2)
$Kint_{mp}$ for transfer from maternal blood to placenta	-0.6 (0.04)	+ 0.3 (0.07)	+ 5.3 (0.02)	–
$Kint_{mp}$ for transfer from maternal blood to placenta	-1.3 (0.08)	- 0.3 (0.08)	+ 24.6 (0.10)	+ 3.1 (0.87)
$Kint_{pf}$ for transfer from placenta to fetus	–	–	–	–
$Kint_{fp}$ for transfer from fetus to placenta	–	–	–	–
$Kint_{faf}$ for transfer from fetus to amniotic fluid	–	–	+ 0.3 (0.20)	-30.3 (28.8)
$Kint_{aff}$ for transfer from amniotic fluid to fetus	–	+ 0.25 (0.05)	+ 0.4 (0.33)	- 3.0 (6.1)

Note: Interaction constant value of 0 was indicated by - in the table.

Table 5.5 Optimal log-likelihood values and Akaike Information Criterion (AIC) values of interaction models fitting to the kinetic data in placenta and fetuses.

	Removed Parameters from the full model	Df[1] for LLR[2] Test	LLF[3]	AIC[4]
3TC-AZT				
Model 0	Full Model [a]	NA	-54.2	124.4
Model 1	$K\,\mathrm{int}_{pf}^{3TC:AZT}$, $K\,\mathrm{int}_{fp}^{3TC:AZT}$	2	-55.6	123.2
Model 2	$K\,\mathrm{int}_{pf}^{3TC:AZT}$, $K\,\mathrm{int}_{fp}^{3TC:AZT}$, $K\,\mathrm{int}_{pf}^{AZT:3TC}$	3	-55.6	121.2
Model 3 (Final Model)	$K\,\mathrm{int}_{pf}^{3TC:AZT}$, $K\,\mathrm{int}_{fp}^{3TC:AZT}$, $K\,\mathrm{int}_{pf}^{AZT:3TC}$, $K\,\mathrm{int}_{fp}^{AZT:3TC}$	4	-56.6	121.2
ModelN	No interaction on transplacental transfer [b]	8	-103.1*	206.2
ABC-AZT				
Model 0	Full Model [a]	NA	-71.4	158.8
Model 1	$K\,\mathrm{int}_{pf}^{AZT:ABC}$, $K\,\mathrm{int}_{fp}^{AZT:ABC}$	2	-71.5	155.0
Model 2	$K\,\mathrm{int}_{pf}^{AZT:ABC}$, $K\,\mathrm{int}_{fp}^{AZT:ABC}$, $K\,\mathrm{int}_{mp}^{AZT:ABC}$, $K\,\mathrm{int}_{pf}^{ABC:AZT}$	4	-71.5	151.0
Model 3 (Final Model)	$K\,\mathrm{int}_{pf}^{AZT:ABC}$, $K\,\mathrm{int}_{fp}^{AZT:ABC}$, $K\,\mathrm{int}_{mp}^{AZT:ABC}$, $K\,\mathrm{int}_{pf}^{ABC:AZT}$, $K\,\mathrm{int}_{fp}^{ABC:AZT}$	5	-71.5	149.0
ModelN	No interaction on transplacental transfer [b]	8	-95.0*	190

[a] Full models are the initial models including 8 interaction constants: $K\,\mathrm{int}_{mp}^{3TC:AZT}$, $K\,\mathrm{int}_{pm}^{3TC:AZT}$, $K\,\mathrm{int}_{pf}^{3TC:AZT}$, $K\,\mathrm{int}_{fp}^{3TC:AZT}$ and $K\,\mathrm{int}_{mp}^{AZT:3TC}$, $K\,\mathrm{int}_{pm}^{AZT:3TC}$, $K\,\mathrm{int}_{pf}^{AZT:3TC}$, $K\,\mathrm{int}_{pf}^{AZT:3TC}$ for 3TC-AZT concentration-time profile in placenta and fetuses; $K\,\mathrm{int}_{mp}^{ABC:AZT}$, $K\,\mathrm{int}_{pm}^{ABC:AZT}$, $K\,\mathrm{int}_{pf}^{ABC:AZT}$, $K\,\mathrm{int}_{fp}^{ABC:AZT}$ and $K\,\mathrm{int}_{mp}^{AZT:ABC}$, $K\,\mathrm{int}_{pm}^{AZT:ABC}$, $K\,\mathrm{int}_{pf}^{AZT:ABC}$, $K\,\mathrm{int}_{fp}^{AZT:ABC}$ for ABC-AZT concentration-time profile in placenta and fetuses.

[b] In ModelN, all the interaction constants were fixed to 0 ($Kint_{mp} = Kint_{pm} = Kint_{pf} = Kint_{fp} = 0$) assuming no interactions on transplacental transfer and the parameter values for the combination-therapy data are the same as for the mono-therapy data.

[1] dgree of freedom. [2] log-likelihood ration. [3] log-likelihood function values. [4] Akaike Information Criterion.

* Significantly worse then the Model 3 LLF using LLR test for nested model ($\alpha = 0.05$).

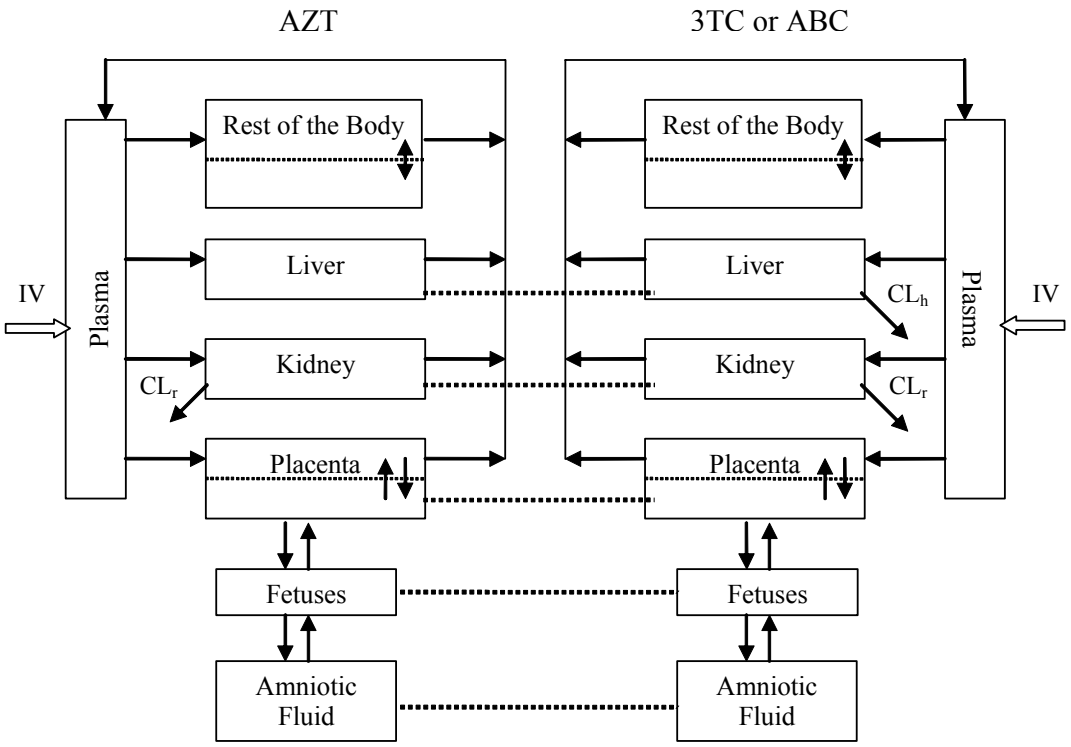

Figure. 5.1 Schematic PBPK model structure for NRTIs combination therapy. Dashed lines indicate the potential interactions of the two drugs in the maternal clearance (in kidney and liver) and maternal-fetal transfer (in placental, fetal and amniotic fluid compartments).

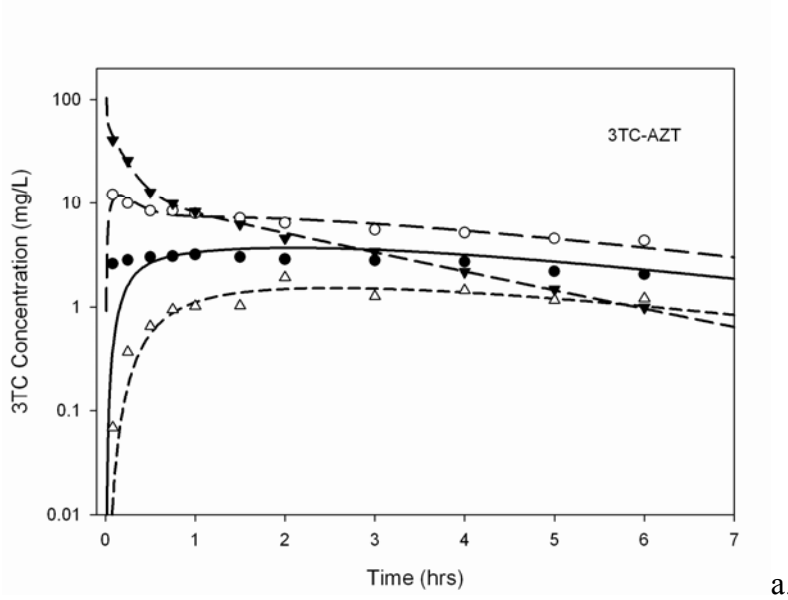

a.

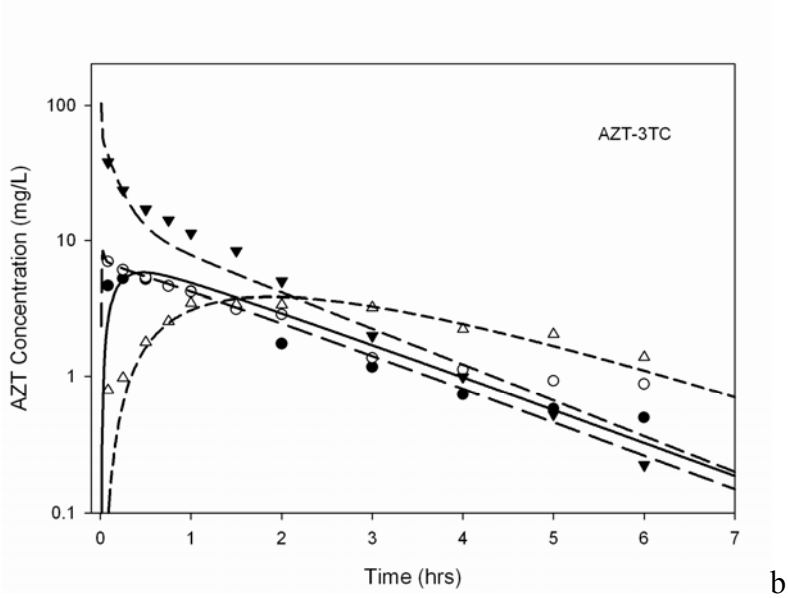

b.

Figure. 5.2 Independent active transport model predictions and observed average 3TC and AZT concentrations in maternal plasma (▼), placenta (○), fetuses (●) and amniotic fluid (Δ) following 3TC-AZT (25 mg/kg each) iv bolus in pregnant rats at gestation day 19. (a) 3TC concentration time profiles, (b) AZT concentration time profiles. Model specific parameter values are shown in Table 5.3.

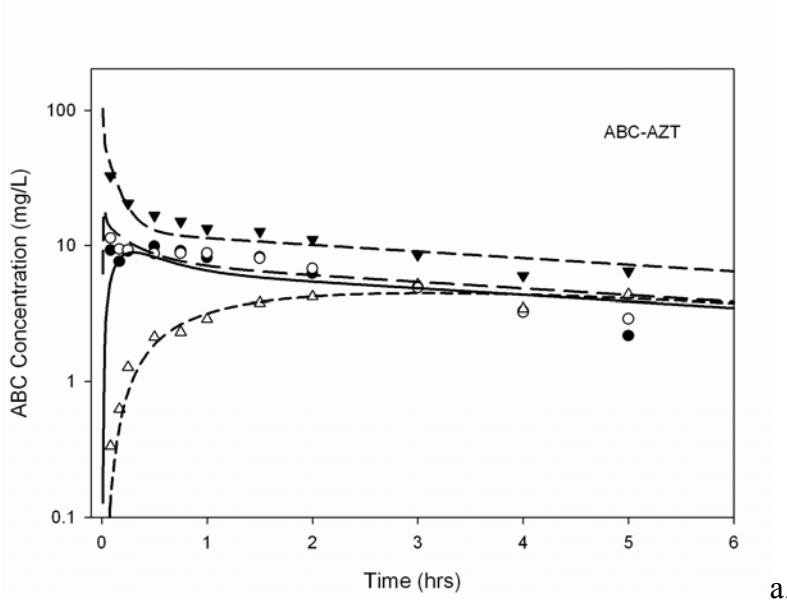

a.

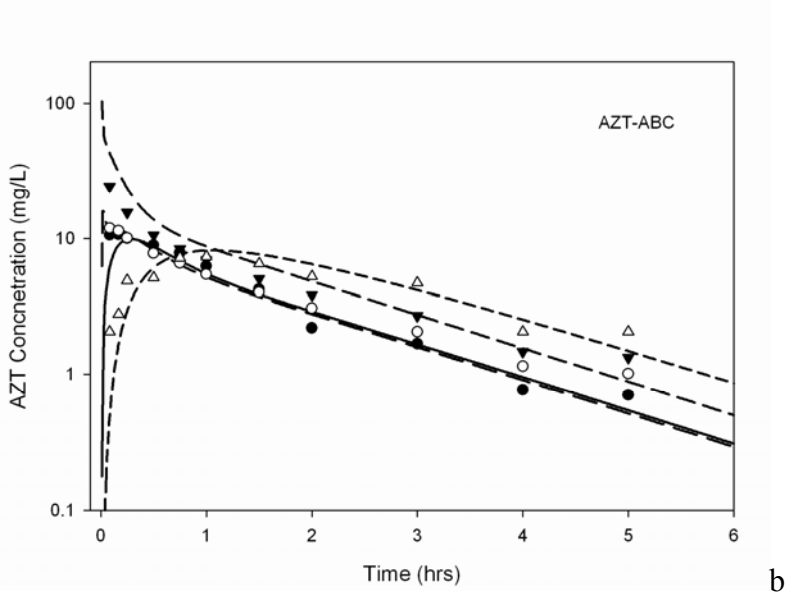

b.

Figure. 5.3 Independent active transport model predictions and observed average ABC and AZT concentrations in maternal plasma (▼), placenta (○), fetuses (●) and amniotic fluid (Δ) following ABC-AZT (25 mg/kg each) iv bolus in pregnant rats at gestation day 19. (a) ABC concentration time profiles, (b) AZT concentration time profiles. Model specific parameter values are shown in Table 5.3.

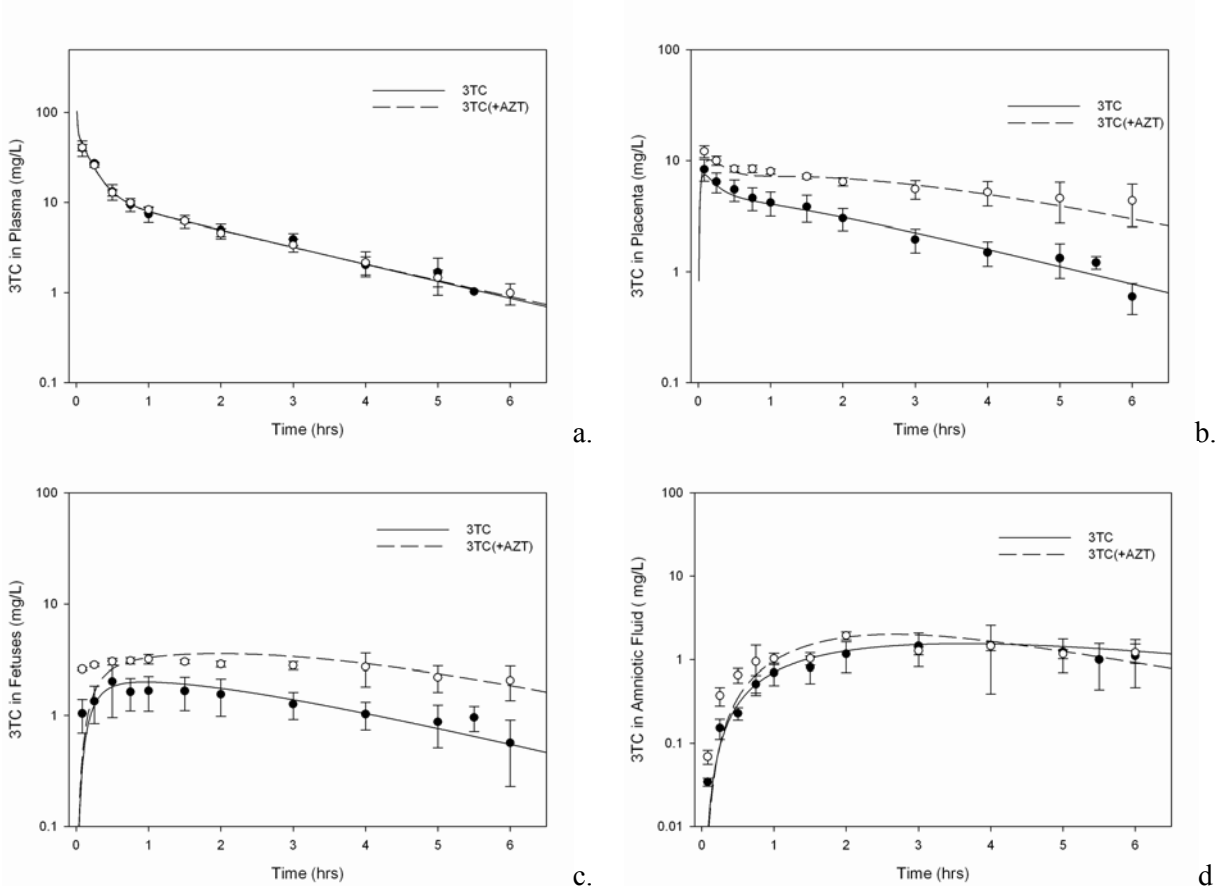

Figure. 5.4 Model predcitions and observed 3TC concentration time course data for mono-therapy (− and ●, respectively) and combination therapy with AZT (--- and ○, respectively). (a) In maternal plasma. (b) In placenta. (c) In fetuses. (d) In amniotic fluid. The vertical bars represent the SD of the observed mean values.

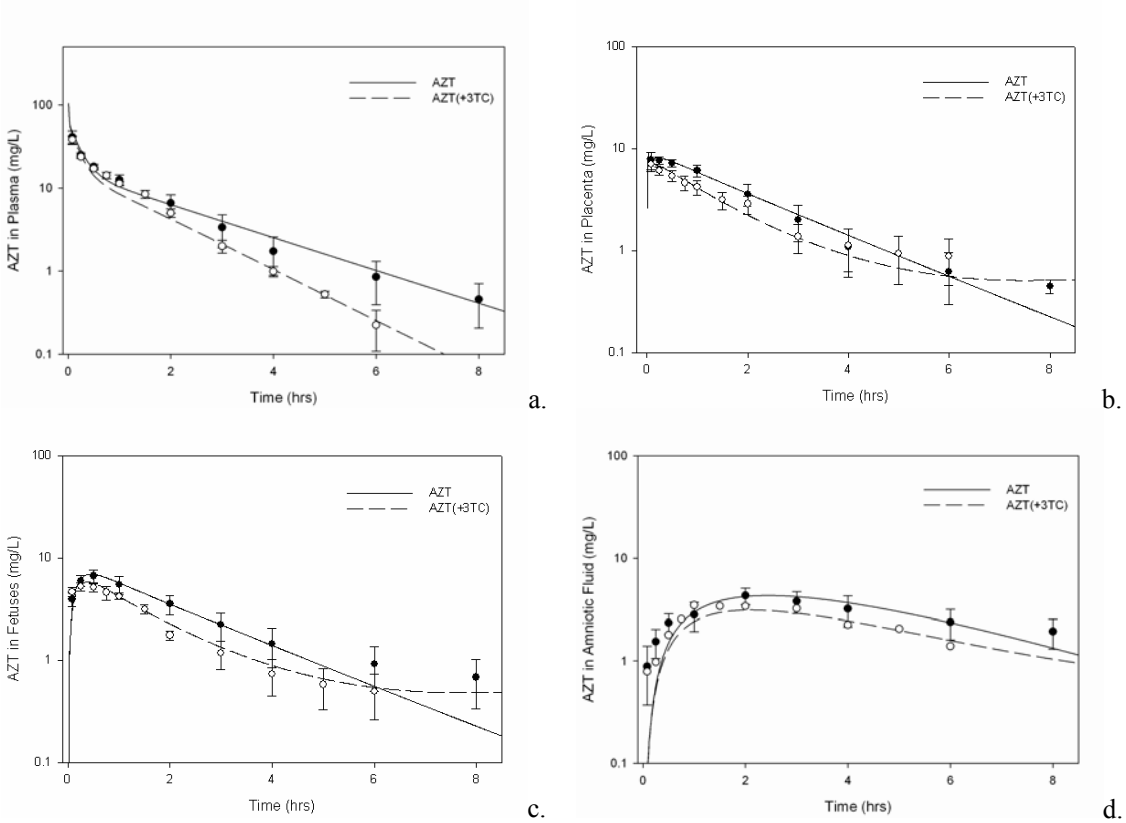

Figure. 5.5 Model predictions and observed AZT concentration time course data for mono-therapy (− and ●, respectively) and combination therapy with 3TC (--- and ○, respectively). (a) In maternal plasma. (b) In placenta. (c) In fetuses. (d) In amniotic fluid. The vertical bars represent the SD of the observed mean values.

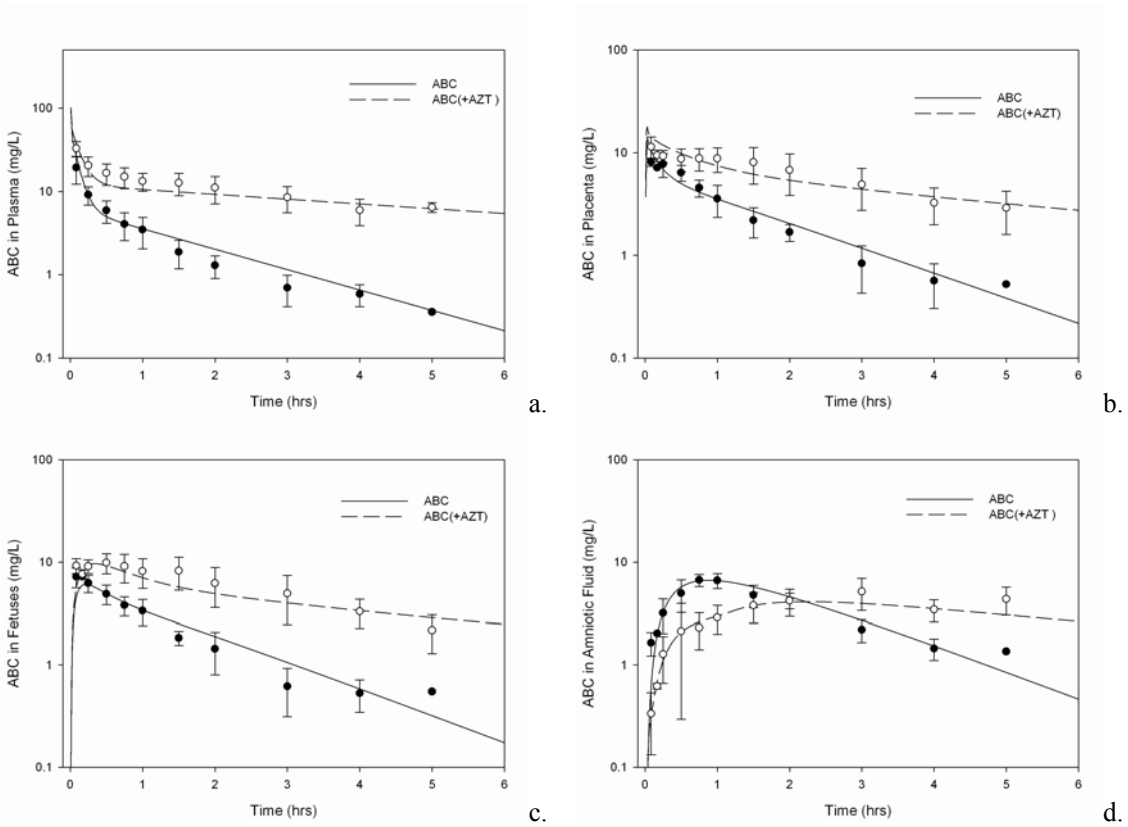

Figure. 5.6 Model predictions and observed ABC concentration time course data for mono-therapy (− and ●, respectively) and combination therapy with AZT (--- and ○, respectively). (a) In maternal plasma. (b) In placenta. (c) In fetuses. (d) In amniotic fluid. The vertical bars represent the SD of the observed mean values.

.

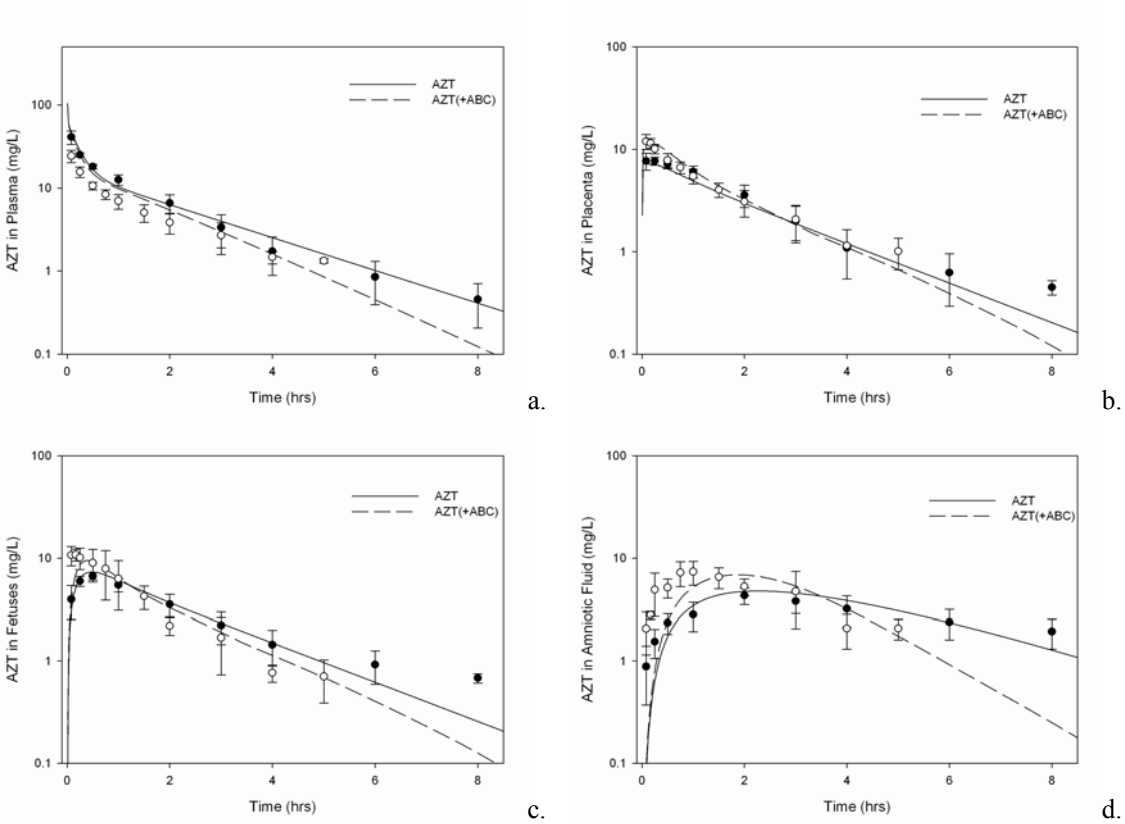

Figure. 5.7 Model simulations and observed AZT concentration time course data for mono-therapy (− and ●, respectively) and combination therapy with ABC (--- and ○, respectively). (a) In maternal plasma. (b) In placenta. (c) In fetuses. (d) In amniotic fluid. The vertical bars represent the SD of the observed mean values.

CHAPTER 6

CONCLUSIONS

PBPK model for DCA in human

The PBPK developed for DCA in human describes the uptake, distribution and metabolism across multiple independent studies with doses ranging from 2.5 μg/kg to 50 mg/kg. The model adequately predicted the kinetic data following high dose repeated exposure, lending support to the mathematical description of DCA-mediated GSTzeta inhibition (suicide inhibition). The primary metabolic parameters were derived either from *in vitro* experiments (the affinity constant, K_m) or estimated by fitting to the kinetic data (V_{max}, k_d and k_{de}). Model estimates for V_{max}, k_d and k_{de} were smaller for humans as compared to the values previously estimated for rodents, which is in agreement with the experimental observations. A low capacity and high affinity plasma protein binding was required to describe the observed kinetic data following 2.5 μg/kg dosing. Based on model simulations, after 50 mg/kg/day iv infusion until steady state, only 13 % of the initial metabolic capacity remained. While at 2.5 μg/kg/day dose level, more than 99% of the enzyme activity remains at steady state. Regardless of the dose, urinary excretion is a minor elimination pathway that less than 1% of the administered DCA was recovered unchanged from urine. In conclusion, using the human DCA PBPK model to predict a human equivalent dose for the dosimetric, AUC for total DCA in plasma and the point of departure liver cancer in mice (2.1 mg/kg/day), a 10% increase in incidence of liver cancer is equated to ingestion of 700 μg DCA per L of water assuming 2 L consumed per day.

PBPK model for NRTIs in pregnant rat

PBPK models were developed to capture the concentration time profile in maternal plasma, placenta, fetuses and amniotic fluid of four NTRIs (ddC, 3TC, AZT and ABC) administered intravenously to pregnant rats on GD 19. Three model structures including flow limited, passive diffusion and active transport were investigated for their ability to describe the transplacental distribution of the NRTIs. Based on visual and statistical evaluations (Akaike Information Criterion), the model structure including active transport provided significantly better fits to the observed kinetic data. The model predicted that the drug with higher lipophilicity crosses the placenta faster resulting in higher estimated transplacental distribution clearances in both directions as compared the more hydrophilic NRTIs. Asymmetrical transplacental transfer rates were identified for all four NRTIs. A trend toward a larger efflux transfer rate from the fetus back to the maternal blood was identified, which is in agreement with the observation that the relative exposures of NRTIs in fetuses ($AUC_{fetuses}/AUC_{maternal\ plasma}$) are less than 1. Studies have shown that NRTIs are substrates for multiple transporters expressed in placenta. Our studies support this hypothesis that transporter-mediated placental transport may play a significant role in fetal NRTI exposure *in vivo*.

PBPK models for NRTIs drug-drug interactions in pregnant rat

PBPK models were developed to characterize the concentration-time profiles of NRTIs in pregnant rats following 3TC-AZT and ABC-AZT combination therapy. The pharmacokinetic alterations in maternal clearance and transplcental distribution of one NRTI were mathematically described as a first order process related to the concentration of the co-administered NRTI. Maternal systemic clearance of AZT was increased in the presence of both 3TC and ABC while maternal systemic clearance of ABC was inhibited significantly by AZT. Therefore, these

interactions do not agree with simple competitive inhibition as the primary mode of interaction and may be attributed to up or down-regulating transporter activities in maternal kidney and liver. Without affecting the systemic clearance of 3TC, AZT increased 3TC accumulation in both placental and fetal compartments through increasing of the distribution clearances from maternal blood to the placental compartment and decreasing of the efflux rate from placenta to maternal blood. 3TC reduced the placneta and fetal exposure to AZT by reducing AZT placental transfer on the maternal side. AZT increased the efflux transfer of ABC from placenta to maternal blood and reduced significantly ABC transfer between fetus and amniotic fluid. ABC appeared to up-regulate the transplacental distribution rate of AZT in both directions, resulting in both higher and more rapid peak concentrations and clearances in both placental and fetal compartments. The most likely mechanisms behind the observed complex interactions on transplacental transfer are that NRTIs interaction with one another through multiple influx/efflux transporters located on the placenta. Co-administration of NRTIs with known cellular transporter inhibitors and even transporter gene knock-out animals will aide the identifying the critical transporters and their functions on maternal clearance and tranplacental distribution of NRTIs.

APPENDICES

APPENDIX A

THE PRO-FS PEPTIDE OF HIV-1 ACTIVATES LTR-DRIVEN GENE EXPRESSION VIA NF-KB WHEN EXPRESSED AS A SELENOPROTEIN, BUT NOT AS A CYSTEINE MUTANT

Ting Li, Lianchun Xiao, Lijun Zhao, and Ethan Will Taylor. Submitted to *Free Radical Research*, 07/20/2007.

Abstract

Pro-fs is a transframe peptide encoded via a –1 frameshift from the HIV-1 protease gene. The pro-fs coding sequence contains two in-frame UGA codons, potentially encoding selenocysteine. Pro-fs has significant similarity to the DNA binding loop of NF-κB, and has been shown to activate HIV-1 long terminal repeat (LTR) driven reporter gene expression. In the present study, pro-fs failed to stimulate gene expression driven by a κB^- LTR mutant, from which the NF-κB binding sites had been deleted. Use of a mutant pro-fs construct in which the two UGA codons of wild-type pro-fs were mutated to cysteine codons led to loss of ability to stimulate wild-type HIV-1 LTR. These mutagenesis studies show that 1) pro-fs stimulates the LTR through an NF-κB mediated pathway, and that 2) the expression of pro-fs as a selenoprotein is crucial to its ability to activate NF-κB. Using the yeast two-hybrid system to screen a human fetal liver cDNA library, we identified several potential targets of pro-fs, including β1-INTEGrin, stimulation of which is known to induce NF-κB activation. These observations confirm a critical role for selenium in HIV infection, and provide a basis for further investigations of the mechanism by which pro-fs activates NF-κB-dependent gene expression.

Introduction

The RNA genome of HIV-1 (~ 9-kb) encodes nine open reading frames (ORFs), which overlap each other either partially, or in some cases entirely, for several of the smaller ORFs. After proteolytic processing, at least 15 distinct proteins are expressed during the process of viral replication and assembly (Frankel and Young, 1998). The high protein encoding capability of HIV relative to its genome size is achieved by a combination of gene overlap, ribosomal frameshifting, alternative splicing, and the production of polycistronic mRNAs.

The protease frameshift protein, pro-fs (~10 kDa) is a putative HIV-encoded polypeptide expressed by a -1 frameshift from the protease (Toschi *et al.*) reading frame. It was first identified by computational analysis (Taylor *et al.*, 1994) and the functionality of the -1 ribosomal frameshift required for its expression was later demonstrated *in vitro* (Taylor *et al.*, 2000). Pro-fs was initially proposed to be a selenoprotein because there are two in-frame UGA codons in the 303 bp mRNA sequence, potentially encoding selenocysteine (SeCys), the selenium homologue of cysteine. Various selenoproteins have been identified in both eukaryotic and prokaryotic genomes, as well as in viruses (Shisler *et al.*, 1998; Driscoll and Copeland, 2003; Gromer *et al.*, 2005).

Selenium is an essential micronutrient, largely due to the fact that selenoproteins mediate a variety of biological process in mammals, such as antioxidant defense, thyroid action, reproductive function, regulation of gene expression, and immune function (Taylor *et al.*, 2000). Several of the most well characterized selenoproteins, glutathione peroxidase (GPx) and thioredoxin reductase (TR), together control two major redox systems in mammalian cells. An HIV-encoded homologue of GPx has been reported to have antioxidant and anti-apoptotic functions in transfected cells (Zhao *et al.*, 2000; Cohen *et al.*, 2004; Zhao *et al.*, 2006).

Clinically, serum selenium is commonly decreased in AIDS patients relative to uninfected controls, and in association with HIV-1 infection, selenium deficiency is associated with a high risk of disease progression and mortality (Cirelli *et al.*, 1991; Dworkin, 1994; Constans *et al.*, 1995; Baum *et al.*, 1997; Look *et al.*, 1997; Campa *et al.*, 1999; Kupka *et al.*, 2004). Several recent studies have shown that selenium, either alone or as part of a multivitamin-mineral supplement, can enhance the survival of HIV-1 infected patients not receiving antiretroviral drug treatment, as well as lead to decreased viral loads and improved CD4 cell count recovery in HIV patients, when used alone or in combination with antiretroviral therapy (Jiamton *et al.*, 2003; Odunukwe *et al.*, 2006; Hurwitz *et al.*, 2007). The study by Hurwitz et al. is the most definitive to date in that it demonstrates that Se supplementation can "suppress the progression of HIV-1 viral burden and provide indirect improvement of CD4 count" (Hurwitz *et al.*, 2007). These and other observations suggest a close relationship among selenium, selenoproteins, the immune response and HIV-1 disease progression and pathogenesis (Taylor *et al.*, 2000).

The long terminal repeat (LTR) of HIV serves as the promoter-enhancer for HIV transcription; it incorporates DNA binding sites for various cellular transcription factors, including SP-1, NF-κB, NF-AT and AP-1. Two adjacent κB sites just upstream of the TATA box in the LTR enable NF-κB to serve as the predominant cellular regulator of HIV transcription. Proteins of the NF-κB family serve as central mediators of host immune and inflammatory responses. NF-κB activity can be upregulated by inflammatory cytokines, such as tumor necrosis factor (TNF)-α and interleukin (IL)-1β, viral and bacterial antigens, and various oxidant stimuli. Its activity can be down-regulated by antioxidants such as α-lipoic acid, selenium, and protein kinase C (PKC) inhibitors (Kretz-Remy and Arrigo, 2001; Zhang and Frei, 2001; Baba, 2006). By incorporating κB sites in the viral LTR, HIV takes advantage of the

activation of NF-κB during the immune response, in order to activate its own gene expression and replication. The gp120, tat, vpr and nef proteins of HIV-1 can also at least indirectly activate NF-κB and further promote viral gene expression, as well as the expression of various cellular genes (e.g., certain cytokines).

Our group previously identified a region of local sequence similarity between pro-fs and the DNA binding loop of NF-κB, which is also the target of thioredoxin (Trx), a thiol reductant that is essential for activation of NF-κB in the cell nucleus (Matthews *et al.*, 1992; Hirota *et al.*, 1999; Taylor *et al.*, 2000). In co-transfection studies in MDCK cells, pro-fs was found to activate LTR-regulated β-gal activity (Xiao *et al.*, 2006). The diet-derived antioxidant ergothioneine showed consistent inhibitory activity on the HIV-1 LTR when assessed using either TNF-α or pro-fs as the activator (Xiao *et al.*, 2006). Using co-immunoprecipitation and GST-pulldown assays, Su et al. (2005) showed that pro-fs interacts with thioredoxin in cell-free systems, and also in the nucleus of living cells, by means of FRET assays in 293T cells (Su *et al.*, 2005).

In light of the central role of Trx in the regulation and nuclear activation of NF-κB (Matthews *et al.*, 1992; Hirota *et al.*, 1999), the results reviewed above support the hypothesis that pro-fs stimulates LTR-driven gene expression via an NF-κB mediated pathway, mostly likely via a redox-related mechanism involving an interaction with Trx, which is the only known biomolecule that has been proven to interact with pro-fs (Su *et al.*, 2005).

In the present study, a κB site deletion mutant of the HIV-1 LTR-β-gal reporter gene plasmid pHIVLacZ was used to assess the hypothesis that NF-κB is the transcription factor that mediates the effects of pro-fs on LTR-driven gene expression. Furthermore, the role of potential selenocysteine residues in the stimulatory activity of pro-fs was examined by creating a double SeCys → Cys mutant of pro-fs, since it is known that UGA codons can be decoded as Cys at low

efficiency by certain $tRNA_{Cys}$ isoacceptors (Urban and Beier, 1995), which can occur because of the high similarity between UGA and the Cys UGY codons. Finally, host proteins that might interact with pro-fs were investigated by yeast two-hybrid cDNA library screening.

Materials and methods

Construction of κB deletion mutant of pHIVLacZ (pHIVLacZκB⁻)

The 2 NF-κB binding sites in HIV-LTR were deleted by a PCR method. Briefly, the HIV-LTR fragment in the pHIVLacZ plasmid (obtained from the NIH AIDS Research and Reference Reagent Program, Rockville, MD) was excised using *Xho*I and *Hind*III and sequenced to confirm. Q1702: 5'-TTCTCGAGACCTGGAAAAACATGGAG-3' was used as sense primer (*Xho*I site was underlined) and Q82: 5'-CTGTTGACATCGAGCTTGTTAC------GGAGGCGTGGCCTGGGCGGGAC-3' as antisense primer (dashed line represents missing NF-κB binding sites) to synthesize the 5' fragment of LTR without the κB sites. The 3' fragment of LTR without NF-κB binding site was synthesized by using Q83: 5'-GTCCCGCCCAGGCCACGCCTCC------GTAACAAGCTCGATGTCAACAG-3'(dashed line represents missing κB sites) and Q783: 5'-ACAAGCTTTATTGAGGCTTAAGCAGTGGGTTC-3' (*Hind*III site was underlined) as anti-sense primer. The 5' fragment and 3' fragment then was used as template and amplified using Q1702 and Q783 as sense and antisense primers, respectively. The PCR products was cloned into pGEM-T vector and sequenced. The confirmed HIV-LTR fragment without NF-κB binding sites replaced the original HIV-LTR fragment between *Xho*I and *Hind*III sites in pHIVLacZ. The successful replacement of the mutated LTR was confirmed by sequencing.

Construction of double Cys mutant of HIV-1 pro-fs

The pro-fs eukaryotic expression vector **(**pEGFP-C1-profs) was previously constructed based upon the pEGFP-C1 plasmid (Xiao *et al.*, 2006). The pEGFP-C1-profs plasmid was used as the template for PCR-based site-directed mutagenesis. The two mutations (^{29}SeCys → ^{29}Cys and ^{58}SeCys → ^{58}Cys**)** were introduced sequentially. The primers used in this procedure were:

NhPfs: 5'- TCCGCTAGCATGGACCCTCAGATCA- 3'

Pfm29as: 5'- TCTTCTAATACTGTA**ACA**TCTGCTCCTGTATCTAAT – 3'

Pfm29s: 5'- ATTAGATACAGGAGCAGA**TGT**TACAGTATTAGAAGA -3'

Pfm58as: 5'- AGATTTCTATGAGTATCTGA**ACA**TACTGTCTTACTTTGAT- 3'

Pfm58s: 5'- ATCAAAGTAAGACAGTA**TGT**CTCAGATACTCATAGAAATCT- 3'

HinPfas: 5'- TTCGAAGCTTGTCTCAATAGGGCTAATG-3'

Underlined residues in NhPfs and HinPfas represent the *NheI* and *HindIII* site, respectively. Bold residues in other primers represent the mutated SeCys codon. To introduce the ^{29}Cys mutation, NhPfs /Pfm29a were used as sense/antisense primers for the preparation of the 5' fragment and Pfm29s / HinPfas were used as sense/antisense primers for the preparation of the 3' fragment. The 5' and 3' fragment served as template and were amplified by second PCR with NhPfs and HinPfas as primers. The PCR product then was connected into the pGEM-T vector (Promega) and the mutation was confirmed by DNA sequencing (pGEM-T-29Cys). The ^{58}Cys mutation was introduced similarly using pGEM-T-29Cys as the template. NhPfs / Pfm58as were used as sense/antisense primers for the preparation of the 5' fragment and Pfm58s / HinPfas were used as sense/antisense primers for the 3' fragment. The final PCR product was digested with *NheI* and *HindIII* and cloned into pEGFP-C1. The sequence of the entire transcribed region of the resultant plasmid pMPro-fs was verified by DNA sequencing. Sequencing and oligonucleotide syntheses were performed at the University of Georgia Molecular Genetics Instrumentation Facility.

Restriction enzymes were obtained from Promega (Madison, WI); other chemicals were obtained from Sigma (St. Louis, MO) unless otherwise specified.

Cell culture

The MDCK (canine kidney) cell line was a gift from Dr. Fengxiang Gao, Centers for Disease Control and Prevention, Atlanta GA. Cells to be used for the transfection studies were grown under 5% CO_2 at 37°C, in Dulbecco's modified Eagle's medium (DMEM/F12) supplemented with 2 mM L-glutamine, 5 μg/ml gentamycin, 0.5 mM sodium pyruvate, 1.2 g/L sodium bicarbonate and 10% calf serum (Atlanta Biologicals).

Generation of stably transfected MDCK cell lines

MProfs-MDCK, Profs-MDCK and P2-MDCK cell lines were created by transfection of MDCK cells with pMProfs, pPro-fs or P2 plasmids respectively, as described previously (Xiao *et al.*, 2006). Briefly, $2.5x10^5$ cells/well were seeded in 6-well plates the day before transfection. When cells attained 90 % confluency, 3 μg plasmid DNA complexed with 6 μg lipofectamine-2000 was added to each well and left overnight. After 24 hours, cells were diluted 100-fold and transfectants were selected with 500 μg/ml G418 (GIBco), by changing G418-containing medium every 3 days for 4-6 weeks, after which the positive clones were pooled.

Transient transfection and β-galactosidase assays

To study whether pro-fs stimulates the LTR through an NF-κB mediated pathway, the deletion mutant pHIVLacZκB$^-$ was created by deleting the tandem NF-κB biding sites from the LTR in pHIVlacZ, as described above. The stably transfected cell lines Profs-MDCK and P2-MDCK were then transiently transfected with pHIVLacZκB$^-$ using lipofectamine-2000, on 6-well plates, with each well seeded with 2.5×10^5 cells and 3 μg of pHIVLacZκB$^-$ plasmid DNA. Approximately 48 hours later, cells were washed with PBS, then harvested by trypsin digestion,

centrifuged at 12,000 g, and washed once with PBS. Then 400 μl cell lysis buffer (Promega) was added to each tube, and vortexed for 30 seconds, allowed to stand for 15 min, then vortexed again. After centrifugation at 12,000 g for 10 minutes, the supernatants were collected and assayed for β-gal activity using Promega's assay kit, according to the manufacturer's instructions. Briefly, 150 μL of cell extract supernatant for each sample was mixed with the same volume of 2X assay buffer, vortexed, and incubated at 37°C for 30 min. Then 500 μl of 1M aqueous Na_2CO_3 was added to stop the reaction, and absorption at 420 nm was determined. Measurements were standardized relative to protein concentration, and expressed as OD420 absorption per mg protein. Lysate protein concentration was determined by the Lowry method, using 15 μl of cell extract for each sample.

Transient transfection and luciferase assays

The stably transfected cells (P2-MDCK, Profs-MDCK, or MProfs-MDCK) were seeded on 24-well plates (each cell line in 3 wells, 1.0 x 10^5 cells per well) 24 hours before the transfection. The second day, cells was transfected with 0.9 μg of pNFκB-Luc plasmid DNA (Panomics) per well using lipofectamine-2000 (Invitrogen). The TransLucent NF-κB(1) reporter vector (LR0051) contains 6 copies of the κB motif (NF-κB binding sequence, 5'-GGGAATTTCC-3') upstream of a firefly luciferase reporter gene. At 48 hours post-transfection, luciferase activity was determined using the assay system provided by the manufacture (Promega). Briefly, cells in each well were rinsed with PBS, then collected using 200 μl cell lysis buffer and transferred into microcentrifuge tubes and placed on ice. Each tube was vorexted 10-15 seconds, then centrifuged at 12,000 g for 2 minutes at 4°C; then 20 μl of the cell lysate and 100 μl of the luciferase assay reagent were added to a luminometer tube and mixed by pipetting. The mixture was placed in a luminometer (Turner TD 20/20; Promega, Madison, WI) and relative

luminescence intensity was read for ten seconds, following a programmed two second delay. Lysate protein concentration was determined by the BCA protein assay (Pierce), using 15 μl of cell extract for each sample. Measurement of both the luciferase activity and the BCA assay were repeated 3 times for each well.

Construction of pro-fs bait strain

Yeast two-hybrid experiments were conducted using the Hybrid-Hunter System (Invitrogen, Carlsbad, CA). The pro-fs-Cys open reading frame was amplified by PCR from pET43.1b-Pro-fs, in which the two in frame SeCys were already mutated to Cys for bacterial expression (Su *et al.*, 2005); the same constraints apply to the requirement for expression in yeast, so it was not possible to use a selenoprotein expression construct of pro-fs for the two-hybrid experiments. For the PCR to excise the coding region, the sense primer was PfEco, 5'-CTCGTGAATTCGTTCAACTTCCCGCAGATCA - 3', containing an *EcoR*I site (underlined residues). The antisense primer was PfXho,
5'- CCTGTACACTCGAGTTATGTCCACAGATTTC - 3', containing a *Xho*I site (underlined residues). The PCR product was cloned into pHybLex/Zeo vector between the *EcoR*I and *Xho*I sites, transformed into XL1-Blue Competent *E. coli* cells (Stratagene, Cedar Creek, TX) and grown overnight on LB plates with 200ug/ml Zeocin^{TM}. Single Zeocin^{TM}-resistant clones were amplified and plasmids were purified from the cells and sequenced to confirm that the pro-fs gene was cloned in-frame with LexA. The pHybLex/Zeo-Pro-fs-Cys bait plasmid was transformed into EGY48 + pSH18-34 yeast cells to create the bait strain using the small-scale yeast transformation protocol provided by the manufacture. The cells were tested for nonspecific autoactivation of the reporter genes in order to confirm that the bait yeast strain was $Leu^{-}LacZ^{-}$ as expected.

cDNA library screening

The cDNA library of human fetal liver in vector pYESTrp (Invitrogen) was used to perform the library screening. The two-step selection method described in the protocol of small-scale library transformation using EGY48 from the manufacturer was followed. Briefly, EGY48-pHybLex/Zeo-Pro-fs + pSH18-34 yeast cells were transformed with the pYESTrp –cDNA and the double transformants were first grown 2 days at 30^{o}C on YC-WUZ200 plates (lacking trytophan, uracil and with supplement of 200ug/ml Zeocin^{TM}). The primary transformant was collected and resuspend in 1 volume of glycerol solution. The yeast suspension was immediately diluted in 10 volumes of YC-WUZ200 Gal/Raff dropout medium (lacking trytophan, uracil and supplemented with 200ug/ml Zeocin^{TM}, 2% galactose and 1% raffinose instead of glucose) and incubated with shaking for 4 hours, so that the GAL promoter was induced to express the library. The suspension was then plated on YC-WULZ200 Gal/Raff dropout plates (lacking trytophan, uracil, leucine and supplemented with 200ug/ml Zeocin^{TM}, 2% galactose and 1% raffinose instead of glucose). The plates were incubated for 3 days at 30^{o} C. Single clones were picked and re-plated on new YC-WULZ200 Gal/Raff plates to select for leucine prototrophism. The β-galactosidase activity of the Leu+ colonies was determined using a β-galactosidase filter lift assay according to the manufacturer's instructions (Hybrid Hunter, Invitrogen). Colonies that were positive for both leucine prototrophy and β-galactosidase activity were chosen as putative positive clones for further study.

Plasmids from the initial positive clones were isolated from the yeast cells as described in the manufacture's protocol. The candidate interacting proteins were amplified by PCR using the pYESTrp forward and reverse primers, 5'-GATGTTAACGATACCAGCC -3' and 5'-GCGTGAATGTAAGCGTGAC -3', respectively. The amplified candidate ORF's were digested

with *EcoR*I and cloned into the pYESTrp plasmid. The plasmids were reintroduced into the bait strain yeast cells and the leucine prototrophy and β-galactosidase activity of the double transformants were tested as described above. The pYESTrp plasmids in the clones that were positive for both reporter genes were sequenced. In all the experiments, pHybLex/Zeo-Fos and pYESTrp2-Jun double transformants, and pHybLex/Zeo-lamin and pYESTrp2-cDNA double transformants were tested in parallel with pHybLex/Zeo-Pro-fs-Cys and pYESTrp2-cDNA double transformants and served as positive and negative controls, respectively.

Statistical Analyses

Data are expressed as mean ± SE of 3 replicates. Student's t-test was used to compare the β-gal activity after transfection with pHIVLacZ or pHIVLacZκB$^-$ plasmid into the stably transfected Profs-MDCK and P2-MDCK cell lines. Bonferroni mutiple comparision was used to compare the luciferase activity in P2-MDCK, Profs-MDCK and MProfs-MDCK cell lines. All the analyses were conducted using the SAS program (SAS Institute Inc., NC, USA). Means were considered significantly different at $p<0.05$.

Results

Pro-fs activation of HIV-1 LTR-driven reporter gene expression is mediated by κB sites

Pro-fs has been previously shown to activate the LacZ gene expression under the direction of the HIV-1 LTR (Xiao *et al.*, 2006). To study which transcriptional regulator in the LTR is involved in this process, the pHIVLacZκB$^-$ plasmid, from which the two NF-κB biding sites in the LTR have been deleted, was constructed and transfected into Profs-MDCK and P2-MDCK cell lines. β-galactosidase activity was then measured. The results of a typical triplicate experiment are shown in Figure A.2. The β-gal enzyme activity (expressed as OD420 absorbance per mg protein) in the pHIVLacZκB$^-$ transfected Profs-MDCK cells (0.042 ± 0.02) only accounted for 1.6% of

the β-gal enzyme activity in the wild type pHIVLacZ transfected Profs-MDCK cells (2.60 ± 0.16); the p-value of the t-test for this difference is $p < 0.001$. In cells not expressing pro-fs (the stably transfected P2-MDCK control cell line), the β-gal reporter gene was not activated by either the wild type LTR (pHIVLacZ) or the κB^- LTR (pHIVLacZκB^-), with β-gal enzyme activity being almost undetectable in both cases, and not significantly different ($p < 0.1$). These data demonstrate that HIV pro-fs stimulates reporter gene expression by acting via NF-κB rather than through other promoter/enhancer elements in the LTR. This result is in agreement with the prediction by Taylor et al. that pro-fs may function via mimicry of NF-κB (Taylor *et al.*, 2000).

Mutation of the in-frame UGA codons of pro-fs to Cys codons abolishes its ability to activate reporter gene expression via the LTR

Since the previous result showed that pro-fs stimulates LTR-driven reporter gene expression solely via NF-κB, for further studies of pro-fs we used the pNFkB-Luc plasmid (Panomics) which contains a luciferase gene downstream of 6 copies of the NF-κB binding site. pNFkB-Luc was transiently transfected into Profs-MDCK, MProfs-MDCK and P2-MDCK cells and luciferase levels in each cell line were measured. The results of a typical triplicate experiment are shown in Figure A.3. The luciferase activity (luminescence per μg protein) in P2-MDCK, Profs-MDCK and MProfs-MDCK cells were 2.87 ± 0.45, 8.19 ± 0.22 and 3.97 ± 0.35, respectively. The luciferase activity in Profs-MDCK was more than 2 fold higher than in both P2-MDCK and MProfs-MDCK cell lines ($p < 0.001$). The luciferase activities in P2-MDCK and Mprofs-MDCK cell lines were not different from each other ($p > 0.2$), though the MProfs-MDCK tended to have higher luciferase activity than P2-MDCK cells. These data again confirm that the selenoprotein isoform of pro-fs can stimulate gene expression via activation of κB sites. However, the observation that this activity is largely abolished when the double Cys mutant of pro-fs is used

suggests that decoding of the UGA codons as selenocysteine residues may be essential for pro-fs to serve as a κB activator.

Putative binding partners of pro-fs

To investigate the possible pathway of pro-fs modulation of NF-κB signaling, the yeast two hybrid system was used to identify potential interactions of pro-fs with cellular proteins. A human fetal liver cDNA library was used for the screen. The pHybLex/Zeo-Pro-fs-Cys bait plasmid and pYESTrp –cDNA prey plasmid were co-transformed into EGY48 +pSH18-34 yeast cells and grown for 3 days and 200 colonies were replicated on new YC-WULZ200 Gal/Raff plates to select for leucine prototrophism and positive β-galactosidase activity. Two clones (Pb14 and Pb35) showed as positives to both reporter genes. PCR directly from the yeast cells identified 2 different ORFs from these Pb14 and Pb35 colonies. Re-introduction these two ORFs into individual pYESTrp prey plasmids, and subsequent co-transfection with pHybLex/Zeo-Pro-fs-Cys bait plasmid, activated both reporter genes in each case; thus, the specific biding of Pro-fs-Cys and the proteins encoded in these two ORFs was confirmed. GenBank database BLAST searching identified Pb14 as encoding eukaryotic translation initiation factor 4 γ (EIF4G1, BC010688) and Pb35 as encoding INTEGrin β1 (ITGB1, NP_391988).

Discussion

The ability of recombinant pro-fs to activate HIV-1 LTR-driven gene expression in transfected cells, which has been reported previously (Xiao *et al.*, 2006), has been studied by using deletion mutagenesis. Our results show that activation of the HIV-1 LTR by pro-fs (when expressed as a selenoprotein) is mediated via NF-κB recognition sites, because the effect is abolished when the two NF-κB binding sites are specifically deleted from the LTR (Figure A.2). Pro-fs is an HIV-encoded gene product, so it is possible that pro-fs-mediated activation of HIV-1

transcription via the LTR may be part of a viral autoregulatory mechanism. Such mechanisms have been demonstrated for other viral proteins, such as HIV-1 tat and nef. Pro-fs may activate NF-κB via a redox pathway, since it has been shown to bind directly to Trx (Su *et al.*, 2005), and ergothioneine, an antioxidant, can inhibit the ability of pro-fs to activate NF-κB (Xiao *et al.*, 2006).

The UGA codon in RNA has the potential to encode selenocysteine, an analog of cysteine, with selenium in place of sulfur. Selenocysteine is found in the active sites of several selenoenzymes involved in redox reactions, such as GPx and Trx. These selenoproteins are typically 1-3 orders of magnitude more active than their Cys analogs, though similar catalytic efficiencies have been reported for *E. coli* enzymes (Johansson *et al.*, 2005; Johansson *et al.*, 2006). In our study, the potential role of selenium in pro-fs in the activation of NF-κB was specifically tested using a luciferase expression plasmid having only κB sites in the promoter region. The double Cys mutant of pro-fs lost the ability to mimic or activate NF-κB (Figure A.3), which suggests that the coding function of the in-frame UGA codons of pro-fs is not simply to encode Cys, which is known to occur in other microbial systems because of the high similarity between UGA and the Cys UGY codons (Urban and Beier, 1995). This result is consistent with the hypothesis that expression as a selenoprotein is necessary for pro-fs to be able to stimulate NF-κB.

However, the substrate binding ability of pro-fs may not be substantially affected by the Cys mutations, because it is well known that binding ability can exist in the absence of catalytic or agonist activity. The purified recombinant Cys mutant of pro-fs was previously shown by three different methods to be able to bind *in vitro* not only to Trx, but also, with reduced affinity, to a Trx mutant whose active site Cys residues had been mutated to Ala (Su *et al.*, 2005). This

proves that the Cys mutant of pro-fs still retains protein binding ability, despite its inability to stimulate NF-kB, as compared to the wild-type pro-fs construct in the present study.

This is important because, for our yeast two hybrid studies of its potential *in vitro* interactions with host proteins, the double Cys mutant of pro-fs (Mpro-fs) was used, for reasons similar to those cited previously by Su et al. in the Trx binding study (Su *et al.*, 2005). These include the need to achieve a high level of protein expression, and differences between mammalian and non-mammalian mechanisms of selenoprotein synthesis, making it mandatory that a conventional protein (as opposed to selenoprotein) expression construct be used.

Although our screening of Mpro-fs vs. a human liver library did not generate Trx as a hit, it did lead to the identification of two additional cellular proteins, β1 INTEGrin and eukaryotic initiation factor 4 γ (eIF4G1), that showed specific protein-protein interactions with Mpro-fs. It is possible that 1) Trx may have been sequestered by binding to other targets in the library, or that 2) Trx may interact with its fusion partner in the prey plasmid construct, masking its CXXC active site; either of these conditions would be unfavorable for pro-fs binding to Trx. Nonetheless, the two positive hits that did come up in screening are of considerable interest, because both proteins have potential links to NF-κB regulation and have been at least indirectly implicated in HIV infection, as reviewed below.

INTEGrins are a family of membrane receptors involved extracellular matrix interactions, hence mediating cell adhesion, recognition and signaling in a variety of processes. They are heterodimeric proteins made up of α and β subunits, and are generally classified according to their β subunits. β1 INTEGrins are a minority of the INTEGrin population, and are believed to play an important role in the recirculation of T cells and tissue infiltration in inflammatory and immune responses (Leblond *et al.*, 2000). For example, the β1 INTEGrins

play a critical role in virally mediated epithelial synapse signaling in HIV-1-infected cells and in epithelial cells (Alfsen *et al.*, 2005). INTEGrin α1β1 is involved in the protection of TNF-α-induced neuronal injury (Wang *et al.*, 2006). HIV tat gene expression regulates endothelial cell proliferation and Kaposi's sarcoma progression by binding to α5β1 and αVβ3 INTEGrins through Arg-Gly-Asp (RGD) domains, acting via the Ras/ERK MAPK signaling pathway (Toschi *et al.*, 2006).

HIV-1 infection of human T-lymphocytes results in enhanced expression of α5β1 INTEGrin (Weeks *et al.*, 1991; Torre *et al.*, 1996), also known as the fibronectin receptor (FNR), which mediates phagocytosis, cell motility and the immune response. Most significant for the present study is a body of evidence that has accumulated since the mid 1990s showing that stimulation of β1 INTEGrins (e.g., binding of fibronectin to FNR) leads to NF-κB activation, which has been demonstrated in monocytes, Jurkat T cells, and primary endothelial cells (Lin *et al.*, 1995; Rosales and Juliano, 1996; Klein *et al.*, 2002; Reyes-Reyes *et al.*, 2002; Witte *et al.*, 2004). Witte et al. demonstrated that INTEGrin stimulation with fibronectin caused a 50 to 100-fold enhancement of nef/tat mediated HIV-LTR driven gene transcription in a transfected T cell line, an effect that must be at least partially mediated via NF-κB (Witte *et al.*, 2004). In the same study, HIV-1 nef was shown to mimic an INTEGrin receptor transduction signal by recruiting the Polycomb group (PcG) protein Eed to the plasma membrane, which was also a major factor in enhanced tat/nef-mediated viral gene expression (Witte *et al.*, 2004).

Thus, there is abundant evidence of a role for β1 INTEGrin-mediated effects on transcriptional activation processes in HIV infection, which could contribute to the biological activity of pro-fs, e.g. if pro-fs were able to act as a fibronectin signal mimic and stimulate NF-κB by binding to β1 INTEGrin.

Eukaryotic initiation factor 4γ (eIF-4γ) is a scaffold protein that interacts with many translation factors (Keiper *et al.*, 1999). Interestingly, it was reported that HIV-1 protease can cleave eIF-4γ and thus inhibit cap-dependent translation in host cells during acute HIV-1 infection (Ventoso *et al.*, 2001; Perales *et al.*, 2003). eIF-4γ also can interact with TNF-α receptor-associated factor 2 (TRAF2), a signaling molecule that plays a key role in activation of NF-κB through TNF-α in the cellular stress response (Kim *et al.*, 2005). Thus, again, a putative binding partner of pro-fs has the potential to modulate NF-κB-dependent signal transduction.

In conclusion, our results suggest that both selenocysteine incorporation and NF-κB activation (or mimicry of NF-κB) play critical roles in pro-fs stimulation of gene expression via the HIV-1 LTR. The finding that a selenoprotein isoform of pro-fs can stimulate the LTR, and thus, potentially, HIV-1 replication, would seem to run counter to evidence suggesting that dietary selenium has a net antiviral and beneficial effect in HIV infection (Constans *et al.*, 1995; Baum *et al.*, 1997; Hurwitz *et al.*, 2007). However, the molecular mechanisms involving selenium are sufficiently complex that a balance between stimulatory and inhibitory roles in both host and pathogen are likely to exist. Selenium inhibits HIV-1 replication in cultured cells (Hori *et al.*, 1997), yet enhanced expression of the cellular selenoprotein GPx was shown to enhance viral replication and subsequent appearance of cytopathic effects associated with an acutely spreading HIV infection (Diamond *et al.*, 2001). Similarly, Trx, which is redox cycled by the selenoprotein TR, has dual and opposing effects on NF-κB in the cytosol and the nucleus (Hirota *et al.*, 1999). Furthermore, pro-fs is only one of several potential HIV-encoded selenoprotein modules (Taylor *et al.*, 2000), one of which, an HIV-encoded GPx (Zhao *et al.*, 2006), appears to be a survival marker in HIV infection (Cohen *et al.*, 2004). And finally, pro-fs itself must exist in various isoforms (e.g. higher molecular mass forms not processed by HIV protease, and thus

extended at the N-terminal), and so far we have only investigated a low mass isoform; the biological activity of other isoforms could differ.

In light of our results, it seems highly likely that pro-fs can also activate cellular genes that are regulated by NF-κB, although this has not been explicitly tested. Possible as yet unexplored functions of pro-fs in the HIV life cycle may exist, based on the suggested protein-protein interactions with β1 INTEGrin and eIF-4γ, although, as discussed above, interactions with either of these molecules have the potential to modulate NF-κB signaling, which is a demonstrated activity of pro-fs (Xiao *et al.*, 2006). More specific experiments are needed before these potential interactions can be confirmed. However, the demonstrated ability of pro-fs to mimic NF-κB, the primary cellular activator of HIV, provides a firm basis for the further study of pro-fs as a potential target for antiviral intervention.

Acknowledgments

This work was supported by U.S. Public Health Service grant DA13561 from the National Institute on Drug Abuse, and North Carolina Biotechnology Center grant #2005-FRG-1014, both to EWT.

List of abbreviations

AIDS, acquired immunodeficiency syndrome

AP-1, Activator protein-1

BCA, bicinchoninic acid

EIF-4γ, eukaryotic initiation factor 4γ

FRET, fluorescent resonance energy transfer

HIV-1, human immunodeficiency virus type 1

β-gal, β-galactosidase

GPx, Glutathione peroxidase

ITGB1, β1 INTEGrin

LTR, long terminal repeat

MDCK, Madin-Darby canine kidney

NF-AT, nuclear factor of activated T cells

NF-κB, nuclear factor kappa B

ORF, open reading frame

PBS, phosphate buffered saline

PcG, Polycomb group

PCR, polymerase chain reaction

PKC, protein kinase C

Pro-fs, protease frameshift protein

SeCys, selenocysteine

TNF-α, tumor necrosis factor-α

TRAF2, TNF-α receptor-associated factor 2

TR, thioredoxin reductase

Trx, thioredoxin

References

Alfsen, A., Yu, H. F., Magerus-Chatinet, A., Schmitt, A., and Bomsel, M. (2005). HIV-1-infected blood mononuclear cells form an INTEGrin- and agrin-dependent viral synapse to induce efficient HIV-1 transcytosis across epithelial cell monolayer. *Mol Biol Cell* **16**, 4267-4279.

Baba, M. (2006). Recent status of HIV-1 gene expression inhibitors. *Antivir Res* **71**, 301-306.

Baum, M. K., Shor-Posner, G., Lai, S., Zhang, G., Lai, H., Fletcher, M. A., Sauberlich, H., and Page, J. B. (1997). High risk of HIV-related mortality is associated with selenium deficiency. *J Acquir Immune Defic Syndr Hum Retrovirol* **15**, 370-374.

Campa, A., Shor-Posner, G., Indacochea, F., Zhang, G. Y., Lai, H., Asthana, D., Scott, G. B., and Baum, M. K. (1999). Mortality risk in selenium-deficient HIV-positive children. *J Acquir Immune Defic Syndr* **20**, 508-513.

Cirelli, A., Ciardi, M., Desimone, C., Sorice, F., Giordano, R., Ciaralli, L., and Costantini, S. (1991). Serum selenium concentration and disease progress in patients with HIV infection. *Clin Biochem* **24**, 211-214.

Cohen, I., Boya, P., Zhao, L., Metivier, D., Andreau, K., Perfettini, J. L., Weaver, J. G., Badley, A., Taylor, E. W., and Kroemer, G. (2004). Anti-apoptotic activity of the glutathione peroxidase homologue encoded by HIV-1. *Apoptosis* **9**, 181-192.

Constans, J., Pellegrin, J. L., Sergeant, C., Simonoff, M., Pellegrin, I., Fleury, H., Leng, B., and Conri, C. (1995). Serum selenium predicts outcome in HIV infection. *J Acquir Immune Defic Syndr Hum Retrovirol* **10**, 392.

Diamond, A. M., Hu, Y. J., and Mansur, D. B. (2001). Glutathione peroxidase and viral replication: implications for viral evolution and chemoprevention. *Biofactors* **14**, 205-210.

Driscoll, D. M., and Copeland, P. R. (2003). Mechanism and regulation of selenoprotein synthesis. *Annu Rev Nutr* **23**, 17-40.

Dworkin, B. M. (1994). Selenium deficiency in HIV infection and the Acquired Immunodeficiency Syndrome (AIDS). *Chemico-Biol Interact* **91**, 181-186.

Frankel, A. D., and Young, J. A. (1998). HIV-1: fifteen proteins and an RNA. *Annu Rev Biochem* **67**, 1-25.

Gromer, S., Eubel, J. K., Lee, B. L., and Jacob, J. (2005). Human selenoproteins at a glance. *Cell Mol Life Sci* **62**, 2414-2437.

Hirota, K., Murata, M., Sachi, Y., Nakamura, H., Takeuchi, J., Mori, K., and Yodoi, J. (1999). Distinct roles of thioredoxin in the cytoplasm and in the nucleus. A two-step mechanism of redox regulation of transcription factor NF-kappaB. *J Biol Chem* **274**, 27891-27897.

Hori, K., Hatfield, D., Maldarelli, F., Lee, B. J., and Clouse, K. A. (1997). Selenium supplementation suppresses tumor necrosis factor alpha-induced human immunodeficiency virus type 1 replication in vitro. *AIDS Res Hum Retroviruses* **13**, 1325-1332.

Hurwitz, B. E., Klaus, J. R., Llabre, M. M., Gonzalez, A., Lawrence, P. J., Maher, K. J., Greeson, J. M., Baum, M. K., Shor-Posner, G., Skyler, J. S., and Schneiderman, N. (2007). Selenium Supplementation Suppresses HIV Viral Load: a randomized controlled trial. *Arch Int Med* **In press**.

Jiamton, S., Pepin, J., Suttent, R., Filteau, S., Mahakkanukrauh, B., Hanshaoworakul, W., Chaisilwattana, P., Suthipinittharm, P., Shetty, P., and Jaffar, S. (2003). A randomized trial of the impact of multiple micronutrient supplementation on mortality among HIV-infected individuals living in Bangkok. *Aids* **17**, 2461-2469.

Johansson, L., Arscott, L. D., Ballou, D. P., Williams, J. C. H., and Arner, E. S. J. (2006). Studies of an active site mutant of the selenoprotein thioredoxin reductase: The Ser-Cys-Cys-Ser motif of the insect orthologue is not sufficient to replace the Cys-Sec dyad in the mammalian enzyme. *Free Radic Biol Med* **41**, 649-656.

Johansson, L., Gafvelin, G., and Arner, E. S. J. (2005). Selenocysteine in proteins--properties and biotechnological use. *Biochim Biophys Acta* **1726**, 1-13.

Keiper, B. D., Gan, W. N., and Rhoads, R. E. (1999). Protein synthesis initiation factor 4G. *Int J Biochem Cell Biol* **31**, 37-41.

Kim, W. J., Back, S. H., Kim, V., Ryu, I., and Jang, S. K. (2005). Sequestration of TRAF2 into stress granules interrupts tumor necrosis factor signaling under stress conditions. *Mol Cell Biol* **25**, 2450-2462.

Klein, S., de Fougerolles, A. R., Blaikie, P., Khan, L., Pepe, A., Green, C. D., Koteliansky, V., and Giancotti, F. G. (2002). Alpha 5 beta 1 INTEGrin activates an NF-kappa B-dependent program of gene expression important for angiogenesis and inflammation. *Mol Cell Biol* **22**, 5912-5922.

Kretz-Remy, C., and Arrigo, A. P. (2001). Selenium: a key element that controls NF-kappa B activation and I kappa B alpha half life. *Biofactors* **14**, 117-125.

Kupka, R., Msamanga, G. I., Spiegelman, D., Morris, S., Mugusi, F., Hunter, D. J., and Fawzi, W. W. (2004). Selenium status is associated with accelerated HIV disease progression among HIV-1-infected pregnant women in Tanzania. *J Nutr* **134**, 2556-2560.

Leblond, V., Legendre, C., Gras, G., Dereuddre-Bosquet, N., Lafuma, C., and Dormont, D. (2000). Quantitative study of beta(1)-INTEGrin expression and fibronectin interaction profile of T lymphocytes in vitro infected with HIV. *Aids Research and Human Retroviruses* **16**, 423-433.

Lin, T. H., Rosales, C., Mondal, K., Bolen, J. B., Haskill, S., and Juliano, R. L. (1995). INTEGrin-mediated tyrosine phosphorylation and cytokine message induction in monocytic cells. A possible signaling role for the Syk tyrosine kinase. *J Biol Chem* **270**, 16189-16197.

Look, M. P., Rockstroh, J. K., Rao, G. S., Kreuzer, K. A., Spengler, U., and Sauerbruch, T. (1997). Serum selenium versus lymphocyte subsets and markers of disease progression and inflammatory response in human immunodeficiency virus-1 infection. *Biol Trace Elem Res* **56**, 31-41.

Matthews, J. R., Wakasugi, N., Virelizier, J. L., Yodoi, J., and Hay, R. T. (1992). Thioredoxin regulates the DNA binding activity of NF-kappa B by reduction of a disulphide bond involving cysteine 62. *Nucleic Acids Res* **20**, 3821-3830.

Odunukwe, N. N., Onwujekwe, D., Ezechi, O. O., Ezobi, P., Gbajabiamila, T., Anyanwu, R., Iloka, E., Adu, R., Nwogbe, O., Audu, R., Herbertson, E., Idigbe, E. O., and Kanki, P. (2006). The role of selenium as adjunct to HAART among HIV-infected individuals who are advanced in their disease. Abstract MoAb0403 In *16th Int AIDS Conf*, Toronto, Canada.

Ohta, H., Tsurudome, M., Matsumura, H., Koga, Y., Morikawa, S., Kawano, M., Kusugawa, S., Komada, H., Nishio, M., and Ito, Y. (1994). Molecular and Biological Characterization of Fusion Regulatory Proteins (Frps) - Anti-Frp Mabs Induced Hiv-Mediated Cell-Fusion Via an INTEGrin System. *Embo Journal* **13**, 2044-2055.

Perales, C., Carrasco, L., and Ventoso, I. (2003). Cleavage of eIF4G by HIV-1 protease: effects on translation. *Febs Letters* **533**, 89-94.

Reyes-Reyes, M., Mora, N., Gonzalez, G., and Rosales, C. (2002). beta1 and beta2 INTEGrins activate different signalling pathways in monocytes. *Biochem J* **363**, 273-280.

Rosales, C., and Juliano, R. (1996). INTEGrin signaling to NF-kappa B in monocytic leukemia cells is blocked by activated oncogenes. *Cancer Res* **56**, 2302-2305.

Shisler, J. L., Senkevich, T. G., Berry, M. J., and Moss, B. (1998). Ultraviolet-induced cell death blocked by a selenoprotein from a human dermatotropic poxvirus. *Science* **279**, 102-105.

Su, G., Min, W., and Taylor, E. W. (2005). An HIV-1 encoded peptide mimics the DNA binding loop of NF kappa B and binds thioredoxin with high affinity. *Mut. Res.* **579**, 125-132.

Taylor, E. W., Cox, A. G., Zhao, L., Ruzicka, J. A., Bhat, A. A., Zhang, W., Nadimpalli, R. G., and Dean, R. G. (2000). Nutrition, HIV, and drug abuse: the molecular basis of a unique role for selenium. *J Acquir Immune Defic Syndr* **25 Suppl 1**, S53-61.

Taylor, E. W., Ramanathan, C. S., Jalluri, R. K., and Nadimpalli, R. G. (1994). A basis for new approaches to the chemotherapy of AIDS: novel genes in HIV-1 potentially encode selenoproteins expressed by ribosomal frameshifting and termination suppression. *J Med Chem* **37**, 2637-2654.

Torre, D., Ferrario, G., Issi, M., Pugliese, A., and Speranza, F. (1996). Expression of the alpha 5 beta 1 fibronectin receptor on T lymphocytes of patients with HIV-1 infection. *J Clin Path* **49**, 733-736.

Toschi, E., Bacigalupo, I., Strippoli, R., Chiozzini, C., Cereseto, A., Falchi, M., Nappi, F., Sgadari, C., Barillari, G., Mainiero, F., and Ensoli, B. (2006). HIV-1 Tat regulates endothelial cell cycle progression via activation of the Ras/ERK MAPK signaling pathway. *Mol Biol Cell* **17**, 1985-1994.

Urban, C., and Beier, H. (1995). Cysteine tRNAs of plant origin as novel UGA suppressors. *Nucleic Acids Res* **23**, 4591-4597.

Ventoso, I., Blanco, R., Perales, C., and Carrasco, L. (2001). HIV-1 protease cleaves eukaryotic initiation factor 4G and inhibits cap-dependent translation. *Proc Natl Acad Sci USA* **98**, 12966-12971.

Wang, J. Y., Grabacka, M., Marcinkiewicz, C., Staniszewska, I., Peruzzi, F., Khalili, K., Amini, S., and Reiss, K. (2006). Involvement of alpha 1 beta 1 INTEGrin in insulin-like growth factor-1-mediated protection of PC12 neuronal processes from tumor necrosis factor-alpha-induced injury. *J Neurosci Res* **83**, 7-18.

Weeks, B. S., Klotman, M. E., Dhawan, S., Kibbey, M., Rappaport, J., Kleinman, H. K., Yamada, K. M., and Klotman, P. E. (1991). HIV-1 infection of human lymphocytes-T results in enhanced alpha-5-beta-1 INTEGrin expression. *J Cell Biol* **114**, 847-853.

Witte, V., Laffert, B., Rosorius, O., Lischka, P., Blume, K., Galler, G., Stilper, A., Willbold, D., D'Aloja, P., and Sixt, M. (2004). HIV-1 nef mimics an INTEGrin receptor signal that recruits the Polycomb group protein Eed to the plasma membrane. *Mol Cell* **13**, 179-190.

Xiao, L., Zhao, L., Li, T., Hartle, D. K., Aruoma, O. I., and Taylor, E. W. (2006). Activity of the dietary antioxidant ergothioneine in a virus gene-based assay for inhibitors of HIV transcription. *Biofactors* **27**, 157-165.

Zhang, W. J., and Frei, B. (2001). Alpha-lipoic acid inhibits TNF-alpha-induced NF-kappa B activation and adhesion molecule expression in human aortic endothelial cells. *Faseb J* **15**, 2423-2432.

Zhao, L., Cox, A. G., Ruzicka, J. A., Bhat, A. A., Zhang, W., and Taylor, E. W. (2000). Molecular modeling and in vitro activity of an HIV-1-encoded glutathione peroxidase. *Proc Natl Acad Sci USA* **97**, 6356-6361.

Zhao, L., Olubajo, B., and Taylor, E. W. (2006). Functional studies of an HIV-1 encoded glutathione peroxidase. *Biofactors* **27**, 93-107.

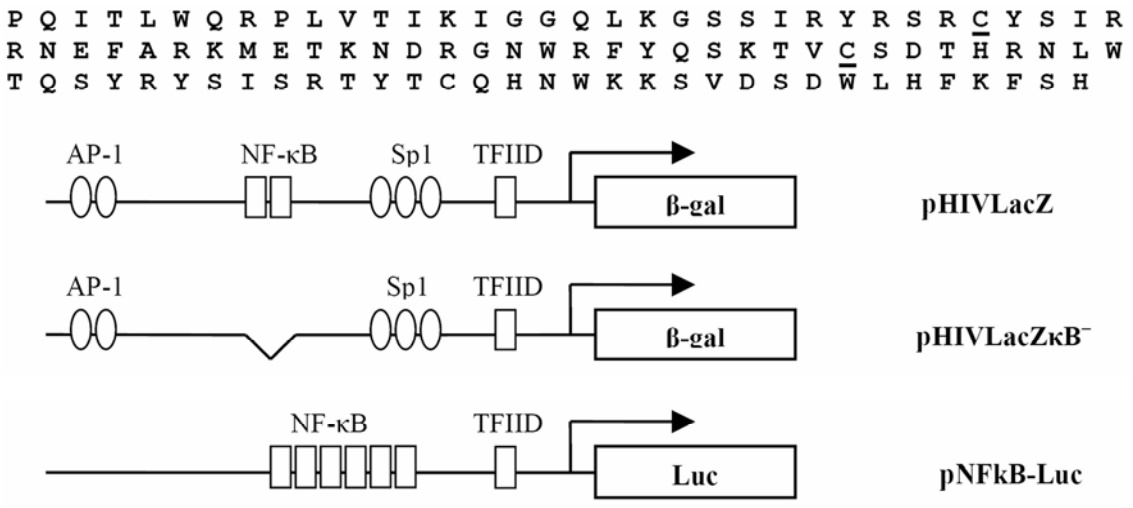

Figure A1. The pro-fs amino acid sequence is shown followed by schematic representations of the pHIVLacZ, pHIVLacZκB^{-} and pNFκB-Luc plasmids used in the experiments. The underlined C residues in the pro-fs sequence are potential selenocysteine codons (Ohta *et al.*) that were mutated to cysteine codons in the MPro-fs construct used in the experiment shown in Figure A.3.

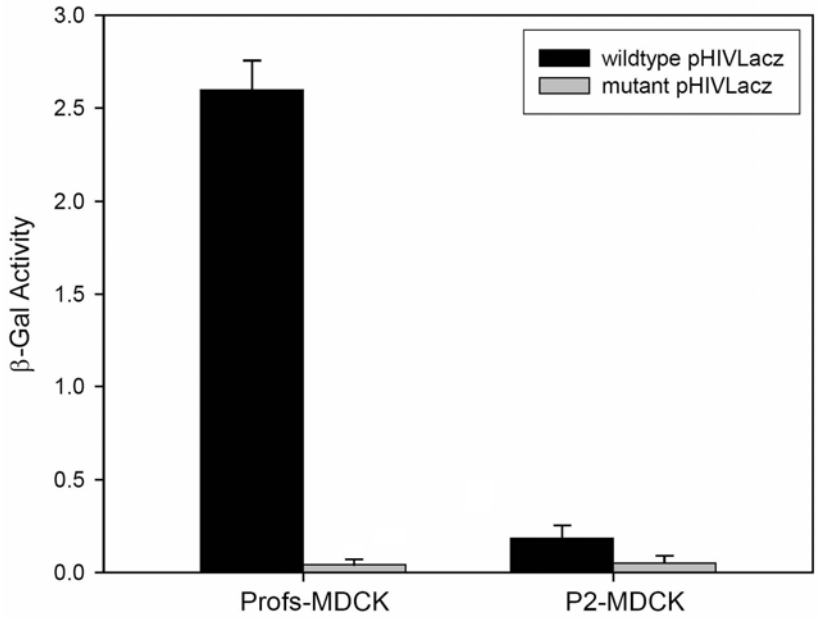

Figure A2. NF-κB binding sites in the LTR are essential for pro-fs activation of gene expression. Pro-fs-MDCK and P2-MDCK were transiently transfected with the pHIVlacZ plasmid or the κB^- deletion mutant plasmid pHIVLacZκB^-, followed by assay for β-gal enzyme activity, expressed in units of OD420 absorption per mg protein ± SE (n=3). In Pro-fs-MDCK cells transfected with the deletion mutant pHIVLacZκB^-, the β-gal enzyme activity was only about 8% of that observed in Pro-fs-MDCK cells transfected with the wild-type LTR pHIVlacZ plasmid ($p<0.001$). The β-gal enzyme activities in P2-MDCK cells after pHIVlacZ plasmid or pHIVLacZκB^- plasmid transfection were not significantly different from each other. This shows that the ability of pro-fs to stimulate the HIV LTR is mediated via NF-κB.

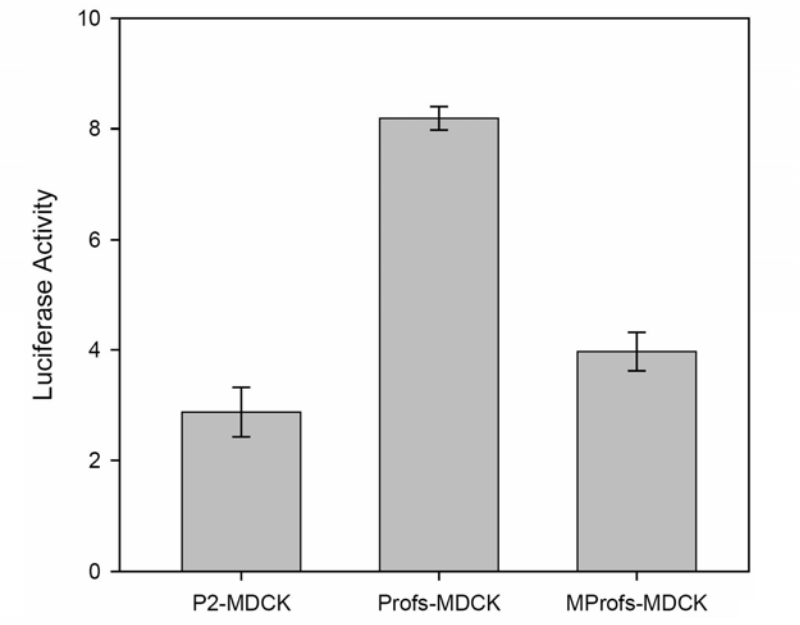

Figure A3. Selenocysteine residues are essential for pro-fs activation of gene expression. Pro-fs-MDCK, MProfs-MDCK (the Cys mutant of pro-fs) and P2-MDCK (negative control) were transiently transfected with the pNFκB-Luc plasmid, which contains an NF-κB promoter-enhancer driving expression of the luciferase gene. Luciferase enzyme activity is expressed in units of luminescence per μg protein ± SE (n=3). In pro-fs transfected cells, there was a 2-fold increase in the induction of luciferase enzyme activity relative to the MProfs-MDCK and P2-MDCK ($p<0.001$). The luciferase activities in MProfs-MDCK and P2-MDCK were not significantly different from each other, showing that, unlike the selenoprotein pro-fs construct (Pro-fs-MDCK), the Cys mutant of pro-fs is relatively ineffective as an NF-κB activator.

APPENDIX B

ACSL MODEL CODE

DCA Model Code

```
PROGRAM

INITIAL
!blood flow rate
CONSTANT QCC = 16.5  !Cardiac output (l/hr-kg):Brown, 1997;
CONSTANT QLC =0.227  !Fractional blood flow to liver: Brown, 1997;
CONSTANT QKC = 0.175 !Fractional blood flow to kidney:Brown, 1997;

!tissue volume
CONSTANT   BW = 70    !Body weight (kg)
CONSTANT   VLC = 0.026 !Fraction liver tissue(male):Brown, 1997;
CONSTANT   VKC = 0.0044 !Fraction Kidney tissue(male):  Brown, 1997
CONSTANT   VPC = 0.044

!partition coefficient for DCA- use mice value
CONSTANT   PL = 1.08   !Liver/blood partition coefficient: Abbas & Fisher, 1997
CONSTANT   PS = 0.37   !Slowly perfused tissue/blood partition: Abbas & Fisher, 1997
CONSTANT   PR = 1.08   !Richly perfused tissue/blood partition: Abbas & Fisher, 1997
CONSTANT   PK = 0.74   !kidney tissue/blood partition: Abbas & Fisher, 1997


!Metabolism Paramters
CONSTANT   VMAXC =27.16  !Maximum velocity of metabolism (mg/hr): Tong, 1998
CONSTANT   KM = 6.1      !Michaelis-Menten constant (mg/l): Tong, 1998
CONSTANT   KD = 0.3      !rate constant for loss of enzyme
CONSTANT   KDE = 0.001   !basal enzyme destruction rate(/hr):Curry, 1991
CONSTANT   KFC = 0.      !First order metabolism rate constant (/hr-1kg)
CONSTANT   Clrc = 0.0007 !1st order urinary elimin. rate constant(/hr):Curry, 1991

!Molecular Weight
CONSTANT   MWDCA = 129. !Molecular weight DCA (g/mol)

!'Scaled parameters'
!Physiological
      QC = QCC*BW**0.75
      QL = QLC*QC
```

```
      QK = QKC*QC
      QR = 0.76*QC-QL-QK  !Brown, 1997
      QS = 0.24*QC        !Brown, 1997
      VL = VLC*BW
      VK = VKC*BW
      VS = 0.747*BW       !Brown, 1997
      VR = 0.129*BW-VL-VK  !Brown, 1997
      VPL = VPC*BW

    !'metabolism and elimination'
     VMAX = VMAXC*BW**0.75
      KF = KFC/BW**0.25
     Clr = Clrc*BW

!resynthesis rate (mg/hr)/hr =kde*vmax so that vmaxt=vmax at steady-state
      KS = KDE*VMAX

!'Dosing'
CONSTANT   PDOSE = 0.      !first oral dose(mg/kg)
CONSTANT   pdose14= 0.02   !dose for 14C-DCA (mg/kg)
CONSTANT   TOR = 0.0         !Start time of first oral dose (hr)
CONSTANT   TOR14 = 24      !start time of 14 day 0.02mg/kg DCA
CONSTANT   IVDOSE1 = 0.    !First IV dose(mg/kg)
CONSTANT   IVDOSE2 = 0.    !Second IV dose (mg/kg)
CONSTANT   TINF = 0.5      !Length of IV infusion(hrs)
CONSTANT   TIV1 = 0.          !Start time of fist iv dosing (hr)
CONSTANT   TIV2 = 8.       !Start time of second iv dosing (hr)
CONSTANT   IVINT1 = 360    !Interval of 1st iv repeat dosing (hrs)
CONSTANT   IVINT2 = 10000  !Interval of 2nd iv repeat dosing (hrs)
CONSTANT   FinalIV =9      !Last IV dosing time (hr)
CONSTANT   FINALOR = 337   !last oral dsoing time (hr)
CONSTANT   ORINT = 360     !Interval of oral dosing (hrs)
CONSTANT   ORINT14 =24     !Interval of 14C-DCA oral dosing (hrs)
CONSTANT   TGAV = 0.05     !Length of oral gavage infusion(hrs)
CONSTANT   K1 =0.01
CONSTANT   K2 = 3
CONSTANT   K3= 5

!Plasma protein binding
CONSTANT Vbp= 91
CONSTANT Kmbp =22.6
CONSTANT kunbp =9

END ! INITIAL
```

```
        DYNAMIC

                ALGORITHM IALG = 2
                NSTEPS    NSTP = 1
                MAXTERVAL MAXT = 1.0e9
                MINTERVAL MINT = 1.0e-9
                CINTERVAL CINT = 0.01

DERIVATIVE

!--------------iv multiple dose
     !IV = Intravenous infusion rate(mg/hr)
           iflag1 = pulse(TIV1,ivint1,tinf)*pulse(0,tstop,finaliv)
      iflag2 = pulse(TIV2,ivint2,tinf)
           IV1 = IVDOSE1*BW/TINF*iflag1  !'rate iv dosing(mg/hr)
     AIV1 = INTEG(IV1,0.)   ! Amount iv dosed(mg)
      IV2 = IVDOSE2*BW/TINF*iflag2  !'rate iv dosing(mg/hr)
     AIV2 = INTEG(IV2,0.)   ! Amount iv dosed(mg)

!--------------oral bolus
!ODOSE = oral gavage infusion rate(mg/hr) for 1st& 2nd challenge
!first dose
  OFLAG = PULSE(TOR,ORINT,TGAV)
  ODOSE = PDOSE*BW/tgav*oflag    !'rate oral gavage dosing(mg/hr)
  AO = INTEG(ODOSE,0.)

 RST = -(K1*AST)-(K2*AST)
 AST = AO + INTEG(RST,0.0)
 RUG = (K2*AST)-(K3*AUG)
 AUG = INTEG (RUG, 0.)
 RAO = K1*AST + K3*AUG
 AAO = INTEG(RAO, 0.)

  !14ODOSE = oral gavage infusion rate(mg/hr) for 14 days (Schultz) and Jia
   oflag14 = pulse(TOR14,orint14,tgav)*pulse(0,tstop,finalor)
   ODOSE14 = PDOSE14*BW /tgav*oflag14   !'rate oral gavage dosing(mg/hr)
   AO14 = INTEG(ODOSE14,0.)

 RST14 = -(K1*AST14)-(K2*AST14)
 AST14 = AO14 + INTEG(RST14,0.0)
 RUG14 = (K2*AST14)-(K3*AUG14)
 AUG14 = INTEG (RUG14, 0.)
 RAO14 = K1*AST14 + K3*AUG14
 AAO14 = INTEG(RAO14, 0.)

!------VMAXT in liver-----------------!
```

```
! two compounds(12C-DCA&13C-DCA) in liver
        CVL = (AL12+AL13)/(VL*PL)
        RLME = -kd*(Vmaxt*CVL/(km+CVL))*(Vmaxt*Km/(km+CVL))
        RCME =  RLME+KS - (KDE*VMAXT)
        VMAXT = INTEG(RCME,VMAX)


!proportion of original Vmax inhibited
        VMAXP = VMAXT*100/VMAX


!-------- model for IV dosed DCA (13C-DCA & 12C-DCA high dose)----------!

    !blood 13C-DCA

        CV13 = (QL*CVL13 + QS*CVS13 + QR*CVR13 + QK*CVK13+ IV1 +IV2)/QC
        RPL13 = QC*(CV13-CA13)- Rbind13
        APL13 = INTEG(RPL13, 0.0)
        CA13 = APL13/Vpl
        Rbind13 = (Vbp*Kunbp*Ca13)/(Ca13+Kmbp)-kunbp*Vpl*Cabind13
        ! Rbind13 = (Vbp*Ca13)/(Ca13+Kmbp)-CLunbp*Cabind13
        Rmax13 = (Vbp*Ca13)/(Ca13+Kmbp)
        Abind13 = INTEG(Rbind13, 0.0)
        Cabind13 = Abind13/Vpl

        ! Total 13C-DCA in plasma
        Apltot13 = APL13+Abind13
        Cat13 = (APL13+Abind13)/Vpl

        Pbind = 100*Cabind13/(Cat13+0.0000000001)
        Maxbound13 = INTEG (Rmax13, 0.0)
        AUC13 = INTEG(CAt13, 0.)

    !AS = Amount in slowly perfused tissues (mg)'
    RAS13 = QS*(CA13-CVS13)
    AS13 = INTEG(RAS13,0.)
    CVS13 = AS13/(VS*PS)
    CS13 = AS13/VS

    !AR = Amount in rapidly perfused tissues (mg)'
    RAR13 = QR*(CA13-CVR13)
     AR13 = INTEG(RAR13,0.)
    CVR13 = AR13/(VR*PR)
     CR13 = AR13/VR
```

```
    !AL = Amount in liver tissue (mg)'
    RAL13 = QL*(CA13-CVL13) - RAMi
     AL13 = INTEG(RAL13,0.)
    CVL13 = AL13/(VL*PL)
    CL13 = AL13/VL
   AUCL13 = INTEG(CL13,0.)

    !metabolism in liver
          !AM1i : GSTZ-mediated metabolism (mg)
           RAM1i=(VMAXT*CVL13)/(KM+CVL13+CVL12)
           AM1i = INTEG(RAM1i,0)

          !AM2i: non-specific degradation (mg)
          RAM2i=(KF*CVL13*VL)
          AM2i = INTEG(RAM2i,0)

          !AMi: total metabolism amount(mg)
          RAMi = RAM1i + RAM2i
          AMi = AM1i + AM2i


    !AK = Amount in kidney tissue (mg)
    RKu13 = CLr*Cvk13
    AKu13 = INTEG(RKu13,0.)   !amount excreted in urine(mg)
    RAK13 = QK*(CA13-CVK13) -RKU13
     AK13 = INTEG(RAK13,0.)
    CVK13 = (AK13+1.0e-9)/(VK*PK)
     CK13 = AK13/VK
   AUCK13 = INTEG(CK13,0.)

   !TMASS = mass balance (mg)'
   TMASS13 =(AL13+AK13+AS13+AR13+Apltot13)+(AMi+AKu13) ! Amount distributed +
Amount out (mg)


!------------Model for oral dosed DCA (12C-DCA)-------------------------------!
    !blood 12C-DCA
         CV12 = (QL*CVL12 + QS*CVS12 + QR*CVR12 + QK*CVK12)/QC
         RPL12 = QC*(CV12-CA12)- Rbind12
         APL12 = INTEG(RPL12, 0.0)
         CA12 = APL12/Vpl
         Rbind12 = (Vbp*Ca12)/(Ca12+Kmbp)-kunbp*Cabind12
         Abind12 = INTEG(Rbind12, 0.0)
         Cabind12 = Abind12/Vpl

         ! Total 12C-DCA in plasma
```

```
      Apltot12 = APL12+Abind12
      Cat12 = (APL12+Abind12)/Vpl
      AUC12 = INTEG (cat12, 0.0)

!AS12 = Amount in slowly perfused tissues (mg)'
RAS12 = QS*(CA12-CVS12)
 AS12 = INTEG(RAS12,0.)
CVS12 = AS12/(VS*PS)
 CS12 = AS12/VS


!AR12 = Amount in rapidly perfused tissues (mg)'
RAR12 = QR*(CA12-CVR12)
 AR12 = INTEG(RAR12,0.)
CVR12 = AR12/(VR*PR)
 CR12 = AR12/VR


!AL12 = Amount in liver tissue (mg)'
RAL12 = QL*(CA12-CVL12) + RAO + RAO14 - RAMw
 AL12 = INTEG(RAL12,0.)
CVL12 = AL12/(VL*PL)
 CL12 = AL12/VL
AUCL12 = INTEG(CL12,0.)


!metabolism in liver
      !AM1w : GSTZ-mediated metabolism (mg)
       RAM1w=(VMAXT*CVL12)/(KM+CVL12+CVL13)
       AM1w = INTEG(RAM1w,0)

      !AM2w: non-specific degradation (mg)
       RAM2w=(KF*CVL12*VL)
       AM2w = INTEG(RAM2w,0)

      !AMw: total metabolism amount(mg)
       RAMw = RAM1w + RAM2w
       AMw = AM1w+AM2w

!AK12 = Amount in kidney tissue (mg)'
 RKu12 = Clr*Ca12
AKu12 = INTEG(RKu12,0.)
RAK12 = QK*(CA12-CVK12) -RKU12
 AK12 = INTEG(RAK12,0.)
CVK12 = AK12/(VK*PK)
 CK12 = AK12/VK
```

```
    AUCK12 = INTEG(CK12,0.)


     !TMASS = mass balance (mg)'
      TMASS12 =(AL12+AK12+AS12+AR12+Apltot12)+(AMw+AKu12)+Ast+Aug + Ast14 +
Aug14

   ! BALtotal = TMASS12+ TMASS13-AIV1-AIV2-ao-ao14 ! Amount in = Amount out (mg)
         BALtotal = TMASS12+ TMASS13-AIV1-AIV2-ao-ao14
               END ! DERIVATIVE


               ! Add discrete events here as needed
               !  DISCRETE
               !  END

               ! code that is executed once at each communication interval goes here

               CONSTANT TSTOP = 500.0
               TERMT (T .GE. TSTOP, 'checked on communication interval: REACHED
TSTOP')

         END ! DYNAMIC


         TERMINAL
               ! code that is executed once at the end of a simulation run goes here
         END ! TERMINAL

END ! PROGRAM
```

Code for NRTI mono-therapy

```
!Model for NRTIs in pregnant rats at gestation day19
!Mono-therapy
!Active transport in maternal plasma - placenta and placenta-fetuses transfer
!last modified June 22, 2007

PROGRAM

         INITIAL
         ! Tissue Volumes
         CONSTANT BW = 0.3       !Body weight of the dam(kg)
         CONSTANT VBC = 0.86
         CONSTANT VKC = 0.0076
```

```
CONSTANT VLC = 0.041
CONSTANT VPC = 0.04    !Volume of plasma


! Blood Flows
CONSTANT  QCC= 14.0
CONSTANT  QLC =0.18
CONSTANT  QKC =0.14

! Scaled tissue volume
VB = VBC*BW
VK = VKC*BW
VL = VLC*BW
VP = VPC*BW
VAF = 0.0032    !measured (kg) by Lewis (2006)
VPLA = 0.0045  !volume of rat placenta (kg) by Lewis (2006)
Ve=0.025  !tissue voulme of fetus (kg)


! Scaled blood flow
QCI = QCC*BW**0.75
QL = QLC*QCI
QK = QKC*QCI
QB = QCI-QK-QL

!Conversion Factors
CONSTANT mgkg=1.0e6
!Tissue volunes and blood flows for fetuses
CONSTANT VfetD18 = 1051.74 ! Volume of fetus on GD18
CONSTANT numfet =10     !number of fetuses in litter


!Partition coefficients
CONSTANT PA=0.2       ! Permeability-area cross product (L/h)
CONSTANT PB = 0.8     !Richly perfused tissues
CONSTANT PPL = 0.8   !Placenta
CONSTANT PE= 0.8
CONSTANT Paf= 1.0
CONSTANT PL = 0.8
CONSTANT PK = 0.9


!Kinetic Parameters
CONSTANT Kmp = 0.1       !Distribution clearance maternal blood – placenta (L/h)
CONSTANT Kpm=0.1         !Distribution clearance placenta – maternal blood(L/h)
CONSTANT Kpf=0.1         !Distribution clearance placenta – fetuses (L/h)
```

```
        CONSTANT Kfp =0.1         !Distribution clearance fetuses – placenta (L/h)
        CONSTANT Keaf = 0.1      ! First-order distribution clearance (fetuses-AF)
        CONSTANT Kafe = 0.1      ! First-order distribution clearance (AF-Fetuses)
        CONSTANT CLrc=0.0        !Urinary clerance
        CONSTANT CLhc = 0.0      !Hepatic clearance

        !Dosing parameter and timing commands
        CONSTANT Div = 25.          !dose NRTI iv (mg/kg)
        CONSTANT TINF = 0.0167  !Length of iv dosing
        CONSTANT TIV = 0.0         !Start time of iv dosing
        CONSTANT Days=19
        CONSTANT ivint=60
        CONSTANT tor= 0.0
        CONSTANT tgav = 0.0167
        CONSTANT orint = 10000

        !Blood flow to placenta(ml/hr)
        QCAP = (0.1207*(Days-12.0))**4.36/24
        QDEC2 = 2.2*exp(-0.23*(Days-10))/24
        Qpla = NumFet* (QCAP + QDEC2)
        QCON = (0.25)*QDEC2 + NumFet*QCAP

        !Changing body weigth through pregnancy(kg)
        QC=QCI + Qpla
        BWt = BW+Vpla + Ve + Vaf

        END ! INITIAL

        DYNAMIC

                ALGORITHM IALG = 2
                CINTERVAL CINT = 0.01

                DERIVATIVE

!--------------iv dose
     !IV = Intravenous infusion rate(mg/hr)
    IFLAG = pulse(TIV,ivint,tinf) !'iflag = pulse (0.,tstop,tinf)
    IV = IVDOSE/TINF*IFLAG  !'rate iv dosing(mg/hr)
    AIV = INTEG(IV,0.)   ! Amount iv dosed(mg)
    IVDOSE = Div*BW      ! MASSIV = AIV


!NRTI Concentration in Plasma (Cp):
         RBL = QB*Cvb + Qpla*Cvpla + QK*CVK + QL*CVL+IV
         RABL = RBL - (QC*Cap)
```

```
ABL = INTEG(RABL, 0.)
Cap = ABL/Vp

!NRTI Concentration in the rest of the body tissues (Cr):
RAEb = QB*(Cap-Cvb)+ PA*(Ctb/pb - Cvb)
AEb = INTEG(RAEb,0.0)
RAIb = PA*(Cvb - Ctb/pb)
AIb = INTEG(RAIb, 0.0)
Cvb = AEb/(0.3*BW)
Ctb = AIb/(0.56*BW)
Ab = AEb + AIb

!NRTI concnetration in the Kidney
CLR=CLRc*BWt
RCLr= CLr*Cvk
RAK = QK*(Cap-CvK) - RCLr
AK = INTEG(RAK,0.0)
CvK = AK/(VK*PK)
CK = AK/VK
ACLr = INTEG (RCL, 0.0)

!NRTI concnetration in the Liver
CLh =CLHc*BWt
RCLh = CLh*CVL
RAL = QL*(Cap-CvL)- RCLh
AL = INTEG(RAL,0.0)
CvL = AL/(VL*PL)
CL = AL/VL
ACLh = INTEG (RCLH, 0.0)

!NRTI Concentration in maternal Placental blood:
Rplab = Qpla*(Cap-Cplab)+ Kpm*Cplac/ppl - Kmp*Cplab
Aplab = INTEG(Rplab, 0.0)
Cplab = Aplab/(0.5*Vpla)

! NRTI In placneta

Rplac = Kmp*Cplab - Kpm*Cplac/ppl + Kfp*Ce/pe - Kpf*Cplac/ppl
Aplac = INTEG(Rplac, 0.0)
Cplac = Aplac/(0.5*Vpla)
Apla = Aplab + Aplac
AUCpla = INTEG (Cplac, 0.0)

!NRTI Concentration in Embryo (Ce):
RAe = Kpf*Cplac/ppl - Kfp*Ce/pe + Kafe*Caf/Paf - Keaf*Ce/pe
Ae = INTEG(RAe,0.0)
```

```
      Ce = Ae/Ve
      Cve= Ce/Pe
       AUCe = INTEG(Ce, 0.0)

!NRTI Concentration in AF
       Raaf = Keaf*Ce/Pe -Kafe*Caf/Paf
       Aaf = INTEG(Raaf, 0.0)
       Caf = Aaf/Vaf
       Cvaf = Caf/Paf
        AUCaf = INTEG(Caf, 0.0)

Constant TSTOP=24.

Bal = Aaf + Ae + Apla + AL + AK + AB + ABL + ACLr + ACLh - IVDOSE
                  TERMT (T .GE. TSTOP, 'checked on communication interval: REACHED
TSTOP')

          END ! DYNAMIC
          TERMINAL
          END ! TERMINAL

END ! PROGRAM
END
```

Interaction Model for NRTI Combination Therapy

```
!ModelIII of NRTIs in pregnant rats at gestation day19
!Mono-therapy
!Active transport in maternal plasma - placenta and placenta-fetuses transfer
!last modified Nov 6, 2006

PROGRAM

          INITIAL
          ! Tissue Volumes
          CONSTANT BW = 300       !Body weight of the dam(g)
          CONSTANT VBC = 0.86
          CONSTANT VKC = 0.0076
          CONSTANT VLC = 0.041
          CONSTANT VPC = 0.04    !Volume of plasma

          ! Blood Flows
          CONSTANT  QCC= 14.0
          CONSTANT  QLC =0.18
          CONSTANT  QKC =0.14
```

```
! Scaled tissue volume
VB = VBC*BW
VK = VKC*BW
VL = VLC*BW
VP = VPC*BW
VAF = 3.2    !measured (g) by Lewis (2006)
VPLA = 4.5  !volume of rat placenta (g) by Lewis (2006)
Ve=25  !tissue voulme of fetus (g)


! Scaled blood flow
QCI = 1000* QCC*(BW/1000)**0.75      ! Cardiac output (ml/h)
QL = QLC*QCI
QK = QKC*QCI
QB = QCI-QK-QL

!Conversion Factors
CONSTANT mgkg=1.0e6
!Tissue volunes and blood flows for fetuses
CONSTANT VfetD18 = 1051.74 ! Volume of fetus on GD18
CONSTANT numfet =10     !number of fetuses in litter


!Partition coefficients
CONSTANT PA=0.2       ! Permeability-area cross product (mL/h)
CONSTANT PB = 0.8     !Richly perfused tissues
CONSTANT PPL = 0.8   !Placenta
CONSTANT PE= 0.8
CONSTANT Paf= 1.0
CONSTANT PL = 0.8
CONSTANT PK = 0.9

CONSTANT PA_azt=0.2       ! Permeability-area cross product (mL/h)
CONSTANT PB_azt = 0.8     !Richly perfused tissues
CONSTANT PPL_azt = 0.8   !Placenta
CONSTANT PE_azt= 0.8
CONSTANT Paf_azt= 1.0
CONSTANT PL _azt= 0.8
CONSTANT PK_azt = 0.9


!Kinetic Parameters
CONSTANT Kmp = 0.1       !Distribution clearance maternal blood – placenta (ml/h)
CONSTANT Kpm=0.1         !Distribution clearance placenta – maternal blood(ml/h)
CONSTANT Kpf=0.1         !Distribution clearance placenta – fetuses (ml/h)
```

```
CONSTANT Kfp =0.1         !Distribution clearance fetuses – placenta (ml/h)
CONSTANT Keaf = 0.1      ! Distribution clearance fetuses-AF (ml/h)
CONSTANT Kafe = 0.1      ! Distribution clearance AF-fetuses (ml/h)
CONSTANT CLrc=0.0        !Urinary clerance
CONSTANT CLhc = 0.0      !Hepatic clearance

CONSTANT kmp_azt = 0.1
CONSTANT kpm_azt=0.1
CONSTANT kpf_azt=0.1
CONSTANT kfp_azt =0.1
CONSTANT Keaf_azt = 0.1
CONSTANT Kafe = 0.1
CONSTANT CLrc=0.0        !Urinary clerance of AZT


!Dosing parameter and timing commands
CONSTANT Div = 25.          !dose NRTI iv (mg/kg = ug/g)
CONSTANT Div_azt = 25.    !dose AZT iv (mg/kg = ug/g)

CONSTANT TINF = 0.0167  !Length of iv dosing
CONSTANT TIV = 0.0         !Start time of iv dosing
CONSTANT Days=19
CONSTANT ivint=60
CONSTANT tor= 0.0
CONSTANT tgav = 0.0167
CONSTANT orint = 10000

!Blood flow to placenta(mL/hr)
QCAP = 1000* (0.1207*(Days-12.0))**4.36/24
QDEC2 = 1000* 2.2*exp(-0.23*(Days-10))/24
Qpla = NumFet* (QCAP + QDEC2)
QCON = (0.25)*QDEC2 + NumFet*QCAP

!Changing body weigth through pregnancy(g)
QC=QCI + Qpla
BWt = BW+Vpla + Ve + Vaf

END ! INITIAL

DYNAMIC

        ALGORITHM IALG = 2
        CINTERVAL CINT = 0.01

        DERIVATIVE
```

```
!--------------iv dose
     !IV = Intravenous infusion rate(mg/hr)
    IFLAG = pulse(TIV,ivint,tinf) !'iflag = pulse (0.,tstop,tinf)
    IV = IVDOSE/TINF*IFLAG  !'rate iv dosing(ug/hr)
    AIV = INTEG(IV,0.)   ! Amount iv dosed(ug)
    IVDOSE = Div*BW      ! MASSIV = AIV


!NRTI Concentration in Plasma (Cp):

          RBL = QB*Cvb + Qpla*Cvpla + QK*CVK + QL*CVL+IV
          RABL = RBL - (QC*Cap)
          ABL = INTEG(RABL, 0.)
          Cap = ABL/Vp

!NRTI Concentration in the rest of the body tissues (Cr):
          RAEb = QB*(Cap-Cvb) + PA*(Ctb/pb - Cvb)
          AEb = INTEG(RAEb,0.0)
          RAIb = PA*(Cvb - Ctb/pb)
          AIb = INTEG(RAIb, 0.0)
          Cvb = AEb/(0.3*BW)
          Ctb = AIb/(0.56*BW)
          Ab = AEb + AIb

!NRTI  concnetration in the Kidney
          CLr=CLrc*BWt
          Rclr = CLrt*Cvk
          RAK = QK*(Cap-CvK) - RCLr
          AK = INTEG(RAK,0.0)
          CvK = AK/(VK*PK)
          CK = AK/VK
          AUCk = INTEG (CK, 0.0)
          Aku = INTEG (Rclr, 0.0)

!AZT effects on 3TC in the kidney
          CONSTANT Kint3tc = 0       ! Interaction rate constant
          RinCLr = Kint3tc*Cvk_azt
          CLrt = INTEG(Rinclr, Clr)

 !NRTI concnetration in the Liver
       CLh =CLhc*BWt
       Rclh = CLht*CVL
       RAL = QL*(Cap-CvL)-RCLh
      AL = INTEG(RAL,0.0)
      CvL = AL/(VL*PL)
      CLh = AL/VL
```

```
      AUCL = INTEG(CLh, 0.0)
      ACLh = INTEG(RCLh, 0.0)

     !AZT effects on ABC in the liver
      CONSTANT Kintabc = 0       ! Interaction rate constant
      CONSTANT minabc =0.001   ! Minimum hepatic clerance of ABC

      RinCLt = Kintabc*Cvl_azt
      CLhabc = INTEG (RinCLh, Clh)
      CLht = MAX (Clhabc, minabc)

!NRTI Concentration in maternal Placental blood:
    Rplab = Qpla*(Cap-Cplab)+ Kpmt*Cplac/ppl – Kmpt*Cplab
    Aplab = INTEG(Rplab, 0.0)
    Cplab = Aplab/(0.5*Vpla)
    AUCplab = INTEG(Cplab, 0.0)

!NRTI Concentration in placneta
  Rplac = Kmpt*Cplab – Kpmt*Cplac/ppl + Kfpt*Ce/pe – Kpft*Cplac/ppl
   Aplac = INTEG(Rplac, 0.0)
   Cplac = Aplac/(0.5*Vpla)
   Cvplac = Cplac/ppl
   AUCplac = INTEG (Cplac, 0.0)
   Apla = Aplab + Aplac

!NRTI Concentration in Embryo (Ce):
      RAe = Kpft*Cplac/ppl  - Kfpt*Ce/pe + kafet*Caf/Paf - keaft*Ce/pe
     Ae = INTEG(RAe,0.0)
     Ce = Ae/Ve
     Cve= Ce/Pe
      AUCe = INTEG(Ce, 0.0)

!NRTI Concentration in AF
       Raaf = keaft*Ce/Pe -kafet* Caf/Paf
      Aaf = INTEG(Raaf, 0.0)
      Caf = Aaf/Vaf
      Cvaf = Caf/Paf
     AUCaf = INTEG(Caf, 0.0)

! First-order interaction Placental Transfer
CONSTANT Kintmp = 0      ! interaction on distribution clearance(maternal blood - placenta)
CONSTANT Kintpm = 0      ! interaction on distribution clearance (placenta – maternal blood)
CONSTANT Kintpf = 0      ! interaction on distribution clearance  (Placenta- Fetuses)
CONSTANT Kintfp = 0      ! interaction on distribution clearance  (Fetuses – Placenta)

Rclmp = Kintmp *Cplab_azt
```

```
KmpT = INTEG (Rclmp, Kmp)

Rclpm = Kintpm*Cvplac_azt
KpmT = INTEG (Rclpm, Kpm)

Rclpf = Kintpf*Cvplac_azt
KpfT = INTEG (Rclpf, Kpf)

Rclfp = Kintfp*Cve_azt
KfpT = INTEG(Rclfp, Kfp)

!Fetuses-AF Transfer
CONSTANT Kineaf = 0      ! Interaction on fetuses-AF transfer
CONSTANT Kinafe =0       !Interaction on AF-Fetuses transfer
CONSTANT minKeafabc= 0.2  !Minimum transfer fetuses-AF for ABC

RCLeaf = Kinteaf*Cve_azt
ValKeafT = INTEG (RCLeaf, Keaf)
Keaft = MAX (Valkeaft, minKeafabc)

RCLafe = Kintafe*Cvaf_azt
ValKafeT = INTEG (RCLafe, Kafe)
Kafet = MAX (Valkafet, minKeafabc)


!******************AZT Model*****************************************

!--------------iv dose
     !IV = Intravenous infusion rate(mg/hr)
    !IFLAG = pulse(TIV,ivint,tinf) !'iflag = pulse (0.,tstop,tinf)
    IV_azt = IVDOSE_azt/TINF*IFLAG  !'rate iv dosing(ug/hr)
    AIV_azt = INTEG(IV_azt,0.)   ! Amount iv dosed(ug)
    IVDOSE_azt = Div_azt*BW      ! MASSIV = AIV


!AZT Concentration in Plasma (Cp):
          RBL_azt = QB*Cvb_azt + Qpla*Cplab_azt + QK*CVK_azt + QL*CVL_azt+IV_azt
          RABL_azt = RBL_azt - (QC*Cap_azt)
          ABL_azt = INTEG(RABL_azt, 0.)
          Cap_azt = ABL_azt/Vp


!AZT Concentration in the rest of the body tissues (Cr):

         RAEb_azt = QB*(Cap_azt-Cvb_azt)+ PA_azt*(Ctb_azt/pb_azt - Cvb_azt)
         AEb_azt= INTEG(RAEb_azt,0.0)
```

```
        RAIb_azt = PA_azt*(Cvb_azt - Ctb_azt/pb_azt)
        AIb_azt = INTEG(RAIb_azt, 0.0)
        Cvb_azt = AEb_azt/(0.3*BW)
        Ctb_azt = AIb_azt/(0.56*BW)

!AZT concnetration in the Kidney
      CLr_azt=CLrc_azt*BWt
      Rclr_azt = CLrt_azt*Cvk_azt
      RAK_azt = QK*(Cap_azt-CvK_azt) - RCLr_azt
      AK_azt = INTEG(RAK_azt,0.0)
      CvK_azt = AK_azt/(VK*PK_azt)
      CK_azt = AK_azt/VK
      Aku_azt = INTEG (Rclr_azt, 0.0)

!Interactions in the Kidney
        CONSTANT Kintazt = 0            ! Effects on AZT urinary clerance by 3TC or ABC

        RinCLR_azt = Kintazt*Cvk
        CLrt_azt = INTEG(RinCLR_azt, CLr_azt)
 !AZT concnetration in the Liver
        RAL_azt = QL*(Cap_azt-CvL_azt)
        AL_azt = INTEG(RAL_azt,0.0)
        CvL_azt = AL_azt/(VL*PL_azt)
        CL_azt = AL_azt/VL
        AUCL_azt = INTEG(CL_azt, 0.0)

!AZT Concentration in maternal Placental blood:
        Rplab_azt = Qpla*(Cap_azt-Cplab_azt)+ Kpmt_azt*Cplac_azt/ppl_azt -
Kmpt_azt*Cplab_azt
        Aplab_azt = INTEG(Rplab_azt, 0.0)
        Cplab_azt = Aplab_azt/(0.5*Vpla)
        AUCplab_azt = INTEG(Cplab_azt, 0.0)

!AZT Concentration in placneta
        Rplac_azt = Kmpt_azt*Cplab_azt - Kpmt_azt*Cplac_azt/ppl_azt +
Kfpt_azt*Ce_azt/pe_azt - Kpft_azt*Cplac_azt/ppl_azt
        Aplac_azt = INTEG(Rplac_azt, 0.0)
        Cplac_azt = Aplac_azt/(0.5*Vpla)
        Cvplac_azt = Cplac_azt/ppl_azt
        AUCplac_azt = INTEG (Cplac_azt, 0.0)
        Apla_azt = Aplac_azt+Aplab_azt

!AZT Concentration in Embryo (Ce):
        RAe_azt = Kpft_azt*Cplac_azt/ppl_azt  - Kfpt_azt*Ce_azt/pe_azt +
Kafet_azt*Caf_azt/Paf_azt - Keaft_azt*Ce_azt/pe_azt
        Ae_azt = INTEG(RAe_azt,0.0)
```

```
        Ce_azt = Ae_azt/Ve
        Cve_azt= Ce_azt/Pe_azt
        AUCe_azt = INTEG(Ce_azt, 0.0)

!AZT Concentration in AF
        Raaf_azt = keaft_azt*Ce_azt/Pe_azt -kafet_azt*Caf_azt/Paf_azt
        Aaf_azt = INTEG(Raaf_azt, 0.0)
        Caf_azt = Aaf_azt/Vaf
        Cvaf_azt = Caf_azt/Paf_azt
        AUCaf_azt = INTEG(Caf_azt, 0.0)


!Transplacental distribution interactions
CONSTANT Kintmpazt = 0
CONSTANT Kintpmazt = 0
CONSTANT Kintpfazt = 0
CONSTANT Kintfpazt = 0

Rclmp_azt = Kintmpazt*Cplab
ValKmpT_azt = INTEG(Rclmp_azt, Kmp_azt)
Kmpt_azt = MIN(315.5, ValKmpt_azt)

Rclpm_azt = Kintpmazt*Cvplac
ValKpmT_azt = INTEG (Rclpm_azt, Kpm_azt)
KpmT_azt = MIN(315.5, ValKpmT_azt)

Rclpf_azt = Vmaxpfazt*Cvplac
ValKpfT_azt = INTEG(Rclpf_azt, Kpf_azt)
Kpft_azt = MIN(202.7, ValKpft_azt)

Rclfp_azt = Vmaxfpazt*Cve
ValKfpT_azt = INTEG (Rclfp_azt, Kfp_azt)
KfpT_azt = MIN(202.7, ValKfpt_azt)


        !Fetuses-AF transfer
        CONSTANT Kinteafazt= 0
        CONSTANT Kintafeazt =0

        RCLeaf_azt = Kinteafazt*Cve
        KeafT_azt = INTEG (RCLeaf_azt, Keaf_azt)

         RCLafe_azt = Kintafeazt*Cvaf
         KafeT_azt = INTEG (RCLafe_azt, Kafe_azt)

Constant TSTOP=24.
```

```
Bal = Aaf + Ae + Apla + AL + AK + AEB + AIB + ABL + AKu + ACLh - IVDOSE
Bal_azt = Aaf_azt + Ae_azt + Apla_azt + AL_azt + AK_azt + AEB_azt + AIB_azt + ABL_azt +
AKu_azt - IVDOSE_azt
Baltotal = Bal + Bal_azt
                TERMT (T .GE. TSTOP, 'checked on communication interval: REACHED
TSTOP')

        END ! DYNAMIC
        TERMINAL
        END ! TERMINAL

END ! PROGRAM
END
```

APPENDIX C

EXPERIMENTAL DATA FOR NRTI IN PREGNANT RATS

ddC Monotherapy

ddC concentrations in materal plasma

Time (min)	rat1	rat2	rat3	rat4	rat5	rat6	Mean
5	32.9	34.7	33.8	32.5	31.3	32.4	32.93333
15	14.4	18.9	17.4	23.4	15.2	13.8	17.18333
30	7.5	9.6	8.9	8.6	7.1	7.6	8.216667
45	5.6	6.1	5.7	5.6	5.6	6.1	5.783333
60	3.8	4.9	4.1	4.2	4.8	5.02	4.47
90	2.8	3.2	3	3	3.2	4.8	3.333333
120	2.1	2.2	2	2.2	2.3	2.9	2.283333
180	1.3	1.4	1.4	1.5	1.8	2.7	1.683333
240	1.1	1.03	1.05	1.3	1.3	1.67	1.241667
300	0.75	1.02	0.78	1.1	1.06	1.35	1.01
360	0.63	0.76	0.71	0.81	1.01		0.784

ddC concentrations in placenta

Time (min)	rat1	rat2	rat3	rat4	rat5	rat6	Mean
5	17.8	21.4	17.4	11.6	15.8	18.2	17.03333
15	11.6	12.4	6.8	18.6	9.68	10.1	11.516
30	11	11.6	8.3	8.14	7.53	8.3	9.145
45	10.6	6.7	6.8	8.22	7.1	6.8	7.703333
60	9.74	6.4	2.9	8.17	5.72	5.15	6.346667
90	8.53	5.7	4.6	4.94	4.8	4.9	5.578333
120	7.08	5.3	3.7	2.5	4.2	4.4	4.53
180	4.4	2.5	2.3	2.2	3.7	3.8	3.15
240	3.54	1.76	1.01	1.9	2.9	2.86	2.328333
300		1.5	1.5	0.78	2.3	2.5	1.716
360	2.42	1.06	2	1.6	1.51		1.718

ddC concentrations in fetus

Time (min)	rat1	rat2	rat3	rat4	rat5	rat6	Mean
5	0.83	1.21	1.19	1.25	0.85	0.89	1.036667
15	1.53	1.56	1.31	1.57	0.99	0.94	1.316667
30	1.83	1.8	1.44	1.52	0.98	1.01	1.43
45	2.12	1.84	1.93	1.64	1.18	1.29	1.666667

60	2.13	1.97	1.86	1.72	1.35	1.33	1.726667
90	2.82	2.11	1.31	1.71	1.42	1.38	1.791667
120	2.11	2.66	1.68	1.83	1.52	1.48	1.88
180	1.96	1.62	1.63	1.45	1.16	1.44	1.543333
240	1.71	1.39	1.11	1.08	1.11	1.21	1.268333
300		1.01	0.87	0.93	1.31	1.09	1.042
360	1.33	0.94	1.35	0.86	1.27		1.15

ddC concentrations in amniotic fluid

Time (min)	rat1	rat2	rat3	rat4	rat5	rat6	Mean
5	0.19			0.18	0.14	0.12	0.146667
15	0.26	0.2	0.17	0.23	0.23	0.19	0.213333
30	0.41	0.49	0.44	0.47	0.45	0.68	0.49
45	0.46	0.59	0.52	0.61	0.61	0.6	0.565
60	0.79	0.78	0.59	0.68	1.07	1.15	0.843333
90	1.27	1.08	1.01	1.25	0.83	1.08	1.086667
120	1.79	1.2	1.38	1.44	1.43	1.11	1.391667
180	1.37	1.5	1.07	1.1	1.26	1.29	1.265
240	1.01	1.31	1.33	1.21	1	1.24	1.183333
300		0.89	0.91	0.97	0.94	1.04	0.95
360	0.62	0.7	0.73	1.05	1.07		0.834

3TC Monotherapy

3TC concentrations in maternal plasma

Time (min)	rat 3	rat4	rat 6	rat 8	rat 9	rat 16	rat18	Mean
5	22.9	45	41	44.67	41.7	45.29	41.63	40.313
15		25.4	26.9	28	27	28.11	26.92	27.055
30	11.9	11.7	14.1	10.3	12.3	18.24	13.4	13.134
45	6.48	9.11	10.3	8.97	9.56	11.5	10	9.417
60	4.87	8.48	7.4	6.37	7.8	8.95	7.81	7.383
90	4.72	6.03	6.3	5.56	6.41	7.88	6.5	6.200
120	3.98	5.07	4.9	4.17	5.1	6.39	5.06	4.953
180	2.66	4.23	4	3.82	3.96	4.67	4.12	3.923
240	1.48	1.52	2.18	2.65	2.05		2.39	2.045
300	1.21	1.14	1.55	1.55		2.98		1.686
330			1.03					1.030
360	0.8	0		1.2				0.667

3TC concentrations in placenta

Time (min)	rat 3	rat4	rat6	rat8	rat 9	rat 16	rat18	Mean
5	4.37	9.72	8.32	9.46	8.46	9.01	8.948	8.326857
15	3.52	7.21	6.4	7.16	6.98	6.828	6.745	6.406143

30	2.81	6.25	5.48	5.53	6.11	6.1	5.996	5.468
45	2.24	5.21	5.104	4.44	4.82	5.207	5.06	4.583
60	1.91	4.93	4.583	4.3	4.25	4.667	4.538	4.168286
90	1.77	5.15	4.206	3.99	3.41	4.203	4.051	3.825714
120	1.81	3.91	3.12	2.704	2.81	3.457	3.305	3.016571
180	1.04	2.53	1.78	2.01	1.86	2.284	2.156	1.951429
240	0.754	1.77	1.779	1.41	1.37	1.805	1.576	1.494857
300	0.681	1.48	1.395			1.755		1.32775
330			1.103			1.325		1.214
360	0.397	0.768			0.631			0.598667

3TC concentrations in fetus

Time (min)	rat3	rat4	rat6	rat8	rat9	rat16	rat18	Mean
5	0.396	1.5	1.212	0.917	0.969	1.269	1.037	1.042857
15	0.442	1.82	1.721	1.033	1.206	1.753	1.406	1.340143
30	0.734	2.02	2.109	1.155	1.46	3.904	2.785	2.023857
45	0.726	2.39	1.912	1.35	1.44	1.906	1.677	1.628714
60	0.669	2.44	2.064	1.39	1.43	1.962	1.708	1.666143
90	0.639	2.46	1.808	1.44	1.64	1.933	1.697	1.659571
120	0.661	2.55	1.487	1.4	1.35	1.856	1.573	1.553857
180	0.617	1.73	1.201	1.34	1.133	1.5	1.342	1.266143
240	0.475	1.32	1.125	0.985	1.01	1.328	0.953	1.028
300	0.361	1.07	0.891			1.174		0.874
330			0.787			1.134		0.9605
360	0.188	0.839			0.675			0.567333

3TC concentration in amniotic fluid

Time (min)	rat 3	rat4	rat6	rat8	rat9	rat 16	rat18	Mean
5		0.0363	0.0378	0.0295	0.0341	0.038	0.03	0.034283
15	0.0684	0.198	0.1562	0.149	0.1711	0.178	0.146	0.152386
30	0.184	0.22	0.2	0.267	0.21	0.296	0.221	0.228286
45	0.223	0.655	0.524	0.55	0.503	0.597	0.52	0.510286
60	0.377	1.04	0.691	0.644	0.616	0.857	0.654	0.697
90	0.337	1.28	0.732	0.777	0.763	0.997	0.745	0.804429
120	0.333	1.85	1.02	1.11	1.215	1.51	1.12	1.165429
180	0.923	2.79	0.9504	1.267	1.49	1.356	1.39	1.452343
240	0.616	3.84	1.096	0.988	0.933	1.725	1.169	1.481
300		1.75	0.69			1.254		1.231333
330			0.6			1.394		0.997
360	0.581	1.81			0.912			1.101

AZT Monotherapy

AZT concentrations in maternal plasma

Time (min)	Rat T	Rat N	Rat P	Rat Q	Rat R	Rat S	Mean
5	30.9	37.4	36.3	50.6	43.2	47.7	41.01667
15	24.6	24.8	22.5	25.9	26.5	26	25.05
30	17.4	18.2	16.1	18.4	19	19.3	18.06667
60	12.9	11.5	10.4	13.3	11.5	15.6	12.53333
120	6.7	6.4	5.4	6.4	5	9.7	6.6
180	2.9	3.1	2.6	3.1	2.2	6.2	3.35
240	2	1.5	1.3	1.4	0.9	3.3	1.733333
360	1	0.67	0.67	0.67	0.4	1.7	0.851667
480	0.3	0.4	0.3	0.39		0.9	0.458

AZT concentrations in placenta

Time (min)	rat T	rat N	rat P	rat Q	rat R	rat S	Mean
5	7.7	6.3	8.8	6.2	7.3	9.9	7.7
15	7.9	7.5	7.4	6.6	8.4	8.3	7.683333
30	6.9	6.5	7	7.2	8.2	7.1	7.15
60	6.1	5.5	5.9	6.8	4.9	7.1	6.05
120	3.5	3.5	2.9	3.7	2.7	5.2	3.583333
180	1.3	2.2	2	2.1	1.1	3.3	2
240	1.1	0.9	1.1	0.9	0.45	2.1	1.091667
360		0.6	0.4	0.4		1.1	0.625
480			0.4			0.5	0.45

AZT concentrations in fetus

Time (min)	rat T	rat N	rat P	rat Q	rat R	rat S	mean
5	4	3.6	3.9	3.3	3.9	5.1	3.966667
15	5.7	5.1	5.3	6.1	6.9	6.7	5.966667
30	6	5.3		7.3	7.6	7.2	6.68
60	5.7	4.9	4.9	6.6	3.9	6.9	5.483333
120	3.7	3.1	3.1	3.8	2.7	4.9	3.55
180	1.9	1.7	1.7	3	1.8	3.2	2.216667
240	1.1		1.2	1.8	0.8	2.3	1.44
360	0.84	0.5	0.63	1.5	0.67	1.4	0.923333
480	0.61	0.3	0.57	1.3	0.5	0.8	0.68

AZT concentrations in amniotic fluid

Time (min)	rat T	rat N	rat P	rat Q	rat R	rat S	mean
5	0.5	0.4	0.5	1.4	0.9	1.6	0.883333
15	1.7	1.2	1.1		2.3	1.4	1.54

30	2.8	1.9	1.9	2.2	3.2	2.1	2.35
60	3.5	1.5	2	3.4	2.8	3.7	2.816667
120	5.1	3.4	4.1	4.2	3.7	5.4	4.316667
180	3.8	3.6	2.6	4.4	3.2	5.2	3.8
240	3	2.5	2.7	3.4	2.4	5.3	3.216667
360	2.5	1.9	1.6	2.8	1.8	3.7	2.383333
480	1.6	1.7	1.8	1.7	1.6	3.2	1.933333

ABC Monotherapy

ABC concentrations in maternal plasma

Time (min)	Rat 1	Rat 2	Rat 3	Rat 4	Rat 5	Rat 6	Mean
5	11.767	13.669	17.601	21.284	20.083	31.950	19.392
15	6.152	6.546	9.484	10.961	10.266	11.442	9.142
30	3.140	4.571	6.169	7.108	6.631	7.988	5.934
45	2.097	3.071	3.205	4.934	5.106	5.967	4.063
60	1.640	2.775	3.041	3.702	3.807	5.905	3.479
90	0.631	1.890	1.858	1.946	2.223	2.766	1.886
120	0.678	1.173	1.735	1.085	1.535	1.578	1.297
180		1.107		0.449	0.639	0.600	0.699
240		0.504		0.412	0.819	0.619	0.589
300		0.358					0.358

ABC concentrations in placenta

Time (min)	Rat 1	Rat 2	Rat 3	Rat 4	Rat 5	Rat 6	Mean
5	8.105	8.403	7.924	7.820	9.342	7.073	8.111
10						7.137	7.137
15	9.168	5.387	6.773	6.395	10.848	7.937	7.751
30	7.444	5.550	6.072	5.431	8.116	5.694	6.385
45	4.777	4.854	3.453	4.782	3.644	5.778	4.548
60	4.174	5.219	1.713	4.131	3.339	2.814	3.565
90	3.202	2.583	1.013	2.089	2.268	2.022	2.196
120	1.926	1.995	1.682	1.157	1.485	1.863	1.685
180		0.854		0.460	0.633	1.392	0.835
240		0.919		0.288	0.505	0.555	0.567
300		0.524					0.524

ABC concentrations in fetus

Time (min)	Rat 1	Rat 2	Rat 3	Rat 4	Rat 5	Rat 6	Mean
5	8.983	7.199	8.597	4.586	7.247	6.546	7.193
10						7.222	7.222
15	6.030	7.341	6.178	4.004	6.727	7.141	6.237
30	6.739	4.866	4.126	4.110	4.112	5.448	4.900

45	5.244	3.984	3.055	3.104	3.800	3.578	3.794
60	3.656	5.136	3.077	2.763	3.045	2.483	3.360
90	2.090	1.805	1.799	1.294	1.975	2.057	1.836
120	2.460	1.341	1.140	0.763	0.993	1.943	1.440
180		0.567		0.398	0.448	1.066	0.619
240		0.691		0.278	0.507	0.646	0.531
300		0.551					0.551

ABC concentrations in amniotic fluid

Time (min)	Rat 1	Rat 2	Rat 3	Rat 4	Rat 5	Rat 6	Mean
5	1.395	1.856	1.806	0.952	2.200	1.671	1.647
10						2.034	2.034
15	1.656	2.569	4.777	2.622	3.156	4.362	3.190
30	4.218	3.734	7.019	2.614	6.734	5.535	4.976
45	6.458	7.456	6.132	5.542	6.508	7.998	6.682
60	6.379	7.777	5.340	5.807	8.141	6.323	6.628
90	6.321	5.937	4.132	3.828	3.434	4.960	4.769
120	5.318	4.271	3.185	3.682	4.491	4.432	4.230
180		2.237		1.511	2.220	2.852	2.205
240		1.795		0.973	1.505	1.517	1.447
300		1.355					1.355

3TC-AZT Combination Therapy

3TC concentration in plasma

Time (min)	rat7c	rat11c	rat12c	rat13c	rat14c	rat17c	Mean
5	40	46.4	39.1	38.7	37.3	42.64	40.69
15	27.3	24.8	26.91	24.1	25.3	26.69	25.85
30	14.2	12	11.4	12.4	13.4	13.44	12.80667
45	10	10.21	9.88	9.06	10.2	10.18	9.921667
60	7.6	8.12	8.83	7.57	8.87	8.7	8.281667
90	6	5.87	6.24		6.7	6.41	6.244
120	4.6	4.1	4.97	3.61	5.04	5.09	4.568333
180	3.7	3.81	3.76	2.54	2.83	3.71	3.391667
240	2.6	2.58	2.6	1.19	1.44	2.65	2.176667
300	1.6	1.87	1.47	1.139	1.09	1.69	1.4765
360	0.9	1.4	1.04	0.728	0.725	1.18	0.9955

3TC concnetration in placenta

Time (min)	rat7c	rat11c	rat12c	rat13c	rat14c	rat17c	Mean
5	13.96	12.23	10.47	10.32	13.49	12.051	12.08683
15	11.105	10.3	8.49	9.19	10.13	10.535	9.958333
30	7.806	8.78	7.82	8.16	8.81	8.947	8.387167
45	7.54	9.3	8.09	8.54	7.99	8.916	8.396
60	7.313	8.5	8.03	7.71	7.87	8.349	7.962

90	7.106	7.72	7.01	6.8	6.94	7.399	7.1625
120	5.492	7.2	6.44	6.45	6.55	6.502	6.439
180	3.55	6.43	6.13	5.886	5.948	5.177	5.520167
240	2.703	5.9415	5.906	5.998	5.631	4.851	5.17175
300	1.414		5.637	5.853	5.424	4.452	4.556
360	1.056	5.408	5.441	5.441	5.345	3.381	4.345333

3TC concnetration in fetus

Time (min)	rat7c	rat11c	rat12c	rat13c	rat14c	rat17c	Mean
5	2.65	2.676	2.51	2.5415	2.611	2.627	2.602583
15	2.98	2.816	2.662	2.825	2.833	2.835	2.825167
30	3.33	3.13	2.741	2.951	2.926	3.073	3.025167
45	3.45	3.11	2.878	2.942	2.956	3.125	3.076833
60	3.7	3.3	2.892	2.909	3.05	3.265	3.186
90	3.1	3.18	2.825	2.923	2.993	3.104	3.020833
120	2.54	2.98	2.871	2.906	3.03	2.919	2.874333
180	2.47	3.1345	2.605	2.77	2.899	2.912	2.798417
240	1.58	2.606	2.567	2.525	2.62	4.393	2.715167
300	1.1	2	2.549	2.696	2.432	2.395	2.195333
360	0.62	2.398	2.375	2.346	2.304	2.327	2.061667

3TC concentration in amniotic fluid

Time (min)	rat7c	rat11c	rat12c	rat13c	rat14c	rat17c	Mean
5	0.0532	0.0703	0.0899	0.0614	0.0639	0.078	0.06945
15	0.232	0.501	0.325	0.349	0.389	0.432	0.371333
30	0.414	0.791	0.678	0.638	0.669	0.737	0.6545
45	0.58	1.94	0.406	0.812	0.8	1.126	0.944
60	0.859	0.849	0.951	1.22	1.15	1.119	1.024667
90	0.926	0.85	0.922	1.12	1.05	1.32	1.031333
120	1.94	1.72	1.64	2.14	2.05	2.068	1.926333
180	1.192	1.44	1.1	1.24	1.22	1.425	1.2695
240	1.25	1.22	1.495	1.58	1.64	1.491	1.446
300	1.1	0.997	1.27	1.33	1.03	1.263	1.165
360	0.972	1.51	0.933	0.9499	1.65	1.259	1.212317

AZT concentration in plasma

Time (min)	rat7c	rat11c	rat12c	rat13c	rat14c	rat17c	Mean
5	45.5	33.8	37.3	37.1	36.7	38.163	38.09383
15	24.3	21.9	23.3	23.8	25	24.005	23.7175
30	17.5	17.3	17.7	16.1	16.6	17.224	17.07067
45	14.8	12	15.5	13.76	14.8	14.309	14.19483
60	11.9	10.6	12.12	10.49	11.48	11.273	11.3105
90	8.8	8.33	9.6		7.16	8.256	8.4292
120	5.7	4.65	5.8	4.69	4.51	4.729	5.013167
180	2.5	1.83	2.3	1.884	1.5	1.979	1.998833
240	1.24	0.963	0.857	0.885	1.039	0.966	0.991667

300	0.603	0.538	0.458	0.545	0.496	0.507	0.5245
360	0.389	0.189	0.351	0.1405	0.133	0.14	0.22375

AZT concnetration in placenta

Time (min)	rat7c	rat11c	rat12c	rat13c	rat14c	rat17c	Mean
5	6.89	6.54	7.66	5.395	8.25	7.242	6.996167
15	5.05	6.19	6.52	5.83	6.5	6.318	6.068
30	4.04	5.81	5.65	5.67	5.46	5.548	5.363
45	3.14	5.2	4.91	4.86	4.75	4.815	4.6125
60	2.8	4.24	4.61	4.7	4.36	4.436	4.191
90	1.97	2.97	3.43	3.49	3.46	3.474	3.132333
120	1.73	3.06	3.283	3.28	3.04	2.833	2.871
180	0.492	1.596	1.65	1.36	1.531	1.593	1.370333
240	0.152	1.2355	1.51	1.524	1.196	1.115	1.122083
300	0.163		1.298	1.249	1.0967	0.84	0.92934
360	0.0552	1.0817	1.177	1.119	1.059	0.797	0.881483

AZT concentration in fetus

Time (min)	rat7c	rat11c	rat12c	rat13c	rat14c	rat17c	Mean
5	4.48	4.68	5.35	3.95	4.84	4.642	4.657
15	5.64	4.82	5.12	4.77	5.88	5.169	5.233167
30	5.55	4.49	5.21	4.84	5.77	5.061	5.1535
45	4.93	4.07	5.9	4.21	4.13	4.438	4.613
60	4.28	3.86	4.63	4.45	4.03	4.139	4.2315
90	2.72	3.29	3.72	3.01	3.02	3.181	3.156833
120	1.62	1.5	2.06	1.838	1.75	1.729	1.7495
180	0.467	1.178	1.35	1.463	1.257	1.318	1.172167
240	0.208	0.706	0.963	0.9982	0.821	0.722	0.736367
300	0.101	0.6986	0.744	0.6999	0.724	0.501	0.578083
360	0.0458	0.632	0.6468	0.6196	0.63	0.413	0.497867

AZT concentrations in amniotic fluid

Time (min)	rat7c	rat11c	rat12c	rat13c	rat14c	rat17c	Mean
5	0.783	0.848	0.549	0.879	0.954	0.721	0.789
15	0.507	1.28	0.881	1.166	1.134	0.887	0.975833
30	1.05	2.69	1.26	1.91	2.09	1.713	1.7855
45	1.46	2.93	2.25	3.11	3.05	2.524	2.554
60	2.19	3.23	3.81	4.08	4.14	3.433	3.4805
90	2.01	3.83	3.02	3.39	4.57	3.608	3.404667
120	2.12	3.42	4.64	3.62	3.19	3.345	3.389167
180	2.18	3.5	4.2	3.6	2.29	3.605	3.229167
240	1.47	2.76	3.47	1.77	1.88	2.107	2.242833
300	0.834	2.01	3.3	2.33	1.84	1.977	2.0485
360	0.639	1.48	2.07	1.449	1.375	1.342	1.3925

ABC-AZT Combination Therapy

ABC concentrations in the maternal plasma

Time (min)	Rat 3	Rat 4	Rat 5	Rat 6	Rat 7	Rat 8	Rat 9	Mean
5	34.981	41.908	39.658	29.606	33.628	22.51	27.724	32.85929
15	22.464	24.637	30.001	16.829	17.057	14.514	18.278	20.54
30	18.527	20.757	24.481	13.605	14.303	10.416	14.609	16.67114
45	18.028	18.884	20.707	12.679	12.247	8.725	14.151	15.06014
60	16.749	14.203	17.484	11.182	12.099	8.196	13.263	13.31086
90	16.914	17.687	13.666	9.777	11.604	6.792	12.485	12.70357
120	15.718	15.728	12.794	9.133	10.732	4.687	8.903	11.09929
180	12.846	11.505	7.321	7.769	8.864	3.839	7.546	8.527143
240			7.038		8.076	3.304	5.474	5.973
300			5.874		7.06			6.467
360							1.213	1.213

ABC concentrations in placenta

Time (min)	Rat 3	Rat 4	Rat 5	Rat 6	Rat 7	Rat 8	Rat 9	Mean
5	13.943	10.68247	15.91	10.156	12.075	9.23	7.904	11.41435
10					10.258		8.569	9.4135
15	10.317	10.4661	10.444	9.184	7.202	9.243	7.998	9.264872
30	8.972	11.73383	10.265	7.991	7.351	6.138	7.609	8.579975
45	8.889	11.61482	11.392	8.282	8.436	5.501	7.426	8.791546
60	9.684	9.548669	10.599	7.688	7.962	5.413	7.559	8.350524
90	10.01	11.14842	8.747	5.877	6.307	4.495	7.177	7.680203
120	11.149	9.145332	7.798	5.401	5.824	2.799	4.77	6.698047
180	7.718	7.958189	3.548	5.146	4.626	1.922	3.685	4.943313
240			3.524		4.512	1.498	3.47	3.251
300			2.815		4.244		1.646	2.901667
360							0.816	0.816

ABC concentrations in fetus

Time (min)	Rat 3	Rat 4	Rat 5	Rat 6	Rat 7	Rat 8	Rat 9	Mean
5	10.682	10.53667	9.378	7.575	9.973	9.646	6.751	9.220239
10					8.186		7.092	7.639
15	10.466	10.42969	8.768	6.796	9.742	9.634	7.86	9.099384
30	11.733	12.68581	10.924	5.631	10.44	10.457	8.187	10.00826
45	11.615	11.56673	11.847	4.106	8.627	7.606	8.32	9.098247
60	9.549	12.61283	11.225	3.161	8.914	6.666	7.985	8.587548
90	11.148	13.87025	9.719	2.779	7.992	7.545	7.206	8.608464
120	9.145	9.694614	5.871	1.781	7.438	4.707	5.521	6.308231
180	7.958	7.587781	3.78	2.763	6.477	2.131	3.482	4.882683

240			3.439		4.534	1.997	3.254	3.306
300			2.584		2.807		1.153	2.181333
360							0.623	0.623

ABC concentrations in amniotic fluid

Time (min)	Rat 3	Rat 4	Rat 5	Rat 6	Rat 7	Rat 8	Rat 9	Mean
5	0.099	0.589	0.19	0.265	0.441	0.175	0.577	0.333714
10					0.649		0.595	0.622
15	0.33	2.109	1.529	1.719	0.807	0.922	1.509	1.275
30	1.382	6.061	1.051	1.221	1.52	0.935	2.718	2.126857
45	2.624	3.142	1.293		2.04	1.323	3.443	2.310833
60	3.178	2.704	2.442	2.756	3.204	1.474	4.447	2.886429
90	5.054	4.383	3.838	1.854	4.393	2.267	4.745	3.790571
120	5.431	5.461	4.222	3.785	4.324	1.773	4.434	4.204286
180	6.678	7.817	4.35	4.805	4.838	2.216	5.382	5.155143
240			3.475		4.26	2.276	3.793	3.451
300			3.432		5.302			4.367
360							2.695	2.695

AZT concentrations in maternal plasma

Time (min)	Rat 3	Rat 4	Rat 5	Rat 6	Rat 7	Rat 8	Rat 9	Mean
5	25.269	31.849	25.206	19.713	25.762	21.032	21.707	24.36257
15	17.389	19.585	16.015	13.131	13.372	14.323	15.533	15.62114
30	11.025	11.316	12.175	8.749	10.054	10.041	11.023	10.62614
45	9.341	9.341	9.406	6.985	7.576	7.142	8.891	8.383143
60	7.356	9.374	7.76	5.332	5.828	5.962	7.185	6.971
90	5.964	7.162	5.236	4.138	4.175	3.717	5.064	5.065143
120	5.086	5.34	3.964	3.453	3.163	2.423	3.484	3.844714
180	4.473	3.745	2.295	3.182	1.844	1.393	1.992	2.703429
240			1.775		1.32	1.574	1.225	1.4735
300			1.272		1.389			1.3305
360							0.765	0.765

AZT concentrations in placenta

Time (min)	Rat 3	Rat 4	Rat 5	Rat 6	Rat 7	Rat 8	Rat 9	Mean
5	14	12.482	14.268	9.929	13.552	11.787	9.756	12.25343
10					12.382		10.571	11.4765
15	10.524	11.53229	10.564	8.939	10.106	11.996	9.133	10.39918
30	7.569	13.394	10.116	6.777	7.588	6.066	7.647	8.451
45	6.762	13.4454	8.196	5.312	6.313	6.261	7.087	7.6252
60	5.398	10.68421	7.043	4.162	5.305	5.993	5.623	6.315459

90	4.318	5.43953	4.531	3.081	4.275	3.235	4.8	4.239933
120	4.589	2.716308	3.657	2.172	2.248	2.758	2.541	2.954473
180	3.26	2.644097	1.535	2.324	1.583	1.48	1.347	2.024728
240			1.185		1.124	1.121	1.152	1.1455
300			1.171		1.247		0.618	1.012
360							0.503	0.503

AZT cocnetrations in fetus

Time (min)	Rat 3	Rat 4	Rat 5	Rat 6	Rat 7	Rat 8	Rat 9	Mean
5	12.482	10.27143	7.887	7.047	11.432	12.287	11.152	10.36549
10					9.741		11.834	10.7875
15	11.532	9.441813	6.927	6.796	9.474	12.003	12.255	9.775545
30	13.394	8.79576	8.347	5.631	7.14	7.044	7.892	8.320537
45	13.445	6.529289	5.728	4.106	6.849	4.594	6.838	6.869898
60	10.684	4.865558	4.757	3.161	6.317	3.727	4.606	5.445365
90	5.44	4.02107	3.243	2.779	4.737	3.392	4.711	4.046153
120	2.716	3.562166	2.368	1.781	1.815	1.8	2.208	2.321452
180	2.644	2.930594	1.228	2.763	1.036	0.84	0.636	1.725371
240			0.93		0.732	0.827	0.583	0.768
300			0.947		0.824		0.346	0.705667
360							0.254	0.254

AZT concentrations in amniotic fluid

Time (min)	Rat 3	Rat 4	Rat 5	Rat 6	Rat 7	Rat 8	Rat 9	Mean
5	1.106	2.863	1.23	1.829	2.412	1.44	3.585	2.066429
10					2.954		2.612	2.783
15	2.313	8.277	3.019	7.187	3.453	5.031	5.107	4.912429
30	5.575	5.332	3.407	4.259	6.026	4.875	6.702	5.168
45	8.361	8.482	4.136		8.922	5.429	8.019	7.224833
60	10.893	8.128	5.846	4.818	7.031	6.919	7.955	7.37
90	8.541	6.154	7.07	4.023	8.011	6.057	5.872	6.532571
120	6.627	5.906	6.03	4.096	5.275	4.973	4.032	5.277
180	10.393	5.771	3.742	4.054	3.302	2.938	2.937	4.733857
240			2.227		3.047	1.758	1.253	2.07125
300			1.739		2.399			2.069
360							0.807	0.807